

**PETROGENESIS OF THE PODIFORM CHROMITITES IN THE
LUOBUSA OPHIOLITE, SOUTHERN TIBET**

By

Mei-Fu Zhou

**Submitted in partial fulfilment of the requirements
for the degree of Doctor of Philosophy**

at

**Dalhousie University
Halifax, Nova Scotia
September, 1995**

© Copyright by Mei-Fu Zhou, 1995



National Library
of Canada

Bibliothèque nationale
du Canada

Acquisitions and
Bibliographic Services Branch

Direction des acquisitions et
des services bibliographiques

395 Wellington Street
Ottawa, Ontario
K1A 0N4

395, rue Wellington
Ottawa (Ontario)
K1A 0N4

Your file *Votre référence*

Our file *Notre référence*

The author has granted an irrevocable non-exclusive licence allowing the National Library of Canada to reproduce, loan, distribute or sell copies of his/her thesis by any means and in any form or format, making this thesis available to interested persons.

L'auteur a accordé une licence irrévocable et non exclusive permettant à la Bibliothèque nationale du Canada de reproduire, prêter, distribuer ou vendre des copies de sa thèse de quelque manière et sous quelque forme que ce soit pour mettre des exemplaires de cette thèse à la disposition des personnes intéressées.

The author retains ownership of the copyright in his/her thesis. Neither the thesis nor substantial extracts from it may be printed or otherwise reproduced without his/her permission.

L'auteur conserve la propriété du droit d'auteur qui protège sa thèse. Ni la thèse ni des extraits substantiels de celle-ci ne doivent être imprimés ou autrement reproduits sans son autorisation.

ISBN 0-612-15828-4

Canada

DALHOUSIE UNIVERSITY

FACULTY OF GRADUATE STUDIES

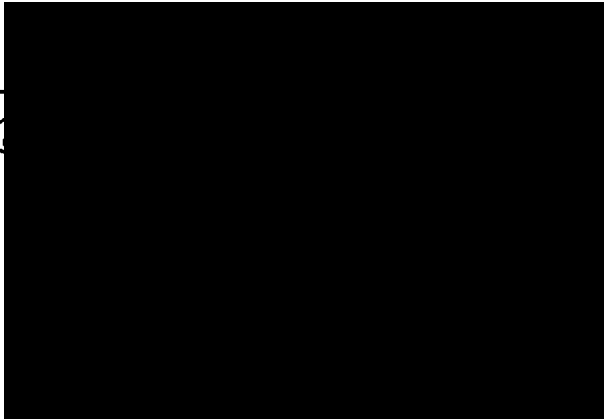
The undersigned hereby certify that they have read and recommend to the Faculty of Graduate Studies for acceptance a thesis entitled "Petrogenesis of the podiform chromitites in the Luobusa Ophiolite, Southern Tibet"

by Mei-Fu Zhou

in partial fulfillment of the requirements for the degree of Doctor of Philosophy.

Dated September 19, 1995

External Examiner
Research Supervisor
Examining Committee



DALHOUSIE UNIVERSITY

DATE: Nov. 1995

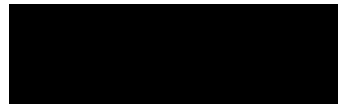
AUTHOR: Mei-Fu Zhou

TITLE: Petrogenesis of the podiform chromitites in the Luobusa ophiolite,
southern Tibet

DEPARTMENT OR SCHOOL: Earth Sciences

DEGREE: PHD CONVOCATION: _____ YEAR: _____

Permission is herewith granted to Dalhousie University to circulate and to have copied for non-commercial purposes, at its discretion, the above title upon the request of individuals or institutions.



Signature of Author

THE AUTHOR RESERVES OTHER PUBLICATION RIGHTS, AND NEITHER THE THESIS NOR EXTENSIVE EXTRACTIONS FROM IT MAY BE PRINTED OR OTHERWISE REPRODUCED WITHOUT THE AUTHOR'S WRITTEN PERMISSION.

THE AUTHOR ATTESTS THAT PERMISSION HAS BEEN OBTAINED FOR THE USE OF ANY COPYRIGHTED MATERIAL APPEARING IN THIS THEISS (OTHER THAN BRIEF EXCEPTS REQUIRING ONLY PROPER ACKNOWLEDGEMENT IN SCHOLARLY WRITING), AND THAT ALL SUCH USE IS CLEARLY ACKNOWLEDGED).

TABLE OF CONTENTS

| | |
|---|-----------|
| Table of contents | iv |
| List of Figures | vii |
| List of Tables | xii |
| Abstract | xiii |
| List of Abbreviations | xiv |
| Acknowledgements | xv |
| Chapter 1. INTRODUCTION | 1 |
| 1.1. Review of theories on the origin of podiform chromitites | |
| <u>1.1.1. Definition and chemical compositions</u> | |
| <u>1.1.2. Genetic relations between podiform bodies and host rocks</u> | |
| <u>1.1.3. Segregation mechanisms of chromite from magmas</u> | |
| 1.2. Problems and objectives | |
| 1.3. Geography and history of the Luobusa chromite deposits | |
| Chapter 2. GEOLOGY | 21 |
| 2.1. Tectonic framework of the Tibetan Plateau | |
| 2.2. The Ngari and Xigaze ophiolites in the Indus-Yarlung Zangbo Suture | |
| 2.3. Geological background of the Luobusa region | |
| <u>2.3.1. General geology</u> | |
| <u>2.3.2. The Luobusa ophiolite</u> | |
| 2.4. Summary | |
| Chapter 3. FIELD RELATIONS AND PETROGRAPHY | 49 |
| 3.1. Nomenclature | |

3.2. Rock types and their distribution

3.3. Petrography

3.3.1. Harzburgite

3.3.2. Dunite

3.3.3. Podiform chromitite

3.3.4. Deformation history

3.4. Summary

Chapter 4. GEOCHEMISTRY

101

4.1. Whole rock geochemistry

4.1.1. Major oxides

4.1.2. Platinum-group elements, Cu, Zn, V and Mn

4.2. Mineral chemistry

4.2.1. Chromite

4.2.2. Olivine

4.2.3. Pyroxenes

4.3. Summary

Chapter 5. PETROGENESIS

136

5.1. Origin of the harzburgites

5.2. Magmatic origin of the podiform chromitites

5.3. Melt/rock interaction around the podiform bodies

5.4. Mechanism of chromite segregation

5.5. MORB mantle peridotites versus boninitic magmas

5.6. Summary

Chapter 6. DISCUSSION

155

6.1. Controls on high-Cr and high-Al chromitites

6.1.1. Similarities and differences of high-Cr and high-Al chromitites

6.1.2. Effects of partial melting

6.1.3. Melt/rock interaction around high-Al chromitites

| | |
|---|------------|
| 6.2. Tectonic setting of podiform chromitites | |
| 6.3. Applications to chromite exploration | |
| 6.4. Summary | |
| Chapter 7. CONCLUSIONS AND FUTURE WORK | 183 |
| 7.1. Conclusions | |
| 7.2. Suggestions for future work | |
| Appendix I: ANALYTICAL METHODS | 187 |
| I.1. Petrochemistry | |
| I.2. Whole rock PGE abundances | |
| I.3. Mineral compositions | |
| Appendix II: PETROCHEMISTRY | 190 |
| Appendix III: MINERAL CHEMISTRY | 196 |
| III-1. Chromite | |
| III-2. Olivine | |
| III-3. Orthopyroxene | |
| III-4. Clinopyroxene | |
| BIBLIOGRAPHY | 216 |

LIST OF FIGURES

| | |
|--|----|
| 1-1. Distribution of major podiform chromite deposits in Chinese orogenic belts..... | 3 |
| 1-2. Cr# vs. Mg# of chromites in podiform chromitites from Chinese ophiolites..... | 4 |
| 1-3. PGE patterns of podiform chromitites from Chinese ophiolites..... | 5 |
| 1-4. Idealized ophiolite section, showing chromitite pods with dunites..... | 9 |
| 1-5. Phase relations in the system Ol-quartz-chromite..... | 15 |
| 1-6. Geographic location of Luobusa, southern Tibet..... | 19 |
| | |
| 2-1. Tectonic map of the Himalayas and the Tibetan Plateau..... | 22 |
| 2-2. Model showing the geologic evolution of the Tibetan Plateau..... | 23 |
| 2-3. Geologic map of the Ngari area, western Tibet..... | 25 |
| 2-4. A cross section of the Erkongba ophiolite in the IYS, western Tibet..... | 30 |
| 2-5. Geologic map of the Xigaze ophiolite, southern Tibet..... | 31 |
| 2-6. Geologic map of the Zedong ophiolitic massif, southern Tibet..... | 34 |
| 2-7. Geologic map of the Luobusa ophiolite, southern Tibet..... | 35 |
| 2-8. South verging fold in Triassic flysch..... | 36 |
| 2-9. Contact between the Luobusa ophiolite and the Luobusa Formation..... | 39 |
| 2-10. Sheared molasse deposits of the Luobusa Formation..... | 40 |
| 2-11. Contact between the Luobusa ophiolite and Triassic flysch..... | 42 |
| 2-12. Cross section of the Luobusa ophiolite | 43 |
| 2-13. Impregnation texture of transition zone dunite..... | 44 |
| 2-14. Sheared rocks from the melange zone in the Luobusa ophiolite..... | 46 |

| | |
|---|----|
| A. Field photo of serpentinite | |
| B. Photomicrograph of a foliated and folded amphibolite | |
| 2-15. Field photo of pillow lavas in the melange zone..... | 47 |
| 3-1. "Opx-Cpx-Ol" diagram of the mantle peridotites and dunites in Luobusa..... | 52 |
| 3-2. Geologic map of the middle part of the Luobusa ophiolite..... | 54 |
| 3-3. Cross sections showing the distribution of chromitites..... | 55 |
| 3-4. Distribution and shapes of chromitite bodies of Ore Group III..... | 56 |
| 3-5. Subsurface podiform chromitite bodies..... | 58 |
| A. Tabular bodies in Ore Group II; | |
| B. Tabular and podiform bodies in Ore Group XXXI. | |
| 3-6. Field photos of podiform chromitite bodies..... | 59 |
| A. Hand sample showing mineralogical zonation | |
| B. A massive chromitite body and several chromite-rich layers in dunite | |
| C. A sharp boundary between a chromitite body and a dunite envelope | |
| D. Chromitite bands in dunite | |
| E. A chromitite band and its branches in dunite | |
| 3-7. Photomicrographs of harzburgites..... | 63 |
| A. Porphyroclastic texture | |
| B. Porphyroclastic texture | |
| C. An Ol porphyroclast, showing kink-banding and irregular boundaries | |
| D. An Opx porphyroclast set in a granular matrix of Ol | |
| E. Olivine along the cleavage of Opx | |
| F. Opx inclusion in Ol | |
| G. Opx inclusion in Opx porphyroclast | |
| H. Deformed Opx porphyroclast | |
| I. Exsolution of Cpx and chromite along cleavage in Opx | |
| J. Grey and yellow Opx twins. | |
| K. Replacement texture showing an Opx grain replaced by Cpx | |
| L. Clinopyroxene and Opx both of which were replaced by Ol | |
| 3-8. Photomicrographs of Di-harzburgite..... | 71 |
| A. Protogranular texture | |
| B. Well-developed kink-banding in an Ol grain | |
| C. Orthopyroxene, Cpx and chromite cluster | |

| | |
|---|----|
| 3-9. Photomicrographs of sheared harzburgite..... | 73 |
| A. Porphyroclastic texture | |
| B. Bent exsolution lamellae of Cpx in Opx | |
| C. Olivine porphyroclasts in a matrix of thinned and elongated Ol | |
| 3-10. Field photo of a dunite dyke in protogranular Di-harzburgite..... | 76 |
| 3-11. Photomicrographs of dunite..... | 77 |
| A. Coarse-grained dunite in contact with protogranular Di-harzburgite | |
| B. Aligned chromite grain in coarse-grained dunite | |
| C. Coarse-grained dunite | |
| D. A large, sheared Ol grain | |
| E. Large Ol grain sheared in two directions at a small angle | |
| F. Kink-bands in Ol, showing subgrain boundaries | |
| G. A larger, sheared Ol grain | |
| H. Olivine and chromite neoblasts along shear fractures | |
| I. Polygonal Ol and chromite neoblasts, locally forming triple points | |
| J. Poikilitic Ol grain containing Opx, and Ol inclusions | |
| K. Elongate Opx grain in a fracture in dunite | |
| L. Small, rounded chromite grain and a small Cpx grain | |
| 3-12. Hand specimen photographs of chromitite..... | 84 |
| A. Massive chromitite showing pull-apart texture | |
| B. Massive to disseminated chromitite | |
| C. Nodular chromitite | |
| D. Nodular chromitite | |
| E. Nodular chromitite. | |
| F. Fragments of brecciated dunite cemented by disseminated chromite | |
| G. Enlarged from F, showing one nodule in a dunite fragment | |
| H. Massive chromitite in contact with dunite | |
| I. Banded chromitite | |
| J. Deformed chromitite | |
| 3-13. Photomicrographs of chromitite..... | 90 |
| A. Sharp boundary between massive chromitite and coarse-grained dunite | |
| B. Interstitial Ol grains in massive chromitite | |
| C. Massive chromitite interstitial to large Ol grains | |
| D. Two chromite nodules in a matrix of Ol and euhedral chromite | |
| E. Disseminated chromitite | |
| F. Dunite with disseminated, euhedral chromites | |
| G. Layered chromitite | |
| H. Layered chromitite | |
| I. Opx grain near boundary between dunite and massive chromitite | |

J. Orthopyroxene grains associated with Ol grains in chromitite

| | |
|---|-----|
| 4-1. Mg# vs. oxides of harzburgite and dunite..... | 104 |
| 4-2. Al/Si vs. Mg/Si and Ca vs. Al of harzburgite and dunite..... | 105 |
| 4-3. SiO ₂ vs. Al ₂ O ₃ of chromitite, dunite, and harzburgite..... | 107 |
| 4-4. Cr ₂ O ₃ vs. SiO ₂ , Al ₂ O ₃ , MgO and FeO of chromitite, dunite, and harzburgite | 108 |
| 4-5. PGE patterns of harzburgite, dunite, and chromitite..... | 111 |
| 4-6. Pd/Ir ratios vs. Cr ₂ O ₃ , Ni, Zn, Cu, and V of harzburgite, dunite, and chromitite | 113 |
| 4-7. Pd/Ir vs. Cu/Ni and Mg# of harzburgite, dunite, and chromitite..... | 114 |
| 4-8. Inter-elemental relationships of chromite..... | 116 |
| 4-9. Cr# vs. Mg# of chromite in dunite, harzburgite, and chromitite..... | 117 |
| 4-10. TiO ₂ vs. Cr# of chromite..... | 119 |
| 4-11. Compositional differences between large and small chromites..... | 120 |
| 4-12. Compositional variations of chromite in the reaction zone..... | 123 |
| 4-13. Fo vs. NiO of Ol in harzburgite, dunite and chromitite..... | 125 |
| 4-14. Compositional variations of Ol in the reaction zone..... | 127 |
| 4-15. "Di-En-Fs" diagram of pyroxene in harzburgite, dunite and chromitite..... | 128 |
| 4-16. Inter-elemental relationships of Opx in harzburgite, dunite and chromitite... | 129 |
| 4-17. En vs. oxides of Opx in harzburgite, dunite and chromitite..... | 130 |
| 4-18. Inter-elemental relationships of Cpx in harzburgite, dunite and chromitite... | 133 |
| 4-19. Chemical variations of pyroxene in the reaction zone..... | 134 |

| | |
|---|-----|
| 5-1. Genetic relationship among harzburgite, dunite and chromitite..... | 139 |
| 5-2. Phase relations in the system Ol-quartz-chromite..... | 145 |
| 5-3. A model illustrating the formation of podiform chromitites..... | 149 |
| 5-4. Tectonic evolution of the Luobusa massif..... | 151 |
| 6-1. Geologic map of the Sartohay ophiolite..... | 157 |
| 6-2. Hand specimen photos of chromitites from Sartohay..... | 158 |
| A. Massive chromitite intruded by a troctolite dyke | |
| B. Disseminated chromitite transitional to dunite | |
| C. Massive chromitite separated from dunite by a chlorite rim. | |
| 6-3. MgO vs. FeO _{total} of lherzolite, harzburgite and dunite from the Luobusa and Sartohay ophiolites..... | 161 |
| 6-4. Ca vs. Al of lherzolite, Di-harzburgite, and dunite from the Sartohay ophiolite..... | 163 |
| 6-5. Cr# vs. Mg# of chromites in lherzolite, Di-harzburgite, dunite and chromitite from the Sartohay ophiolite..... | 164 |
| 6-6. TiO ₂ vs. Cr# of chromites of high-Al chromitites from the Sartohay ophiolite..... | 165 |
| 6-7. Textures illustrating melt impregnation in high-Al chromitites..... | 169 |
| A-Altered plagioclase interstitial to dunites | |
| B-Plagioclase matrix of dunite | |
| C-Chromite and altered Cpx interstitial to dunite | |
| 6-8. REE patterns of dunites and harzburgites adjacent to chromitites and lherzolites of the Sartohay massif..... | 171 |
| 6-9. Illustration of melt/rock interaction in the upper mantle..... | 173 |
| 6-10. Diagrams illustrating three major tectonic settings and their relationships to the podiform chromitites..... | 178 |

LIST OF TABLES

| | |
|--|-----|
| 1-1. Average chromite compositions of podiform chromitites from China..... | 6 |
| 1-2. PGE abundances and metal ratios of podiform chromitites from China..... | 7 |
| 3-1. Locations of studied samples from the Luobusa ophiolite..... | 50 |
| 3-2. Modal analyses of mantle peridotites, dunites and chromitites in Luobusa..... | 51 |
| 3-3. Characterization of three stages of deformation..... | 96 |
| 4-1. Major oxide, trace element, and PGE abundances and metal ratios of mantle peridotites and chromitites in Luobusa..... | 102 |
| 4-2. Representative analyses (wt%) of chromites from the reaction zone..... | 122 |
| 6-1. A mineralogical and geochemical comparison between the Luobusa and Sartohay ophiolites..... | 160 |

ABSTRACT

Podiform chromitites of the Luobusa ophiolite in the Indus-Yarlung Zangbo Suture of southern Tibet are typical of the high-Cr variety. This ophiolite is composed of a mantle sequence, a transition zone and a melange zone, and is tectonically bounded by Triassic flysch on the south and Tertiary molasse deposits and the Gangdese Batholith on the north. The podiform chromitites in Luobusa occur in the mantle sequence. The mantle peridotites are chiefly harzburgites and Di-harzburgites composed of Ol (Fo=90-92), Opx (En=87-92), Cpx (Mg#=45-53) and chromite (Cr#=18-66). They have porphyroclastic textures, relatively uniform bulk-rock compositions (Mg#=89-91), and unfractionated, chondrite-normalized PGE patterns. These rocks are essentially residua left after extraction of MORB magmas in a mature spreading centre. The chromitites display nodular, massive, disseminated or banded textures and typically have dunite envelopes that grade into the surrounding harzburgite and Di-harzburgite. They consist of relatively uniform chromite (Cr#=74-82) and low-Al pyroxenes and have strongly fractionated PGE patterns depleted in Pt and Pd. They are believed to have formed from a boninitic magma produced by a second stage of melting above a subduction zone. Dunites contain accessory chromites intermediate in composition between those of peridotites and chromitites and are the products of reaction between the boninitic magmas and MORB peridotites. The melt/rock reaction removed pyroxenes from the peridotites and precipitated Ol, forming dunite envelopes. The melts thus became more boninitic in composition and chromite-saturated. The interplay of melt/rock interaction, chromite fractionation and magma mixing would presumably lead to many fluctuations in melt composition, producing both massive and disseminated chromitites as well as phase layering within individual podiform bodies.

High-Cr and high-Al chromitites are believed to have formed by high and low degrees of partial melting and both are precipitated by interaction of newly-formed magmas with old lithospheric mantle peridotites in island arc environments and nascent spreading centres, respectively.

LIST OF ABBREVIATIONS

| | |
|------|---|
| Cpx | Clinopyroxene |
| Di | Diopside |
| En | Enstatite |
| Fs | Ferrosilite |
| Fo | Forsterite |
| OI | Olivine |
| Opx | Orthopyroxene |
| Cr# | $100\text{Cr}/(\text{Cr}+\text{Al})$, atomic ratio |
| Mg# | $100\text{Mg}/(\text{Mg}+\text{Fe}^{2+})$, atomic ratio of Ol and chromite |
| Mg# | $100\text{Mg}/(\text{Mg}+\text{Fe}^{2+}+\text{Ca})$, atomic ratio of Cpx |
| Mg# | $100\text{Mg}/(\text{Mg}+\text{Fe}^{2+})$, mole fraction of bulk-rock petrochemistry |
| LREE | Light rare earth element |
| PGE | Platinum-group element |
| IPGE | Iridium group of PGEs |
| PPGE | Palladium group of PGEs |
| BHT | Bayan Har-Hohoxili Terrane |
| BNS | Bonggong-Nujing Suture |
| ISC | Indian Subcontinent |
| IYS | Indus-Yarlung Zangbo Suture |
| KQS | East Kunlun-Qingling Suture |
| LLS | Longmu-Lancanjiang Suture |
| LT | Lhasa Terrane |
| MBT | Main Boundary Thrust |
| MCT | Main Central Thrust |
| MORB | Mid-oceanic Ridge Basalt |
| QT | Qiangtang Terrane |
| TTT | Tarim-Tsaidam Terrane |

ACKNOWLEDGMENTS

I am greatly indebted to my supervisor, Professor P. T. Robinson, whose interest in Chinese ophiolites and chromites made this project possible. I thank him for many enlightening and enjoyable days we shared during field work in the remote areas, western China. His insightful comments were invaluable in improving the early version of this thesis. It would not have been possible without his guidance, patience, and constant encouragement. Professors J. Malpas, G. K. Muecke and P. H. Reynolds merit special words of appreciation for serving as supervisory committee members, for their help and encouragement through the course of my study, and for critically reading this thesis.

The continuing collaboration with Dr. W.-J. Bai and Mr. X.-F. Hu from the Institute of Geology (CAGS, Beijing) made our field work in China successful. I thank them for sharing their geological ideas developed over many years. Drs. Ba Dengzhu, Guo Jiangzi and Zhang Yizhi from the Geological Team 2 of the Tibetan Geological Survey helped me during my field work in Tibet. Thanks are due to Drs. G. Davies and G. Suhr for an enjoyable field season in 1994. I appreciate the kind assistance of Drs. M. Sun, J. Jain and J. Fan with operation of the ICP-MS at the University of Saskatchewan, Mr. R. McKay with the electron microprobe and Mr. G. Brown with thin section preparation. The debt of gratitude is owed my friends who helped me in various ways, notably S. Anderson, N. Banerjee, Yi Ding, R. Hicks, J. Ketchum, Guodong Li, M. C. Tate, and Jing-Sui Yang.

Advice received from Drs. T. Calon and H. J. B. Dick advanced my understanding of the rocks. Drs. R. G. Coleman, J. Dostal, R. A. Jamieson and P. J. C. Ryall provided insightful comments on the final version of this thesis. I acknowledge the many colleagues who kindly provided helpful comments on various chapters or submitted manuscripts that were later incorporated into this thesis, notably Drs. S. Arai, S. J. Barnes, P. Kelemen, R. Kerrich, B. R. Lipin, E. A. Mathez, S. Roberts, P. Roeder, G. Suhr and M. Sun. Their thoughtful reviews improved substantially the presentation of this thesis.

This work was supported financially by NSERC research grants to P.T. Robinson, NSERC-NSFC (Natural Science Foundation of China) bilateral exchange grants to P. T. Robinson and W.-J. Bai, a Geological Society of America research grant and a Dalhousie graduate scholarship.

Chapter 1. INTRODUCTION

1.1. Reviews of theories on the origin of podiform chromitites

1.1.1. Definition and chemical compositions

Podiform chromitites, as defined by Thayer (1964), are lenticular bodies of chromitite hosted in deformed peridotites in many ophiolites. Individual bodies yield about 1000 tons of chromitite on average (Thayer, 1973). These lens-shaped bodies are usually enveloped by dunite in a harzburgite host. Important examples of such deposits exist in former Yugoslavia, Greece, Turkey, Iran and Pakistan along the Alpine-Himalayan orogenic belt, and in the Philippines and New Caledonia in the western Pacific. Ophiolites in Cuba and the Urals also contain such deposits (Stowe, 1987; and references therein).

The deposits (chromitites) include high-Cr (45-60 wt% Cr_2O_3) and high-Al (>25 wt% Al_2O_3) varieties, reflecting the strong reciprocal variation of Cr_2O_3 (15-65 wt%) and Al_2O_3 (6-43 wt%) (Thayer, 1964, Leblanc and Violette, 1983, Hock et al., 1986). A bimodal compositional distribution of podiform chromitites has been reported in John Day, Oregon (Thayer, 1946); Zambales, Philippines (Leblanc and Violette, 1983, Hock et al., 1986); Kempirsay, Kazakhstan (Pavlov and Chuprynina, 1966) and Coolac, Australia (Golding and Johnston, 1971). Both high-Al and high-Cr chromitites occur in these massifs but they are spatially separated. Many massifs contain only high-Al or high-Cr chromitites. In the Zambales ophiolite of the Philippines, the Coto ultramafic massif contains high-

Al chromitites, whereas the Acoje massif hosts high-Cr chromitites (Leblanc and Violetter, 1983).

In China, the major podiform deposits occur in the Himalayan and Palaeo-asian orogenic belts (Figure 1-1), and include both high-Cr and high-Al varieties (Figure 1-2). Zhou and Bai (1992) noted that the high-Al chromitites have chromites with higher Ti contents than those of the high-Cr variety (Table 1-1). All podiform chromitites exhibit relatively constant FeO, in contrast to stratiform chromitites with variable FeO but relatively uniform Cr#'s.

Podiform chromitites show Os, Ir and Ru enriched PGE patterns (Barnes et al., 1985). Podiform chromitites from China have variable PGE contents (Table 1-2) and exhibit three types of PGE patterns on chondrite-normalized diagrams (Zhou et al., 1995b): (1) a negatively sloping pattern with variable positive Ru anomalies (type I), (2) a smooth, negatively sloping pattern (type II, sample XD-2), and (3) an irregular, enriched pattern (type III, sample GI-2) [Figure 1-3]. Although high-Al chromitites (samples XS-2, NII-2) have a type I pattern, they are poorer in total PGEs than their high-Cr counterparts (samples NI-2, NI-3, XD-1, GD), and particularly so in Ir and Rh (Figure 1-3). Podiform chromitites from the Rizo ophiolite, Greece, have type II PGE patterns (Konstantopoulou and Economou, 1991). PGE-rich rocks with type III patterns, having high Ru and Rh contents, have been reported in chromite-rich samples from the Rizo and Zambales ophiolites (Bacuta et al., 1990; Konstantopoulou and Economou, 1991). However, compared with stratiform chromitites, PGE

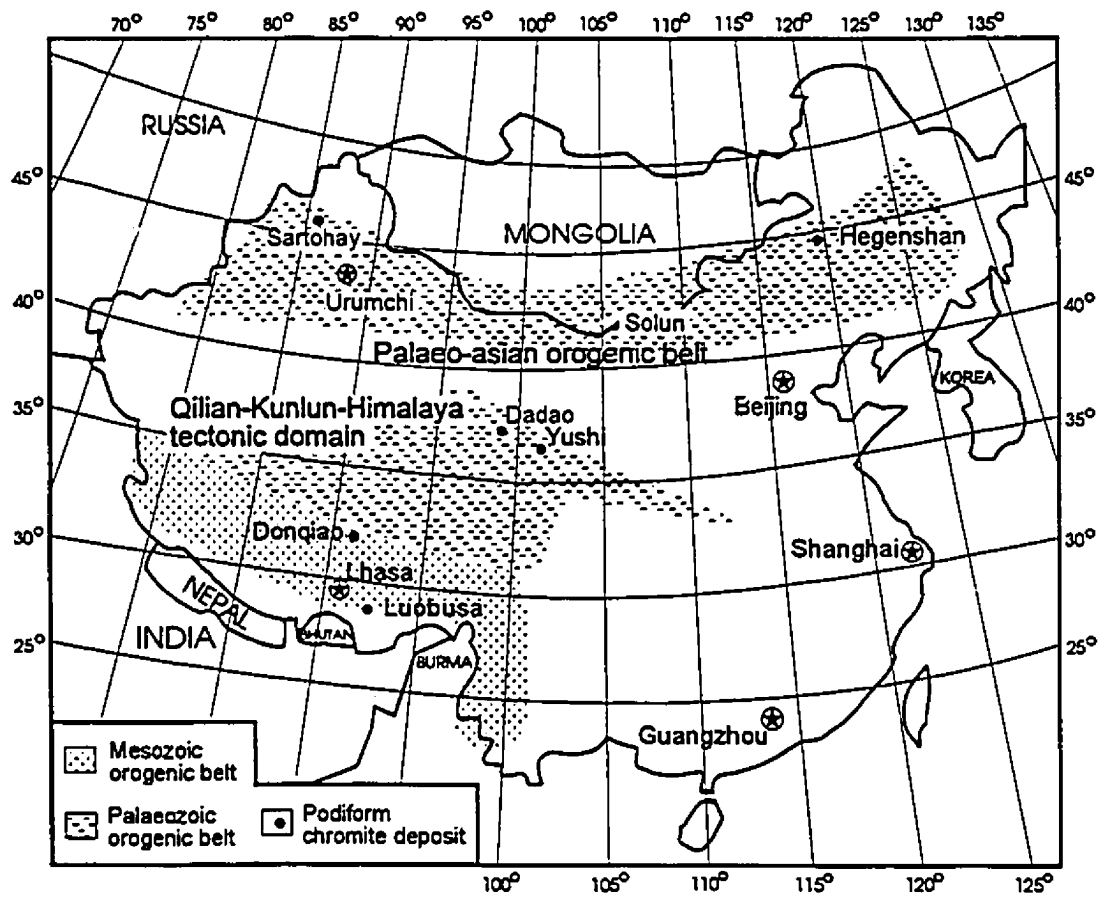


Figure 1-1. Distribution of major podiform chromite deposits in Chinese orogenic belts (modified from Zhou and Bai, 1992).

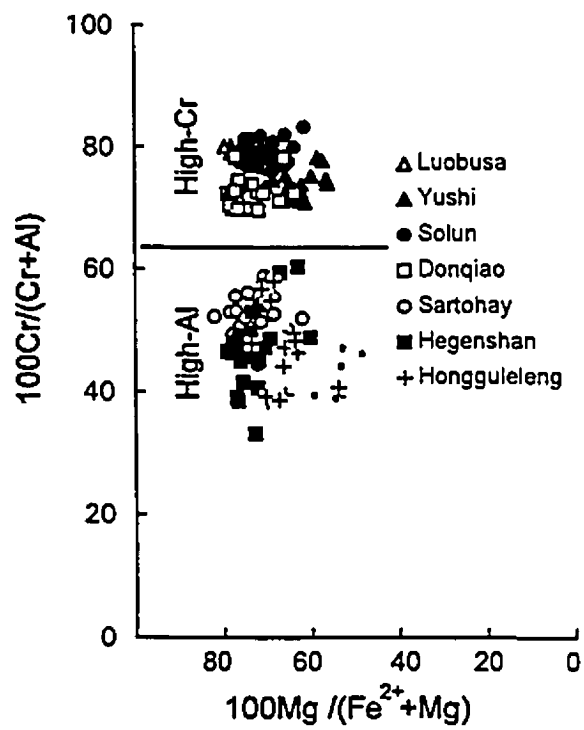


Figure 1-2. Cr# versus Mg# of chromites in podiform chromitites from Phanerozoic ophiolites in China

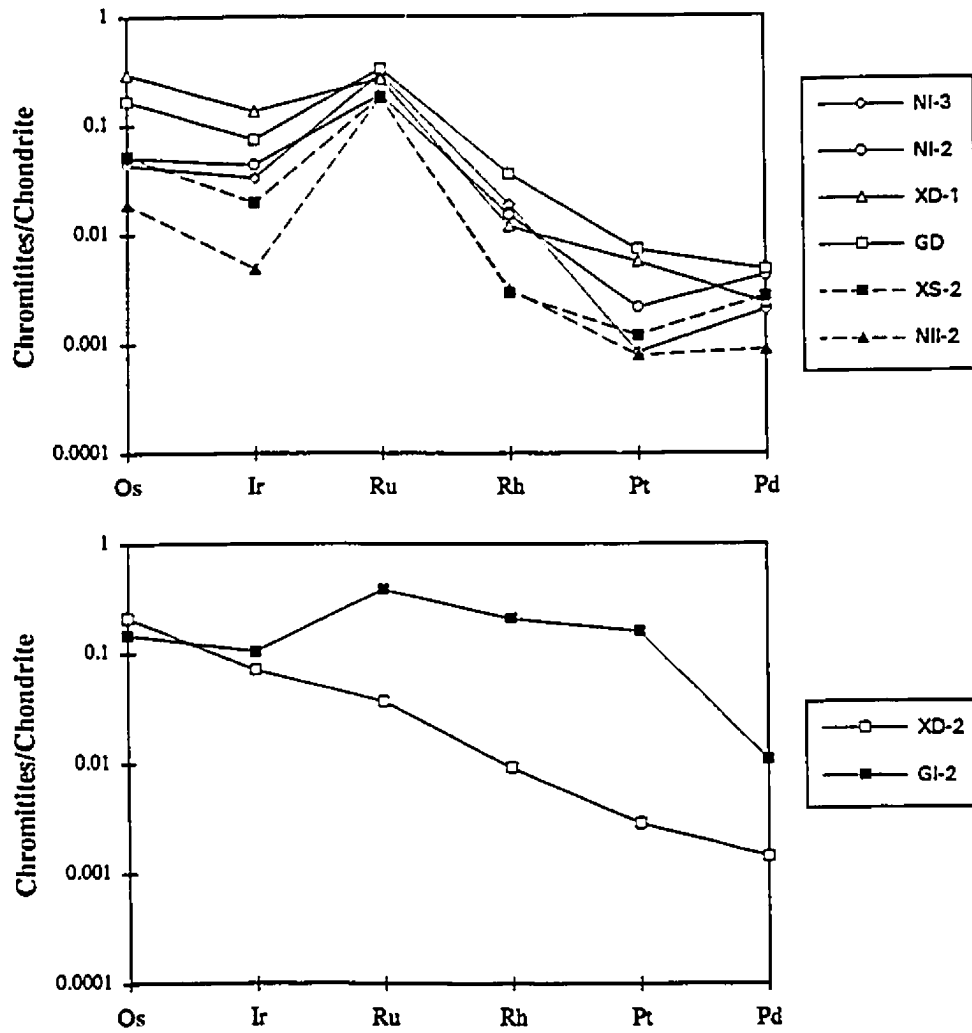


Figure 1-3. Chondrite-normalized PGE patterns of podiform chromitites from Phanerozoic ophiolites in China.

Table 1-1. Average chromite compositions of podiform chromitites from China

| | 1 | 2 | 3 | 4 | 5 | 6 | 7 | 8 |
|--------------------------------|------|------|------|------|------|------|------|------|
| No. | 30 | 40 | 22 | 16 | 24 | 37 | 36 | 38 |
| Al ₂ O ₃ | 23.4 | 27.7 | 28.1 | 14.6 | 10.5 | 11.1 | 13.7 | 15.8 |
| Cr ₂ O ₃ | 42.7 | 40.1 | 38.9 | 53.2 | 58.7 | 59.0 | 53.7 | 50.6 |
| Fe ₂ O ₃ | 5.56 | 4.34 | 4.34 | 4.32 | 2.81 | 3.69 | 4.54 | 3.73 |
| FeO | 11.4 | 11.5 | 12.9 | 14.1 | 10.7 | 10.1 | 9.81 | 17.5 |
| MgO | 15.5 | 16.2 | 15.1 | 12.9 | 14.3 | 15.2 | 15.4 | 10.8 |
| TiO ₂ | 0.29 | 0.20 | 0.28 | 0.15 | 0.04 | 0.19 | 0.07 | 0.15 |
| MnO | 0.18 | 0.15 | 0.19 | 0.17 | 0.14 | 0.13 | 0.08 | 0.29 |
| NiO | 0.13 | 0.17 | 0.15 | 0.08 | 0.11 | 0.15 | 0.12 | 0.10 |
| Total | 99.1 | 100 | 100 | 99.5 | 97.2 | 99.6 | 97.0 | 98.5 |
| Mg# | 70 | 72 | 66 | 61 | 69 | 72 | 73 | 51 |
| Cr# | 55 | 49 | 48 | 71 | 79 | 78 | 72 | 68 |

Ophiolites: 1-Sartohay; 2-Hegenshan; 3-Hongguleleng;
 4-Yushi; 5-Solun; 6-Luobusa; 7-Donqiao; 8-Dadao.
 Abbreviations: No.=numbers of analyses; Mg#=100Mg/
 (Mg+Fe²⁺), Cr#=100Cr/(Cr+Al).

Table 1-2. PGE abundances (ppb) and metal ratios of podiform chromitites from China

| | Os | Ir | Ru | Rh | Pt | Pd | Pd/Ir | Pu/(Pt+Pd) | Description |
|---------------------|-----|------|-----|------|------|------|-------|------------|-------------|
| Yushi (high-Cr) | | | | | | | | | |
| GI-2 | 75 | 56 | 262 | 41 | 162 | 5.94 | 0.107 | 0.96 | Massive |
| Solun (high-Cr) | | | | | | | | | |
| NI-3 | 22 | 18 | 201 | 3.73 | 0.86 | 1.10 | 0.062 | 0.44 | Banded |
| NI-2 | 26 | 23 | 128 | 3.00 | 2.19 | 2.25 | 0.096 | 0.49 | Nodular |
| Donqiao (high-Cr) | | | | | | | | | |
| XD-1 | 151 | 72 | 182 | 2.34 | 5.75 | 1.27 | 0.018 | 0.82 | Massive |
| XD-2 | 107 | 38 | 25 | 1.82 | 2.96 | 0.78 | 0.021 | 0.79 | Banded |
| Sartohay (high-Al) | | | | | | | | | |
| XS-2 | 27 | 11 | 123 | 0.58 | 1.22 | 1.46 | 0.139 | 0.46 | Massive |
| Hegenshan (high-Al) | | | | | | | | | |
| NI-2 | 10 | 2.61 | 122 | 0.63 | 0.81 | 0.48 | 0.184 | 0.63 | Nodular |
| Dadao (high-Cr) | | | | | | | | | |
| GD | 85 | 40 | 222 | 7.07 | 7.40 | 2.56 | 0.064 | 0.74 | Massive |

patterns of podiform chromitites are relatively uniform (Naldrett and von Gruenewaldt, 1989).

1.1.2. Genetic relations between podiform bodies and host rocks

Despite being compositionally distinct from stratiform varieties, podiform chromitites have cumulate textures and magmatic depositional structures. Early workers related these features, by analogy, to their stratiform counterparts in large layered complexes (Thayer, 1964; 1969). Some of the peculiar features of the podiform deposits were explained as the result of deformation during remobilization and re-emplacement of chromitite bodies as autoliths, and thus, podiform chromitites were thought to be essentially metamorphosed stratiform bodies (Thayer, 1969).

Because their host rocks were recognized as residual peridotites of ophiolitic origin (Figure 1-4) (e.g., Coleman, 1977), the podiform chromitites were later interpreted as being formed by cumulate processes operating in magma chambers located near the crust-mantle boundary (e.g., Dickey, 1975; Malpas and Strong, 1975; Greenbaum, 1977). Dickey (1975) suggested that podiform chromitites form by the sinking of chromitite bodies as autoliths into the upper mantle rocks, whereas Greenbaum (1977) proposed tight infolding of the lower crustal stratiform chromitites into upper mantle rocks. However, structural studies do not support a crustal cumulate origin for the pods (e.g., Cassard et al., 1981; Lago et al., 1982), and mineralogical and geochemical data reveal that podiform deposits are distinctly different from stratiform deposits in the lower

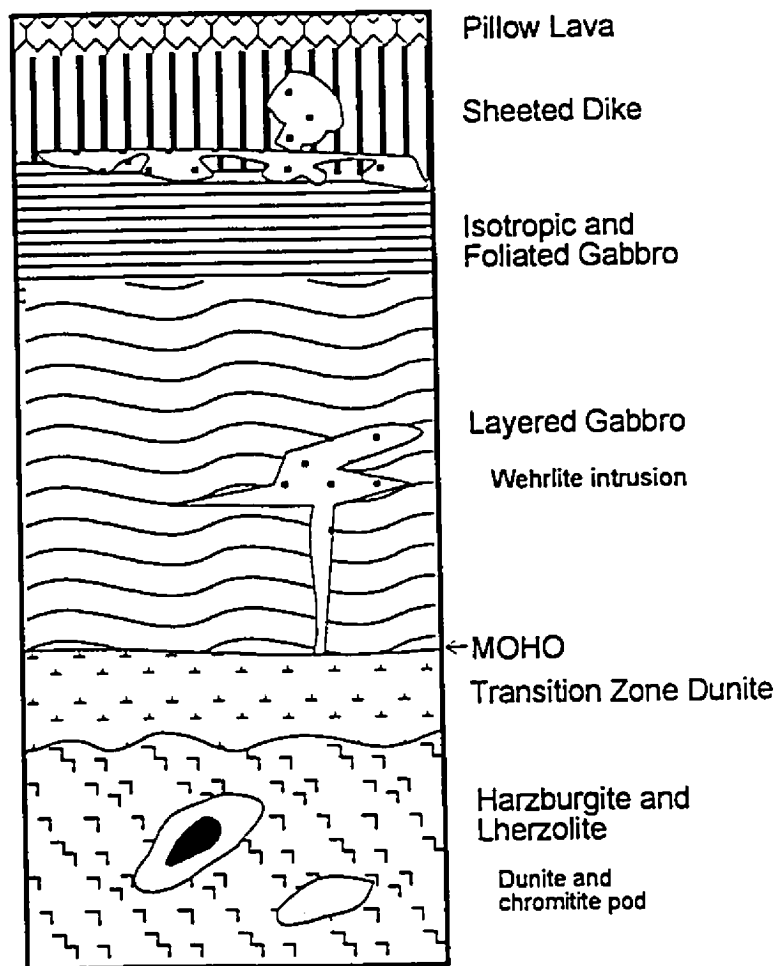


Figure 1-4. Idealized ophiolite section, showing chromitite pods with dunite envelopes in the upper mantle.

crust.

The association of depleted peridotites and chromitites led to the hypothesis that the podiform chromitites also represent residues after partial melting (e.g., Arai, 1980; Wang Xibin et al., 1987). Segregation of residual chromite could produce layers of disseminated chromite in residual harzburgite. Experimental work of Dickey et al. (1971) indicated that chromite can be formed by incongruent melting of chromian diopside. This process was extended to cover other mantle silicates as likely source materials for chromium (Dickey and Yoder, 1972). Some Cpx in lherzolite xenoliths is rich in chromium, with up to 4% Cr₂O₃ being reported from various lherzolite and wehrlite xenoliths (Dawson et al., 1970; Hervig et al., 1986). Textural evidence of the transformation of Opx-spinel symplectites into discrete idiomorphic chromite grains (Leblanc et al., 1980) supports the experimental work of Dickey et al. (1971). Sinigoi et al. (1983) interpreted the Cr-spinel trains in dunites of the Balmuccia peridotite (Italy) as residues of incongruent melting of pre-existing thin Cr-diopsidic layers. However, it is difficult to explain large bodies of chromitite by concentration of residual chromites.

Grafenauer (1977) suggested that chromitites form during upward movement and partial fusion of the upper mantle. In this model, droplets of Cr-rich melt would be formed during deformation of the host peridotites. These droplets would eventually merge together and by a process of liquefaction, nodules would be formed. Thus, the ores would be strung out

along flow lines in the peridotite. Grafenauer suggested that the smaller streaks would coalesce to form thicker plates. Such a process would require extremely high temperatures in the upper mantle in order to sustain chromite melts for a substantial period.

Formation of podiform chromitites has also been related to basaltic melts in the upper mantle. Because chromitites were thought to be restricted to highly depleted harzburgite-type ophiolites, they were related to supra-subduction zone environments where partial melting was enhanced by the addition of volatiles (Pearce et al., 1984; Roberts, 1988; 1992; Paktunc, 1990; Nicolas and Al Azri, 1991; Roberts and Neary, 1993). In lherzolite-type ophiolites chromium is still largely retained in Cpx. With higher degrees of partial melting, the Cpx would be dissolved allowing chromium to be incorporated into the melt and leaving behind a harzburgitic residue (Roberts, 1988; 1992; Roberts and Neary, 1993). High chromium contents in the basaltic magmas would lead to later segregation of chromium into chromite deposits during crystallization (Nicolas and Al Arzi, 1991).

Neary and Brown (1979) and Brown (1980) explained the formation of podiform chromitites by crystal settling in rising mini magma chambers located in the mantle beneath the main crustal cumulate magma chamber. Lago et al. (1982) proposed a somewhat similar model involving dynamic crystallization and accumulation of chromite along vertical/subvertical conduits which channel the magma upward. They suggested that primitive melts are repeatedly replenished

in small magma chambers and residual liquid is withdrawn from the site of chromite crystallization. This is considered here to be a useful model for explaining the formation and distribution of podiform bodies.

1.1.3. Segregation mechanisms of chromite from magmas

There is now widespread acceptance that podiform chromitites crystallize from basaltic magmas in the upper mantle. The problem then becomes how chromium as a minor component in the magma can be concentrated to form large chromitite bodies. Normal crystallization of chromite from basaltic magma can account for the formation of disseminated chromite ores, where small amounts of chromite are hosted in dunite, but a different explanation is needed to account for large bodies of massive chromite ore (Irvine and Sharpe, 1986). The same problem exists in understanding the origin of stratiform chromitites.

Early workers explained the formation of chromitites by crystallization from Cr-rich melts that are immiscible with silicate magmas (e.g., Pavlov et al., 1977). An immiscible Cr-rich liquid was proposed for the formation of some chromitite seams in the Bushveld complex, based on a study of inclusions in chromite (Sampson, 1932; McDonald, 1965). Large liquid miscibility gaps are evident from experimental studies of Cr₂O₃-bearing silicate systems (Muan, 1975). The MgO-Cr₂O₃-SiO₂ system has two immiscible liquids—Si-rich and Cr-rich melts, when the MgO content is low (Keith, 1954). Because of the high temperatures and simple compositions used in these experiments, separation of an immiscible Cr-rich liquid was thought not to be likely in natural magmas

(Dickey, 1975). However, an immiscible Cr-rich phase could occur under magmatic conditions where many more degrees of freedom in the system exist than have been experimentally examined (McDonald, 1965). Studies using the $\text{Fe}_2\text{O}_3\text{-Cr}_2\text{O}_3\text{-SiO}_2$ (Muan and Somiya, 1960) and $\text{CaO-Cr}_2\text{O}_3\text{-SiO}_2$ systems (Glasser and Osborn, 1958) indicate that high CaO and Fe_2O_3 contents in basaltic magmas increase the possibility of liquid immiscibility of Si-rich and Cr-rich melts. More significantly, the presence of volatile- and alkali-rich inclusions within chromite grains of many podiform chromitites (Johan et al., 1983; Wang Hesheng et al., 1983; Bai et al., 1985; McElduff and Stumpfl, 1991) indicates that a fluid phase may play an important role in decreasing the temperature of immiscibility. Unfortunately, immiscible Cr-rich melts in a system similar to a natural assemblage with volatile and alkali elements have not been produced experimentally.

Johan (1986a, b) believes that the chromitite bodies and enclosing dunite of the Massif du Sud (New Caledonia) were formed by interaction of a magma with reducing fluids along pre-existing shear zones. A metasomatic origin for dunite involving replacement of pyroxene by Ol during subsolidus reaction with aqueous fluids is relatively well known (e.g., Dungan and Ave Lallemand, 1977), and formation of J-M Reef (Stillwater Complex) chromites by interaction of a gabbro norite crystal mush with fluid was suggested by Boudreau (1988). The major evidence for the formation of podiform chromitite bodies by metasomatic processes is the presence of hydrous phases as inclusions in chromites.

Contamination by wall rock assimilation was proposed for chromitite formation in the Muskox (Irvine, 1975) and Kemi (Alapieti et al., 1989) layered intrusions because alkali-rich inclusions occur in chromites from these bodies.

Other models focus on migration of melts from the silicate-chromite cotectic into the primary phase volume of chromite. Ulmer (1969) emphasized the importance of oxygen fugacity in expanding the crystallization field of chromite, and Cameron and Desborough (1969) suggested that contamination of the magma by gaseous emanations from the country rock could increase its oxygen fugacity, leading to the formation of monomineralic chromite horizons. Cameron (1980) subsequently abandoned this hypothesis in favor of chromite crystallization in response to changes in total pressure, a mechanism also invoked to explain chromite layers in the Stillwater Complex (Lipin, 1993). However, the magnitude of the pressure change required to form a 1-m-thick chromitite layer would be unrealistically large ($\gg 1$ kb) and, in general, the effect of pressure on mineral stability is small (Hatton and von Gruenewaldt, 1987; Campbell and Murck, 1993).

A magma mixing model for the formation of stratiform chromitite was proposed by Irvine (1977) who suggested that chromitite layers in the Muskox intrusion and other stratiform intrusions were formed by periodic mixing of evolved melts with more mafic parental magmas as illustrated in Figure 1-5. Mixing of fractionated and parental liquids would result in the magma becoming supersaturated in chromite leading to monomineralic precipitation (see mixing

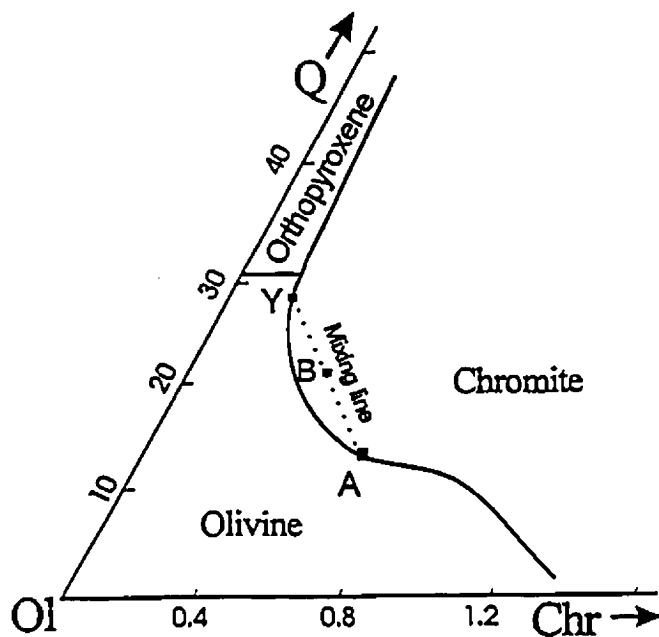


Figure 1-5. Phase relations in the system Ol-quartz-chromite as determined by Irvine (1977). Mixing of primary (A) and evolved magmas (Y) leads to chromite saturation (B).

line in Figure 1-5). This mixing model is consistent with textural evidence pointing to common cotectic crystallization of chromite and OI and also accounts for the presence of laterally extensive chromitite bands within layered intrusions and the observed sequence of layers (e.g., Duke, 1983; Sharpe and Irvine, 1983; Irvine and Sharpe, 1986; Murck and Campbell, 1986; Roeder and Reynolds, 1991; Campbell and Murck, 1993).

Reaction between partial melts and mantle has been experimentally and petrographically documented (Fisk, 1986; Kelemen, 1990; Kelemen et al., 1992, 1995; Daines and Kohlstedt, 1994). Zhou et al. (1994) proposed that the reaction between mantle melts and their host peridotites modifies the liquid compositions, driving them into the field of chromite crystallization, and producing dunite envelopes around the chromitite bodies. They suggest that such melt/rock reaction has played an important role in producing podiform bodies, in a manner similar to that of Irvine (1977).

1.2. Problems and objectives

Podiform chromitites have a much wider range of composition (from high-Cr to high-Al) and more varied textures than stratiform types (Thayer, 1964), and they occur in depleted peridotites (Figure 1-4). These facts cause many major problems regarding their genesis: (1) how chromium, as a minor component in the magmas, is concentrated to form large chromitite ore bodies, (2) why podiform chromitites with cumulate textures are associated with depleted mantle

sequences of ophiolites which commonly exhibit a tectonite fabric, and (3) what controls the chromite compositions of podiform chromitites. Answers to these problems are of fundamental importance for understanding the formation mechanism of podiform chromitite and future chromite exploration. They are also crucial for understanding mantle processes and the evolution of oceanic lithosphere.

Any viable hypothesis should also explain why chromites in podiform chromitites are chemically distinct from those in stratiform complexes, and why the former everywhere have relatively uniform PGE abundances, compared to the more variable PGE distributions of stratiform chromitites.

In order to address these problems, I have focused on the petrogenesis of high-Cr podiform chromitites from the Luobusa ophiolite in southern Tibet. Based on field work in Luobusa, this thesis establishes the lithostratigraphy of the ophiolite. I have sampled the mantle sequence of this ophiolite and carried out petrographic observations and mineral and whole-rock analyses. To compare this ophiolite and its chromitites with ophiolites containing high-Al chromitites, field work and laboratory analyses were also carried out on the Sartohay ophiolite (Xinjiang Province, NW China, see Figure 1-1). The objectives are to test the proposed melt/rock reaction model for explaining the genetic relationships between the mantle peridotites and chromitites, to determine what controls the compositions of the chromitites, to discuss applicability of the model to other ophiolites, and finally to consider possible

tectonic settings for podiform chromitites and their host peridotites.

1.3. Geography and history of the Luobusa chromite deposits

The Luobusa chromite mining area is located on the south bank of the Yarlung Zangbo River (29°5'N, 92°5'E), about 250 km east of Xigaze, and 200 km southeast of Lhasa (Figures 1-1 and 1-6). The lowest elevation is the Yarlung Zangbo River, about 3500 meters above sea level, and the highest peak is 6000 meters above sea level.

Ultramafic rocks of the Luobusa ophiolite were first discovered in 1951 by geologists of Academic Sinica and its chromitites were reported in 1959 by local people to a Tibetan Geological Team. Wang Xibin and co-workers mapped the body and examined the chromite mineralization in 1960 and published a report in 1965 (Wang Xibin et al., 1965). The second geological team of the Tibetan Geological Survey started exploration in 1966. Thus far, this team has sampled the ophiolite through more than 700,000 m of diamond drill holes (Li Zijin et al. 1993), as well as by trenching, channeling and opening pits. This team has written two initial reports on the general geology and on the results of their exploration (GTTGB, 1981; 1989). Wang Hesheng et al. (1983) summarized the basic information on the petrography of the chromitites and their petrochemistry and suggested that they are late magmatic deposits. Wang Xibin et al. (1987) studied the ophiolite and proposed that the Luobusa chromitites represent the most depleted residuum in the upper mantle section. Li Zijin et al. (1993) carried

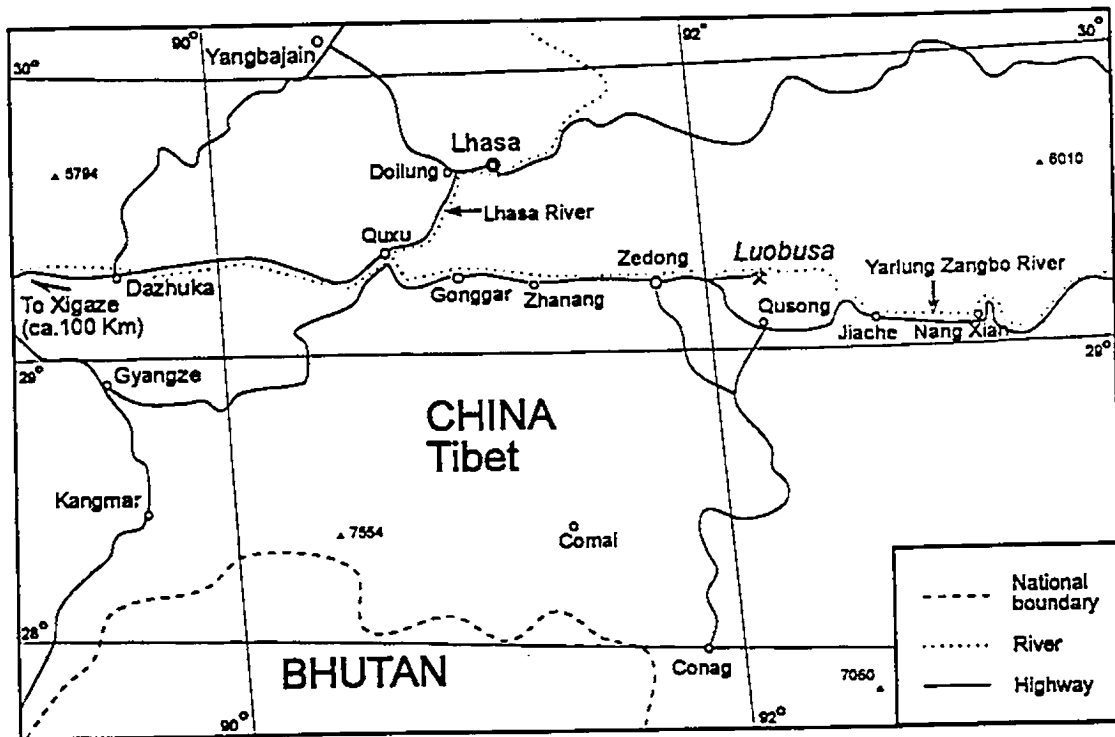


Figure 1-6. Geographic location of Luobusa, southern Tibet.

out a statistical study on the ore reserves. Bai et al. (1993) reported diamonds and other unusual minerals (such as native chrome, Fe-Ni alloy, SiC and graphite) in the mantle peridotites and podiform chromitites of the Luobusa ophiolite and suggested a suprasubduction zone environment for ophiolite formation. The geochemistry of the volcanic rocks supports this suggestion (Zhou et al., 1995c). Zhou and co-workers also examined the petrography and geochemistry of the podiform chromitites in Luobusa and proposed that they formed by melt/rock interaction in the upper mantle (Zhou and Robinson, 1994; Zhou et al., 1995a).

The Luobusa mine has operated for more than 10 years and produces metallurgical chromites which provide the major source of chromium for China. It contains proven reserves (ores with more than 25 wt% chromite) of several million metric tons (Li Zijin et al., 1993). Both the chromitites and their host peridotites are well-preserved and remarkably fresh, providing a unique opportunity for detailed geochemical studies. However, because of its economic value, the area was not open to western geologists until very recently.

Chapter 2: GEOLOGY

2.1. Tectonic framework of the Tibetan Plateau

The Luobusa ophiolite lies in the eastern part of the Indus-Yarlung Zangbo Suture (IYS) within the Tibetan Plateau (Figures 1-1 and 2-1). This plateau consists of several terranes which were accreted successively to the Tarim-Tsaidam Terrane (TTT) in the northernmost part of the Plateau (Figures 2-1 and 2-2) [Zhang et al., 1984; Dewey et al., 1988; Xiao Xuchang et al., 1988]. The Bayan Har-Hohoxili Terrane (BHT) was accreted along the East Kunlun-Qingling Suture (KQS) and is separated from the Qiangtang Terrane (QT) to the south by the Longmu-Lancanjiang Suture (LLS). The Lhasa Terrane (LT) was accreted to the Qiangtang Terrane (QT) along the Bonggong-Nujing Suture (BNS) and is separated to the south from the Indian Subcontinent (ISC) by the IYS.

There are three major units in the ISC: the Higher Himalaya, the Lesser Himalaya, and the Sub-Himalaya, separated by the Main Central Thrust (MCT) and the Main Boundary Thrust (MBT), respectively.

Within the TTT, ophiolites of early Palaeozoic age occur in the Jiliang Mountains and represent remnants of oceanic lithosphere within Eurasia (Xiao Xuchang et al., 1988). During Permian and Triassic time this terrane was separated from Gondwanaland by the Palaeo-Tethyan ocean (Figure 2-2), now represented by ophiolites and wild-flysch of the KQS. The 423-394 Ma East

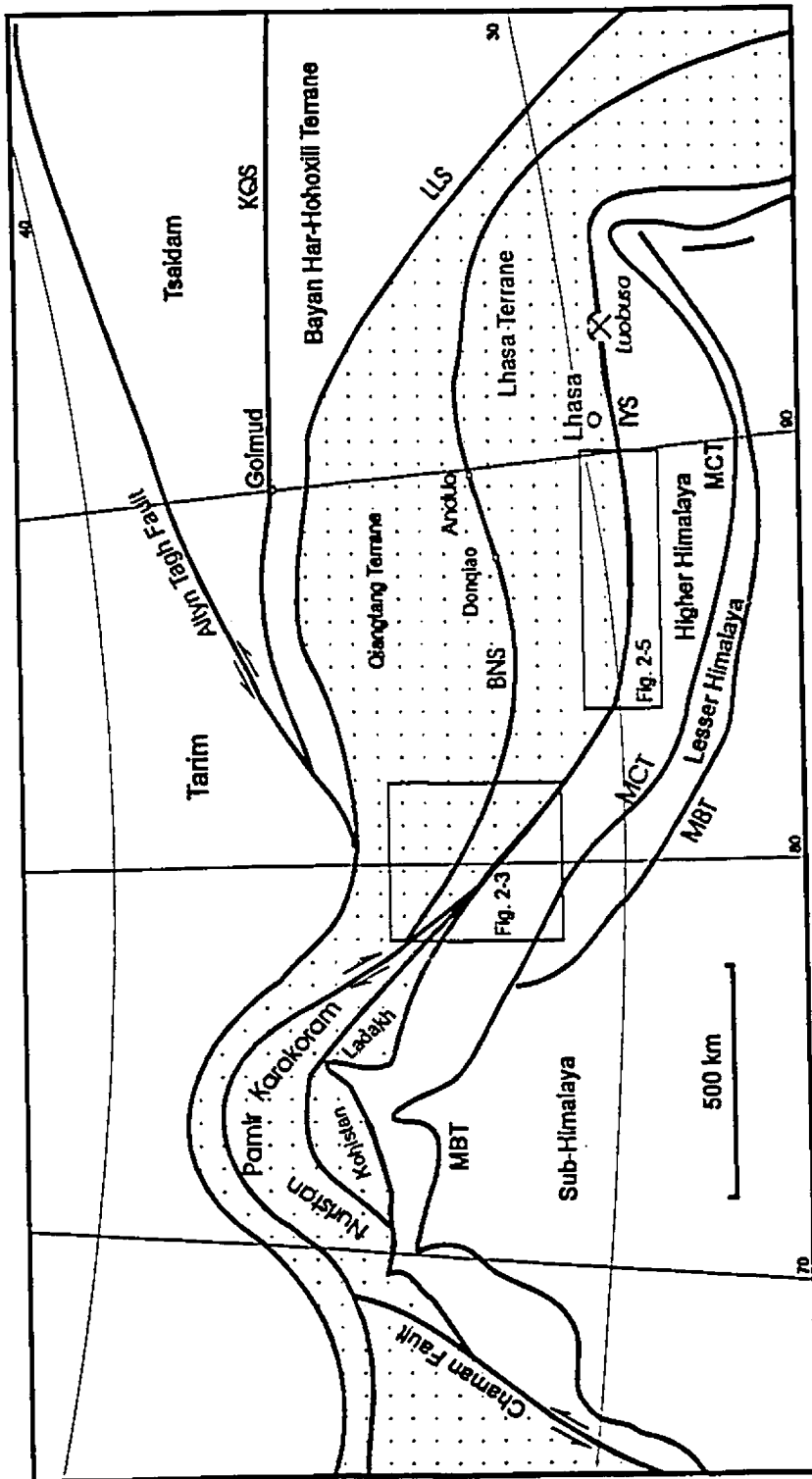
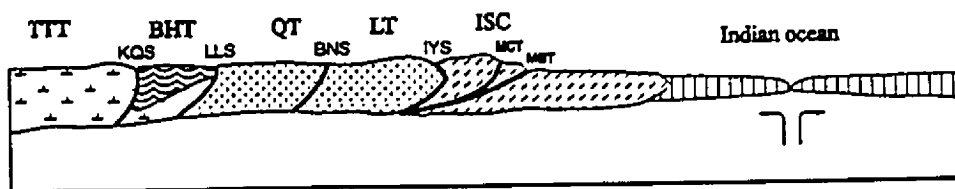
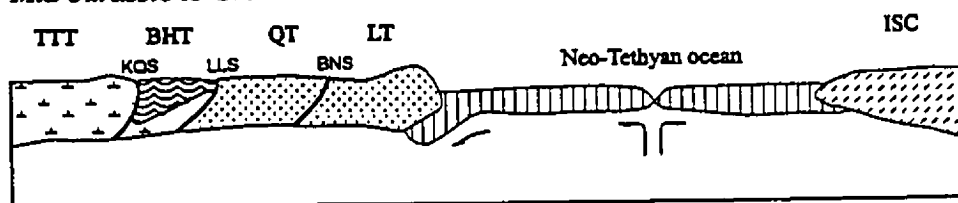


Figure 2-1. Tectonic map of the Himalayas and the Tibetan Plateau showing tectonic divisions, suture zones and major thrusts (after Zhang et al., 1984; Dewey et al., 1988; Xiao Xuchang et al., 1988). The dotted areas were fragments of Gondwanaland before Cretaceous time. Abbreviations: BNS-Bonggong-Nujiang Suture, IYS-Indus-Yarlung Zangbo Suture, KQS-East Kunlun-Qingling Suture, LLS-Longmu-Lancangjiang Suture, MBT-Main Boundary Thrust, MCT-Main Central Thrust.

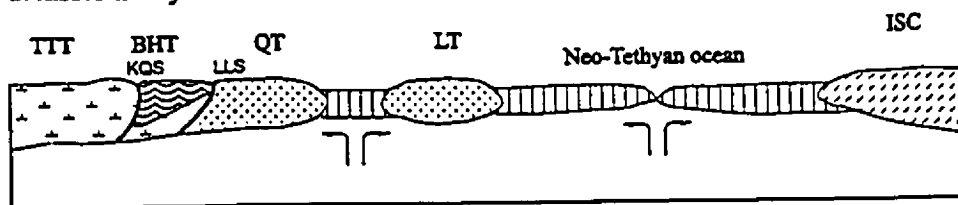
Early Tertiary to Present



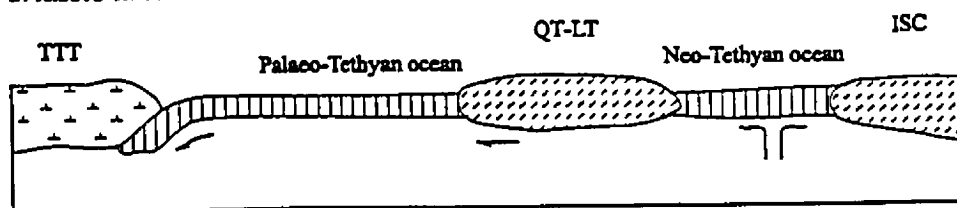
Mid-Jurassic to Cretaceous time



Triassic-Early Jurassic time



Triassic time



Pre-Triassic time

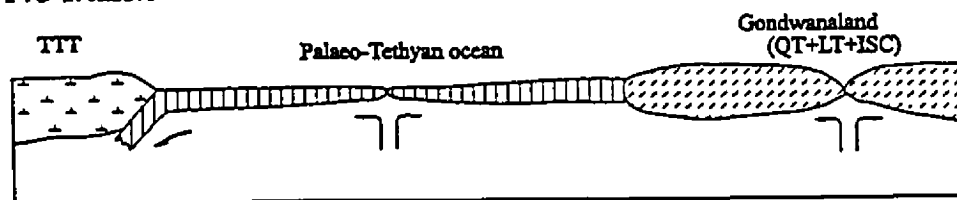


Figure 2-2. Schematic section showing the geologic evolution of the Tibetan Plateau. See text for explanation.

Kunlun granitic batholith north of the suture (Zhang et al., 1984) may have been generated during the northward subduction of the Palaeo-Tethyan lithosphere. The BHT is composed of thick Triassic flysch possibly deposited in the Palaeo-Tethyan ocean.

The LLS extends southward into western Yunnan along the Jinshajiang River and continues further into Thailand (Figure 2-1). This suture is considered to mark the principal boundary between Eurasia and Gondwanaland in Permian and Triassic times. It is marked by Permian and possibly Late Carboniferous ophiolites and ophiolitic melange, as well as by exotic blocks and olistostromes. During Permian time, the Tibetan Block (both QT and LT) separated from Gondwanaland, drifted northward, and approached and collided with the margin of Eurasia so that the Palaeo-Tethyan ocean was closed near the end of the Late Permian.

The QT has a metamorphic crystalline basement, probably consolidated in Precambrian time, and a platform-type Palaeozoic sequence that developed since the Silurian. The terrane also contains a 3,250-m-thick sequence of Carboniferous and Permian sandstones and slates intercalated with basic volcanic rocks. The Lower Permian sequence consists of more than 2,000 m of flysch intercalated with sandy conglomerates.

The BNS extends more than 1,500 km from Banggong Lake (Figure 2-3) on the west to the Nujiang River Valley on the east. A similar suture zone has been described in Farah Rud, Afghanistan, and to the east in Sittang Valley,

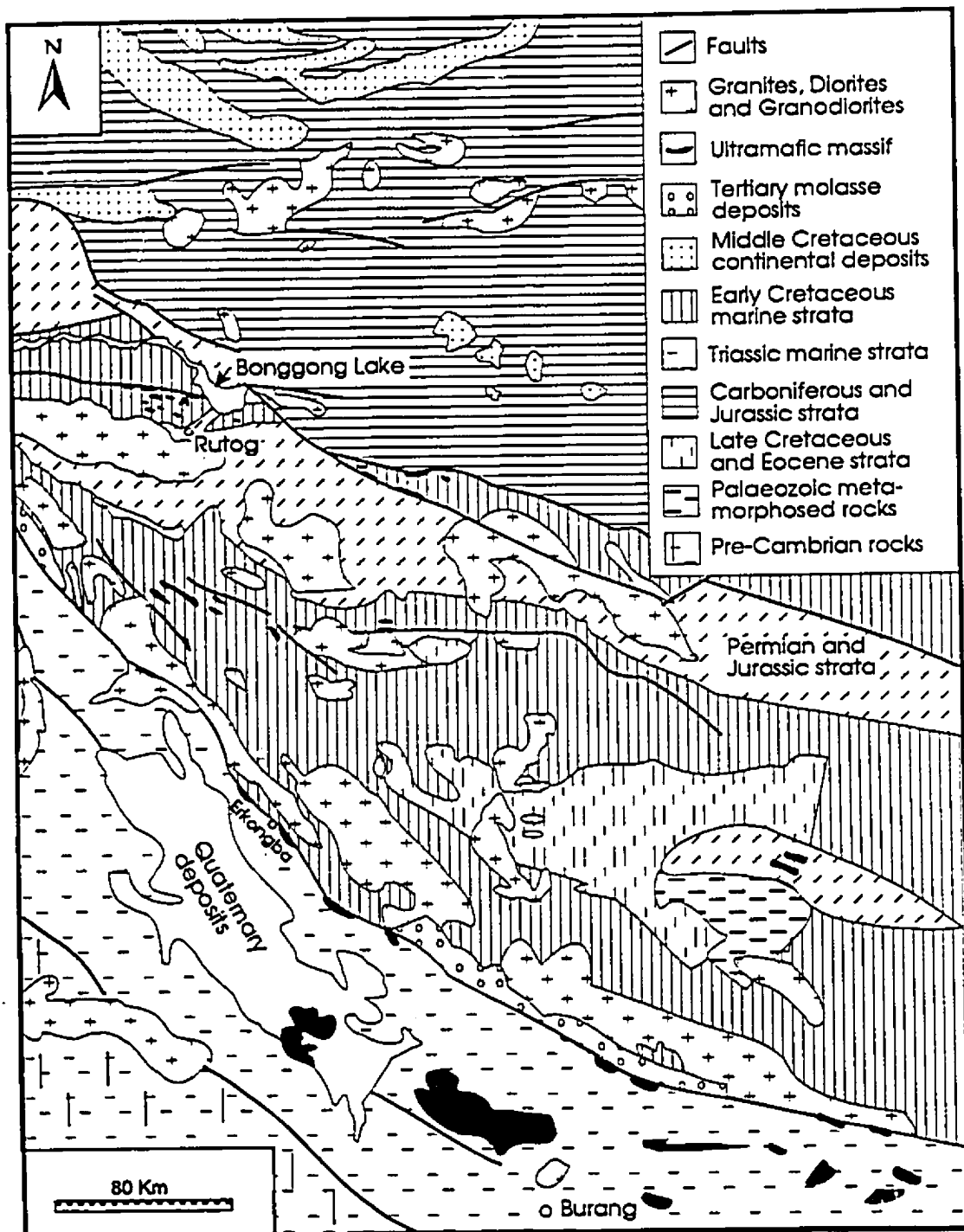


Figure 2-3. Geologic map of the Ngari area, western Tibet (simplified from Guo Teying et al., 1991). See location in Figure 2-1.

Mytkyina of Burma, suggesting an east-west trending oceanic domain during Triassic time (Chang, et al., 1989; Girardeau et al., 1989). Numerous ophiolitic components and melange have been found along this suture. The ophiolites near the Donqiao and Gyangco areas of northern Tibet contain a mantle sequence of depleted residual harzburgites, a cumulate sequence of wehrlites, pyroxenites, dunites and layered gabbros, and a volcanic sequence. In the Bonggong Lake area of western Tibet, ophiolitic material extends 100 km along the suture (Figure 2-3) and consists of ultramafic rocks, gabbros, diabase and pillow lavas. The ophiolite is thrust over Jurassic flysch and is associated with Early Cretaceous sedimentary rocks. Based on their geochemistry, the ophiolites may have formed in a supra-subduction zone environment.

Radiolarian cherts associated with the ophiolites contain foraminifera including *Sethocyrtis*, *Cryptocapsa*, *Dicolacapsa*, *Tricolocapsa*, *Dictyomitra*, *Lithocampe*, *Genellipsis*, and *Rhopalastrum*, indicating a Jurassic age (Wang Xibin et al., 1987). The ophiolites are transgressively covered by Cretaceous shallow-water deposits. In the Donqiao and Gyangco areas, foliated garnet-bearing amphibolites which occur beneath the sheeted diorites and mantle peridotites are interpreted as remnants of a metamorphic sole. Two amphibole-separates from this unit yielded $^{40}\text{Ar}/^{39}\text{Ar}$ isotopic ages of 175 ± 3 Ma and 180 ± 3 Ma, respectively (Zhou et al., 1995b). The Bonggong-Nujiang ocean opened by intra-continental rifting to form a continental marginal basin in Late Triassic time (Figure 2-2). Obduction of the Donqiao ophiolite occurred in Middle Jurassic

resulting in the formation of 172 Ma gneissic rocks in the Anduo area (Xu et al., 1985), although the closure of this ocean might be as late as Early Cretaceous in the Bonggong area (Guo Tieying et al., 1991).

The LT extends southwards into the Zayu-Tengchong Block and is underlain by Lower Palaeozoic to Mesozoic sedimentary rocks with intercalated volcanic rocks. The southeastern portion of this terrane is dominated by the east-west trending Gangdese Batholith and its associated volcanic sequence known as the Linzizhong Formation in which radiometric ages range from 40 to 120 Ma (Scharer et al., 1984; Xu et al., 1985). The Gangdese Batholith is composite, made up of numerous plutonic bodies, commonly with gradational contacts. Compositions range from noritic gabbro to adamellite through quartz-monzonite and granodiorite. Most rocks are typically meta-aluminous and subalkaline (Le Fort, 1988). Isotopic data suggest a largely mantle source for the batholith with small amounts (<30%) of crustal assimilation (Debon et al., 1986). Most of the Gangdese Belt is attributed to magmatism at an active continental margin above a northward-dipping subduction zone (Allegre et al., 1984). This terrane formed the southern margin of the Eurasian continent prior to about 40 Ma. This Andean-type margin progressively passes into the Kohistan-Ladakh Arc in the west (Figure 2-1), branching off the southern Tibet continental crust in the Ladakh region (Le Fort, 1988). In northern Pakistan there are granulites and ultramafic blocks which are thought to be diapirs of subducted oceanic lithosphere underneath the Kohistan-Ladakh Arc (Jan and

Windley, 1990).

The IYS is marked by discontinuous ophiolitic bodies extending from Burma in the east to Ladakh in the west (Figure 2-1). The ophiolites in Burma and the Andaman Sea were obducted eastward prior to Middle Eocene (Sengupta et al., 1990). The Ngari and Xigaze ophiolites west of Luobusa will be discussed in the next section.

The Higher Himalaya, the northernmost exposed part of the ISC, is made up of a thick sequence of Cambrian to Eocene sedimentary rocks of the Tibetan Tethys Zone which overlies a Proterozoic metamorphic basement, known as the "Centre Crystalline". The Centre Crystalline is a thick (5 to more than 10 km) pile of aluminous gneisses and schists. The rocks of the Higher Himalaya are separated from those of the Lesser Himalaya by a major, north-dipping thrust, the MCT. The MCT is a major intracontinental fault zone that accommodated portions of the post-collisional convergence between India and Eurasia.

The Lesser Himalaya comprises Proterozoic to Mesozoic sedimentary rocks overlying earlier basement rocks. South of the Lesser Himalaya, and separated from it by the MBT, are the Sub-Himalayan Siwalik molasse-type deposits which have been affected by the most recent Himalayan deformation.

The leading edge of the Indian plate was deformed and metamorphosed prior to uplift along the major north-dipping thrusts which imbricated and stacked the metamorphic complex.

2.2. The Ngari and Xigaze ophiolites in the IYS

The ophiolites in the Ngari area, western Tibet, have been little studied and very few data are available. The Xigaze ophiolite in the middle of the IYS has been described by a number of Chinese and French geologists (e.g., Nicolas et al., 1981; Girardeau et al., 1985; Girardeau and Mercier, 1988; Nicolas, 1989).

In the Ngari area, ophiolites in the IYS include mantle peridotite, troctolite, layered gabbro, pillow lavas and radiolarian cherts. There are abundant andesites and andesitic basalts interlayered with Cretaceous marine sedimentary rocks. The Erkongba ophiolite has a complete ophiolite sequence including chromite-bearing harzburgite, plagioclase peridotite, troctolite, gabbro, pillow lavas and cherts (Figure 2-4). The Burang ophiolite is among the largest ultramafic massifs in this zone and occurs as a tectonic nappe thrust over the Triassic rocks of the ISC (Figure 2-3).

The Xigaze ophiolite extends east-west along the IYS and forms a continuous belt over 170 km long (Figure 2-5). The ophiolite is covered by cherts and marine pelagic sedimentary rocks of the Xigaze Group. Below are pillowed and massive lavas that pass downward through diorite sills, or dykes, into serpentized dunite and harzburgite. The upper harzburgites and dunites are intruded over a thickness of about 1 km by thick diabase sills which become progressively less abundant down section. Di-rich harzburgite is the dominant ultramafic rock and lies about 2 km below the mafic unit, and thus about 5 km

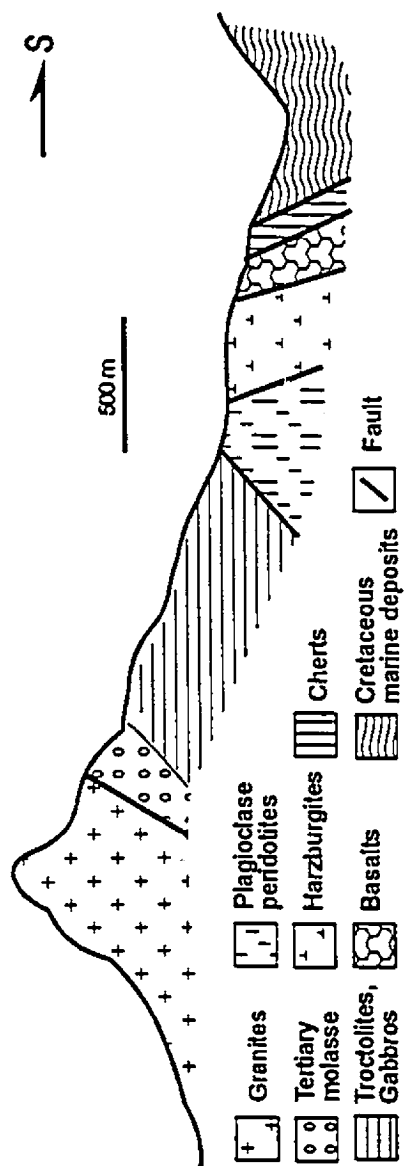


Figure 2-4. A cross section of the Erkongba ophiolite in the IYS, western Tibet (after Guo Tteying et al., 1991).

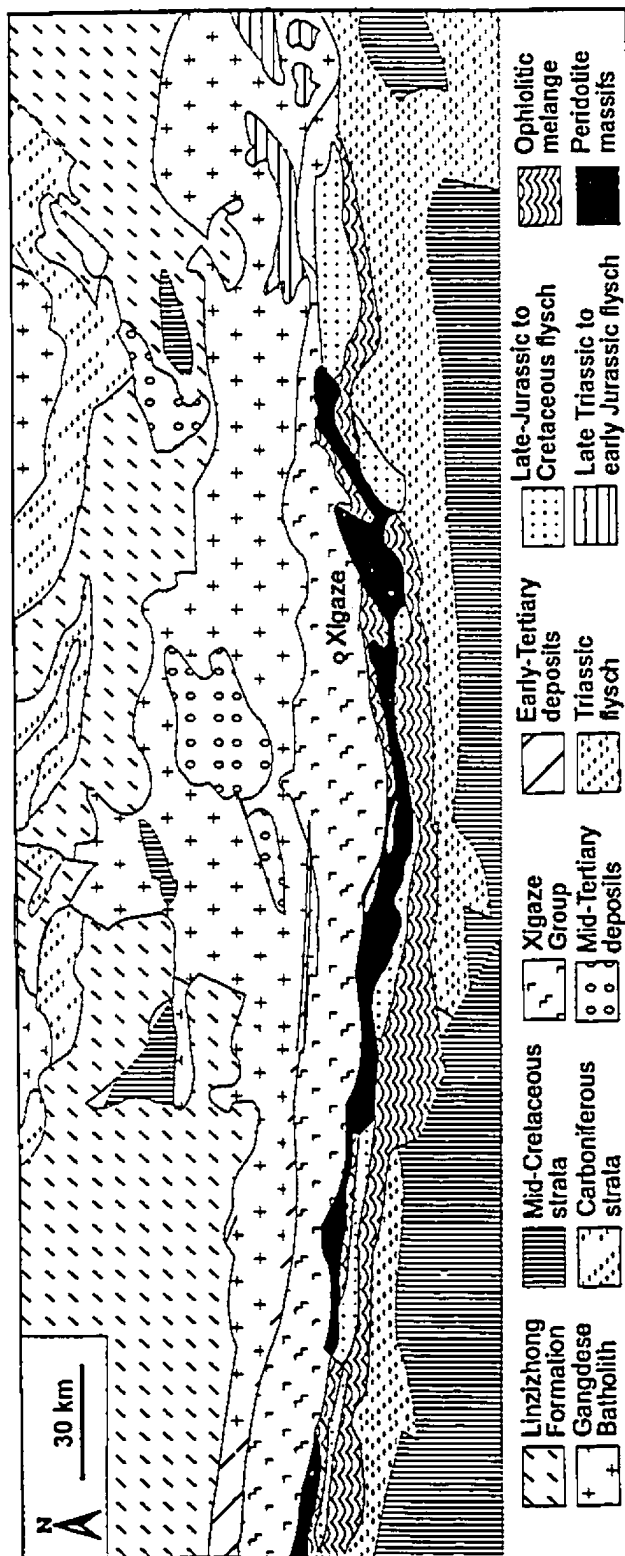


Figure 2-5. Geologic map of the Xigaze ophiolite, southern Tibet (after Wang Xibin et al., 1987).

beneath the sedimentary cover of the ophiolite sequence. The harzburgite grades downward into a more lherzolitic peridotite. Lead isotope data point to an island-arc affinity for the ultramafic tectonites and a depleted-MORB affinity for the mafic rocks (Nicolas, 1989).

Palaeomagnetic data on the pillow lavas and radiolarites of the Xigaze ophiolite show that the ophiolite formed at a latitude of about 10°-20°N (Pozzi et al., 1984), close to the southern margin of Eurasia during Early Cretaceous time. The Xigaze Group flysch was deposited in an oceanic basin at the southern edge of Eurasia. The simultaneous formation of the Gangdese magmatic arc just north of this oceanic basin shows that it was a fore-arc basin, located between an arc and a north-dipping subduction zone (Nicolas, 1989).

The IYS ophiolites formed in the Tibetan Tethys ocean separating the ISC from the LT during Middle Cretaceous time (110-100Ma), as shown by the age of radiolarian cherts directly covering the Xigaze ophiolite (Marcoux et al., 1982). This age is roughly consistent with a $^{238}\text{U}/^{206}\text{Pb}$ age of $120\pm 10\text{Ma}$ (Gopel et al., 1984) and a Nd/Sm age of $109\pm 21\text{ Ma}$ (Prinzhofer, 1987, cited in Nicolas 1989) for the same ophiolite. Formation of the ophiolite at 110-100 Ma in an oceanic basin with MORB affinities was followed by northward subduction that produced the Gangdese Batholith. Girardeau and Mercier (1988) envisage a slow-spreading environment for this ridge on the basis of the geochemistry of the Xigaze ophiolite. After the formation of the subduction zone, the ophiolite became incorporated into the oceanic lithosphere of a fore-arc basin. From

there, it was obducted onto the ISC during the final collision.

The collision of India with Eurasia began in the Cenozoic at about 50 Ma as shown by paleomagnetic data (Patriat and Achache, 1984). The ocean basin was completely closed and the ophiolites obducted before the end of the Eocene (before 40 Ma) (Tapponnier et al., 1981). The subduction of oceanic lithosphere induced island-arc magmatism in the Gangdese Mountains of the LT. Accordingly, the youngest granodiorites dated at 41 Ma (Sharer et al., 1984) record the closure of the ocean and thus the end of oceanic subduction.

2.3. Geological background of the Luobusa region

2.3.1. General geology

In the eastern part of the IYS, from Quxu to Nang Xian, the major ophiolitic massifs include those in Zedong and Luobusa (Figures 2-6 and 2-7). Both the Zedong and Luobusa massifs are tectonically bounded by the Gangdese Batholith and the Luobusa Formation to the north and by Triassic rocks to the south. The Triassic rocks of the ISC are typical Tibetan Tethyan flysch. These strata, dominantly west-east trending, are located south of the IYS and dip to the south. They include low-grade metamorphosed sedimentary rocks such as greywacke and sandstone. There are numerous mafic sills parallel to the strike of the strata. Rocks directly above the ophiolite are extensively fractured and sheared and have well-developed, steeply south-dipping cleavage. Further south, there are south-verging mesoscopic folds (Figure 2-8).

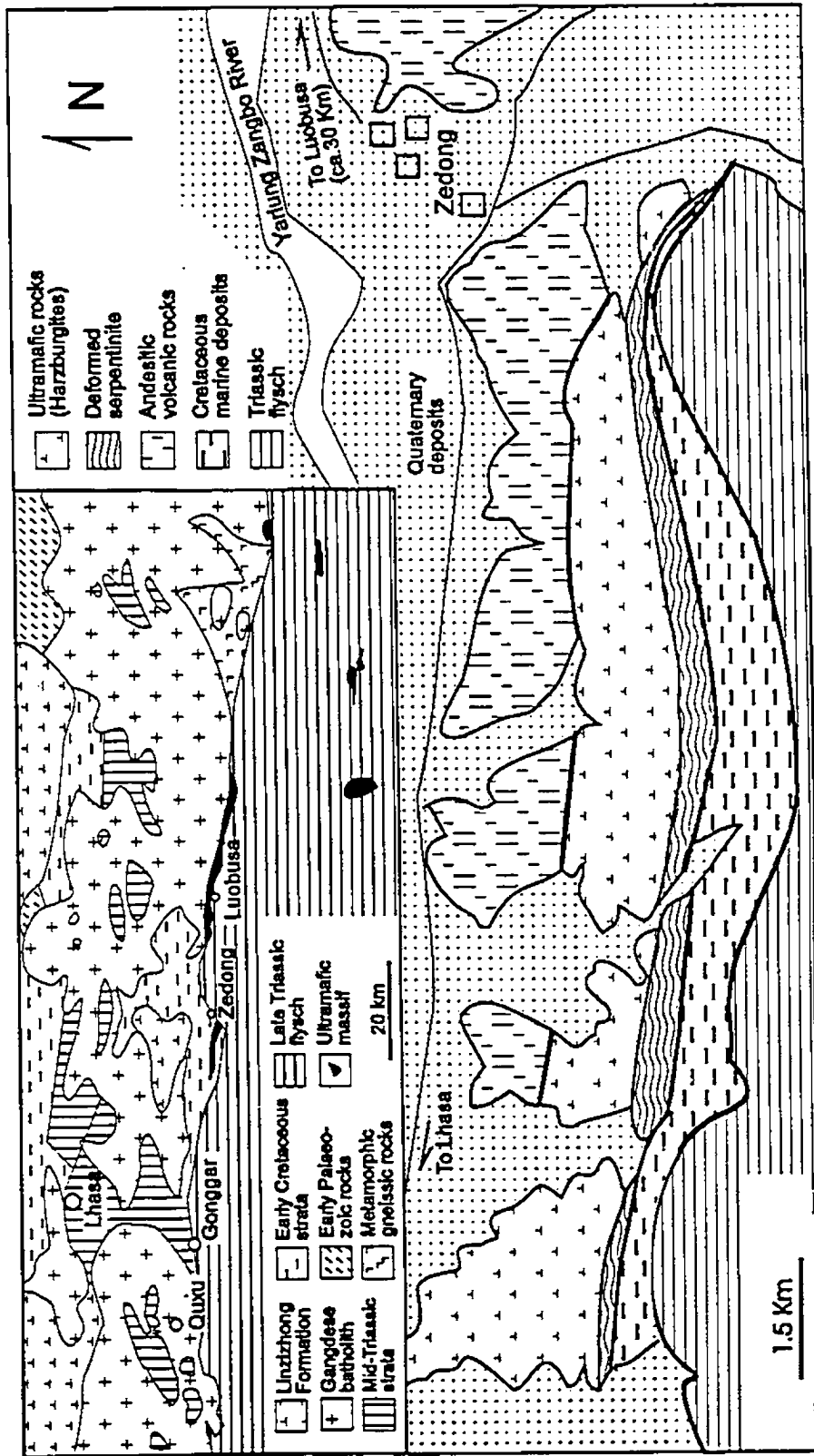


Figure 2-6. Geologic map of the Zedong ophiolitic massif. The left-upper insert is a geologic map of the Quxu-Nang Xian area of southeastern Tibet (modified from Wang Xibin, 1965).

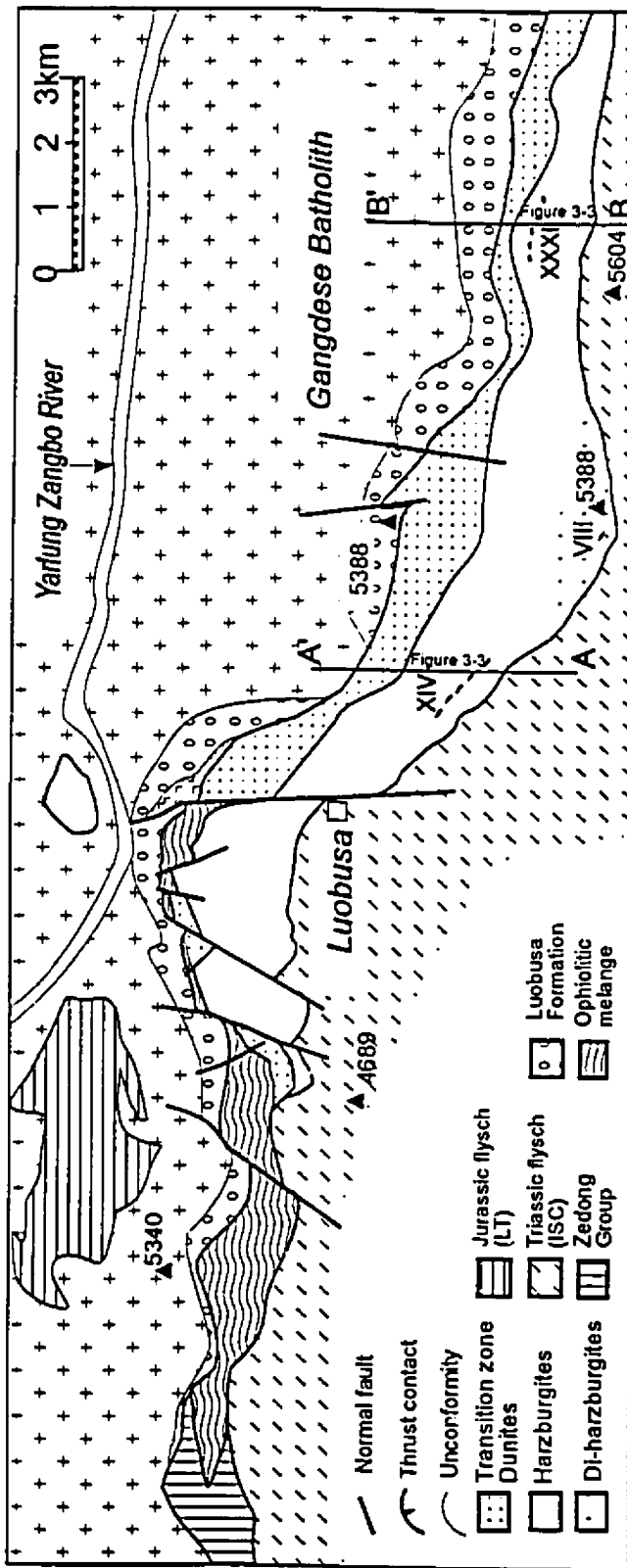


Figure 2-7. Geologic map of the Luobusa ophiolite (see location in Figure 1-6 and Figure 2-6), southern Tibet, showing Ore Groups XXXI, VIII and XIV. The major Ore Groups are near Luobusa (see Figure 3-2). See location in Figures 1-6 and 2-6.

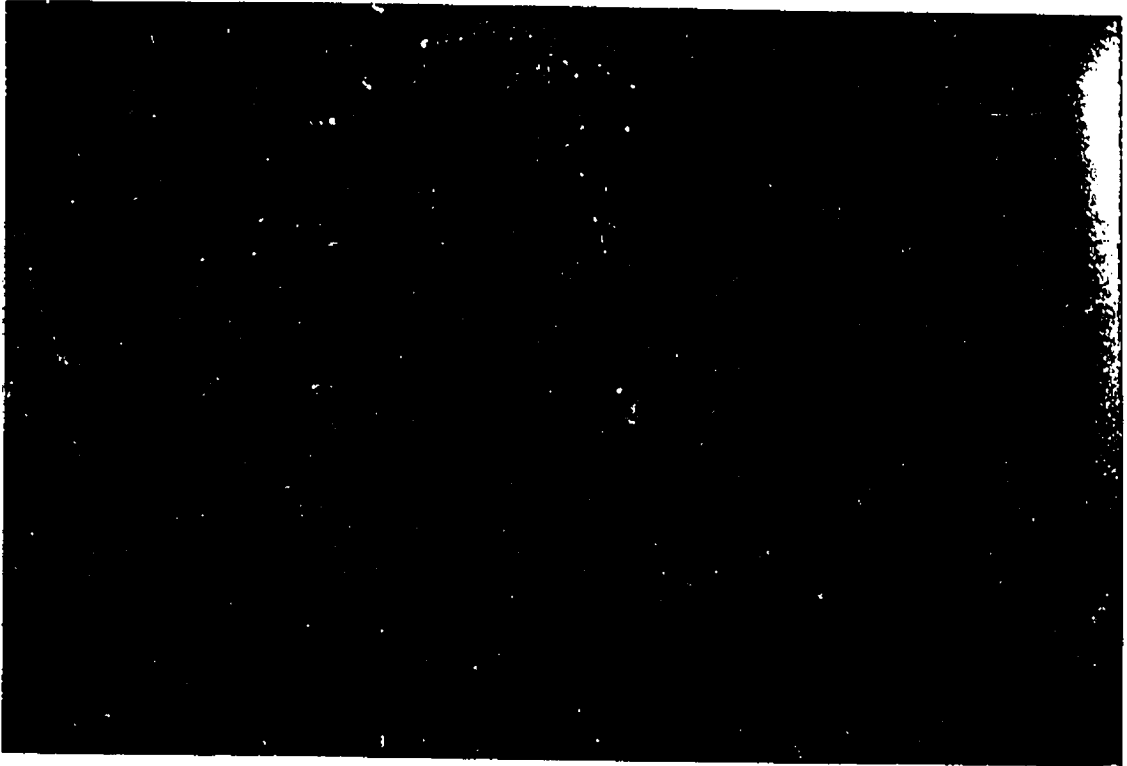


Figure 2-8. South verging fold in Triassic flysch about 20 km south of Zedong, about 30 m across.

Their sense of asymmetry and vergence indicate a southward obduction. However, some of the deformation can be related to northward Tertiary thrusting onto the ophiolite, because the Tertiary molasse deposits are also intensely deformed.

Late Jurassic and Early Cretaceous rocks northwest of the study area belong to the LT (Figures 2-6 and 2-7). These are dark shales, black slates and grey to yellow limestone, as well as intermediate volcanic rocks. The Gangdese Batholith in the area is mainly composed of granodiorites and granites.

The Luobusa Formation along the IYS extends for about 300 km from Nang Xian in the east to Quxu in the west. It consists of typical molasse deposits which are comparable to the Indus Molasse in the Ladakh area of India (Thakur and Misra, 1984). The Luobusa Formation can be divided into three lithologic units, from bottom to top: 1) conglomerates with bedded breccia intercalated with gravel-bearing sandstone (33.9-357 m thick); 2) purplish well-bedded gravel-bearing, medium- to coarse-grained limestone and dolomite, intercalated with siltstone, fine sandstone, conglomerate and lenticular shale (272-428 m thick); 3) polygenetic conglomerate intercalated with thin-bedded sandstone, siltstone and gravel-bearing sandstone (272-428 m thick). These units vary in thickness and lithology along strike.

The Luobusa Formation unconformably overlies the Gangdese Batholith, and the basal unit has abundant clasts of granite and ophiolitic rocks. There are also abundant fossils of Oligocene to Miocene age.

The Luobusa Formation is little deformed. However, strongly sheared deposits occur near Ore Group XXXI at the eastern end of the Luobusa ophiolite, where transition zone dunite is thrust over this unit (Figure 2-9). There, the sedimentary rocks have been mylonitized (Figure 2-10).

These molasse deposits were formed on the north of the fore-arc basin of the convergent margin of Asia, south of the Gangdese Batholith, and post-date the collision of the Eurasian and Indian plates.

As discussed earlier, the Gangdese Batholith and calc-alkaline volcanic rocks of the Linzizhong Formation in the LT suggest a north-dipping subduction zone beneath southern Asia prior to 40 Ma. Field observations, however, show that the IYS is south-dipping in Luobusa, and that the ophiolite overthrusts the Luobusa Formation (see below), suggesting that the suture was deformed subsequent to closure of the ocean that once separated India and Asia. This south-dipping contact represents a Neogene north-directed thrust. Observations by Yin et al. (1994) in the area from Zedong to Xigaze indicate that the present IYS is not the trace of a single fault contact marking the locus of oceanic closure between India and Asia. They suggest that the suture is a composite structural feature resulting from multiphase deformation including both dip-slip and strike-slip faulting since the late Oligocene.

2.3.2. The Luobusa ophiolite

Mantle peridotites, transition zone dunites and ophiolitic melange are present in the Luobusa ophiolite (Figure 2-7). All sequences are crosscut by

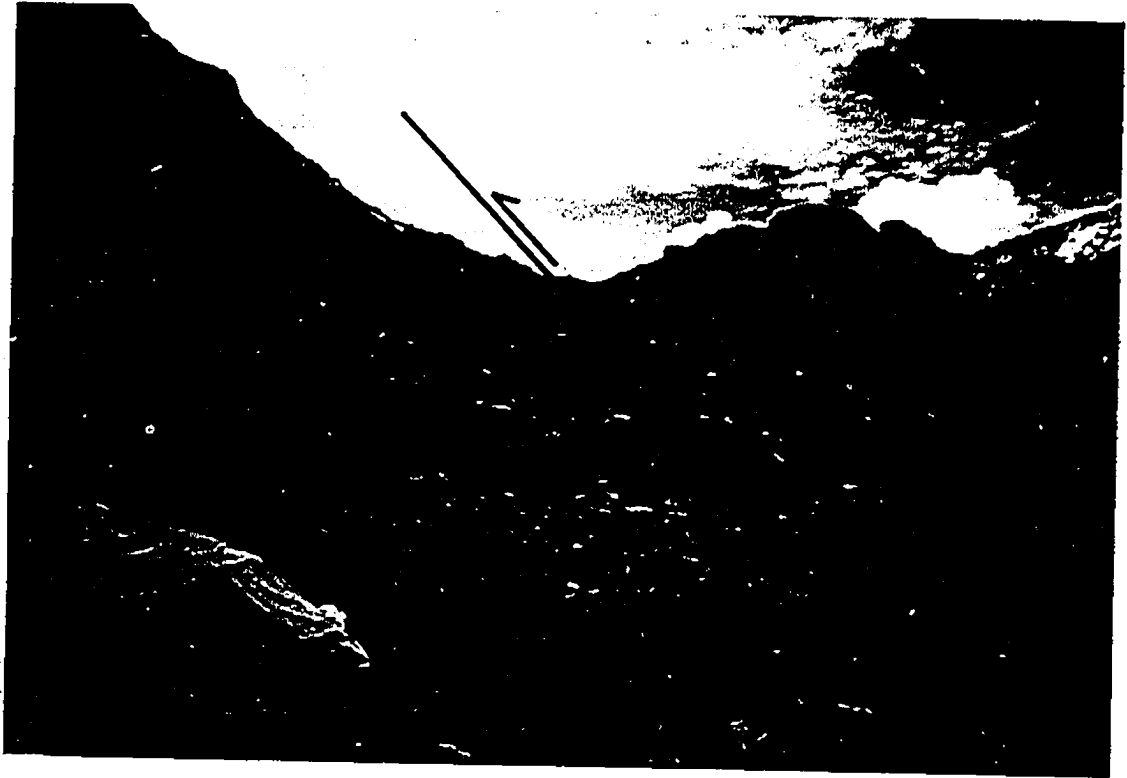


Figure 2-9. Contact between the Luobusa ophiolite (south) and the Luobusa Formation (north), eastern part of the ophiolite.

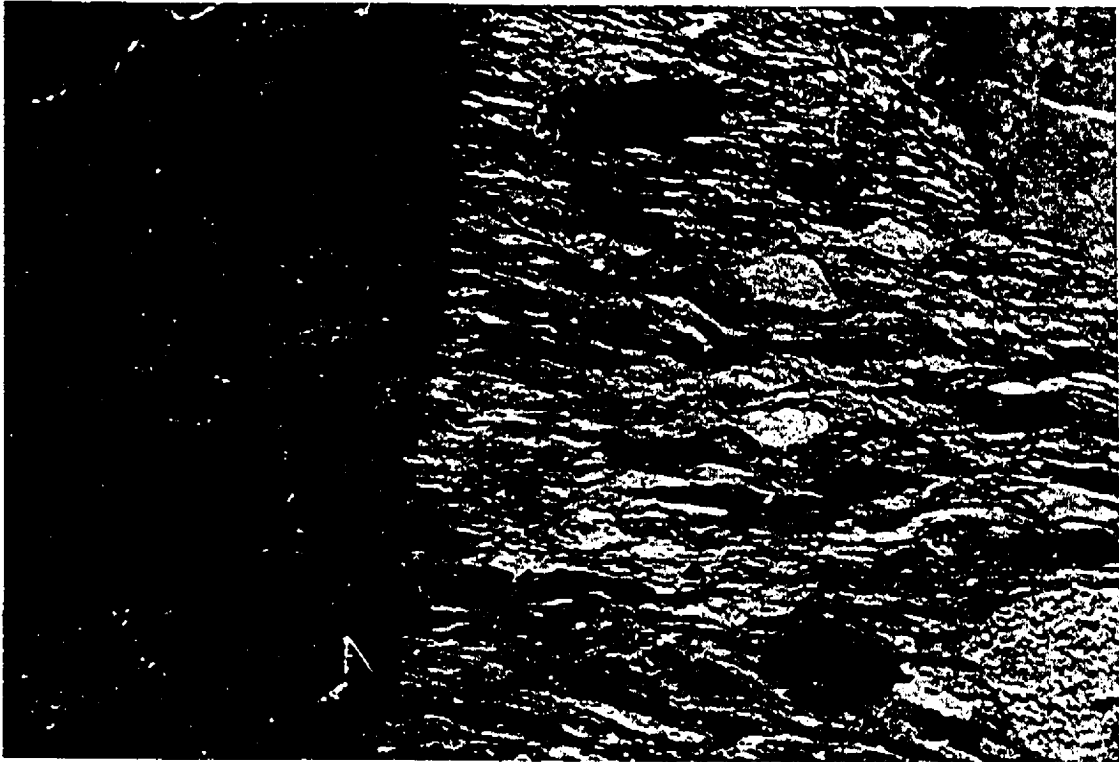


Figure 2-10. Sheared molasse deposits of the Luobusa Formation; note the diversity of clasts in the conglomerate and boudinage structures; same location as Figure 2-9.

north-south trending normal faults. Cumulate rocks, basaltic lavas and cherts occur as blocks in the melange zone. The entire sequence is thrust over either the Luobusa Formation (Figure 2-9) or the Gangdese Batholith to the north (Figure 2-7) and is in turn overthrust by Triassic flysch to the south (Figure 2-11). The boundaries between the major units generally dip southward, suggesting that the section is possibly overturned (Figure 2-12) or that each sequence is an individual thrust slice. The northern thrust contact with the Luobusa Formation dips towards the south at a lower angle than the southern contact (Figure 2-12).

The Luobusa ultramafic massif extends for 42 km in an E-W direction, and the mantle sequence which hosts the chromite deposits is well-preserved. There are numerous gabbro dykes, several hundred metres long by 10-20 m wide, in the sequence but pyroxenite dykes are rare. The gabbro dykes are undeformed and cross-cut the tectonite fabric in the host rocks. Their origin is not yet clear, because similar gabbro dykes are also observed in the Triassic rocks.

Dunite, locally grading into wehrlite, is the most abundant rock type in the transition zone. It consists of coarse-grained Ol, minor Cpx and traces of chromite. The chromite occurs chiefly as euhedral inclusions in Ol grains, but a few thin bands or layers of disseminated chromite are also present. These bands or layers are believed to have formed by precipitation of chromite in a crustal magma chamber (c.f., Malpas, 1978). Clinopyroxene forms small,

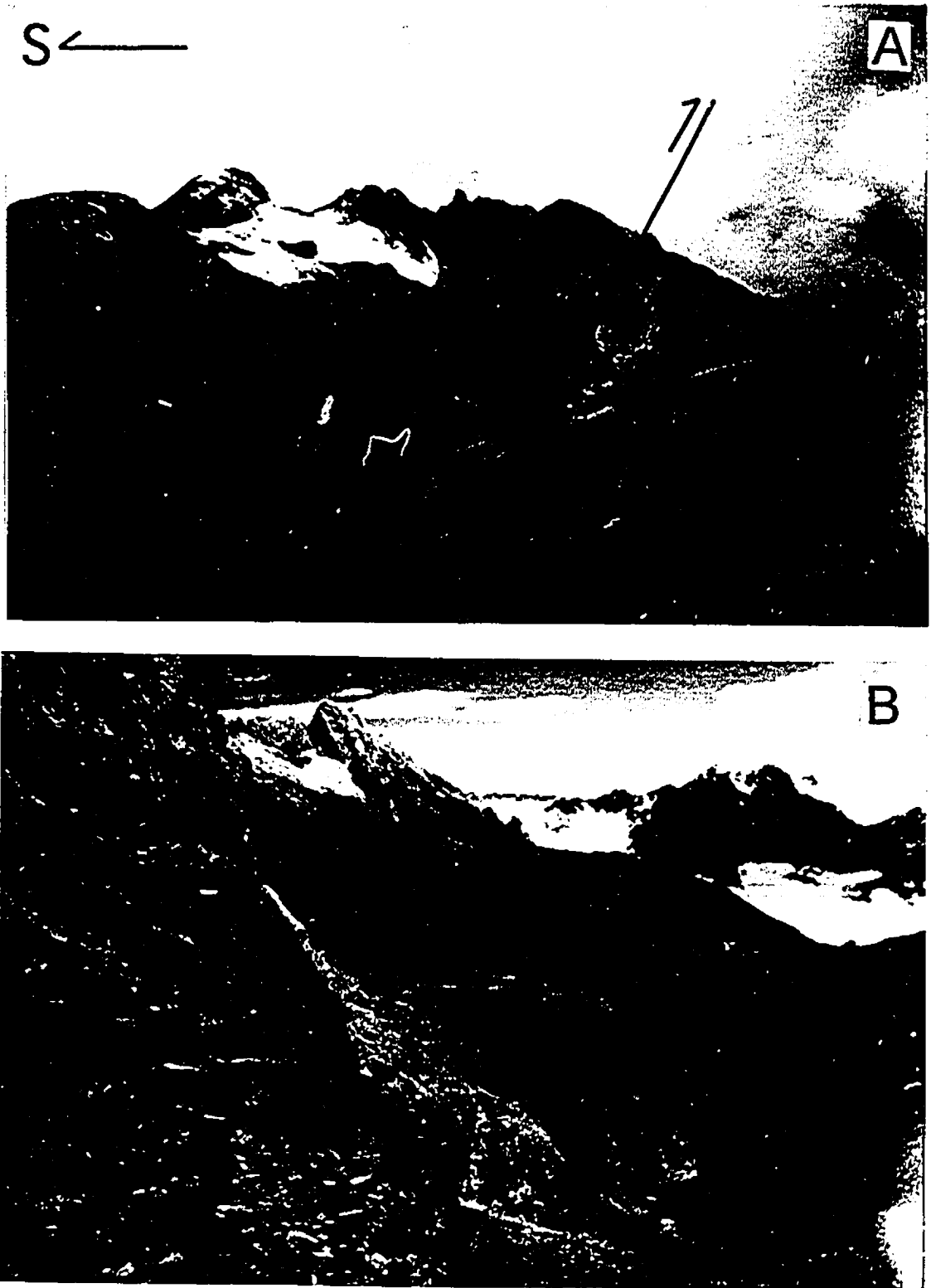


Figure 2-11. Contact between the Luobusa ophiolite (north) and Triassic flysch (south). Picture A faces west, and picture B faces northeast.

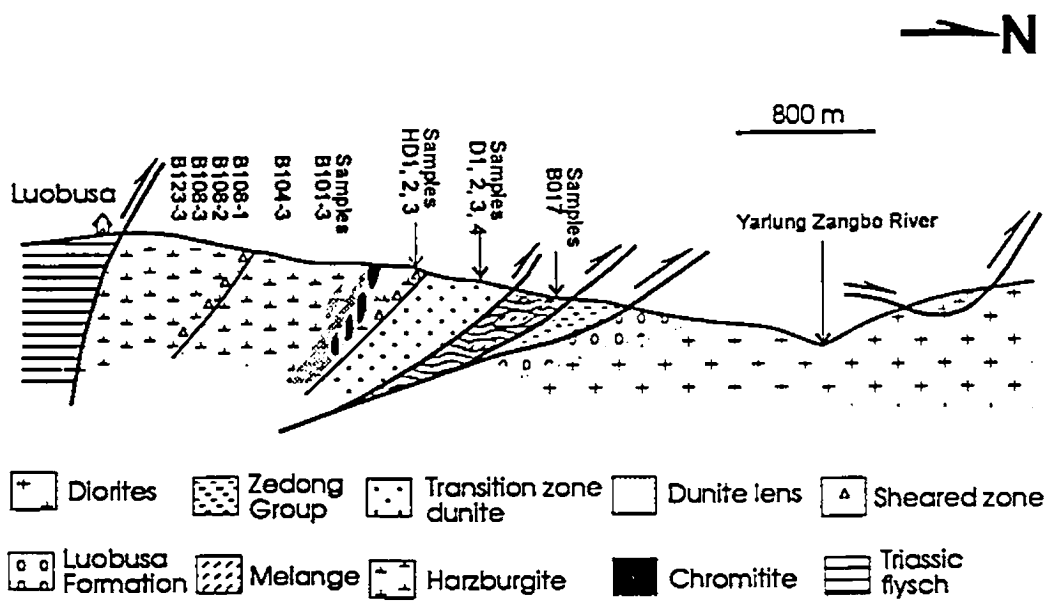


Figure 2-12. Cross section of the Luobusa ophiolite drawn from Figure 2-7.



Figure 2-13. Impregnation texture of transition zone dunite. Clinopyroxenes are interstitial in Ol. Note small, euhedral chromites (black) in Ol. 94L16,

anhedral grains between the larger Ol crystals which have equant shapes (Figure 2-13). This type of texture has been attributed to impregnation (Nicolas, 1989). Although the Ol grains show deformation features such as kink-bands and undulatory extinction, similar to those in the underlying harzburgite, low-Fo Ol and whole-rock chemistry point to major differences in composition between the transition zone and mantle sequence.

Tectonically underlying the transition sequence is a melange zone containing lenses of cumulate rock including wehrlite, pyroxenite, layered and homogenous gabbro and pillow lavas in a strongly serpentized, ultramafic matrix (Figure 2-14A). Individual lithologies are irregularly distributed and all the rocks are highly deformed. There are meta-gabbros that are now amphibolites (Figure 2-14B), although most gabbros have original igneous textures and mineralogies. This zone is several hundred metres wide and is discontinuously distributed along the northern boundary of the ophiolite (Figure 2-7).

The volcanic rocks in the melange zone are pillow lavas (Figure 2-15). They have typically undergone greenschist-facies metamorphism, but some are now amphibolites with some relict volcanic textures. Associated volcanoclastic rocks and cherts are known as the Zedong Group (Figures 2-6 and 2-7). Near Zedong, andesitic rocks are in tectonic contact with ultramafic rocks (Figure 2-6). This group might be part of the ophiolite, because of its close association with the ophiolitic ultramafic rocks. MORB tholeiites, however, have not been identified in the area. Their absence might be due to tectonic removal, such as



Figure 2-14. Sheared rocks from the melange zone in the Luobusa ophiolite:
A. Field photo of serpentinite, north of the Geology Camp (see Figure 2-7);
B. Photomicrograph of a foliated and folded amphibolite, B017.

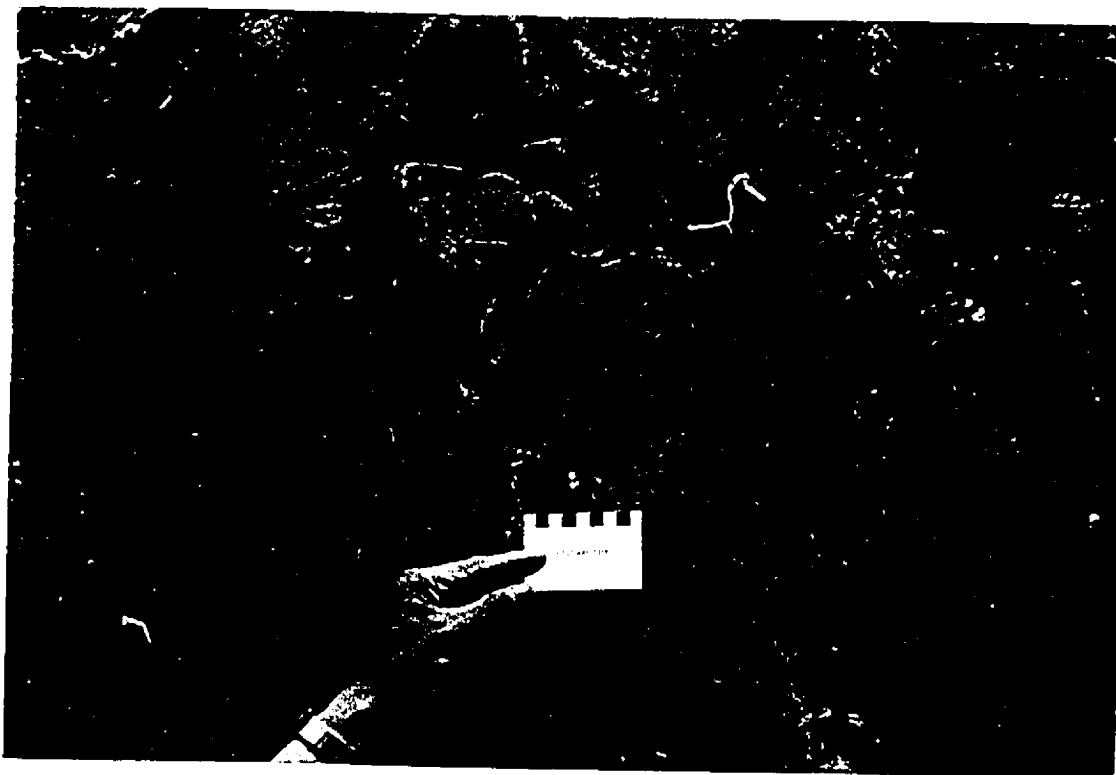


Figure 2-15. Field photo of pillow lavas in the melange zone, north of the Geology Camp (see Figure 2-7).

beneath the Gangdese Batholith.

2.4. Summary

The Tibetan Plateau consists of several terranes which were accreted successively to the southern margin of Eurasia. These terranes are separated by suture zones. The Luobusa ophiolite lies in the IYS in southern Tibet. This suture zone was formed during the collision between Eurasia and India around 41 Ma. The ophiolite is tectonically bounded by Triassic flysch on the south and by the molasse deposits of the Tertiary Luobusa Formation and the Gangdese Batholith on the north. The ophiolite is composed of a mantle sequence, a transition zone and an ophiolitic melange. The boundaries between the major units generally dip southward, possibly indicating that the section is overturned or that each unit is an individual thrust slice. The transition zone is mainly composed of dunites with abundant wehrlites. Wehrlites, pyroxenites, gabbros, pillow lavas and cherts in the melange zone are set in a strongly serpentized, ultramafic matrix.

Chapter 3: FIELD RELATIONS AND PETROGRAPHY

3.1. Nomenclature

Although most samples studied are composed totally of primary minerals, chromitites and adjacent host dunites have been at least partly serpentinized and contain fractures filled by antigorite, lizardite, and chrysotile. Samples with little, if any, alteration were selected for modal analyses by point counting phases (Ol, Cpx, Opx and chromite) [Table 3-2].

The classification of ultramafic rocks is based on the proportions of Cpx-Opx-Ol (Figure 3-1) [Streckeisen, 1973]. Dunite consists of Ol with less than 10 modal% pyroxene. Harzburgite is composed of Ol and Opx with less than 5 modal% Cpx (Di), whereas Di-harzburgite (Di-bearing harzburgite) contains 5-10 modal% Di. Lherzolites have variable proportions of Ol and pyroxene, but are characterized by more than 10 modal% Di (Figure 3-1). Locations of samples used for the descriptions are shown in Table 3-1, Figure 2-12, Figure 3-2 and Figure 3-3.

Textural terminology used for mantle peridotites is from Nicolas and Poirier (1976) and Harte (1977). Textural types of chromitites are from Thayer (1964, 1969), Leblanc (1980) and Cassard et al. (1981).

Table 3-1. Locations of samples used for petrographic description and chemical analyses. For locations see maps on pages 35 and 54.

| Samples | Rock types | Location |
|----------------------------|---|-----------------------|
| 8-1, -2, -3, -4, -5, -6 | Chromitite | Ore Group VIII |
| 94L16 | Dunite (Transition zone) | North of Ore Group IV |
| 94L22 | Pyroxenite (Transition zone) | North of Ore Group IV |
| 11, 2, 3, 4, 5, 6, 7, 8, 9 | Chromitite | Ore Group I |
| XIV-5, -7, -8 | Chromitite | Ore Group XIV |
| B101-3, 104-3, 108-1 | Harzburgite | North of Luobusa |
| B108-2, 108-3, 123-3 | Harzburgite | North of Luobusa |
| B017 | Amphibolite (Melange zone) | North of Geology camp |
| H1, 2, 3, 11, 14 | Harzburgite | Ore Group XIV |
| HZK395, 395-1 | Harzburgite | Ore Group XIV |
| HD1, 2, 3 | Sheared harzburgite | North of Ore Group I |
| L6, 8, 9 | Harzburgite | Ore Group I |
| L10 | Harzburgite | Ore Group II |
| L12 | Harzburgite | Ore Group V |
| L13 | Dunite | Ore Group V |
| L14 | Dunite | Ore Group XI |
| L15, 16 | Dunite | Ore Group X |
| L17 | Harzburgite | Ore Group XIV |
| L18 | Dunite | Ore Group XXXI |
| L19 | Harzburgite | Ore Group XXXI |
| L20 | Di-harzburgite | Ore Group X |
| L22 | Harzburgite | Ore Group VI |
| L23 | Chromitite | Ore Group XIV |
| L24 | Chromitite | Ore Group VI |
| L25 | Chromitite | Ore Group V |
| L26, 27 | Chromitite | Ore Group XI |
| L28, 29 | Chromitite | Ore Group XXXI |
| LH1-1, 2, 3, 4, 5, 6, 8 | Di-harzburgite | Ore Group XXXI |
| LH1-2 | Dunite to Di-harzburgite | Ore Group XXXI |
| LH7 | Dunite dyke | Ore Group XXXI |
| LH9, 10 | Dunite with Di-harzburgite | Ore Group XXXI |
| S1, 2, 3, 5, 6, 7, 8 | Di-harzburgite | Ore Group XXXI |
| S4 | Chromitite bands with dunite transition | Ore Group XXXI |
| S4-1 | Dunite to harzburgite | Ore Group XXXI |
| S9, 10, 11 | Harzburgite | Ore Group XXXI |
| XL1, 5 | Chromitite | Ore Group III |
| ZHK1, 2, 3, 4, 5 | Nodular chromitite | Ore Group XXXI |
| ZHK6-1, 6-1 | Dunite with massive chromitite | Ore Group XXXI |
| ZHK7, 8, 9 | Dunite | Ore Group XXXI |
| ZHK10, 11 | Harzburgite | Ore Group XXXI |
| ZHLs | Chromitite to dunite to Di-harzburgite | Ore Group VIII |

Table 3-2. Modal analyses of the mantle peridotites, dunites and chromitites in Luobusa

| Sample | Chromite | Cpx | Ol | Opx | Other | Counts |
|-----------------------|----------|------|------|------|-------|--------|
| Di-harzburgite | | | | | | |
| H14 | 0.7 | 11.8 | 58.6 | 27.2 | 1.7 | 2240 |
| L6 | 1.6 | 10.5 | 60.3 | 26.7 | 0.8 | 2300 |
| LH4 | 1.1 | 8.0 | 60.0 | 29.9 | 1.0 | 3100 |
| S7 | 1.2 | 6.9 | 61.7 | 28.8 | 1.3 | 2240 |
| S8 | 0.9 | 10.3 | 59.3 | 28.4 | 0.9 | 1280 |
| S6 | 1.0 | 8.6 | 65.9 | 23.6 | 0.9 | 1280 |
| LH3 | 0.7 | 7.2 | 66.7 | 24.1 | 1.3 | 1280 |
| L17 | 0.9 | 10.4 | 58.8 | 28.1 | 1.8 | 2300 |
| S4-4 | 0.7 | 9.2 | 70.9 | 17.7 | 1.5 | 2700 |
| S4-1 | 0.4 | 9.4 | 74.3 | 14.5 | 1.3 | 2700 |
| S4-3 | 0.5 | 9.0 | 67.8 | 20.7 | 2.0 | 1900 |
| L10 | 0.8 | 5.3 | 74.6 | 18.6 | 0.7 | 1600 |
| S3 | 0.7 | 9.9 | 65.4 | 23.1 | 0.9 | 1900 |
| ZHK11 | 0.5 | 7.8 | 66.9 | 22.6 | 2.2 | 3100 |
| LH8 | 0.9 | 11.6 | 60.8 | 25.5 | 1.1 | 1920 |
| S5 | 1.0 | 5.9 | 72.4 | 19.5 | 1.1 | 1920 |
| LH6 | 2.2 | 6.5 | 55.7 | 34.6 | 1.0 | 2300 |
| Harzburgite | | | | | | |
| H2 | 0.6 | 3.1 | 80.5 | 15.0 | 0.8 | 1800 |
| H1 | 0.4 | 2.4 | 72.7 | 23.4 | 1.1 | 1600 |
| ZHK10 | 0.7 | 1.8 | 75.2 | 21.1 | 1.3 | 1900 |
| L19 | 0.4 | 3.6 | 62.6 | 31.6 | 1.7 | 2700 |
| H3 | 0.7 | 2.3 | 77.5 | 18.4 | 1.1 | 2300 |
| LH1-2 | 0.8 | 1.6 | 79.4 | 16.6 | 1.7 | 2700 |
| L6a | 0.5 | 4.3 | 65.4 | 28.3 | 1.6 | 4000 |
| LHs | 0.7 | 2.8 | 75.4 | 20.2 | 0.9 | 2700 |
| L22 | 0.2 | 2.4 | 71.0 | 25.0 | 1.4 | 1900 |
| LH3 | 0.9 | 4.8 | 62.3 | 30.9 | 1.1 | 1900 |
| LH7 | 1.1 | 0.0 | 86.0 | 11.0 | 1.9 | 2300 |
| S4-0 | 0.6 | 3.8 | 80.2 | 14.6 | 0.9 | 1900 |
| L9 | 0.8 | 1.0 | 69.5 | 27.1 | 1.6 | 1600 |
| L8 | 0.7 | 1.2 | 70.8 | 25.4 | 1.9 | 1900 |
| Dunite | | | | | | |
| L18 | 0.9 | 0.6 | 95.1 | 3.0 | 0.4 | 1900 |
| ZHK9 | 1.0 | 0.4 | 96.1 | 2.1 | 0.4 | 1900 |
| ZHK8 | 0.9 | 0.7 | 96.7 | 1.0 | 0.7 | 3100 |
| Chromitite | | | | | | |
| L26 | 25.7 | 0.1 | 66.3 | 6.8 | 1.1 | 1900 |
| L25 | 56.7 | 1.5 | 21.7 | 18.4 | 1.7 | 2300 |
| L27 | 13.6 | 0.1 | 72.2 | 12.5 | 1.6 | 1900 |
| I6 | 63.2 | 0.0 | 20.3 | 15.2 | 1.3 | 2300 |
| 94L12 | 33.7 | 0.1 | 63.2 | 2.6 | 0.3 | 2700 |
| L28 | 65.2 | 0.0 | 29.1 | 2.2 | 3.6 | 1200 |
| VIII-6 | 75.8 | 5.1 | 4.7 | 12.9 | 1.4 | 1600 |

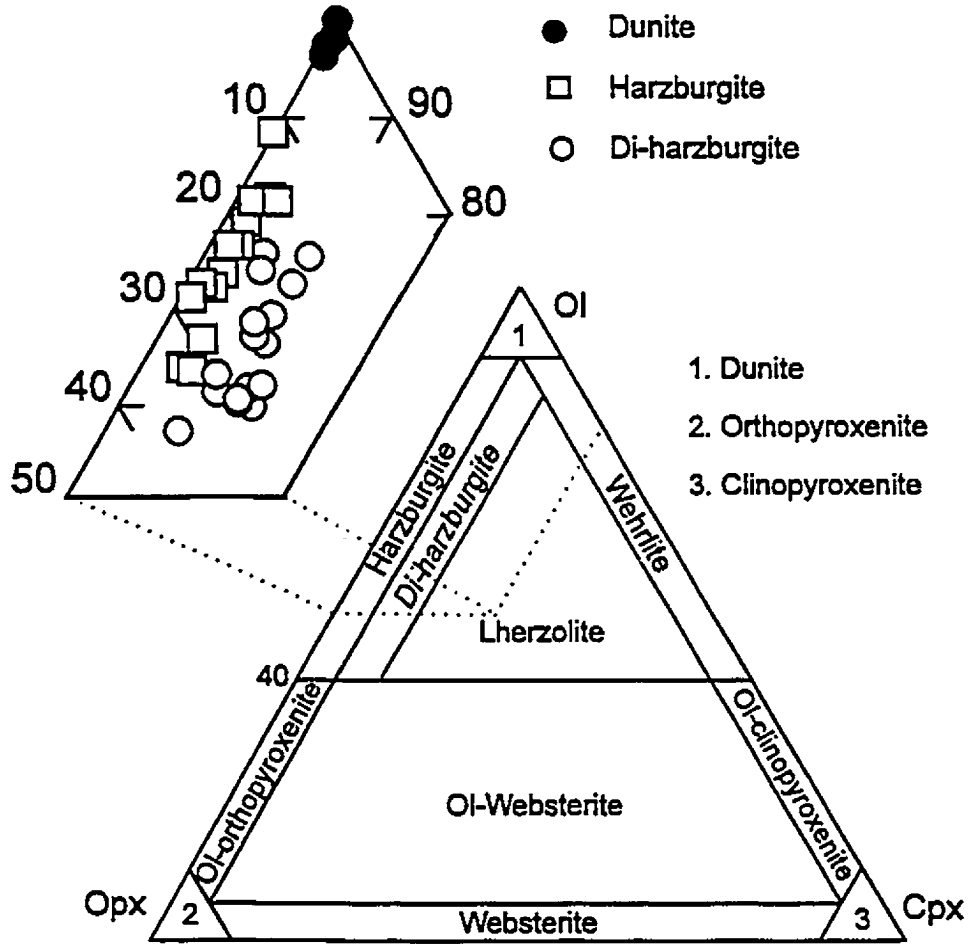


Figure 3-1. Plots of the mantle peridotites and dunites in Luobusa on the diagram "Opx-Cpx-Ol"; classification of ultramafic rocks based on Streckeisen (1973).

3.2. Rock types and their distribution

In Luobusa, harzburgites are composed of 62-86 modal% Ol, 11-32% Opx, 1-5% Cpx and 0.2-1.1% chromite. Most Di-harzburgites have 5.9 to 9.9 modal% Cpx, although a few samples have higher Cpx contents up to 12 modal% (Table 3-2). The mantle sequence also has abundant pods and lenses of dunite and chromitite. Dunites have 0.3-1.0% chromite with small amounts of pyroxene (1.0-3.0% Opx, 0.0-0.7% Cpx), whereas chromitites contain variable amounts of Ol and Opx with very minor Cpx (0.0-1.5%).

The most abundant rock type is harzburgite (Figure 3-2). Di-harzburgite occurs along the southernmost edge of the ophiolite where the mantle section is thickest (about 3 km) and it is believed to represent the deepest mantle exposed (Figure 2-7). Di-harzburgite also occur locally elsewhere in the massif. Dunites are abundant throughout the entire rock body: dunite dykes crosscut Di-harzburgites in the southern portion of the massif and dunite lenses are associated with chromitites in harzburgites (Figure 3-2).

Most chromitite bodies in Luobusa are hosted in harzburgite and occur in a narrow band, generally 500-600 m stratigraphically below the boundary with the transition zone dunite (Figures 3-2, 3-3). This band roughly coincides with the zone in which the mantle tectonite fabric passes from subvertical to subhorizontal (Figure 3-4). It varies from 200-600m wide and is characterized by many dunites. In the band, chromitite pods are arranged in a subparallel fashion with their long axes oriented 120°-160° in the vicinity of Luobusa village and 35°

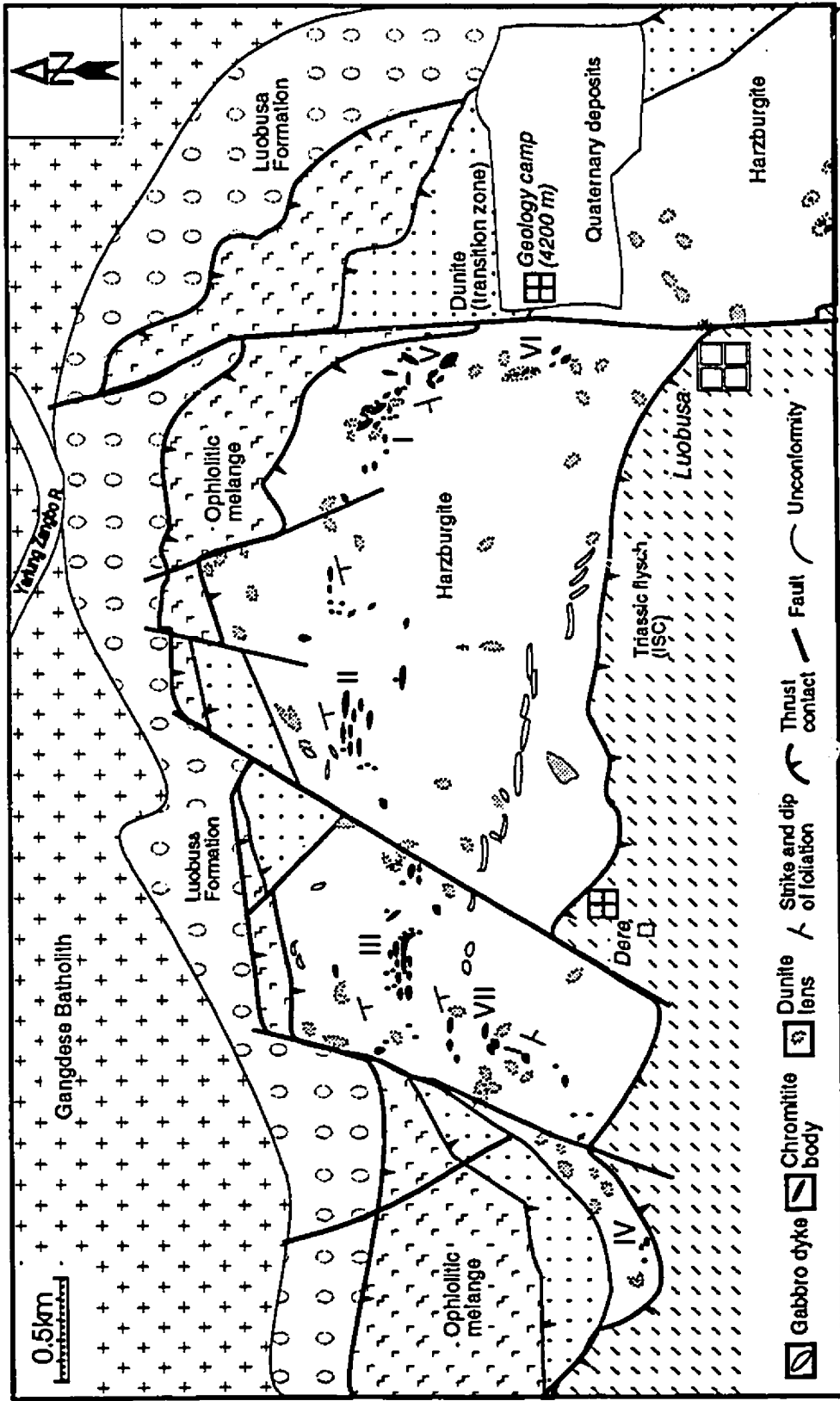


Figure 3-2. Geologic map of the middle part of the Luobusa ophiolite, showing the distribution of podiform chromitites and dunitic lenses (modified from GTTB, 1978, 1981; Bai et al., 1993; Li Zijin, 1993; Zhou and Robinson, 1994). Roman numerals give locations of Ore Group I -VII.

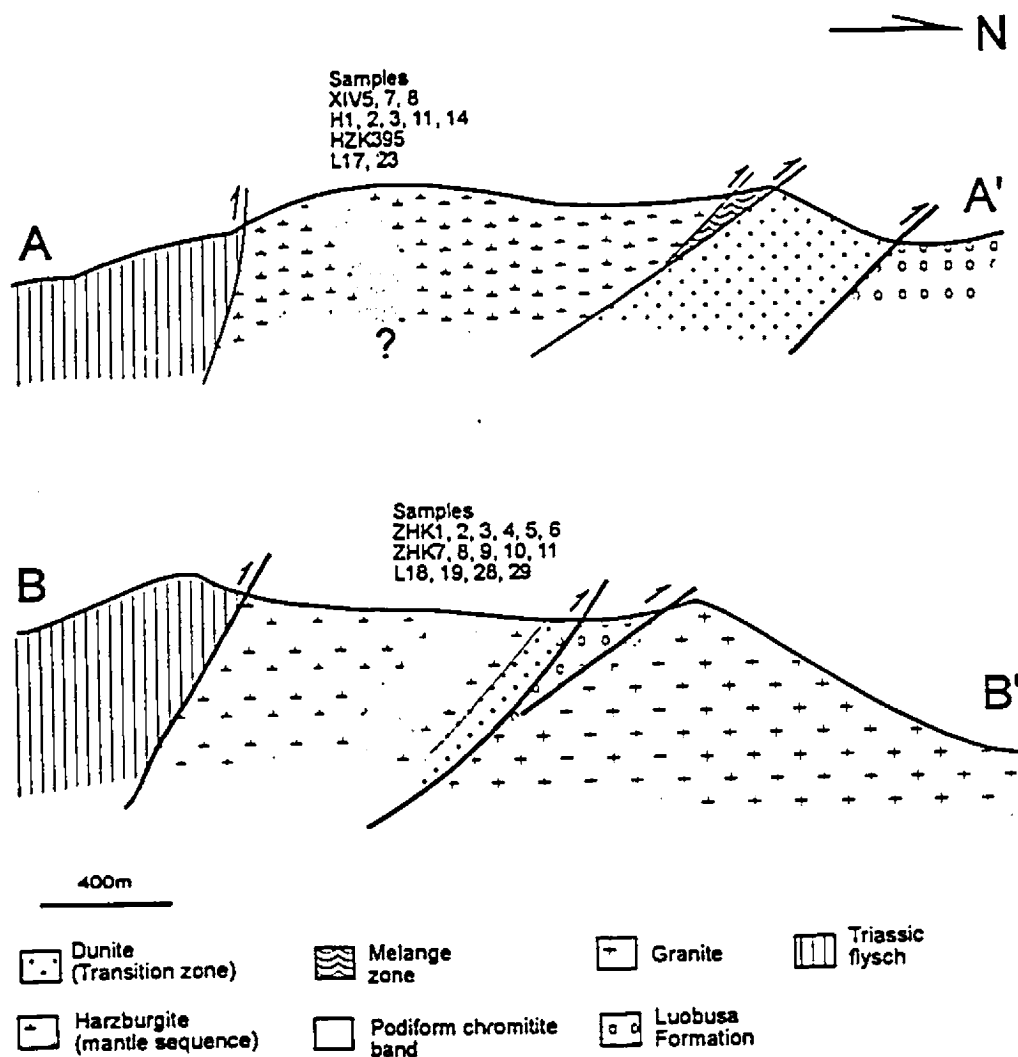


Figure 3-3. Cross sections showing the distribution of chromitites in the mantle peridotites of the Luobusa ophiolite drawn from Figure 2-7.

- 55° east of Luobusa. The change in direction results from N-S normal faulting (Figure 3-2). The chromitite pods and lenses occur in clusters which have been identified as ore groups designated by Roman numerals for mining purposes (see Figures 2-7 and 3-2).

Podiform chromitites in Luobusa are typically lens-shaped although many occur as tabular or pencil-like bodies (Figures 3-4 and 3-5). Most bodies are concordant or sub-concordant to the foliation in the surrounding peridotite and exhibit structures and fabrics interpreted to be the result of solid-state flow and recrystallization at relatively high temperatures (cf. Cassard et al., 1981). Typical chromitite bodies range from 20-250 m long, 10-100 m wide and 0.5-5 m thick. The lenticular bodies of chromitite have an average aspect ratio of 20:8:1. The largest body in Luobusa has yielded 0.6 million tons of ore (Li Zijin et al., 1993).

Most of the chromitites are enclosed in dunite pods or have dunite envelopes several centimetres to several metres thick. Massive chromitites typically have sharp contacts with the enclosing dunite whereas disseminated bodies grade outward into the surrounding rock, in some cases passing into interlayered chromitite and dunite. The chromitite and dunite layers normally have sharp contacts and the chromitite bodies may have branches that intrude the dunitites. The dunitites grade outward into the surrounding harzburgite or Di-harzburgite with increasing modal proportions of pyroxene (Figure 3-6). Although their thickness does not correlate closely with the size of the chromitite body, dunite envelopes are generally thicker around large ore bodies.

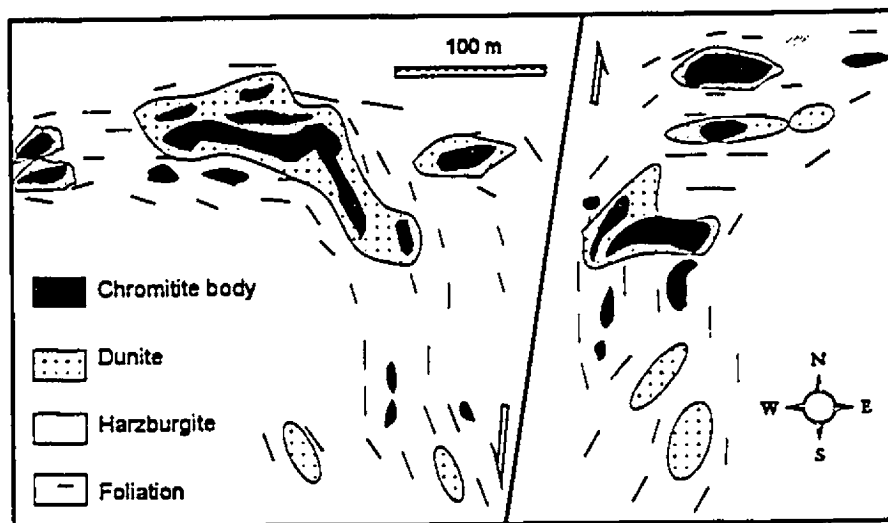


Figure 3-4. Distribution and shapes of chromitite bodies of Ore Group III (see Figure 3-2). Note the close association of dunites and chromitites and the sub-concordant relationship of both with foliation in harzburgite.

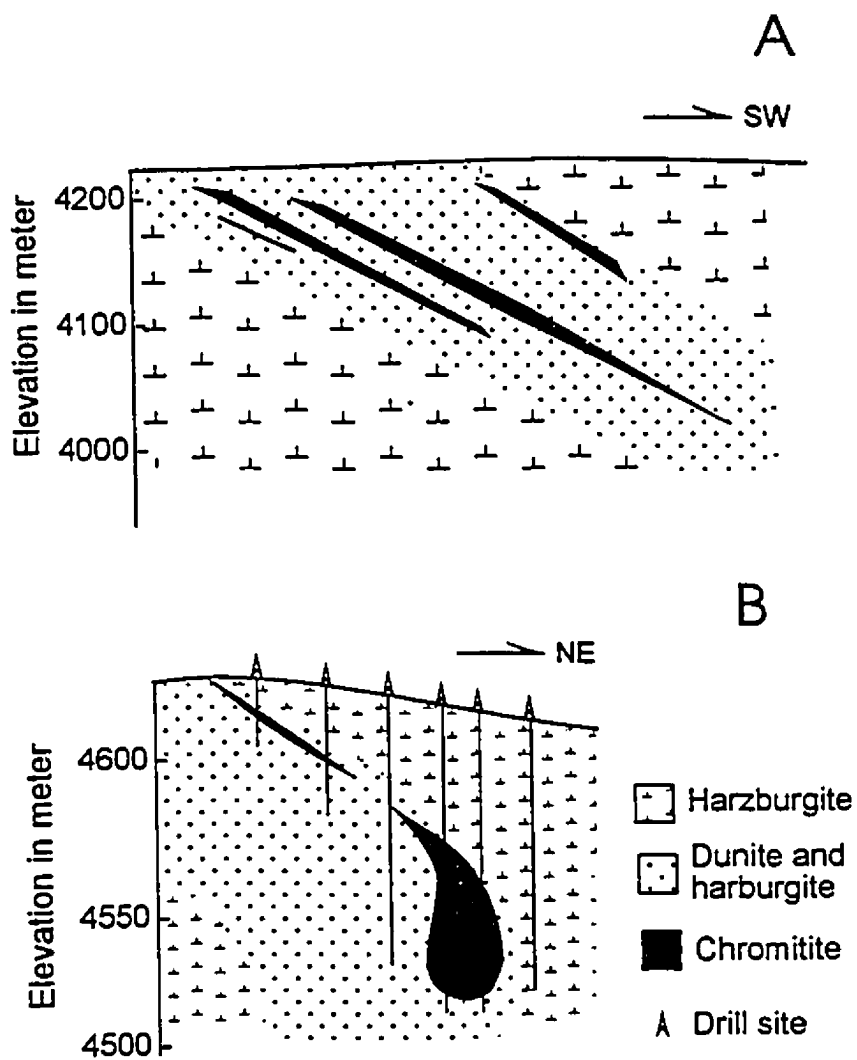


Figure 3-5. Subsurface podiform chromitite bodies:
 A. Tabular bodies in Ore Group II;
 B. Tabular and podiform bodies in Ore Group XIV.

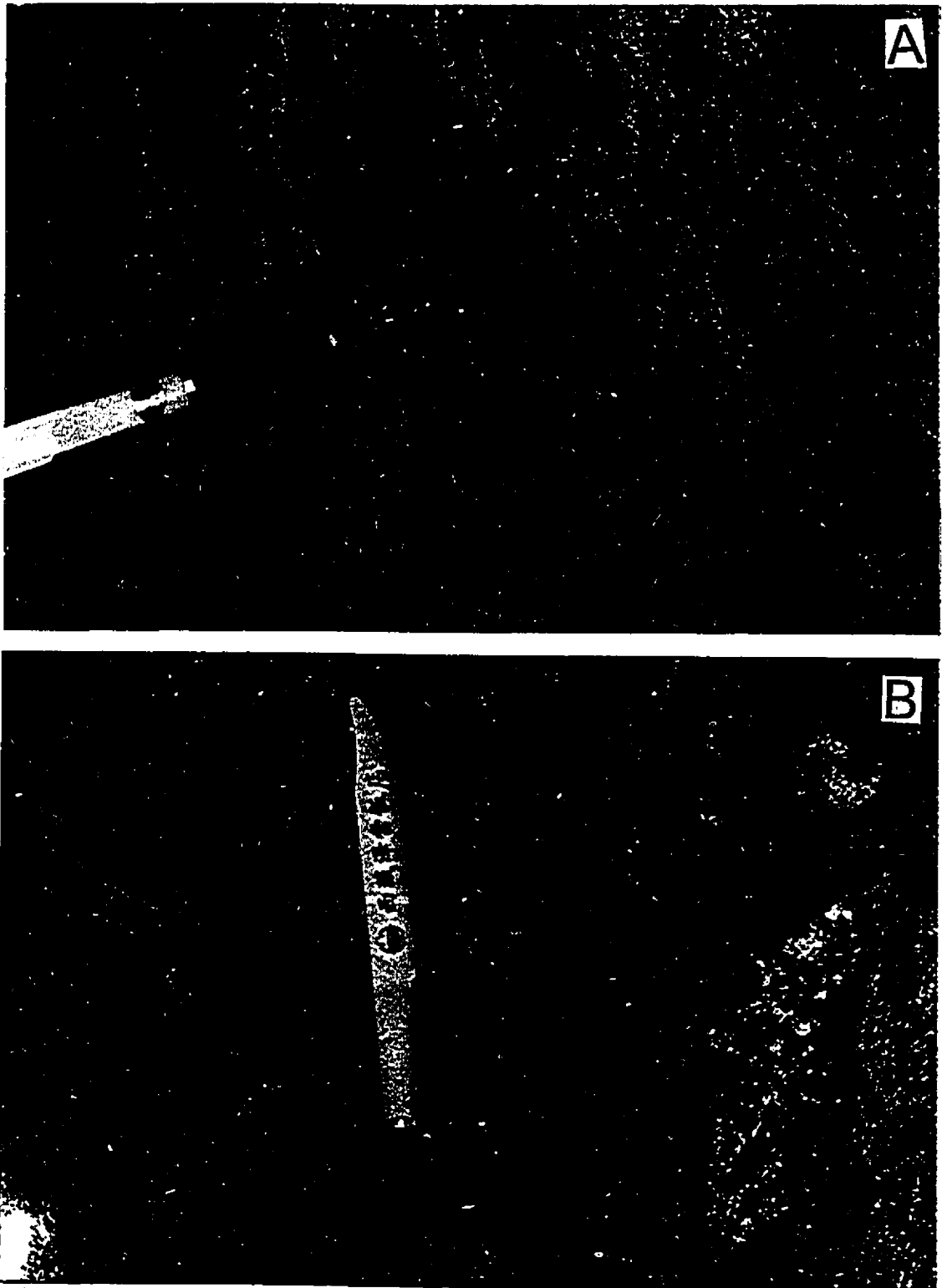


Figure 3-6. Field photos of podiform chromitite bodies: A. A transition zone from chromitite to dunite to harzburgite to Di-harzburgite; Ore Group VIII. B. A massive chromitite body and chromite-rich layers in dunite; Ore Group VIII.

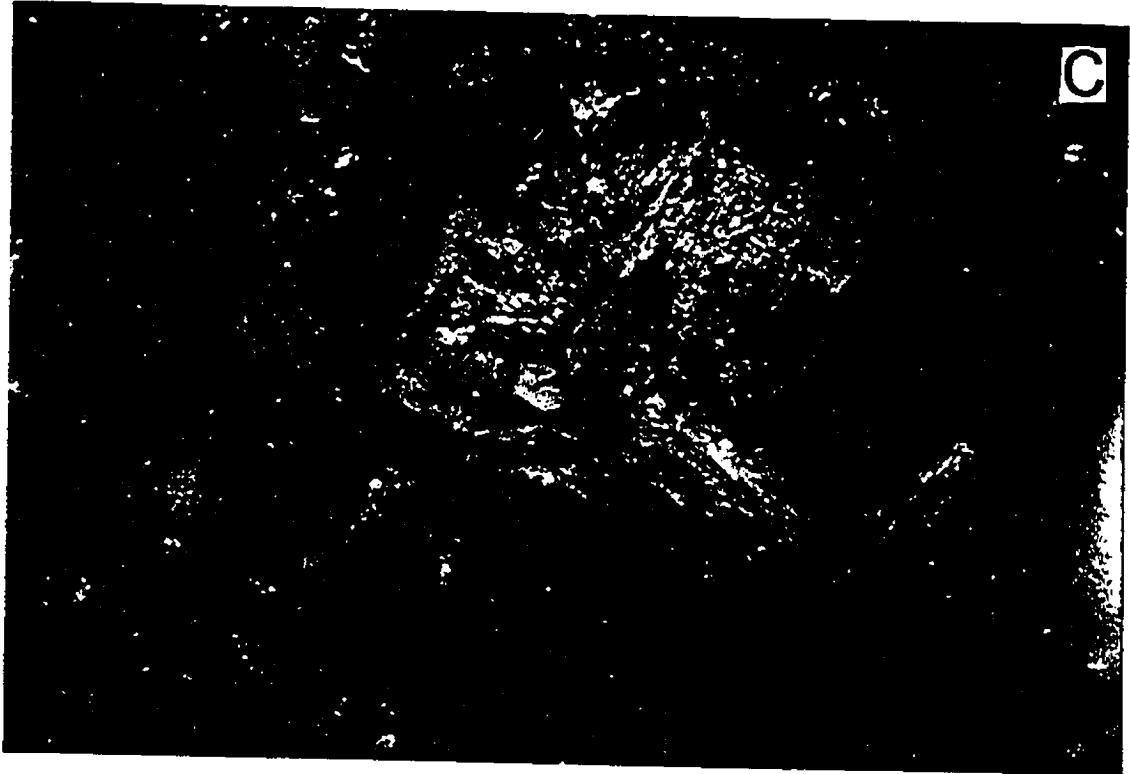


Figure 3-6. C. A sharp boundary between a chromitite body and a dunite envelope; Ore Group VII. D. Chromitite bands in dunite; Ore Group IV.



Figure 3-6. E. A chromitite band and its branches in dunite; Ore Group XIV.

3.3. Petrography

3.3.1. Harzburgite

Most harzburgites show various degrees of deformation and have microstructures similar to the porphyroclastic textures defined by Mercier and Nicolas (1975) [Figure 3-7A, B]. Olivine is the most common porphyroclast phase, although both Cpx and Opx can also form porphyroclasts. The Ol porphyroclasts, 0.5 to 1.5 cm in size, display traces of polygonization in many places and have been partly recrystallized at their peripheries into neoblasts, 0.02 to 0.05 mm in size (Figure 3-7C). The neoblasts are generally subpolygonal, with straight boundaries suggesting that most of the recrystallization occurred through progressive disorientation of subgrains, attributed to subgrain rotation (Ave Lallemant, 1985). The amount of recrystallization ranges from about 10% to 50%. Both Ol porphyroclasts and neoblasts show undulatory extinction, sharp subgrain boundaries and well-developed lamellae or kink-banding (Figure 3-7C), characteristic of internal plastic deformation (Nicolas and Poirier, 1976).

Orthopyroxene porphyroclasts, typically 0.5 to 1.0 cm but up to 2 cm in size, commonly are embayed, resorbed, and are surrounded by granular Ol grains (Figure 3-7D). Some grains of Opx are clearly replaced by Ol along cleavage planes (Figure 3-7E). Many single crystals are elongated subperpendicular to their exsolution lamellae, suggesting they formed by dismembering or pull-apart of originally larger crystals or of Opx bands.

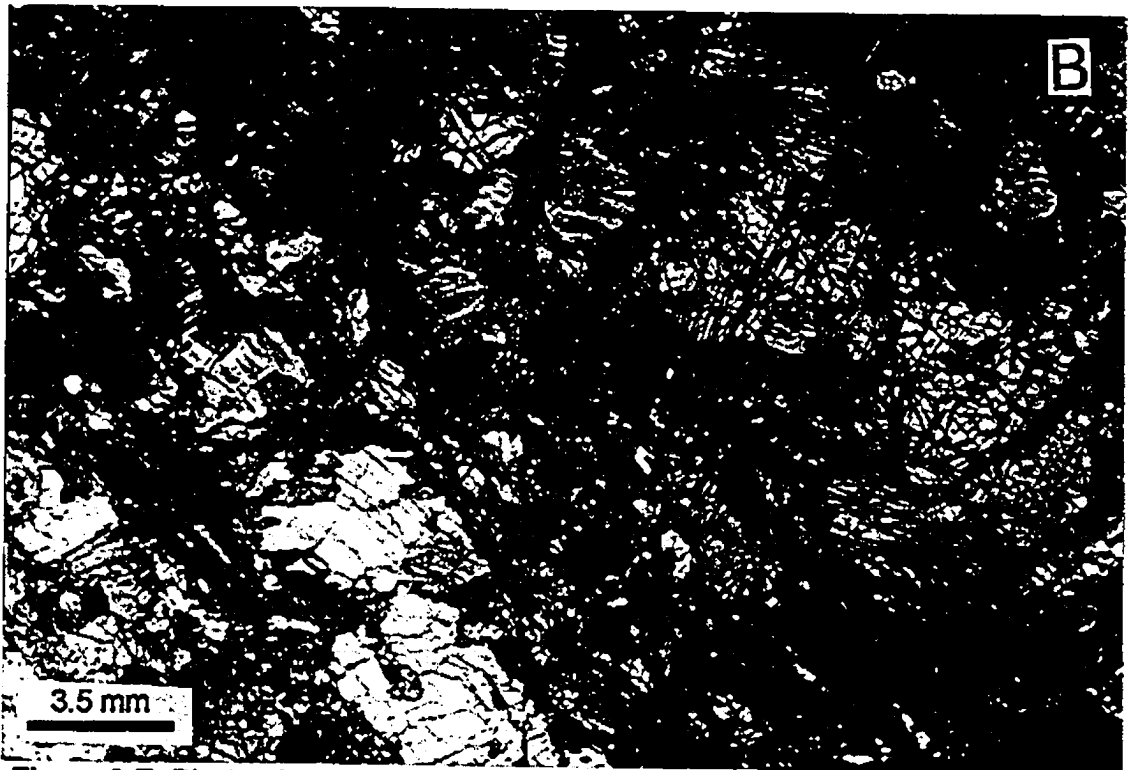
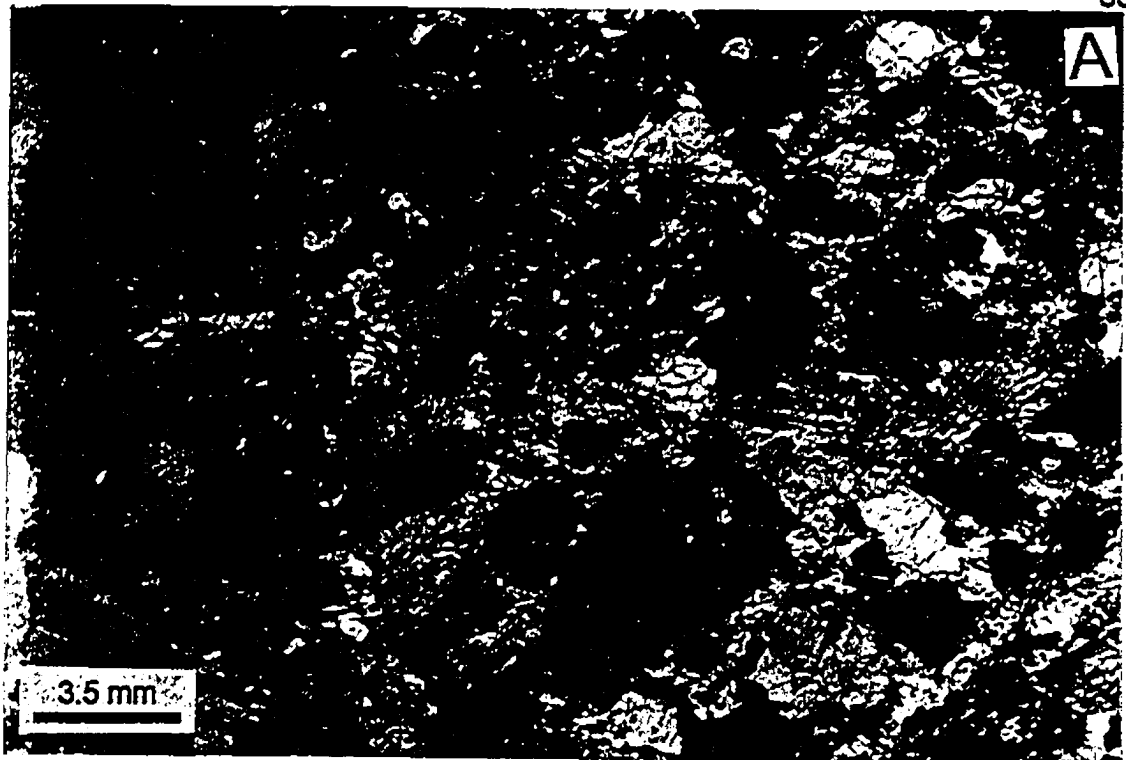


Figure 3-7. Photomicrographs of harzburgites: A. Porphyroclastic texture; note weak orientation of the Ol porphyroclasts with typical high-temperature granular matrix; L10. B. Porphyroclastic texture; note Opx porphyroclasts and thinned, banded Ol possibly representing late stage deformation; L19.

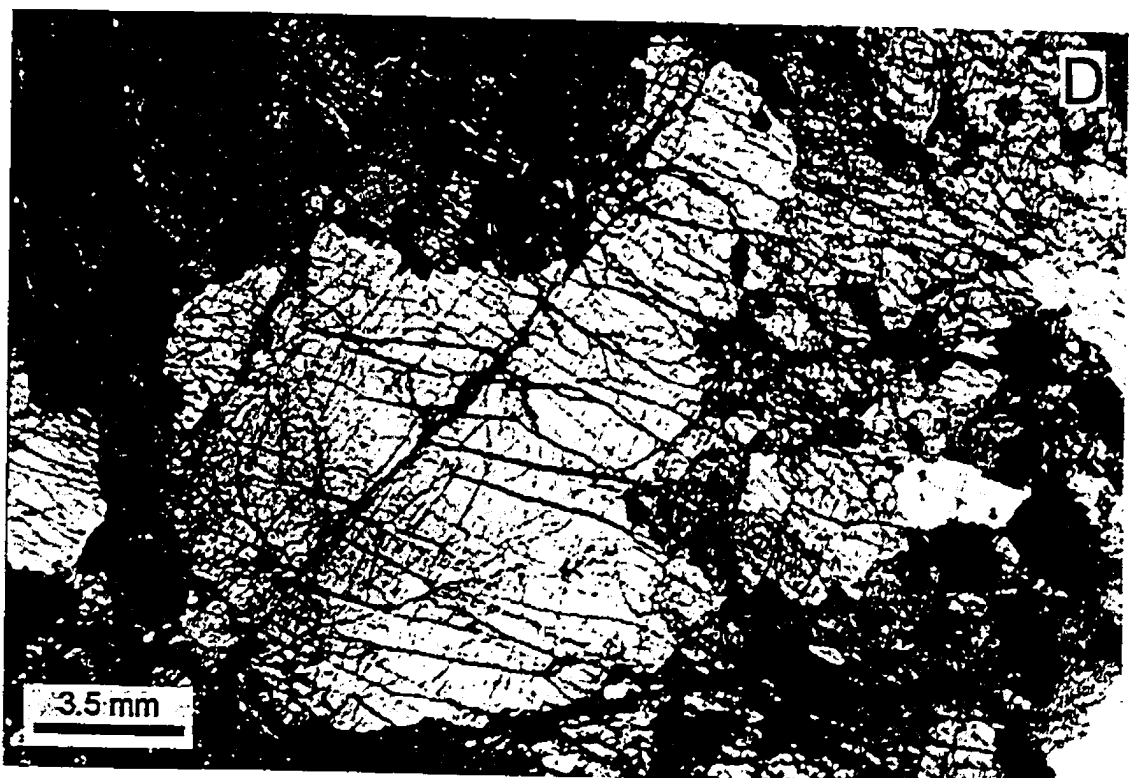
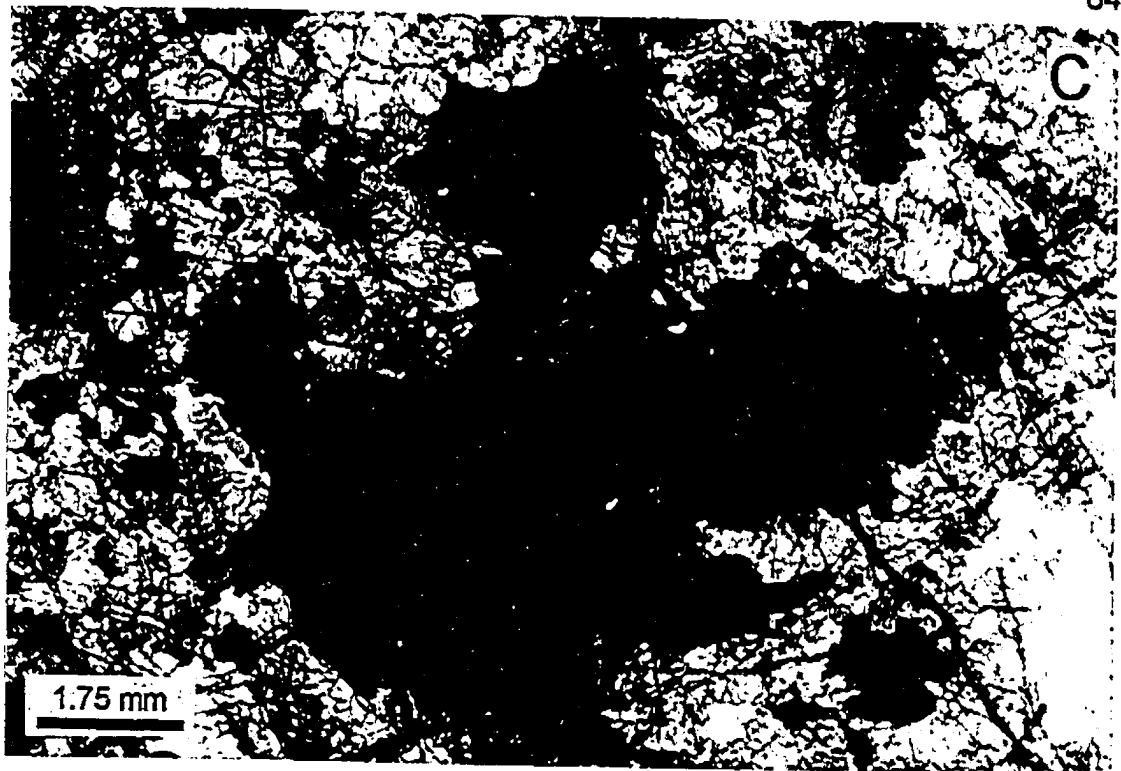


Figure 3-7. C. An Ol porphyroblast, showing kink-banding and irregular boundaries surrounded by a granular Ol matrix; H3. D. An Opx porphyroblast set in a granular matrix of Ol; L12.

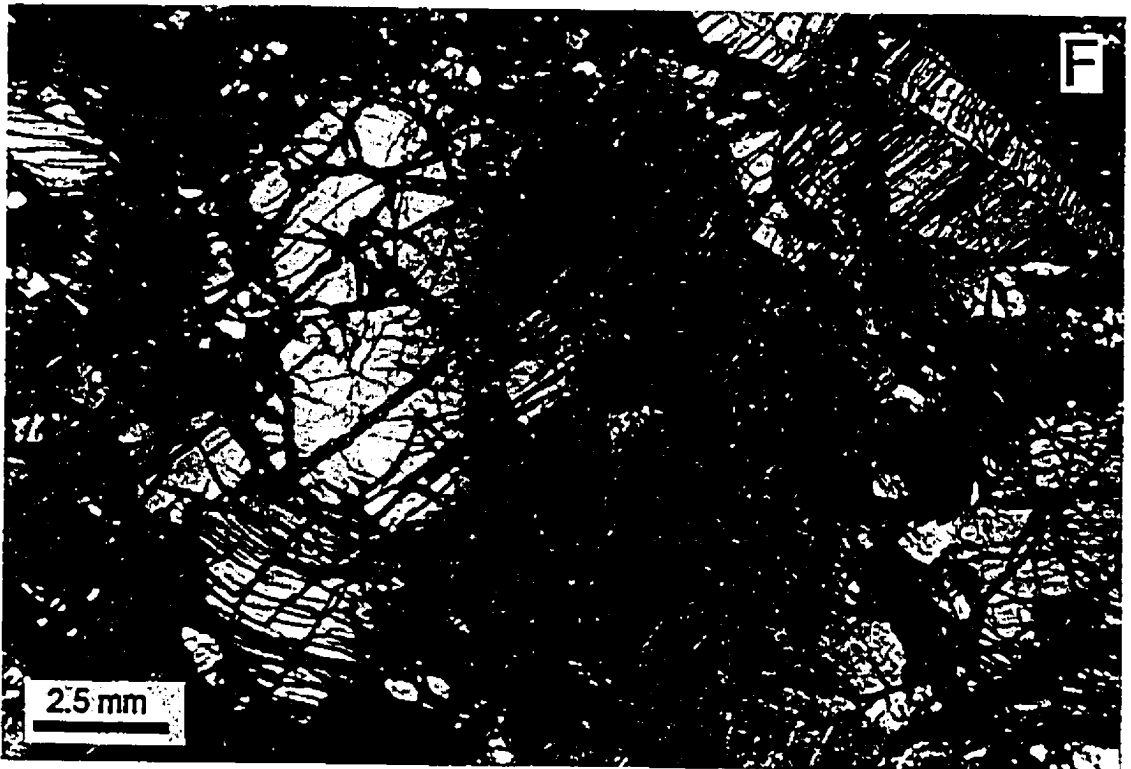
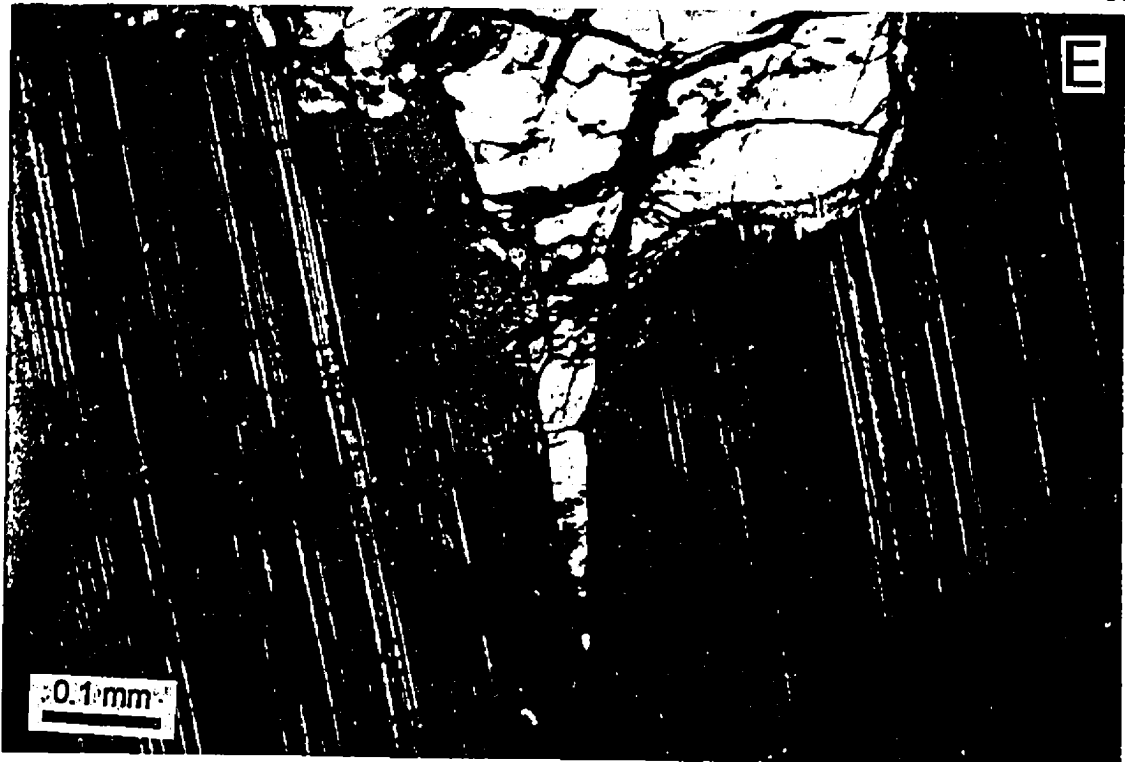


Figure 3-7. E. Olivine along the cleavage of Opx; note also the Cpx exsolution lamellae in Opx; B123-3. F. Opx inclusion in Ol, possibly indicating incongruent melting; L19.

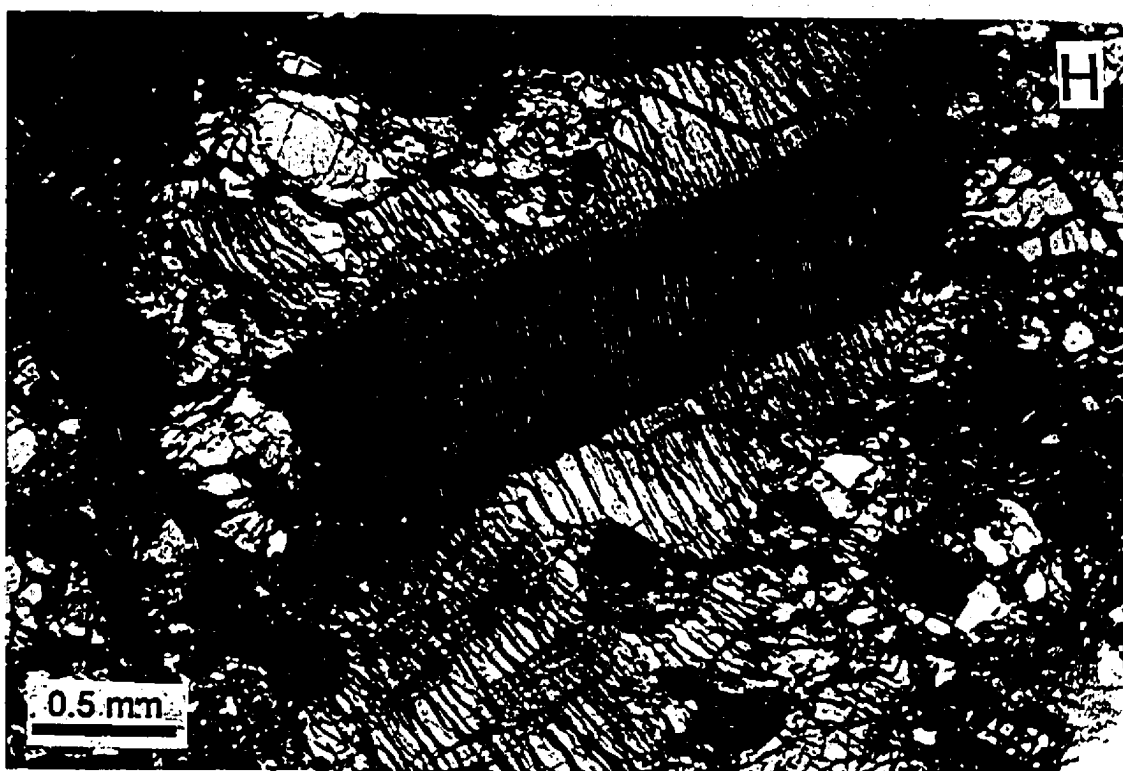
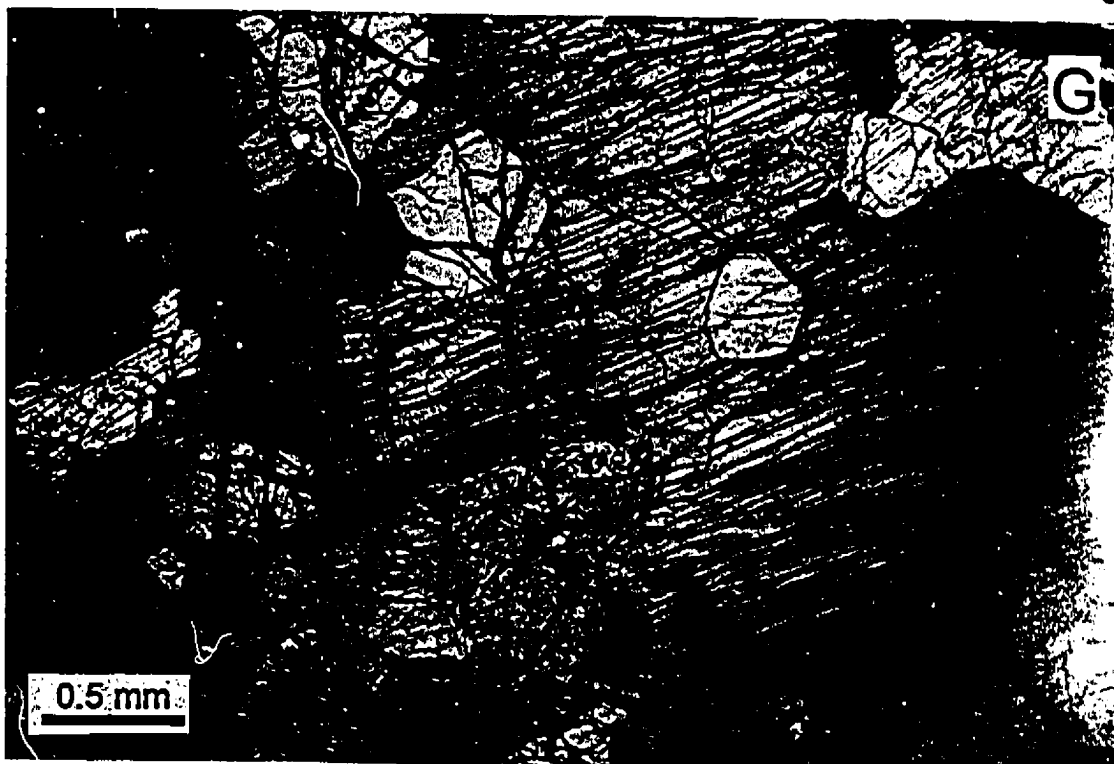


Figure 3-7. G. Opx inclusion in Opx porphyroblast; note also smaller OI grains around the Opx grain, possibly indicating replacement; B104-3. H. Deformed Opx porphyroblast showing mechanical twin and granular edges, B108-2.

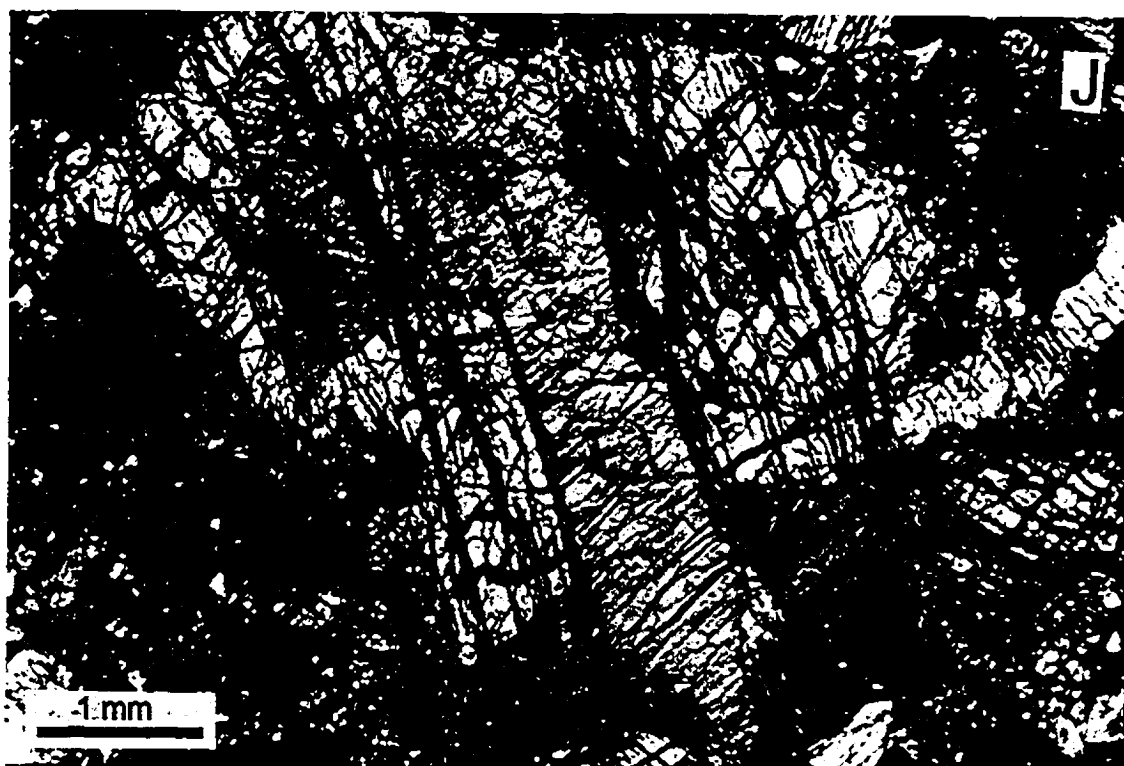
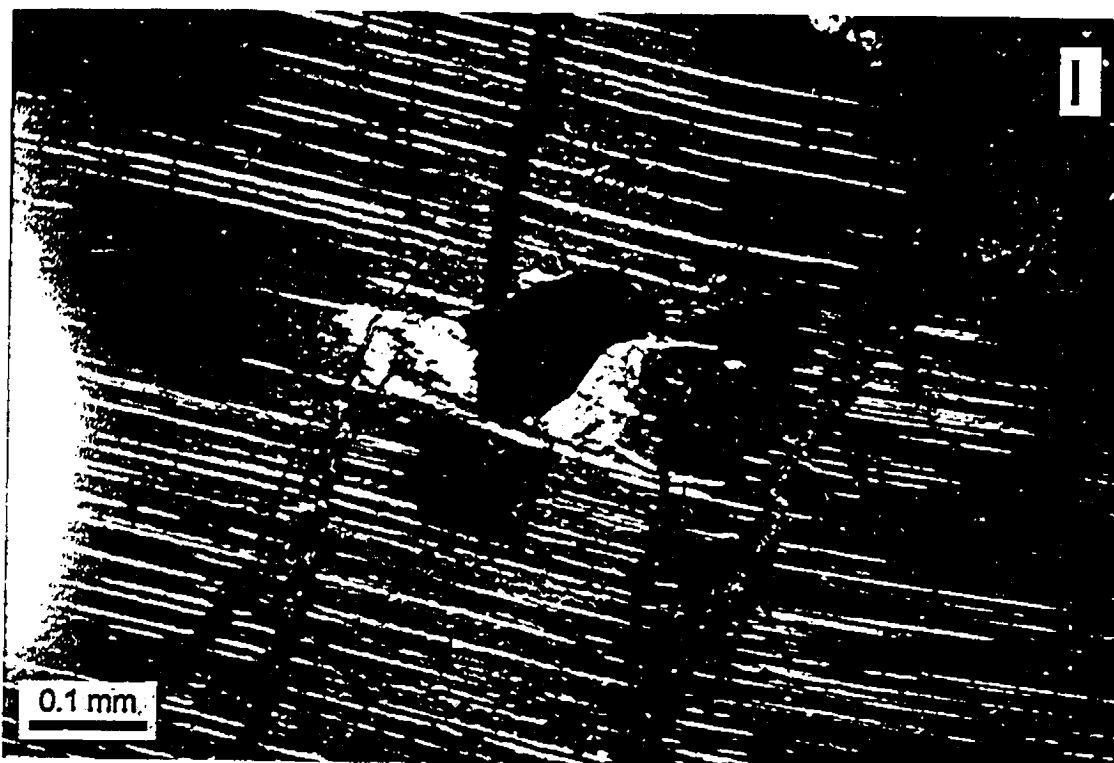


Figure 3-7. I. Exsolution of Cpx and chromite along cleavage in Opx, B104-3. J. Grey and yellow Opx twin. Yellow Opx grains show Cpx exsolution along cleavage. Note chromite along left edge of yellow Opx and rimming large Opx grain. B108-3.

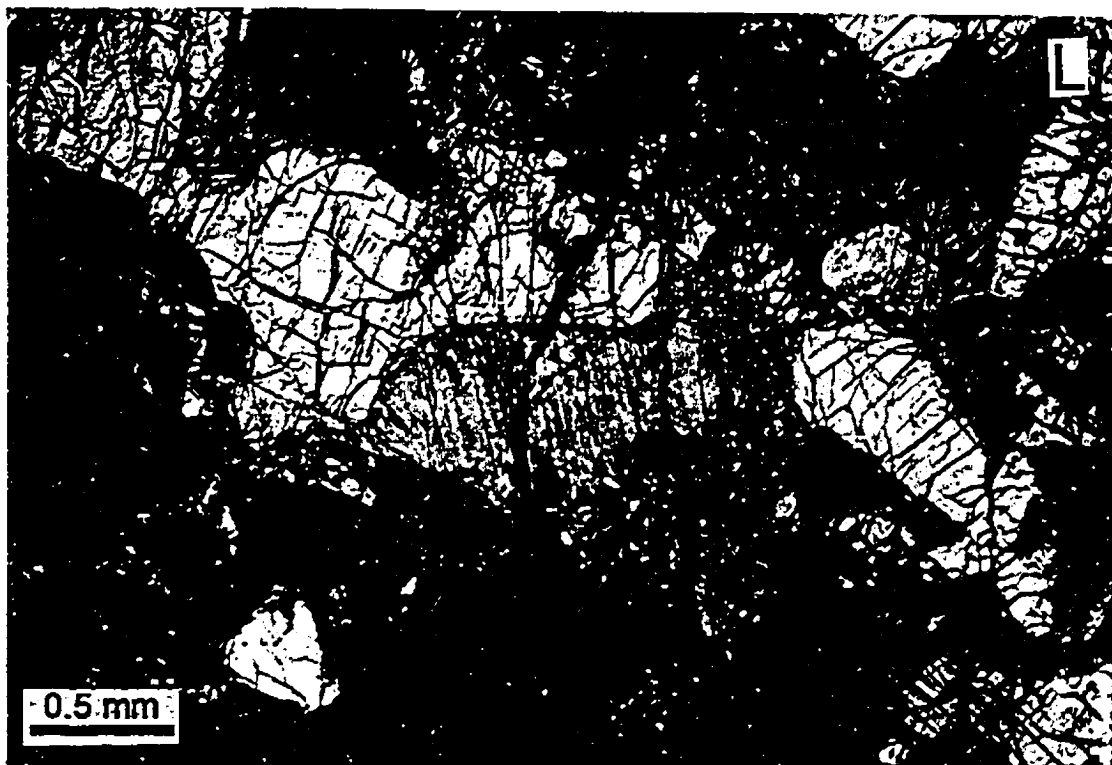
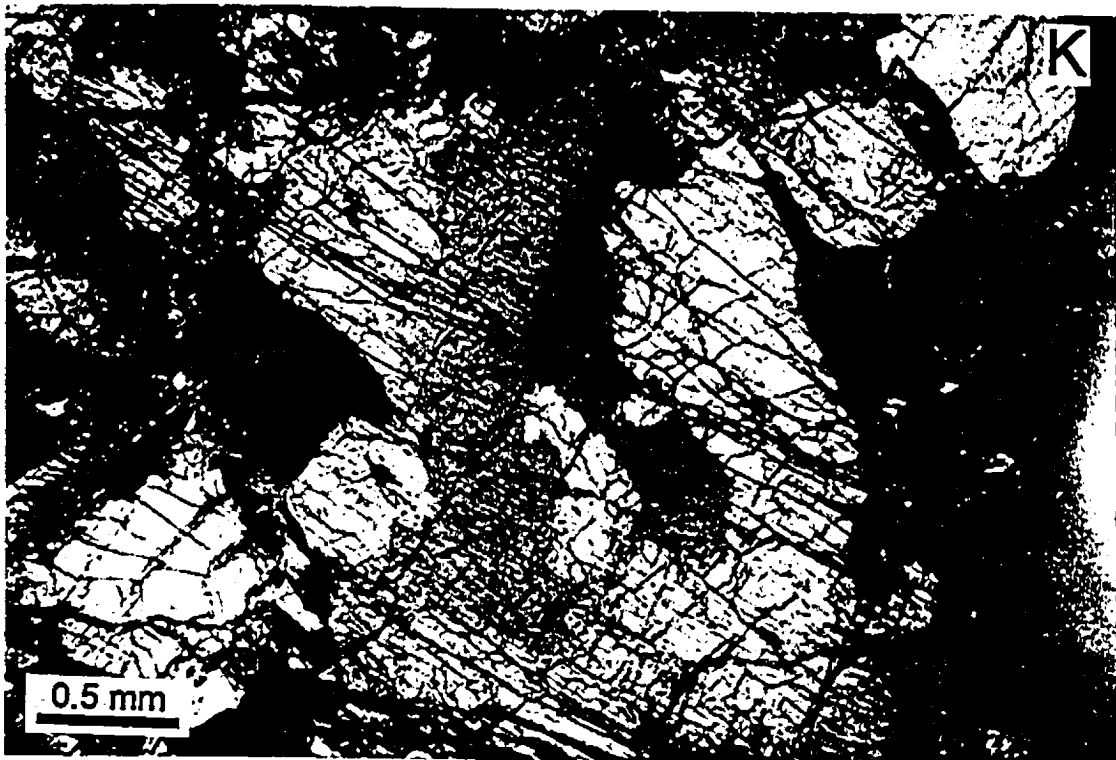


Figure 3-7. K. Replacement texture showing an Opx grain replaced by Cpx (centre) and Ol, B101-3. L. Clinopyroxene and Opx both of which were replaced by Ol; Note also anhedronal chromite (black); B108-1.

Many Ol crystals contain inclusions of Opx (Figure 3-7F), suggesting a replacement process, perhaps due to incongruent melting of the pyroxene (Dick, 1977). In one sample (B104-3), an Opx porphyroclast contains a smaller, euhedral Opx inclusion (Figure 3-7G). This Opx "inclusion" may truly be a coexisting grain.

Most Opx grains have Cpx exsolution lamellae along the slip planes and exhibit deformation (Figure 3-7H). In sample, B104-3, an Opx grain contains chromite and Cpx, possibly formed by exsolution (Figure 3-7I). In sample B108-3, twinned Opx grain has Cpx exsolution along cleavage planes (Figure 3-7J). In some cases Opx has clearly been replaced by Cpx, leaving Opx islands with optical continuity (Figure 3-7K). No Cpx veinlets or segregations have been observed within the rock. Thus, the replacement of Opx by Cpx does not result from melt impregnation.

Individual Cpx crystals are rare and occur as embayed grains generally associated with Opx (Figure 3-7L); these are interpreted to be residual Cpx. Clinopyroxene also occurs as exsolution lamellae in Opx (Figure 3-7E, H, I).

Di-harzburgites exhibit protogranular textures as described by Mercier and Nicolas (1975). Olivine, Opx, and Cpx are similar in size, and all show weak deformation (Figure 3-8A, B, C). Olivine grains also show kink-banding and subgrain boundaries (Figure 3-8B). Orthopyroxene is always associated with Cpx and chromite (Figure 3-8C).

Accessory chromite (0.1-0.5 mm) is ubiquitous in harzburgite where it is

typically anhedral (Figures 3-7I, J, L and 3-8C), similar to those of harzburgites from Bay of Islands ophiolite, Newfoundland (Talkington and Malpas, 1980). It occurs as both isolated crystals scattered in the Ol matrix and in close association with Opx and Cpx. Grains associated with Opx and Cpx are amoeboid and are commonly interpreted as being derived from garnet plus Ol, thus recording a mantle evolution toward lower pressure. The Cpx-chromite assemblage may represent the final products of decomposition of Opx during incongruent melting.

There is a 5-15-m-wide mylonitic shear zone along the boundary between the mantle sequence and the transition zone. The mylonitic microstructures are characterized by thin bands and lenticular domains (Figure 3-9A), a few millimetres thick, made up of fine-grained recrystallized Ol (Figure 3-9B, C). These bands and domains enclose deformed porphyroclasts of Ol and pyroxenes, 0.1 to 1 cm in size. Olivine has been strongly recrystallized into fine-grained (<0.01 mm) neoblasts that are slightly elongated parallel to the shear zone and have irregular contours (Figure 3-9B, C). Opx and Cpx porphyroclasts are elongate and have exsolution lamellae (Figure 3-9B). The intensity of recrystallization decreases away from the centre of the shear zone, but some recrystallization is always present and occurs in pressure shadows of Ol porphyroclast remnants.

The bands and lenticular domains are separated by thin, anastomosing layers of ultrafine-grained (2-30 μm) material (Figure 3-9A, B, C). These

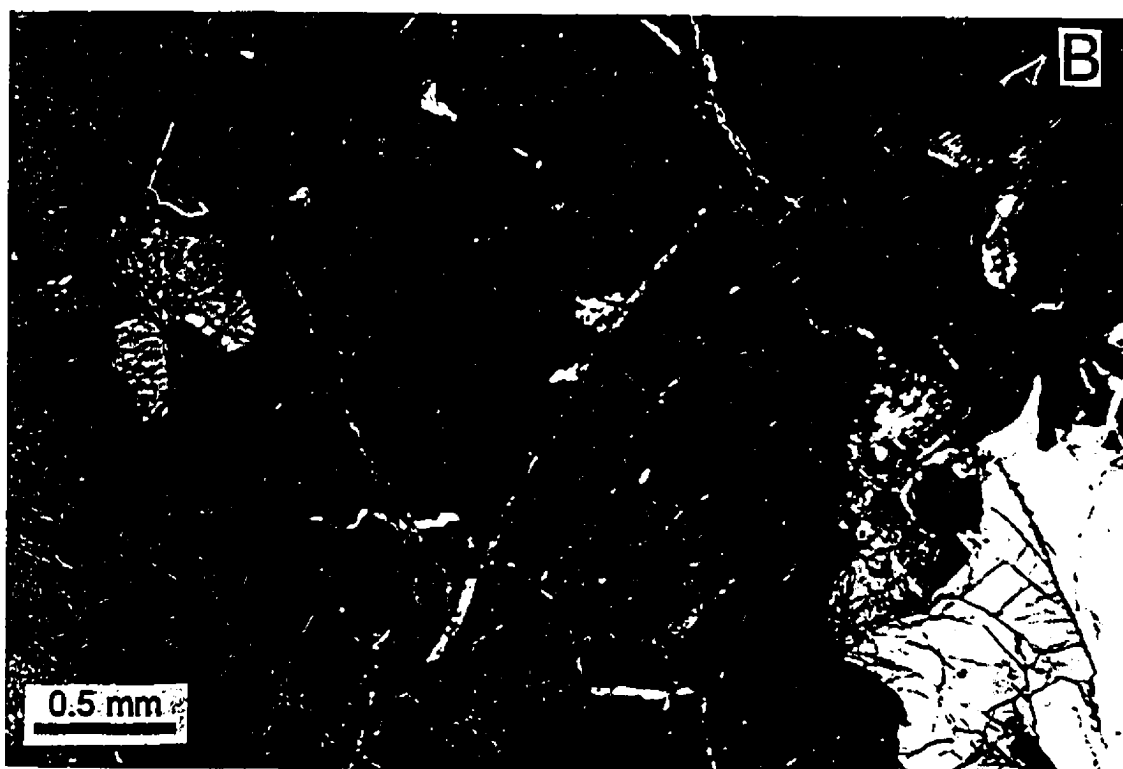
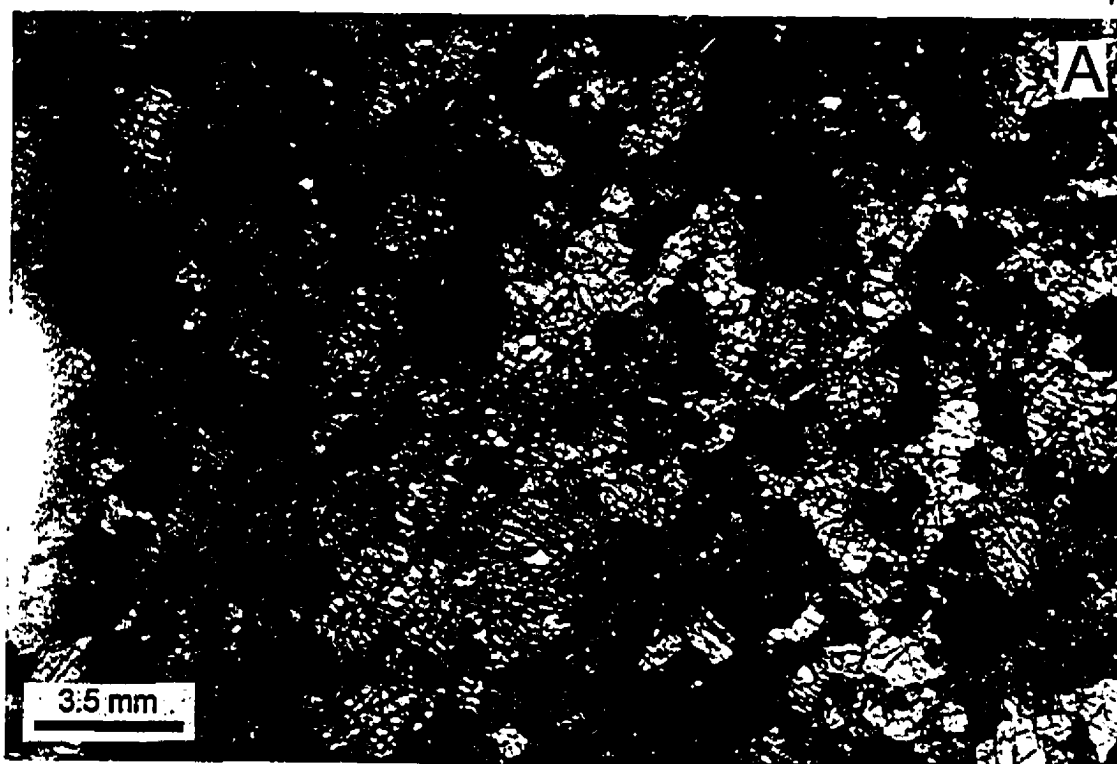


Figure 3-8. Photomicrographs of Di-harzburgite: A. Protogranular texture, showing weak deformation; S7. B. Well-developed kink-banding in an Ol grain; LHS.

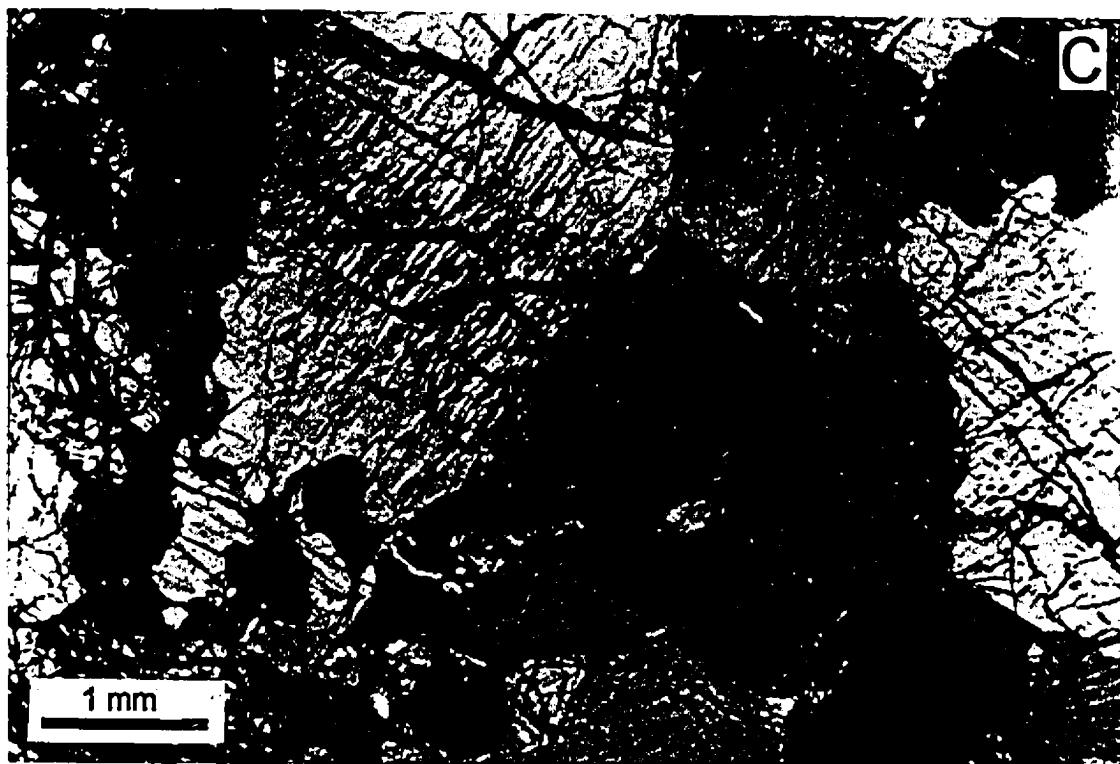


Figure 3-8. C. Orthopyroxene, Cpx and chromite cluster, LH3.



Figure 3-9. Photomicrographs of sheared harzburgite: A. Porphyroclastic texture; Cpx and Opx porphyroclasts set in a matrix of sheared Ol and pyroxene; HD3. B. Bent exsolution lamellae of Cpx in Opx; note bent twin planes in pyroxene porphyroclasts in a matrix that contains elongated and recrystallized Ol; HD3.

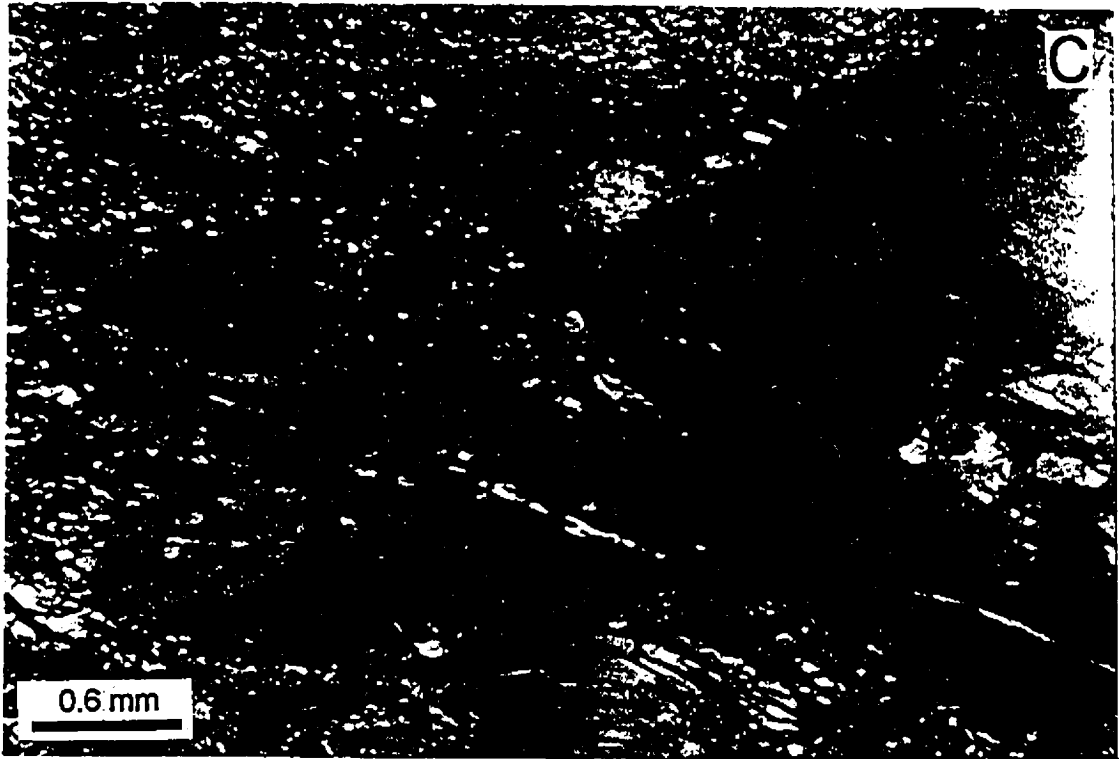


Figure 3-9. C. Olivine porphyroclasts in a matrix of thinned and elongated Ol, HD3

ultrafine-grained bands produce a fluidal aspect to the microstructure and suggest that deformation may have been controlled by some form of grain-size sensitive creep, commonly referred to as "superplasticity" (e.g., Boullier and Gueguen, 1975).

3.3.2. Dunite

Dunites occur in lenses and dykes in harzburgite and as envelopes around podiform chromitites. These dunites are mostly concordant with respect to the foliation of the peridotites. In the dunite dykes, aligned trails of chromite grains are parallel to the walls of the dykes (Figure 3-10). Dunites are composed chiefly of very coarse-grained Ol clearly larger than in the host Di-harzburgites or harzburgites (Figure 3-11A). Some dunites have bands of disseminated chromite which are parallel to the foliation of the enclosing harzburgite and to the boundary between the harzburgite and dunite (Figure 3-11B). Individual Ol grains are generally 0.5-5 mm across, with the largest up to 30 mm, and many show kink-banding and undulatory extinction, suggesting an internal plastic deformation. The boundaries between grains are highly irregular (Figure 3-11B to C). In many cases, porphyroclastic Ol grains show granular edges with recrystallized, small mosaic Ol grains that have triple junctions (Figure 3-11G to I).

Accessory chromites in dunites are 0.05-0.5 mm across, much smaller than the Ol grains. They are normally euhedral or subhedral (Figure 3-11H, I), morphologically distinct from those in the harzburgites (Figure 3-8C), a feature

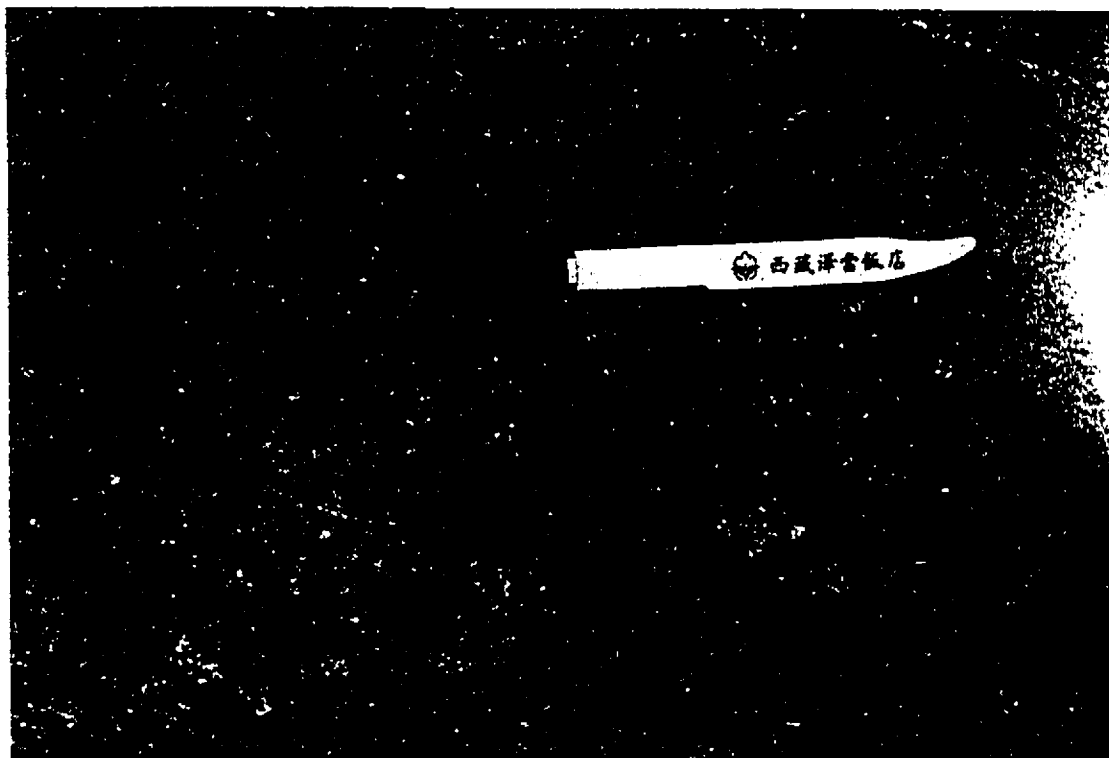


Figure 3-10. Field photo of a dunite dyke in protogranular Di-harzburgite; note chromite string in dunite parallel to dyke margin, taken near Ore Group VIII.

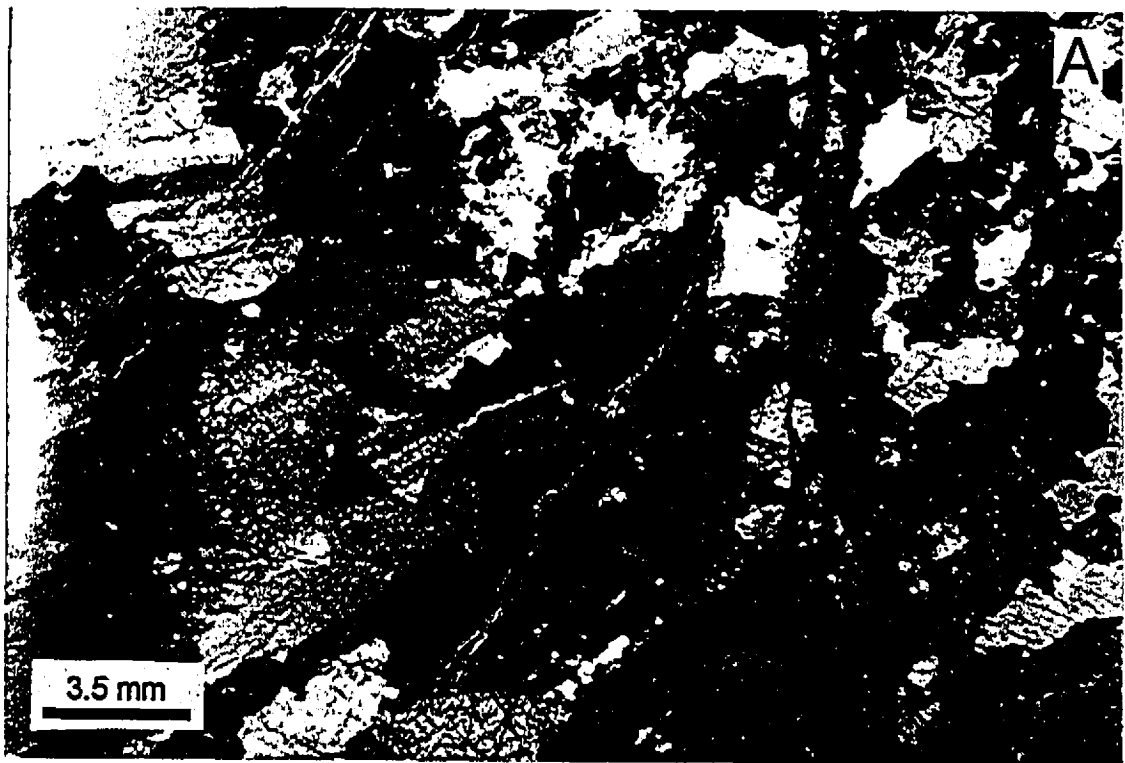


Figure 3-11. Photomicrographs of dunite: A. Coarse-grained dunite (lower left) in contact with protogranular Di-harzburgite (upper right); LH1-2. B. Aligned chromite grain in coarse-grained dunite; LH1-1.

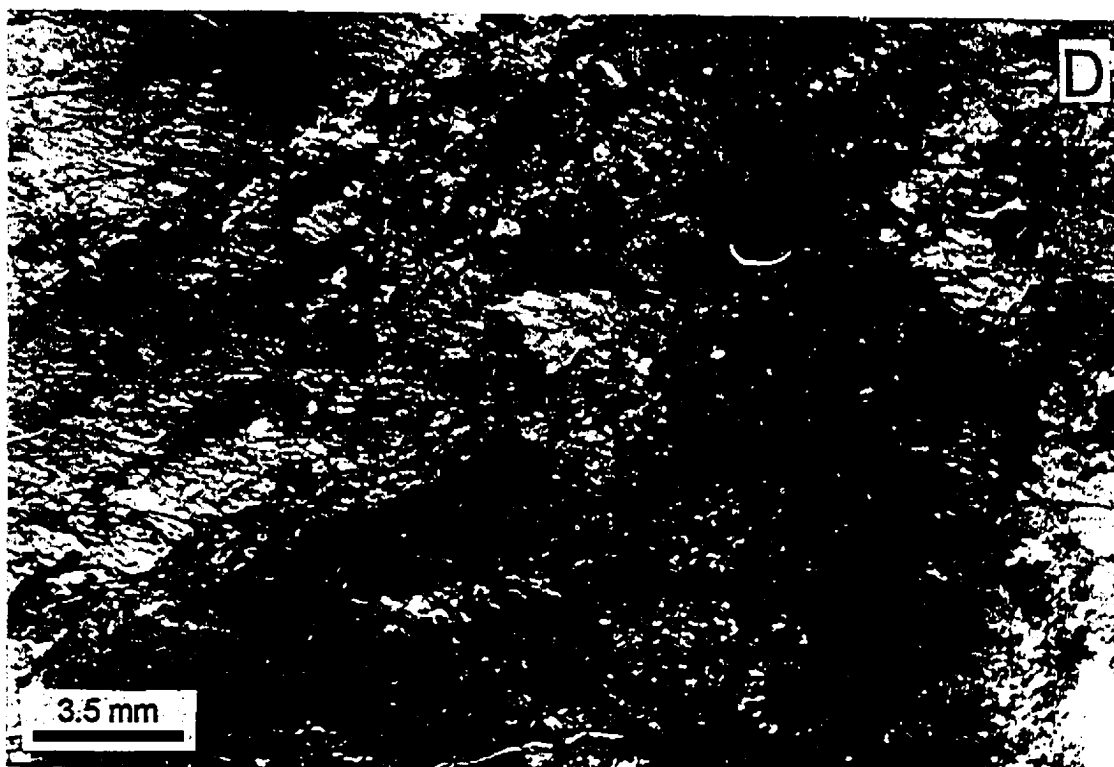
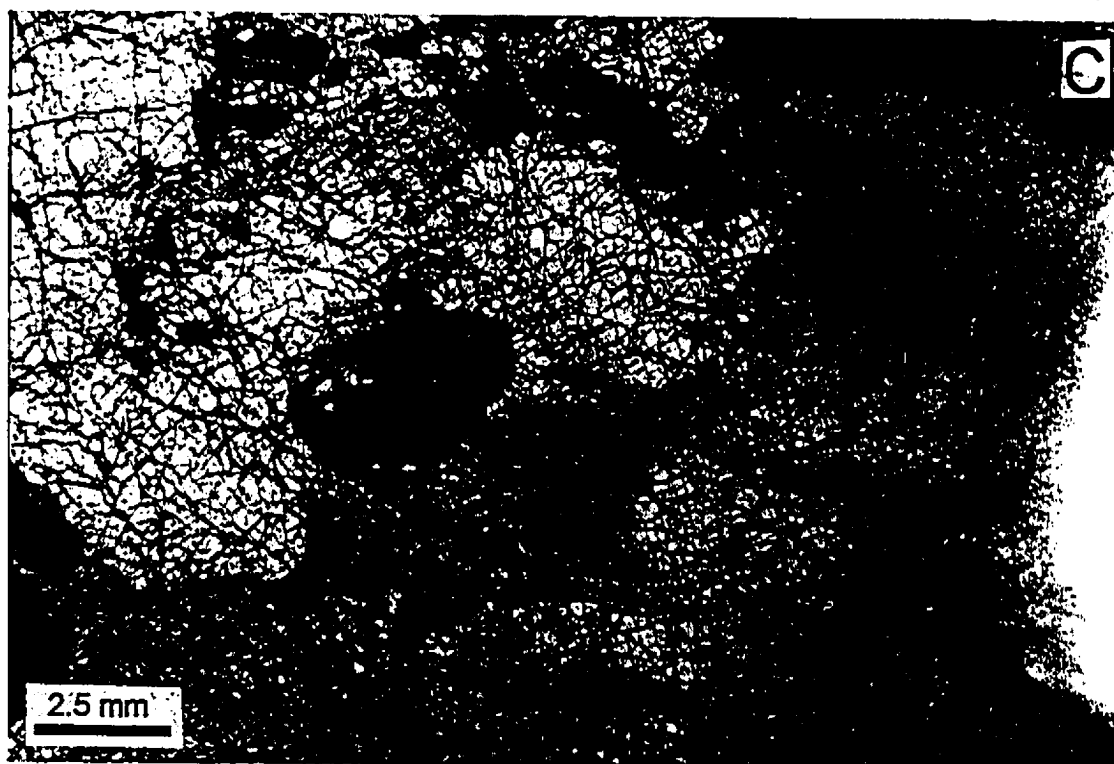


Figure 3-11. C. Coarse-grained dunite; note small, anhedral, elongate chromite grains along the boundaries of Ol grains (left), LH2. D. A large, sheared Ol grain; note small Ol neoblasts in Ol and euhedral chromite grains; L18.



Figure 3-11. E. Large Ol grain sheared in two directions; fractures are filled with smaller Ol grains and euhedral chromite grains, ZHK9. F. Kink-bands in Ol, showing subgrain boundaries, Ol neoblasts and euhedral chromite; ZHK8.

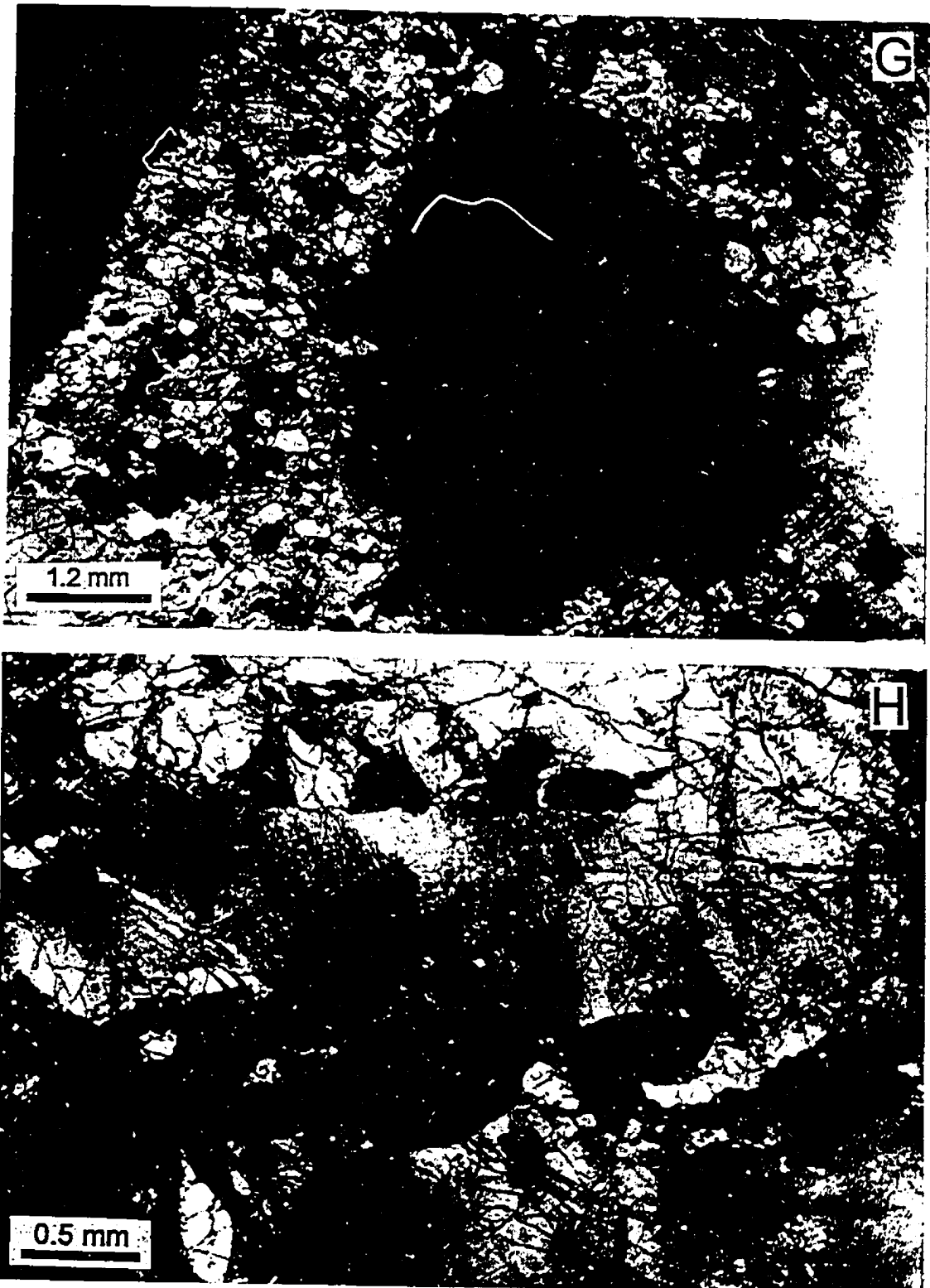


Figure 3-11. G. A larger, sheared Ol grain. Shear zones are filled with fine-grained Ol and euhedral chromite, ZHK6-2. H. Olivine and chromite neoblasts along shear fractures in a large Ol grain; L18.

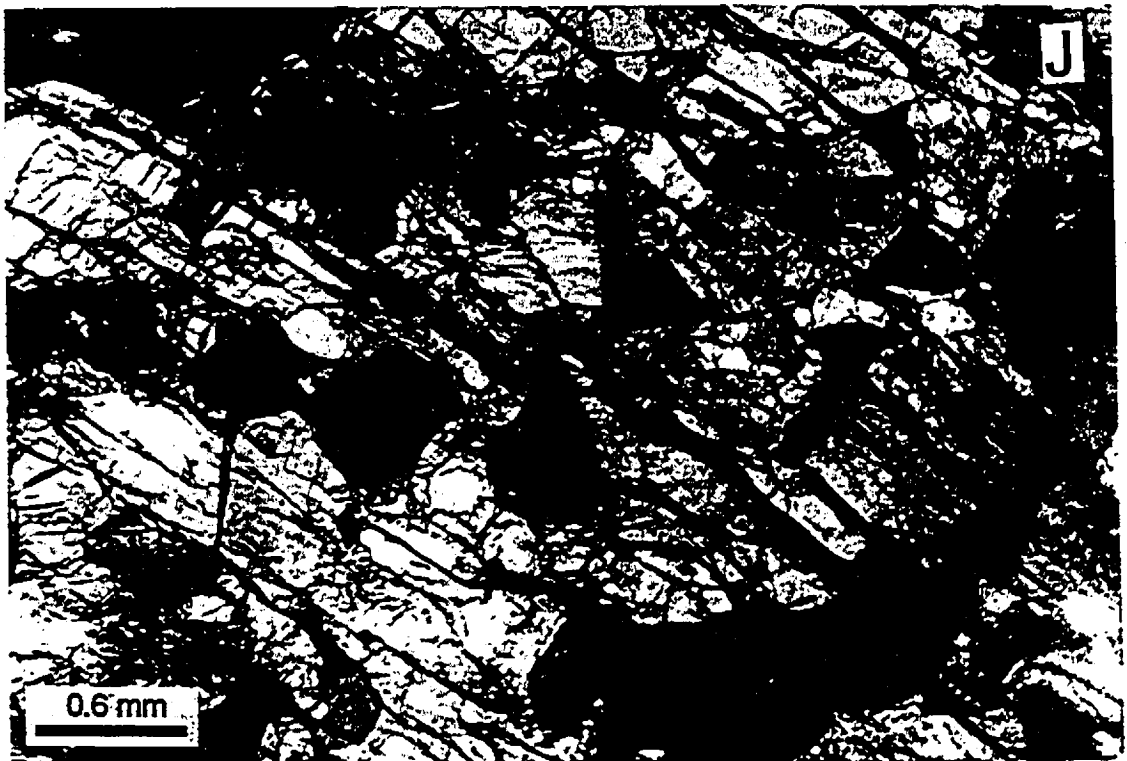
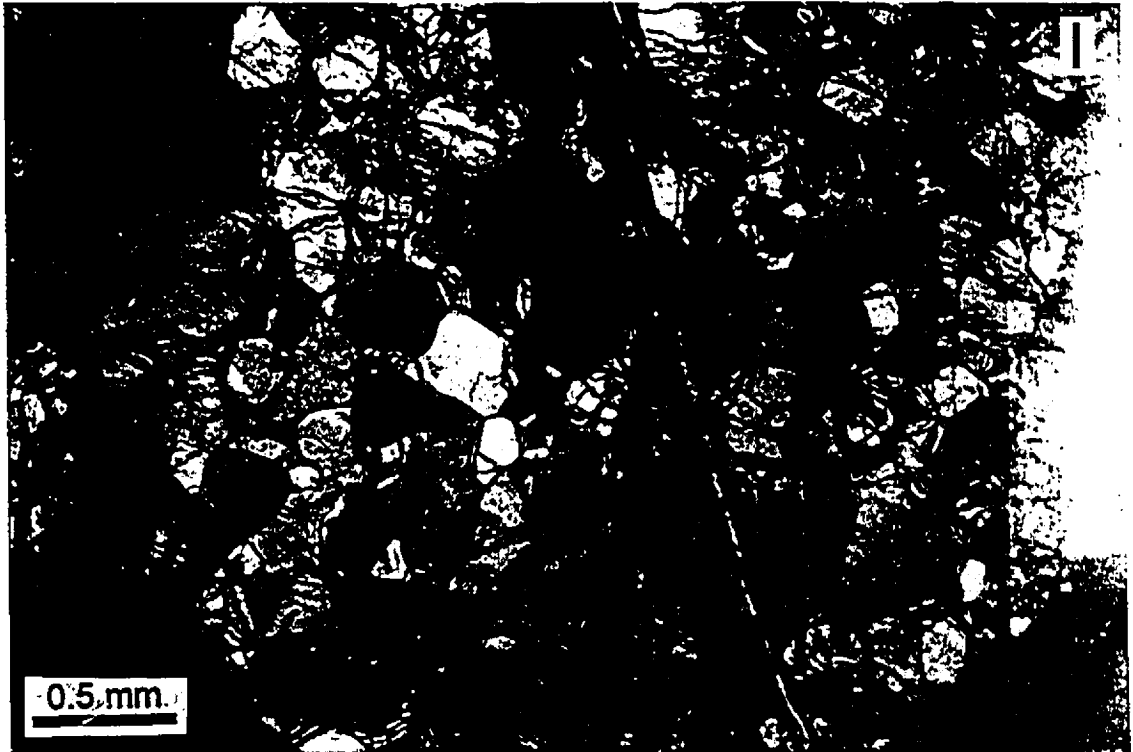


Figure 3-11. I. Polygonal Ol and chromite neoblasts, locally forming triple points; ZHK-L. J. Poikilitic Ol grain containing Opx, and Ol inclusions; VIII-6, 32 x 0.5.

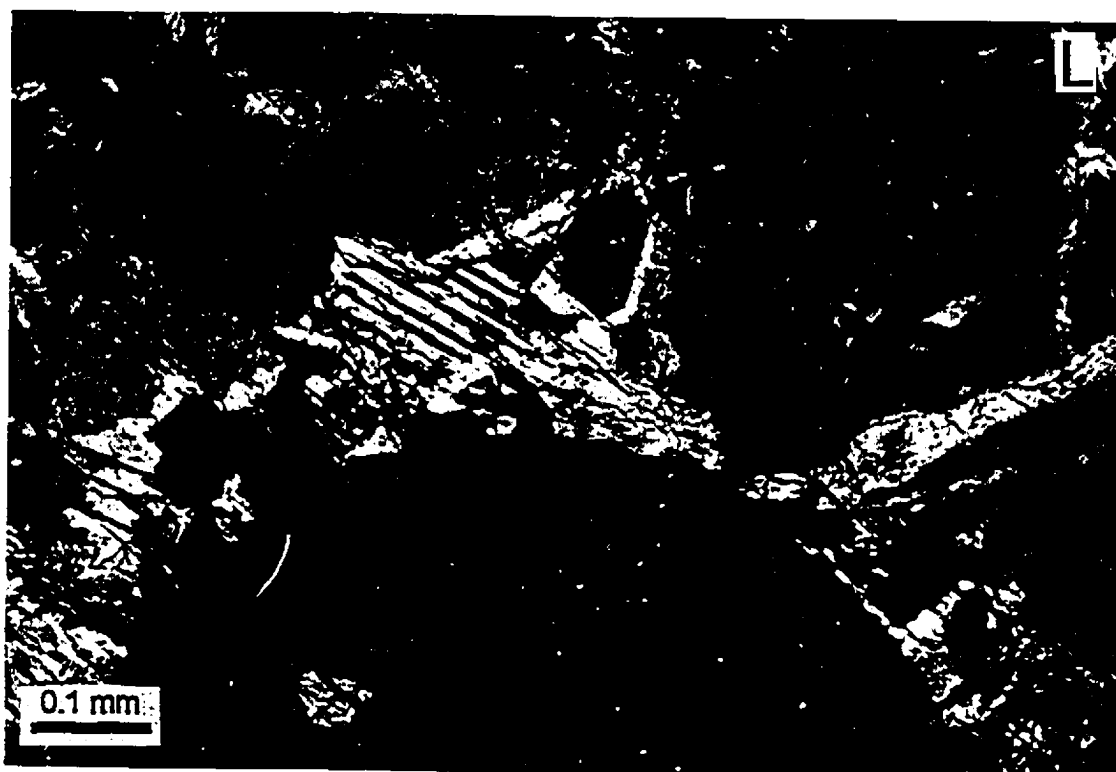
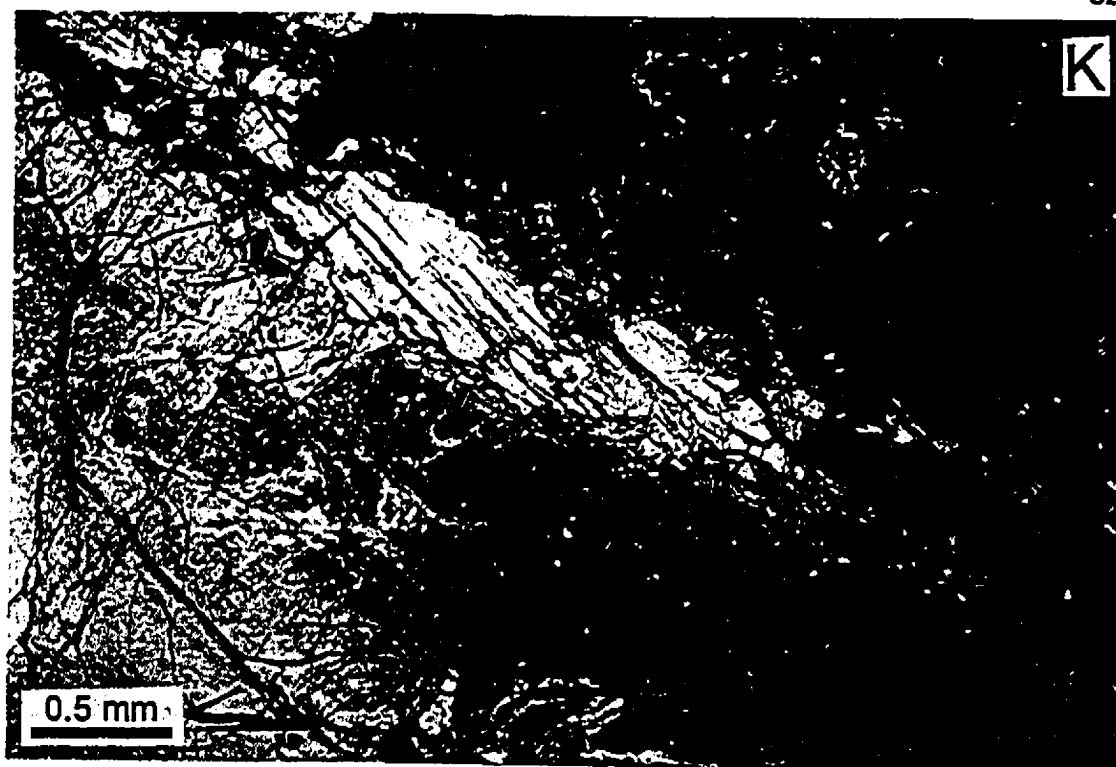


Figure 3-11. K. Elongate Opx grain in a fracture in dunite, ZHK-L. L. Small, rounded chromite grain and a small Cpx grain, both included in a very large Ol grain (at least 5 cm in size). ZHK-L.

noted previously by Leblanc (1980). Some grains have been deformed and recrystallized into smaller and more equant grains and form a mosaic with smaller Ol grains along fractures in the large Ol grains (Figure 3-11H).

The dunites adjacent to chromitites show magmatic textures. In sample VIII-6, the dunite near the chromitite band has a poikilitic texture in which large Ol grains surround smaller Ol and Opx (Figure 3-11J). Orthopyroxene grains occur along shear zones in the dunite (Figure 3-11K). There are also fine chromite and Cpx grains included in large Ol grains (Figure 3-11L).

3.3.3. Podiform chromitite

Massive, disseminated, nodular and brecciated chromitites are the most common textural types (Figure 3-12) and these commonly grade into each other.

Massive chromitites are typically coarse-grained rocks composed of more than 80 modal% chromite. Individual chromite grains are mostly 1 to 5 mm across (some are up to 30 mm), anhedral in shape and show the effects of corrosion or reaction in addition to mechanical disruption (Fig 3-12A). The chromite grains are closely packed, leaving very narrow interstices filled with silicate minerals (cf. Thayer, 1964; Greenbaum, 1977).

Disseminated chromitites consist of 10-65 modal% chromite, uniformly scattered in the host silicates (mainly Ol, Table 3-1). Individual chromite grains are generally smaller (0.5-2 mm) and more regular than in the massive varieties. Many disseminated chromitites grade into massive bodies with increasing chromite contents and larger crystal sizes (Figure 3-12B).

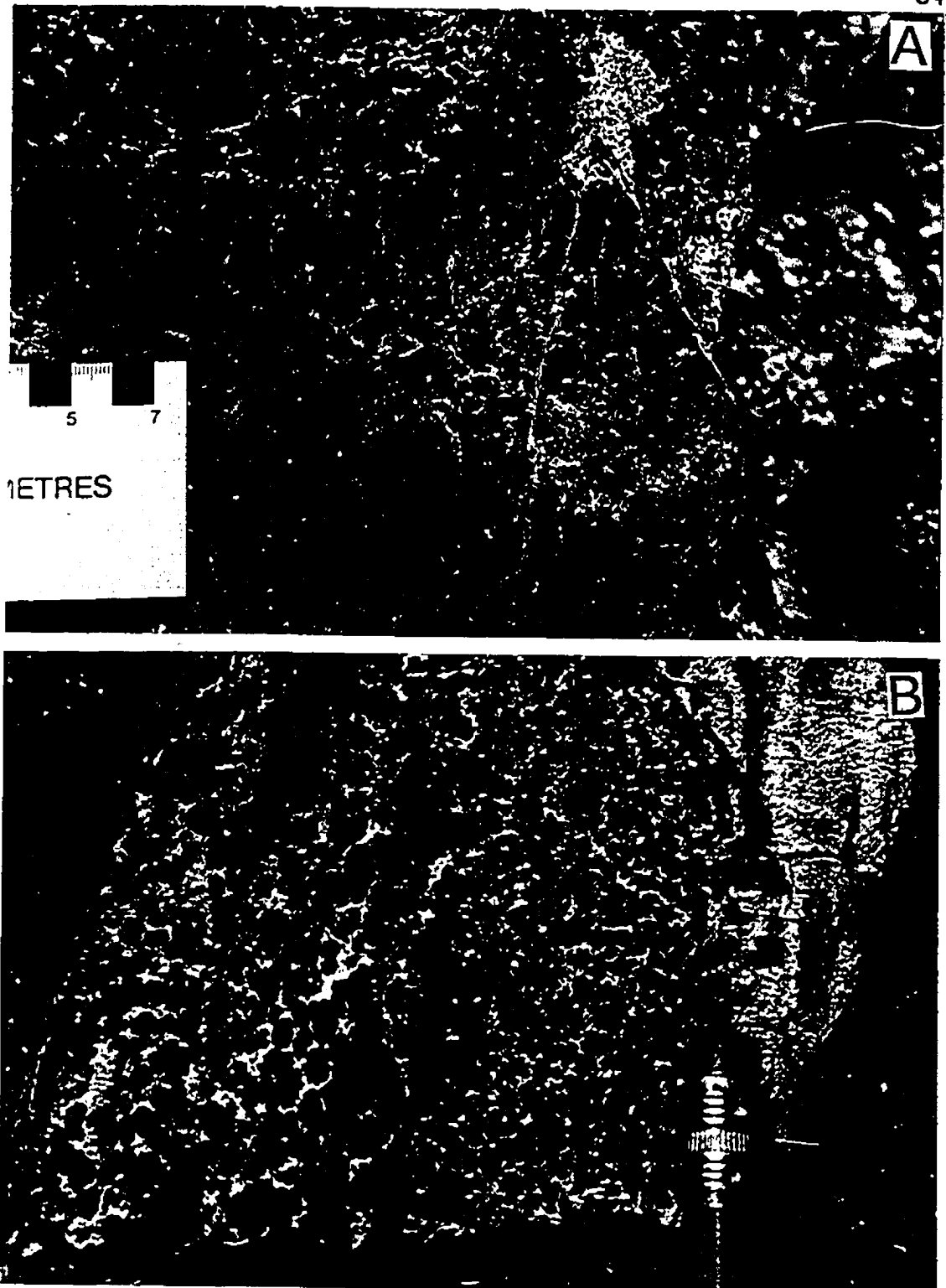


Figure 3-12. Hand specimen photographs of chromitite: A. Massive chromitite showing pull-apart texture; Ore Group I. B. Massive to disseminated chromitite; Ore Group III.

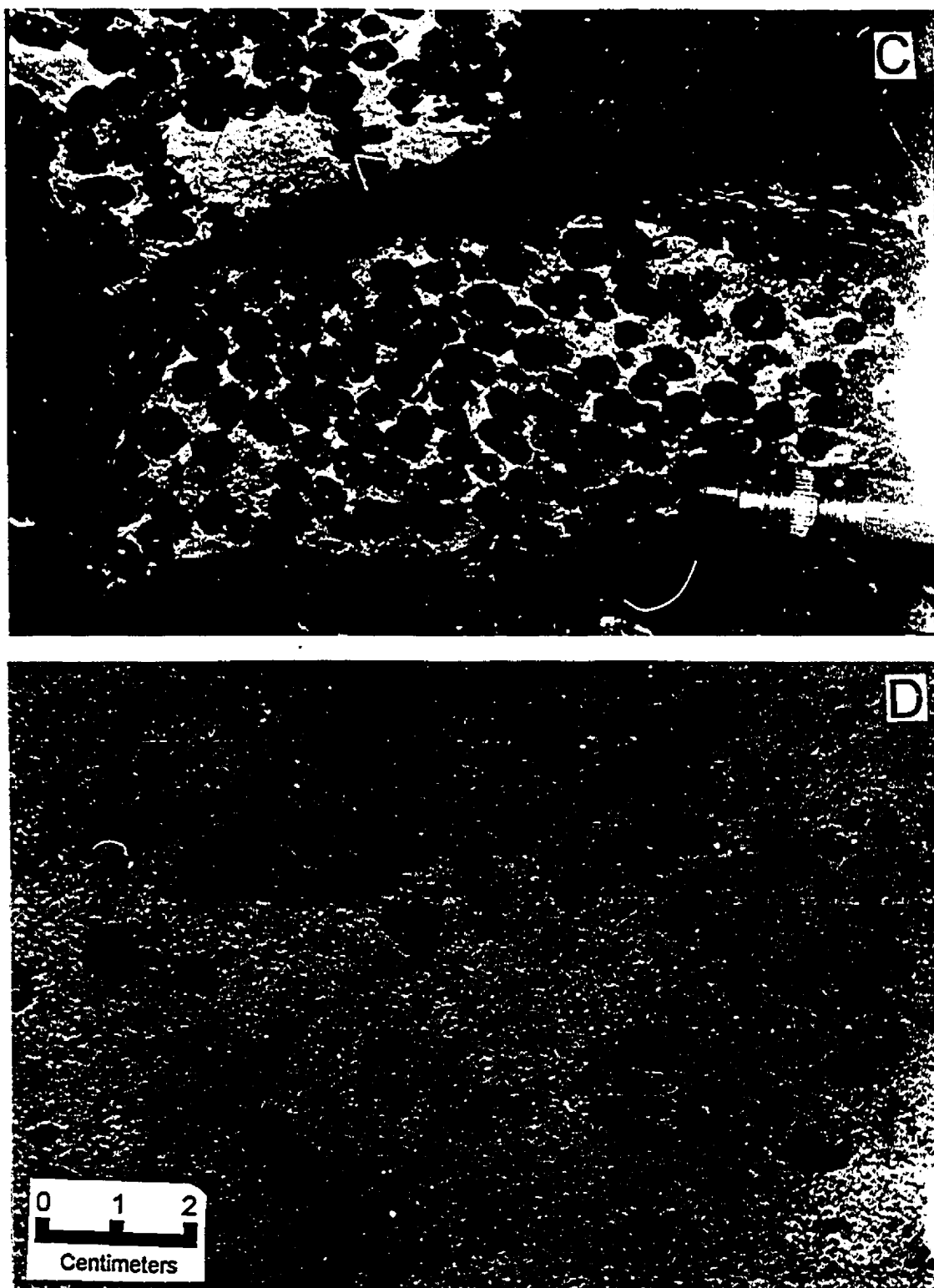


Figure 3-12. C. Nodular chromitite showing weak orientation of individual chromite nodules; Ore Group VII. D. Nodular chromitite composed of large nodules and small euhedral chromite in the matrix; Ore Group XXXI.

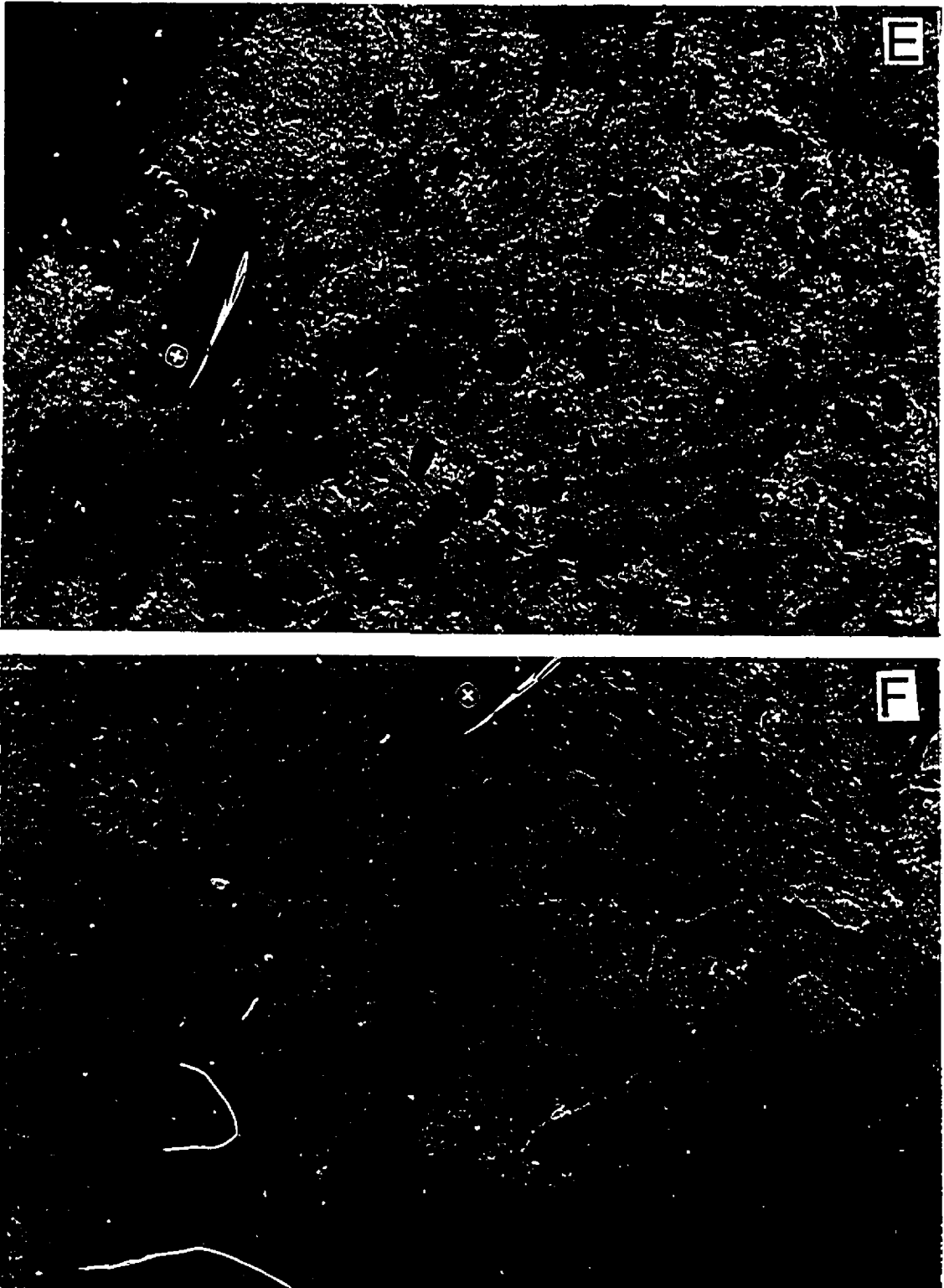


Figure 3-12. E. Nodular chromitite; note elongate individual nodules and folded disseminated grains; Ore Group XXXI. F. Fragments of brecciated dunite cemented by disseminated chromite; Ore Group XXXI.

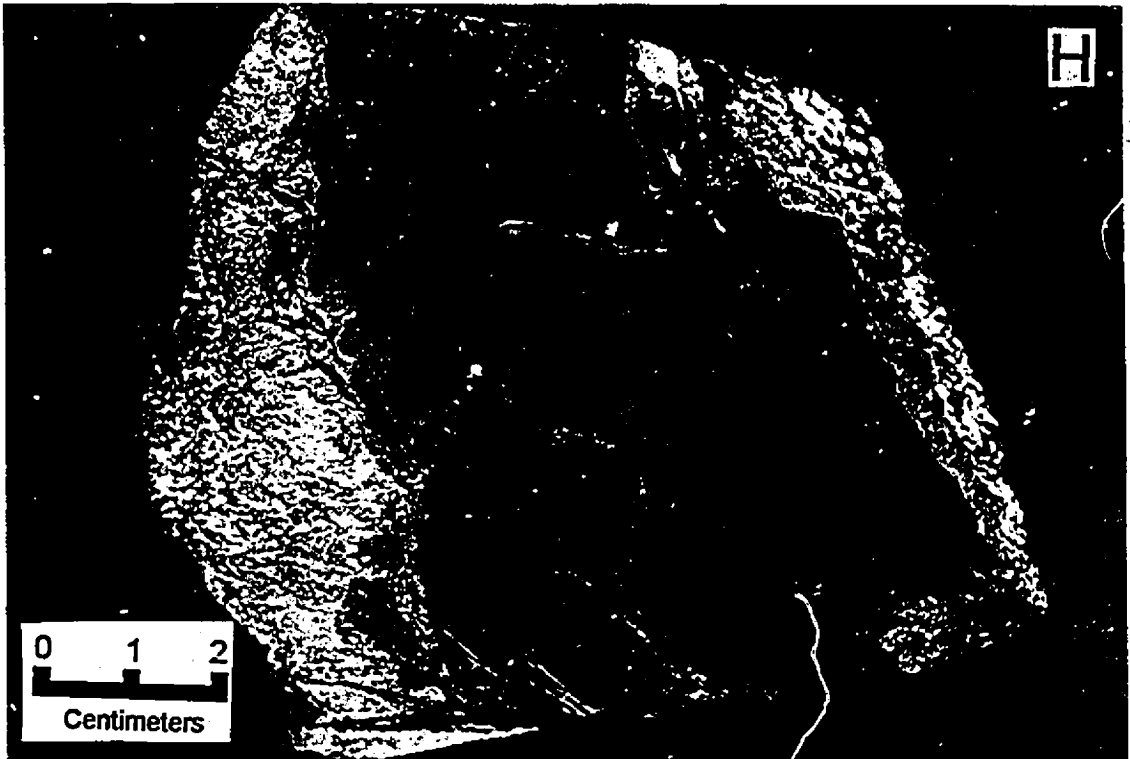
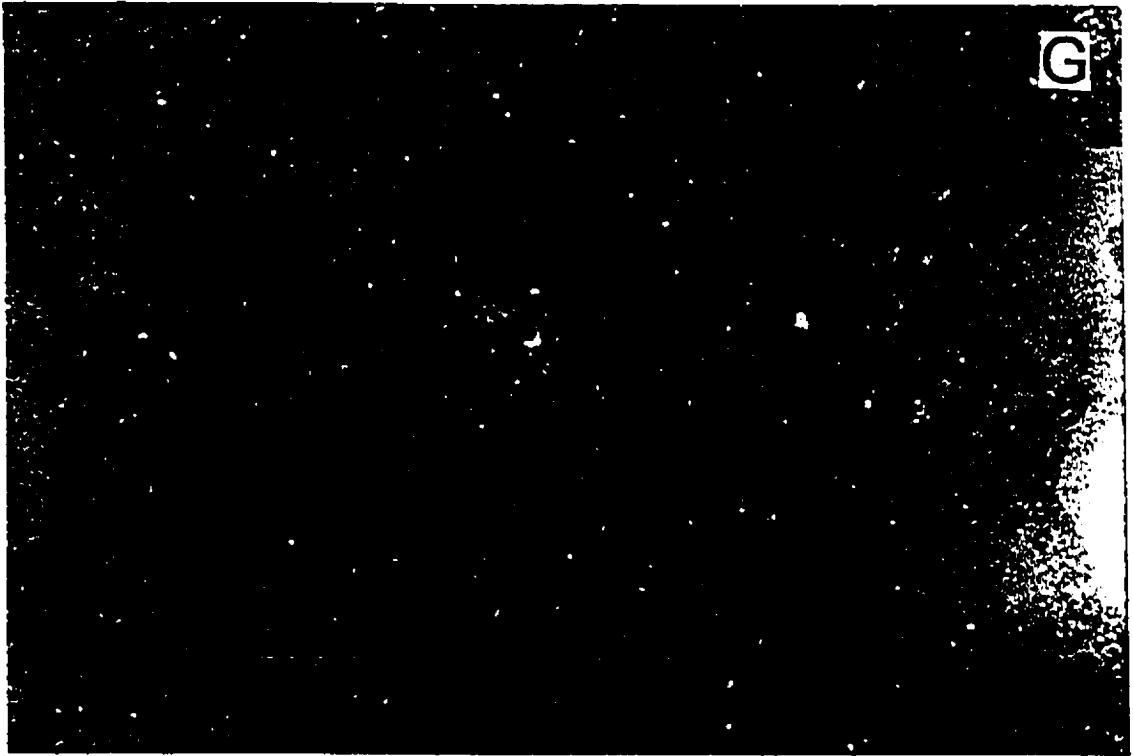


Figure 3-12. G. Enlarged from F, showing one nodule in a dunite fragment; Ore Group XXXI. H. Massive chromitite in contact with dunite that contains nodules and disseminated chromitite; Ore Group XXXI.

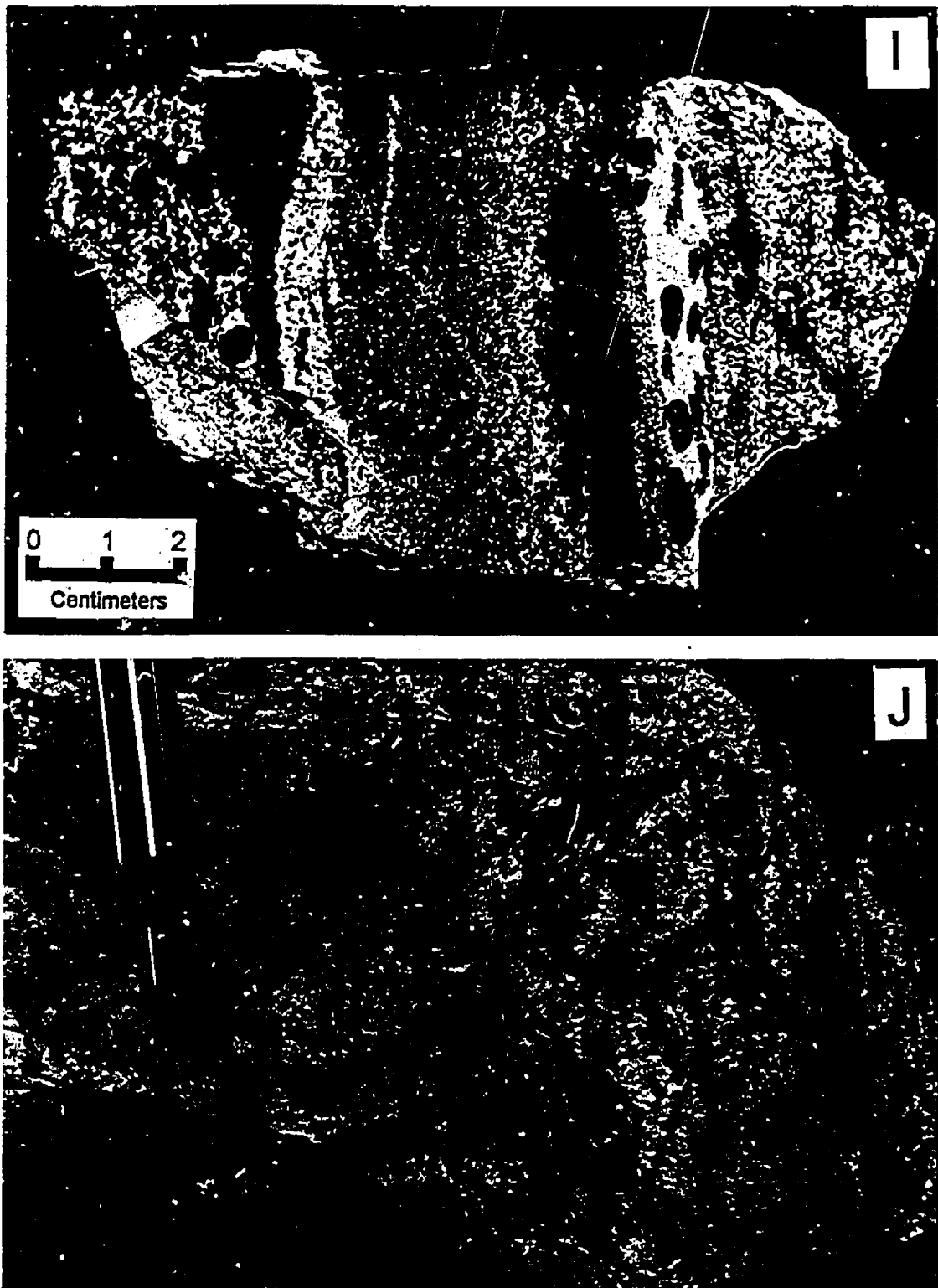


Figure 3-12. I. Banded chromitite composed of massive, disseminated and nodular chromitite layers; Ore Group III. J. Deformed chromitite showing elongate chromite nodules; Ore Group IV.

Nodular varieties consist of small (0.3 to 2.5 cm) spherical or elliptical aggregates of chromite in an Ol-rich matrix that may itself contain disseminated chromite (Figure 3-12C, D). In some cases, individual nodules may be crudely aligned parallel to their long axes (Figure 3-12C, D). Closely associated with nodular chromitites are orbicular types which have a solid, nodule-like nucleus of chromite surrounded by a mantle of Ol and an outermost rim of fine-grained chromite plus Ol. Both types can grade into massive chromitites with increasing amounts of chromite.

In some chromitite bodies, disseminated chromite fills spaces between dunite fragments (Figure 3-12F). The brecciation of the harzburgites or dunites might have been produced by ductile shearing during the late stage of upwelling of a hot mantle diapir.

Banded chromitites, with rhythmically alternating chromite-rich and Ol-rich layers, are present in some chromitite pods (Figure 3-12I). Such banding usually parallels the long axis of the chromitite pods or lenses, which in turn usually parallels the foliation in the host harzburgites. Many bands show small-scale folding, faulting and cataclasis (Figure 3-12J).

The most common silicate mineral in chromitites is Ol. These Ol grains are smaller than those in the adjacent dunites which usually have pegmatitic Ol (Figure 3-13A and B). In addition, typical impregnation textures are present in some samples as chromitites are veinlets in dunite. In such samples, euhedral chromites are interstitial to the large Ol grains (Figure 3-13C). Nodular

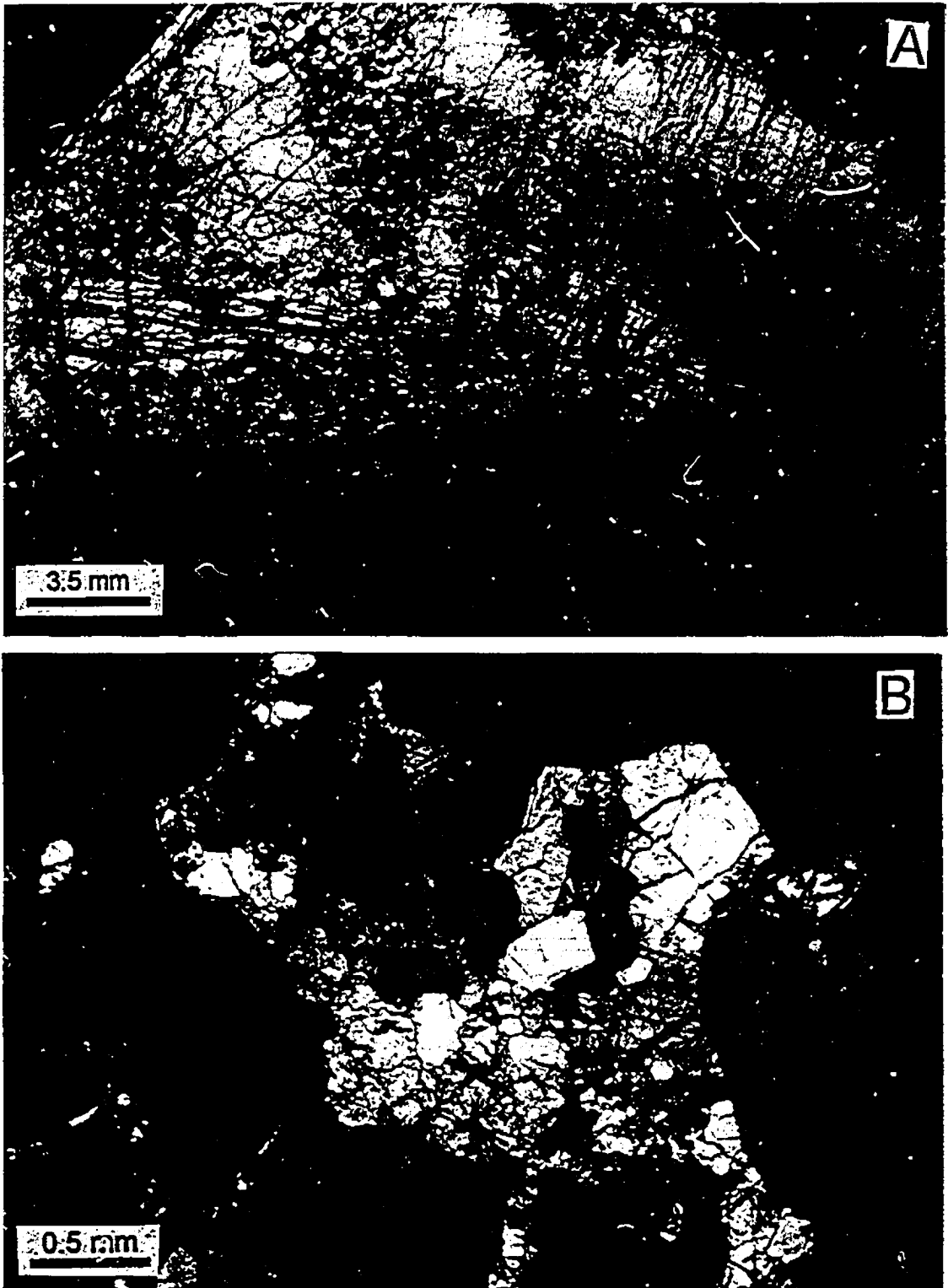


Figure 3-13. Photomicrographs of chromitite: A. Sharp boundary between massive chromitite and coarse-grained dunite; note large sheared Ol grain with recrystallized Ol in shear zones. ZHK6-2, Ore Group XXXI. B. Interstitial Ol grains in massive chromitite; ZHK-L, Ore Group XXXI.

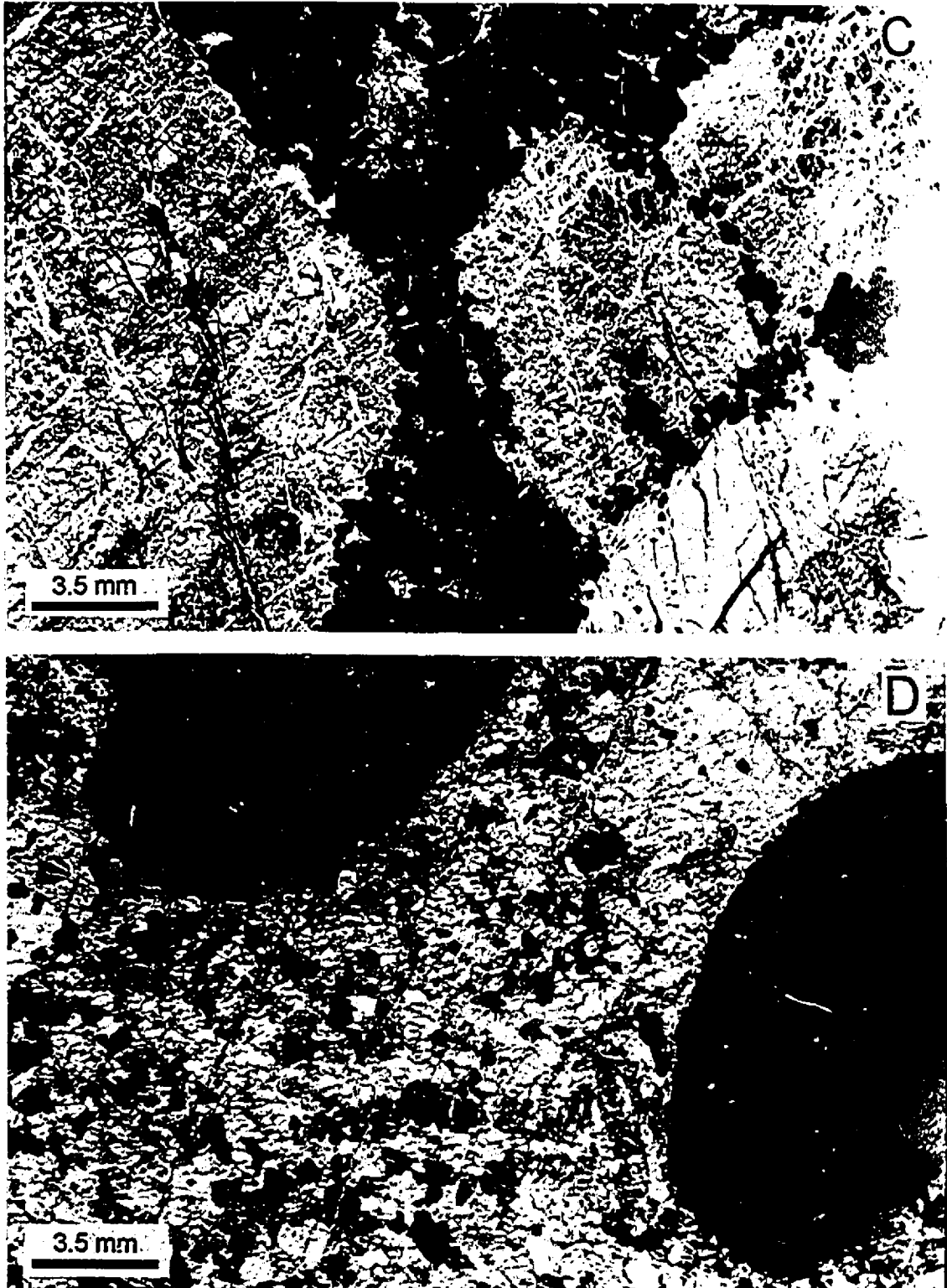


Figure 3-13. C. Massive chromitite interstitial to large Ol grains, resulting from magma impregnation into the dunite; XIV7, Ore Group XIV. D. Two chromitite nodules in a matrix of Ol and euhedral chromite; L29, Ore Group XXXI.

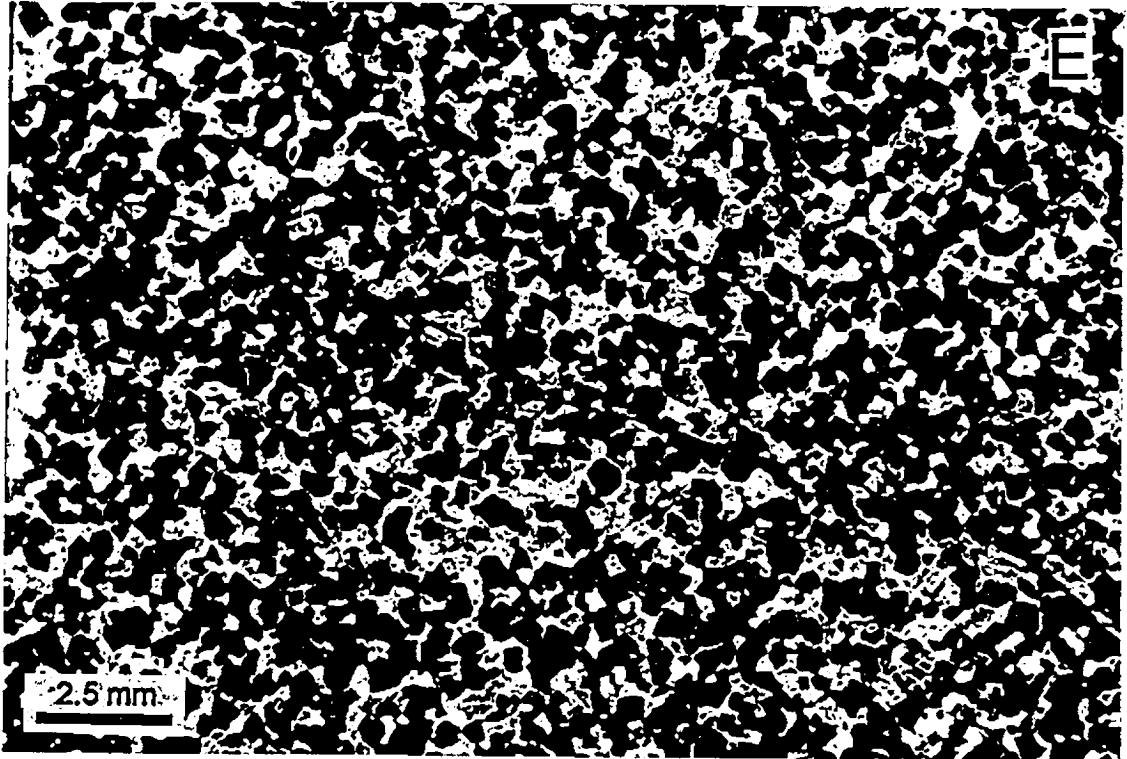


Figure 3-13. E. Disseminated chromitite; nearly euhedral chromite grains form a mesh-texture in an Ol matrix; L25, Ore Group V. F. Dunite with disseminated, euhedral chromites; L27, Ore Group XIV.

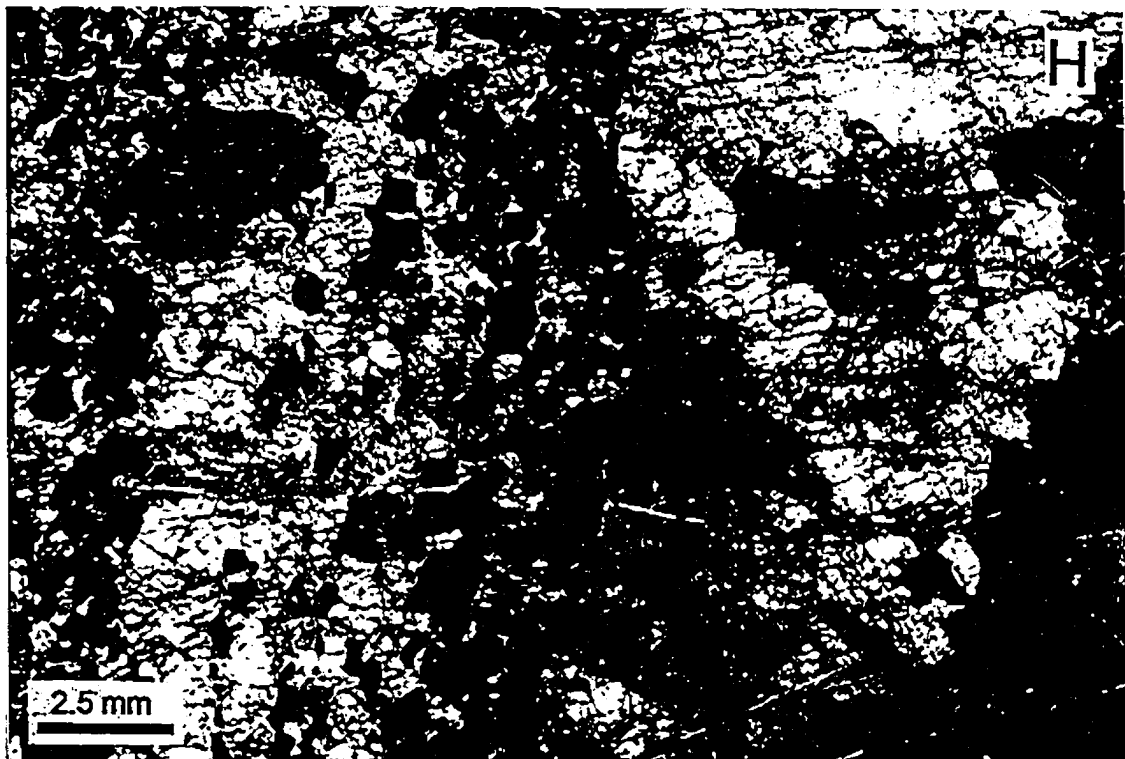


Figure 3-13. G. Layered chromitite. Olivine grains are oriented parallel to the chromitite band. 94L12, Ore Group X. H. Layered chromitite with large Ol grains in dunite, VIII-3, Ore Group VIII.

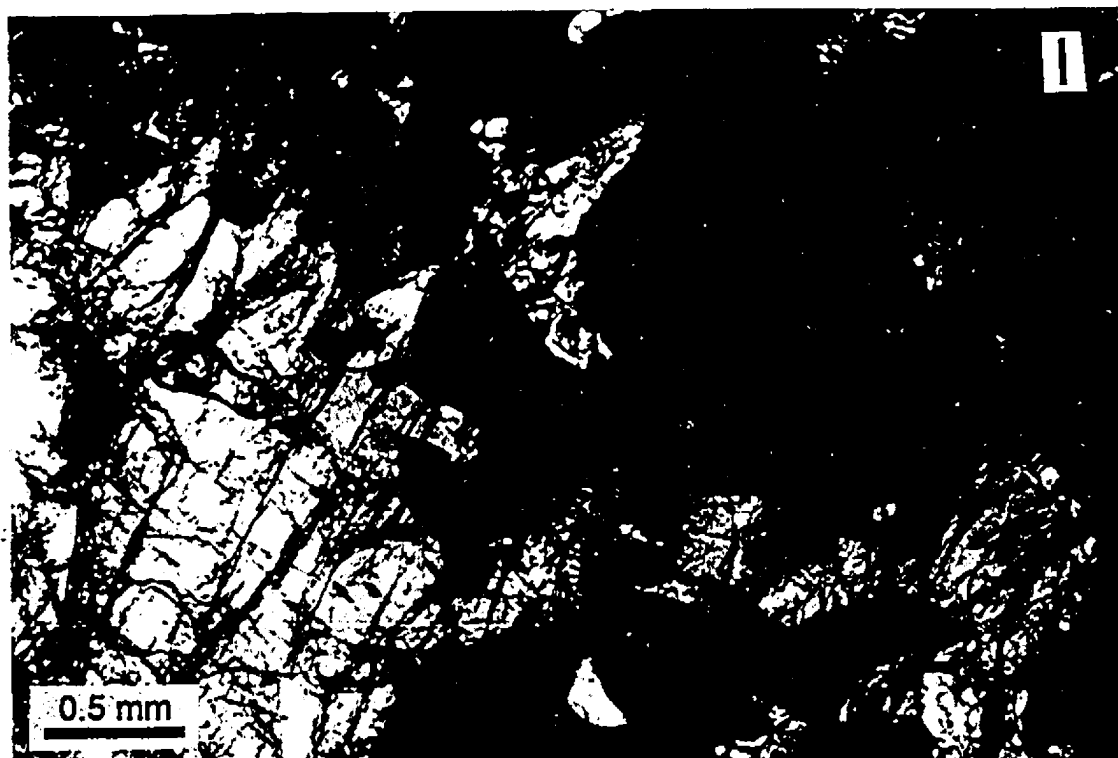


Figure 3-13. I. Opx grain near boundary between dunite and massive chromitite, VIII-6, Ore Group VIII. J. Orthopyroxene grains associated with Ol grains in the matrix of massive chromitite, VIII-6, Ore Group VIII.

chromitites have a matrix of euhedral chromite and Ol, both of which are equal in size (Figure 3-13D). Euhedral or subhedral chromites in some disseminated chromitites form a mesh-texture in which Ol grains are interstitial to the chromite grains (Figure 3-13E) or euhedral chromites are distributed along large Ol grains (Figure 3-13F). In layered chromitites, Ol grains are elongate with their long direction parallel to the layering (Figure 3-13G, H).

Most chromitites contain small amounts of Opx and Cpx that are normally interstitial to the large chromite grains or more often associated with Ol grains (Figure 3-13I, K, J). Some samples have up to 12.9 modal% Opx, suggesting that the parental magma was possibly boninitic.

3.3.4. Deformation history

The microstructures of the harzburgites, dunites and chromitites in Luobusa suggest that they experienced at least three stages of deformation (T. Calon, 1995, personal communication). Stage 1, a high-temperature recrystallization was followed by stage 2, a high-stress deformation. The latter was in turn locally overprinted by stage 3, a mid-crustal level deformation. The characteristics of each stage deformation appear in Table 3-3.

In most samples, the Ol porphyroclasts are clearly elongate, defining a foliation visible only in thin section. The foliation is enhanced by layers of pyroxene or chromite, or by the preferred orientation of elongate grains of pyroxene. These structures have been attributed to "asthenospheric flow" (Nicolas and Poirier, 1976), indicative of ductile, high-temperature deformation in

Table 3-3. Three stages of deformation of the mantle sequence from the Luobusa ophiolite

| | Stage 1 | Stage 2 | Stage 3 |
|-----------------------|--|--|---|
| Stage | Stage 1 | Stage 2 | Stage 3 |
| P, T condition | High T | High P/low T | Mid-P/low T |
| Main features | Recrystallization Foliation of chromite, OI, Opx Coarse-grained OI | Internal plastic deformation (kink-banding), subgrain boundary Exsolution lamellae | Internal plastic deformation (mini-kinking), recrystallization Deformation lamellae |
| Events | Formation of podiform chromite | Subduction of the massif | Uplift of the massif |

the upper mantle. The high-temperature recrystallization textures are also characterized by coarse-grained to very coarse-grained Ol in the dunite (Figure 3-11A to H, K), chromite layering in the chromitites (Figure 3-13G, H), fine Ol tablets in large Ol "porphyroblasts" (Figure 3-11J), and recrystallization of Ol and chromite into a well-developed foam structure (Figure 3-11G, I). These features are typical of a very high temperature, very low differential stress environment as seen in spinel lherzolite mantle xenoliths, and orogenic lherzolite complexes, such as the Ronda, Lherzo, and Beni Bousera massifs (Nicolas and Poirier, 1976). Such high temperature deformation overprinted primary mantle rock microstructures as described in abyssal peridotites (Dick and Natland, 1995; and others). For the large Ol "porphyroblasts", this deformation proceeded largely along the enclosed chromitite bands (Figures 3-11B, 3-13H) [T. Calon, 1995, personal communication].

The intracrystalline extinction band morphology which is typically tapered, wavy, and quite narrowly spaced (Figures 3-7C and 3-8B) is characteristic of the high pressure deformation of the second stage. In addition, exsolution along the slip planes (Figure 3-7F, H), kink banding (Figure 3-7F, H) and dynamic recrystallization (Figure 3-7L) also occurred during this stage.

The stage 2 microstructures were overprinted by a low-temperature/high-differential stress event which led to the development of deformation lamellae along slip planes in Ol (Figure 3-11F), mini-kinking of Ol grains that were unfavourably oriented (Figure 3-11E, F), low-temperature, irregular extinction

band configurations (Figures 3-8B, 3-7C), and very heterogeneously distributed low-temperature, fine-grained dynamic recrystallization within Ol grains, along kinks (Figure 3-11E, G), and along grain boundaries. Sample H3 is a good overview of the stage 3 "cold working" and of low-temperature dynamic recrystallization overprinting of a heterogeneously developed, stage 2 recrystallization, Ol microstructure (Figure 3-7C). This stage of deformation appears to be a characteristic mid-crustal level orogenic overprint that took place in relatively anhydrous conditions.

Discrete low-temperature plastic shear zones which have a "cataclastic" appearance are locally developed (Figure 3-7B). Sample L19 looks like advanced stage 3 deformation (Figure 3-7B). The shears in sample HD3 (Figure 3-9) may truly be cataclastic and possibly later than stage 3.

By considering the tectonic evolution of the region and the mantle peridotites, the first stage recrystallization may have occurred during the formation of podiform chromitites, whereas stage 2 may very well be a deep crustal overprint on the annealed (stage 1) mantle microstructure. During their uplift, these rocks experienced a mid-crustal level dynamic deformation.

The microstructures described above are distinctly different from abyssal mantle peridotites that usually preserve textures of partial melting and plastic deformation (e.g., Dick and Natland, 1995). The deformation succession of the mantle sequence in Luobusa is very similar to what has been described for orogenic, garnet peridotites regionally associated with eclogites (T. Calon, 1995,

personal communication). Therefore the deformation is interestingly consistent with the presence of diamond grains reported earlier (Bai et al., 1993).

3.4. Summary

The mantle sequence of the Luobusa ophiolite is composed of harzburgites and Di-harzburgites with abundant dunites and podiform chromitites. Harzburgites show porphyroclastic textures, whereas dunites are equigranular. The dunites occur as dykes or lenses in the harzburgites or as envelopes surrounding chromitite bodies. The chromitites have nodular, massive and disseminated textures. Silicate minerals in chromitites are chiefly Ol with minor Cpx and variable amounts of Opx.

The mantle peridotites have experienced three stages of deformation (Table 3-3). High-temperature recrystallization occurred along the porphyroclasts of Ol or pyroxenes, possibly during the formation of the podiform chromitites. This recrystallization overprinted the primary mantle microstructure and was, in turn, overprinted by a high-stress deformation. This second stage of deformation is characterized by intracrystalline extinction band morphology of Ol and Opx slip system and exsolution along the slip planes. During uplift, these rocks experienced a third, mid-crustal level, dynamic deformation. This stage of deformation is marked by the development of deformation lamellae along slip planes and mini-kinking of Ol and recrystallization along kinks of Ol. This succession is very similar to what has been described for orogenic garnet

peridotites regionally associated with eclogites (T. Calon, 1995, personal communication).

Chapter 4: GEOCHEMISTRY

4.1. Whole rock geochemistry

4.1.1. Major oxides

Whole-rock major oxides of harzburgites, Di-harzburgites, dunites and chromitites from the mantle sequence of the Luobusa ophiolite are given in Appendix II. Those samples which were also analyzed for trace elements and PGEs are given in Table 4-1.

Whole-rock Mg#s [$100\text{Mg}/(\text{Mg}+\text{Fe})$] range from 91-93 in dunites, 90-91 in harzburgites; and 89-90 in Di-harzburgites. Mg#s correlate negatively with SiO_2 , Al_2O_3 and CaO (Figure 4-1), but are independent of Cr_2O_3 contents (Figure 4-1). Harzburgites and dunites have similar Cr_2O_3 contents ranging from 0.2 to 0.7 wt% (Table 4-1, Appendix II). The harzburgites are depleted rocks with low Al_2O_3 (1.16 ± 0.39 wt%) and CaO (1.25 ± 0.46 wt%) whereas the Di-harzburgites are somewhat less depleted with higher Al_2O_3 (1.73 ± 0.22 wt%) and CaO (1.79 ± 0.43 wt%). As expected, the dunites have very low CaO (0.23 ± 0.11 wt%) and Al_2O_3 (0.20 ± 0.11 wt%) and very high MgO (47 to 50 wt%). These compositions reflect the modal mineralogy of the rocks.

Dunites have much higher Mg/Si ratios (1.79 ± 0.05) than Di-harzburgites (1.38 ± 0.05) or harzburgites (1.49 ± 0.06). In the Al/Si versus Mg/Si diagram (Figure 4-2), Di-harzburgites and harzburgites plot along the geochemical fractionation trend defined by Jagoutz et al. (1979) whereas dunites have higher

Table 4-1. Major oxide (wt%), trace element (ppm) and PGE (ppb) abundances and metal ratios of the mantle peridotites, dunites and chromitites in Luobusa

| Sample | L20 Di-H | L22 Harz | L19 Harz | L6 Harz | L10 Harz | L12 Harz | L17 Harz | L9 Harz | L8 Harz | L13 Dun | L14 Dun | L15 Dun |
|--------------------------------|-------------|-------------|-------------|------------|-------------|-------------|-------------|------------|------------|------------|------------|------------|
| SiO ₂ | 45.1 | 44.4 | 44.9 | 43.8 | 43.7 | 44.7 | 44.8 | 41.5 | 41.2 | 40.6 | 41.2 | 42.5 |
| Al ₂ O ₃ | 0.76 | 0.74 | 0.70 | 1.17 | 1.03 | 0.66 | 1.76 | 0.53 | 0.39 | 0.26 | 0.47 | 0.60 |
| Fe ₂ O ₃ | 9.13 | 8.56 | 8.51 | 9.07 | 8.48 | 8.41 | 8.60 | 8.76 | 10.2 | 6.65 | 7.61 | 5.67 |
| MgO | 42.6 | 45.0 | 44.4 | 43.6 | 44.6 | 45.0 | 42.2 | 47.9 | 47.7 | 51.8 | 50.5 | 50.8 |
| CaO | 1.69 | 0.65 | 0.73 | 1.77 | 1.5 | 0.69 | 1.91 | 0.66 | 0.19 | 0.12 | 0.08 | 0.02 |
| TiO ₂ | 0.02 | 0.02 | 0.02 | 0.03 | 0.03 | 0.02 | 0.04 | 0.02 | 0.02 | 0.01 | 0.02 | 0.01 |
| MnO | 0.15 | 0.15 | 0.15 | 0.15 | 0.14 | 0.13 | 0.15 | 0.14 | 0.18 | 0.12 | 0.13 | 0.12 |
| Cr ₂ O ₃ | 0.54 | 0.47 | 0.51 | 0.43 | 0.46 | 0.36 | 0.49 | 0.51 | | 0.42 | | 0.33 |
| LOI | 12.2 | 2.9 | 3.6 | 2 | 0.2 | 2.6 | 4.7 | 6.2 | 6.1 | 6.9 | 16 | 14.9 |
| Zn | 42 | 45 | 41 | 54 | 52 | 46 | 42 | 45 | | 28 | | 30 |
| Cu | 35 | 13 | 15 | 24 | 16 | 16 | 28 | 5 | | 5 | | 8 |
| Ni | 1787 | 2257 | 2087 | 2261 | 2382 | 2308 | 2045 | 2613 | | 3373 | | 2294 |
| V | 60 | 34 | 49 | 60 | 47 | 37 | 66 | 21 | | 5 | | 9 |
| Cu/Ni | 0.020 | 0.006 | 0.007 | 0.011 | 0.007 | 0.007 | 0.014 | 0.002 | | 0.001 | | 0.003 |
| Os | 3.58 | 1.75 | 3.26 | 2.58 | 1.64 | 0.76 | 1.76 | 1.41 | 0.15 | 1.34 | 1.58 | 2.63 |
| Ir | 6.01 | 5.56 | 5.56 | 5.52 | 3.87 | 1.72 | 4.27 | 2.57 | 1.17 | 2.52 | 2.99 | 5.00 |
| Ru | | | | | | | | | | | | |
| Rh | 1.72 | 2.05 | 1.46 | 1.59 | 1.39 | 0.65 | 1.28 | 0.83 | 0.75 | 0.33 | 0.62 | 0.7 |
| Pt | 10.4 | 8.44 | 10.2 | 8.18 | 5.71 | 2.13 | 7.16 | 2.23 | 5.97 | 1.06 | 2.72 | 1.22 |
| Pd | 11.5 | 4.86 | 7.35 | 7.6 | 3.69 | 3.61 | 7.87 | 1.47 | 1.98 | 3.67 | 4.35 | 2.52 |
| Pt/Pd | 0.90 | 1.74 | 1.39 | 1.08 | 1.55 | 0.59 | 0.91 | 1.52 | 3.02 | 0.29 | 0.63 | 0.48 |
| Pd/Ir | 1.92 | 0.87 | 1.32 | 1.38 | 0.95 | 2.10 | 1.84 | 0.57 | 1.69 | 1.46 | 1.45 | 0.50 |

Table 4-1 (Continued)

| Sample | L16 Dun | L18 Dun | L23 Mass | L24 Diss | L25 Diss | L26 Diss | L27 Diss | L28 Nodu | L29 Nodu | XL1 Nodu | XL5 Nodu |
|--------------------------------|------------|------------|-------------|-------------|-------------|-------------|-------------|-------------|-------------|-------------|-------------|
| SiO ₂ | 40.9 | 40.5 | 0.00 | 9.57 | 14.4 | 32.2 | 25.5 | 6.90 | 16.3 | 9.25 | 7.26 |
| Al ₂ O ₃ | 0.08 | 0.51 | 12.8 | 10.2 | 8.52 | 3.38 | 5.27 | 9.66 | 7.54 | 9.55 | 10.1 |
| Fe ₂ O ₃ | 8.64 | 6.80 | 6.28 | 6.34 | 6.15 | 5.17 | 6.07 | 6.50 | 5.91 | 7.04 | 6.49 |
| MgO | 49.6 | 51.5 | 15.6 | 20.2 | 24.9 | 43.7 | 35.8 | 20.6 | 27.4 | 18.5 | 18.5 |
| CaO | 0.14 | 0.05 | 0.00 | 1.28 | 0.28 | 0.04 | 0.07 | 0.00 | 0.00 | 0.01 | 0.01 |
| TiO ₂ | 0.02 | 0.02 | 0.20 | 0.17 | 0.16 | 0.10 | 0.12 | 0.17 | 0.15 | 0.16 | 0.20 |
| MnO | 0.14 | 0.11 | 0.79 | 0.77 | 0.80 | 0.54 | 0.67 | 0.80 | 0.77 | 0.69 | 0.91 |
| Cr ₂ O ₃ | 0.46 | 0.5 | 64.4 | 51.4 | 44.8 | 14.9 | 26.5 | 55.4 | 420 | 54.8 | 56.5 |
| LOI | 7.1 | 2.4 | 0.0 | 3.8 | 3.1 | 5.6 | 6.8 | 0.9 | 2.2 | 2.4 | 2 |
| Zn | 41 | 27 | 239 | 187 | 178 | 53 | 115 | 224 | 160 | 221 | 289 |
| Cu | 5 | 5 | 44 | 27 | 15 | 5 | 7 | 34 | 14 | 20 | 19 |
| Ni | 2560 | 3468 | 1845 | 2401 | 2922 | 3646 | 3126 | 2262 | 2983 | 2791 | 3075 |
| V | 15 | 8 | 582 | 386 | 323 | 99 | 180 | 462 | 328 | 473 | 443 |
| Cu/Ni | 0.002 | 0.001 | 0.024 | 0.011 | 0.005 | 0.001 | 0.002 | 0.015 | 0.005 | 0.007 | 0.006 |
| Os | 5.1 | 2.48 | 39.7 | 49.1 | 33.4 | 18.5 | 20.9 | 22.3 | 8.57 | 58.1 | 80.6 |
| Ir | 6.53 | 5.75 | 114 | 100 | 72.5 | 62.5 | 96.3 | 50.1 | 18.9 | 38.9 | 64.6 |
| Ru | | | 148 | 145 | 190 | 140 | 114 | 141 | 117 | 212 | 202 |
| Rh | 1.51 | 0.68 | 10.4 | 8.75 | 9.65 | 7.36 | 5.02 | 9.2 | 7.53 | 9.37 | 9.43 |
| Pt | 6.55 | 1.60 | 2.63 | 1.24 | 3.24 | 1.34 | 2.9 | 0.97 | 0.41 | 0.81 | 2.05 |
| Pd | 3.34 | 0.90 | 2.06 | 2.13 | 3.38 | 2.08 | 2.75 | 1.45 | 2.01 | 0.88 | 0.76 |
| Pt/Pd | 1.96 | 1.78 | 1.28 | 0.58 | 0.96 | 0.64 | 1.05 | 0.67 | 0.20 | 0.92 | 2.70 |
| Pd/Ir | 0.51 | 0.16 | 0.02 | 0.02 | 0.05 | 0.03 | 0.03 | 0.03 | 0.11 | 0.02 | 0.01 |

Major oxides were recalculated to 100% on volatile-free basis. Total iron was determined as Fe₂O₃. Blank means that the element was not analyzed. Abbreviations: LOI=loss on ignition; Di-H=Di-harzurgite; Harz=harzburgite; Dun=Dunite; Mass=massive chromitite; Diss=disseminated chromitite Nodu=nodular chromitite.

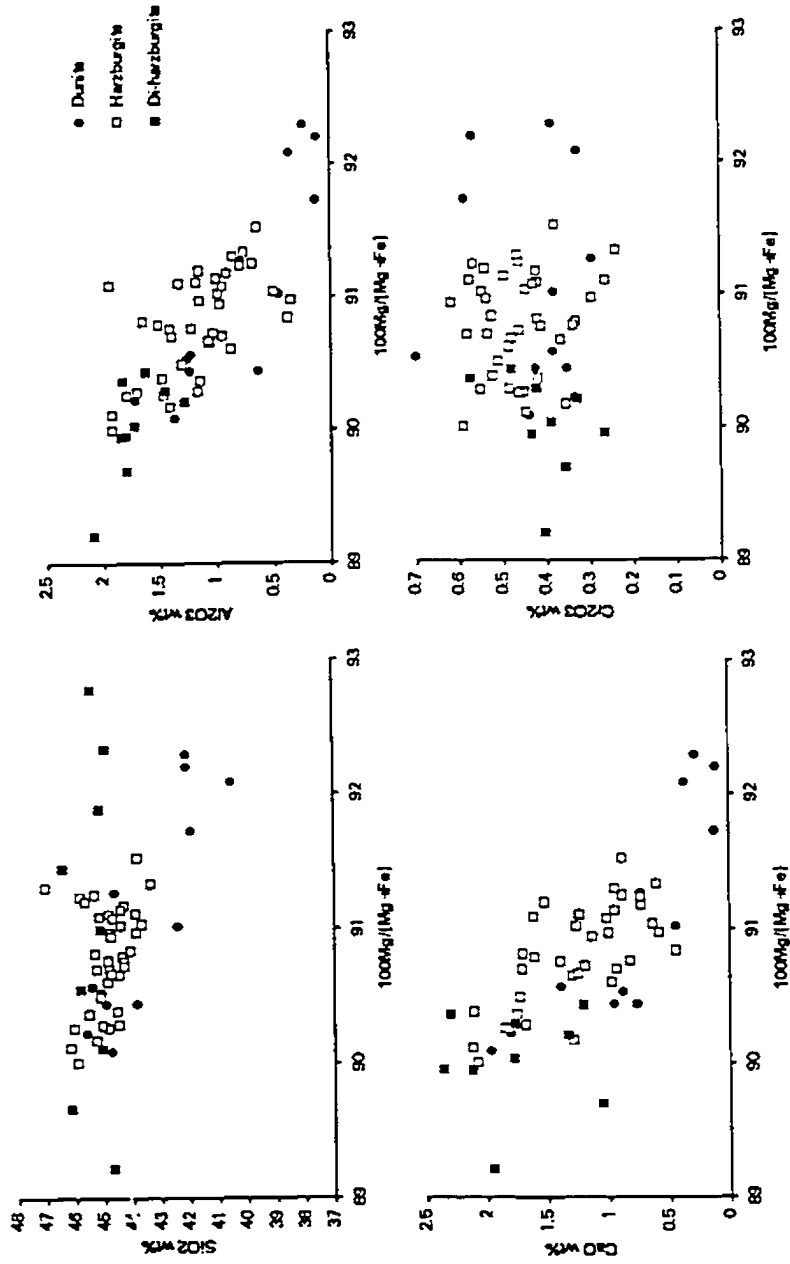


Figure 4-1. Mg# versus oxides of harzburgite and dunite in the mantle sequence of the Luobusa ophiolite.

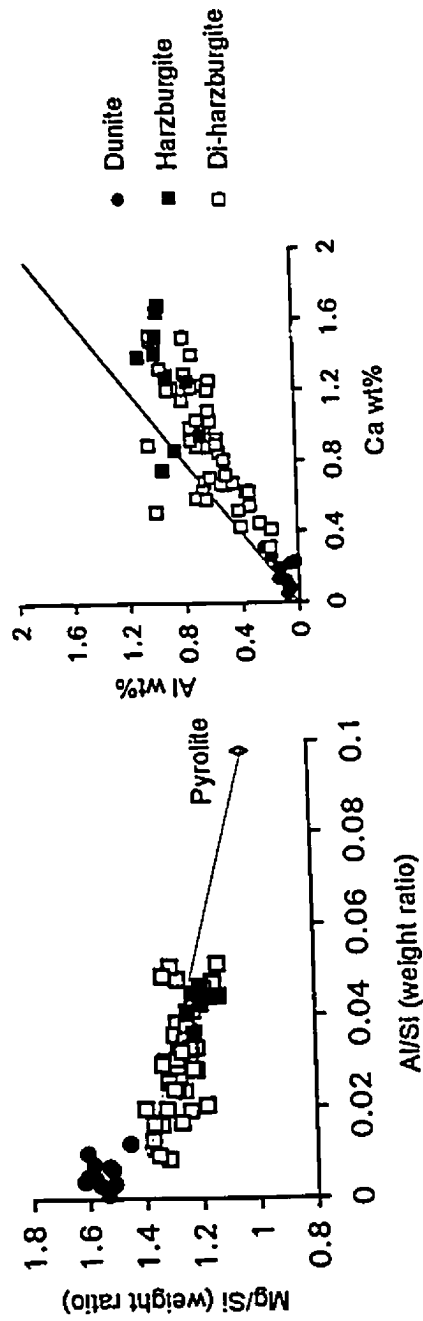


Figure 4-2. Al/Si versus Mg/Si (after Jagoulez et al., 1979) and Ca versus Al (after Boyd, 1989) of harzburgite and dunitite in the mantle sequence of the Luobusa ophiolite.

Mg/Si ratios and lower Al/Si ratios. The peridotites follow an oceanic trend when plotted on a Ca versus Al diagram and are more depleted than the primary mantle (Figure 4-2).

Chromitites vary widely in composition: $\text{SiO}_2=0.42\text{-}34.79$; $\text{Al}_2\text{O}_3=1.07\text{-}12.79$; $\text{FeO}_{\text{total}}=6.73\text{-}15.27$; $\text{MgO}=15.14\text{-}44.08$; $\text{CaO}=0.01\text{-}1.94$; $\text{Cr}_2\text{O}_3=5.97\text{-}64.35$ wt% (Appendix II). The compositions correlate closely with different textural types: Massive chromitites have compositions close to chromite mineral compositions, whereas disseminated chromitites are closer to dunites (Figures 4-3 and 4-4). Exploitable chromitites have an average grade of 48 wt% Cr_2O_3 (Li Zijin et al., 1993), and consist of high-Cr chromite.

In the chromitites, Cr_2O_3 shows a positive correlation with FeO and Al_2O_3 but a negative correlation with SiO_2 and MgO (Figure 4-4). These variations reflect the relative amounts of chromite and Ol.

In a diagram of SiO_2 versus Al_2O_3 (Figure 4-3), the harzburgites have a chemical trend distinct from the chromitites. However, dunites follow the trends defined by both the chromitites and harzburgites. The compositional gap between the chromitites and dunites may be the result of sampling bias. These characteristics indicate that the peridotites and chromitites are different in origin; the peridotites represent a residue left after partial melting and chromitites formed by crystallization from magmas. The dunites bridge the gap between the two.

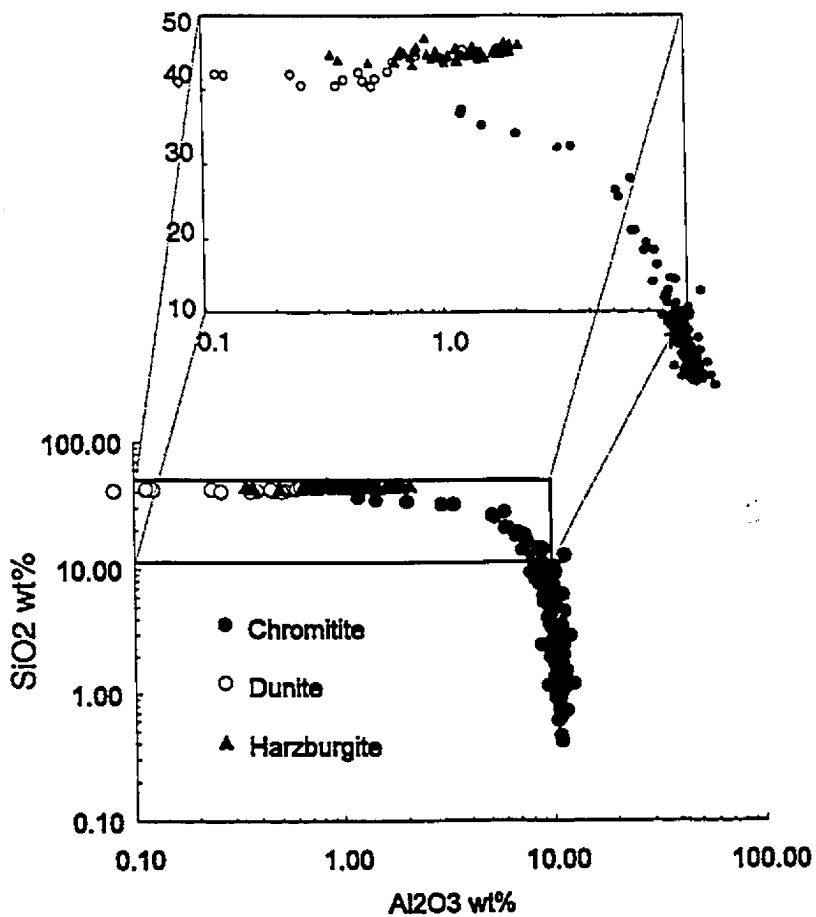


Figure 4-3. Log plots of SiO₂ versus Al₂O₃ of chromitite, dunite, and harzburgite from the mantle sequence of the Luobusa ophiolite, showing two different chemical trends.

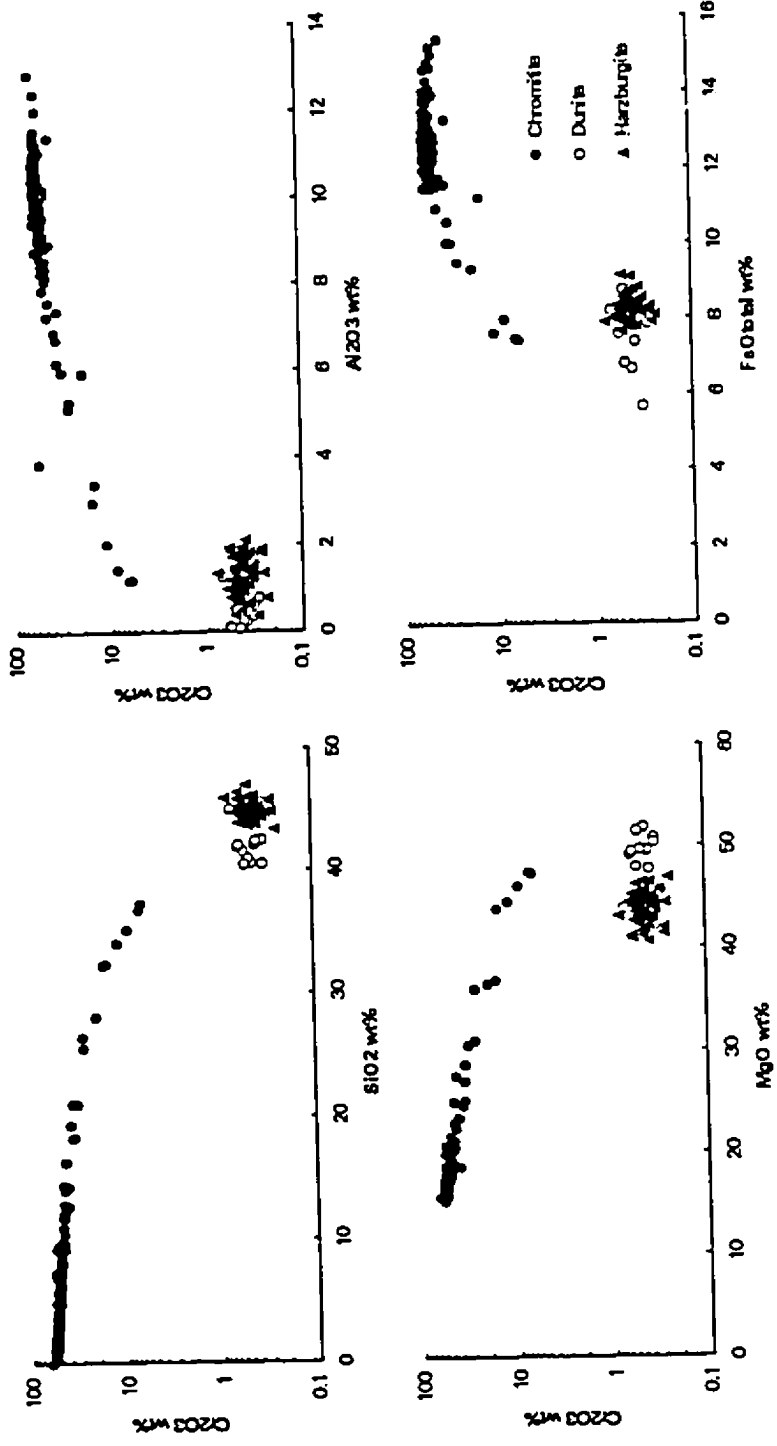


Figure 4-4. Cr₂O₃ versus SiO₂, Al₂O₃, MgO and FeO of chromitite, dunite, and harzburgite from the mantle sequence of the Luobusa ophiolite.

4.1.2. Platinum-group elements, Cu, Zn, V and Mn

Harzburgites and Di-harzburgites in Luobusa have PGE values similar to those of sulphide-bearing residual mantle (Barnes et al., 1985; Lorand, 1989; Edwards, 1990; Leblanc, 1991; Lorand et al., 1993). Overall, the harzburgites and Di-harzburgites have relatively unfractionated, chondrite-normalized PGE patterns (Figure 4-5). Sample L20, a diopsidic harzburgite, has the highest Pd (11.5 ppb) and Pt (10.4 ppb) contents (Table 4-1). This sample is slightly depleted in Os, possibly due to incomplete recovery during preconcentration due to the volatile nature of its oxide (Sun et al., 1993; Zhou, 1994).

Dunites have similar Os and Ir contents as harzburgites but lower Rh, Pt, and Pd contents. All but one of the dunites (sample L13) have negative Pt anomalies (Figure 4-5).

Chromitites have wide ranges of Os (8.57-81 ppb), Ir (19-114 ppb), and Pt (0.07-2.86 ppb) and smaller ranges of Ru (202-212 ppb), Rh (4.92-10 ppb), and Pd (0.52-2.43 ppb) [Table 4-1]. They have relatively uniform PGE-normalized distributions and are characterized by enrichment of Os, Ir, and Ru (IPGE, iridium group of PGEs) and depletion in the Rh, Pt and Pd (PPGE, palladium group of PGEs). They have a negatively sloping, chondrite-normalized pattern (Figure 4-5), a feature typical of podiform chromitites (Page and Talkington, 1984; Naldrett and von Gruenewaldt, 1989). The Pt and Pd contents of chromitites are lower than those of harzburgites and all samples show a slightly negative Pt anomaly (Figure 4-5). Variations in PGE abundances and chondrite-

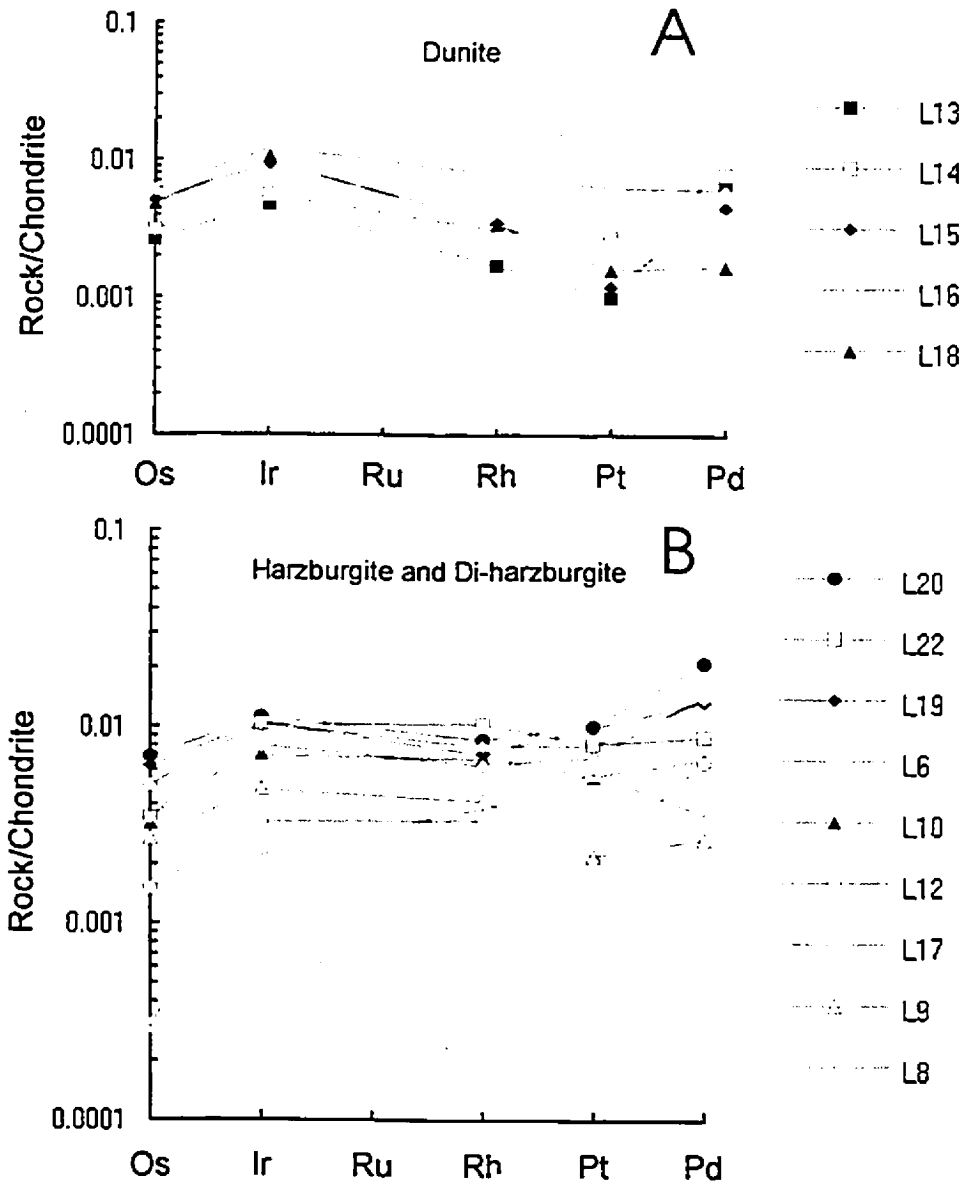


Figure 4-5A and B. Chondrite-normalized PGE patterns of harzburgite and dunite from the mantle sequence of the Luobusa ophiolite. Normalization values are from Naldrett and Duke (1980).

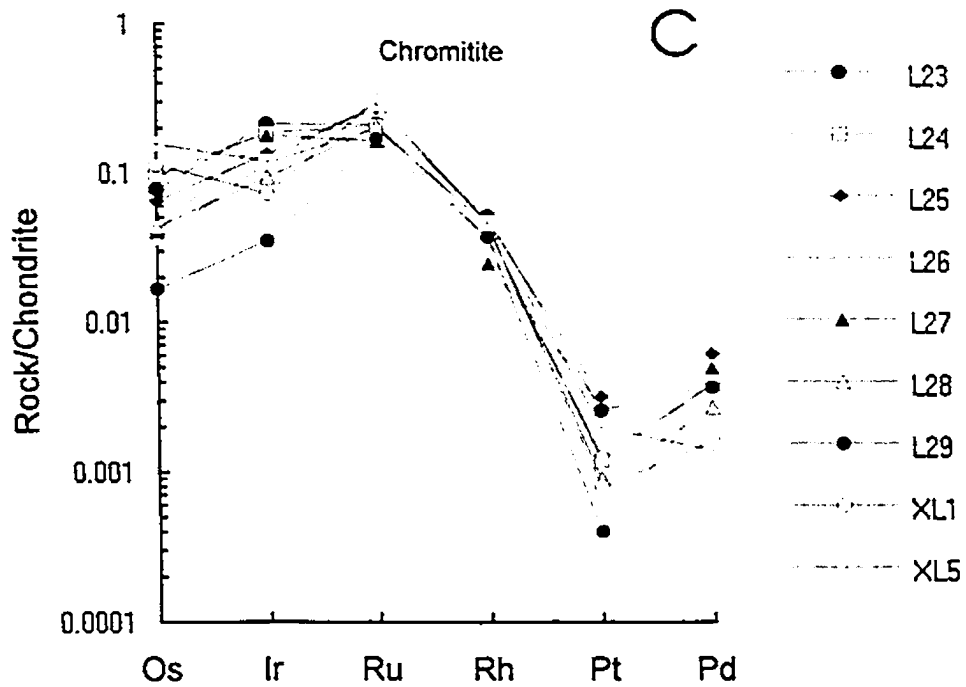


Figure 4-5C. Chondrite-normalized PGE patterns of chromitite from the mantle sequence of the Luobusa ophiolite. Normalization values are from Naldrett and Duke (1980).

normalized patterns of chromitites do not correlate with the distribution of the chromitite bodies, their textural types, their bulk rock compositions, or chrome contents. This is consistent with the observation of von Gruenewaldt et al. (1989) that high IPGE/PPGE ratios are characteristic of all chromite-enriched rocks in the Potgietersrus area of the Bushveld Complex, regardless of the amount of chromite in the rock.

V, Cu, Zn, Mn contents increase with Pd/Ir ratios from harzburgite to Di-harzburgite, whereas Mg#s decrease (Figures 4-6 and 4-7). Both Cu/Ni and Pd/Ir ratios increase from harzburgite to diopsidic harzburgite. This variation suggests a removal of a partial melt enriched in Pd, leaving a refractory residuum relatively enriched in Ir (Leblanc, 1991). The high Pd content and high Pd/Pt ratio (1.1) of sample (L20) indicate fractionation of Pt and Pd. Similar high Pd contents are observed in Iherzolites of the Zabargad ophiolite and in the Ivrea Verbano orogenic-type peridotite massifs (Garuti et al., 1984). These Iherzolites also have higher whole-rock Cu contents than the associated harzburgites, a feature attributed to the low melting point of sulphide components relative to silicate minerals (Garuti et al., 1984; Lorand, 1989).

Chromitites have lower Pd/Ir ratios but higher V, Zn, Cr, Mn contents and Ni/Pd ratios than the mantle peridotites (Table 4-1 and Figures 4-6 and 4-7).

Dunites have Pd/Ir ratios intermediate between harzburgites and chromitites. However, they have the lowest Zn, V and Cu (Figures 4-6 and 4-7). It is known that IPGEs, being more refractory than PPGEs, are removed during

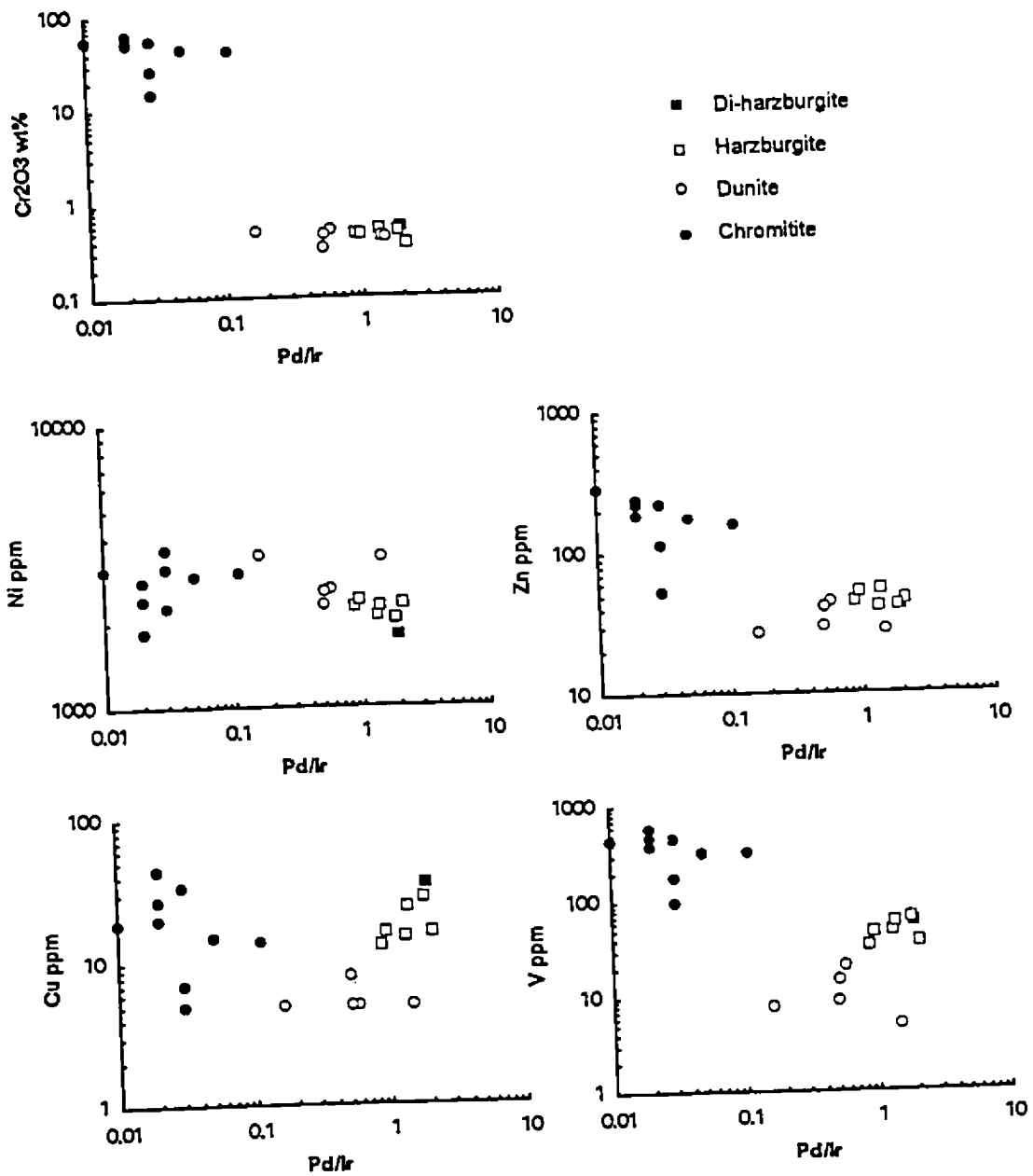


Figure 4-6. Pd/Ir ratios versus Cr₂O₃, Ni, Zn, Cu, and V of harzburgite, dunite, and chromitite from the Luobusa ophiolite.

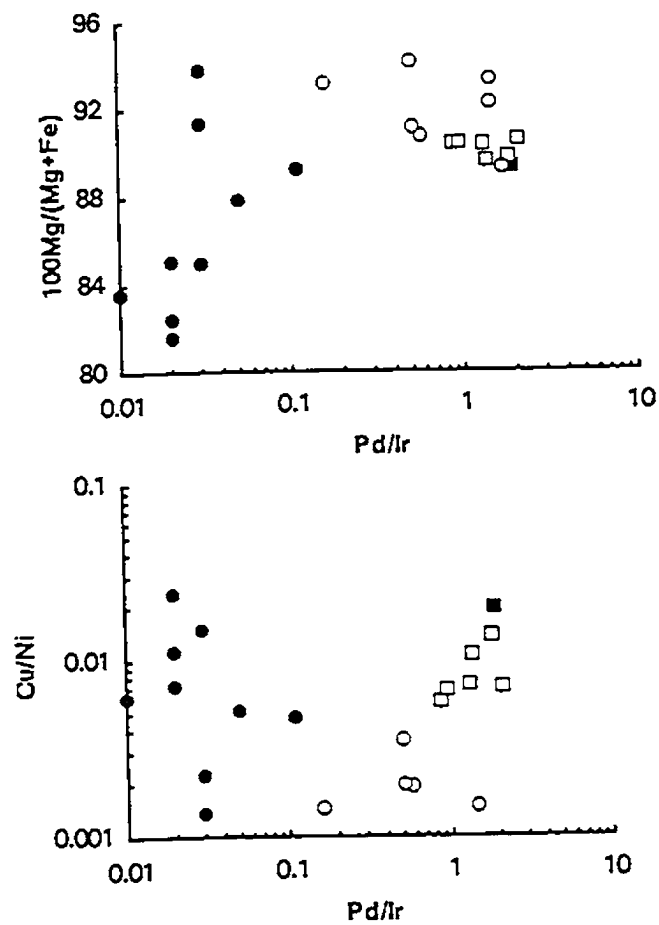


Figure 4-7. Pd/Ir ratios versus Cu/Ni ratios and Mg# of harzburgite, dunite, and chromitite from the Luobusa ophiolite.

the early stages of crystallization from the melt, whereas PPGEs are mostly retained, and are enriched in more fractionated liquids (Barnes et al., 1985, Edwards, 1990). Accordingly, PGE patterns of the chromitites can be explained by precipitation of laurite, erlichmanite and Os-Ir alloys. These IPGE-bearing minerals normally occur as inclusions in chromite grains and might have crystallized earlier than chromite (Stockman and Hlava, 1984; Talkington and Lipin, 1986).

4.2. Mineral chemistry

4.2.1. Chromite

Chromites in harzburgites, dunites and chromitites in the mantle sequence of the Luobusa ophiolite show a wide range of composition with Cr# varying from less than 19 to 82 (Appendix III-1). Overall, Al_2O_3 contents of chromites show a negative correlation with Cr_2O_3 and $\text{FeO}_{\text{total}}$ and a positive correlation with MgO (Figure 4-8). Total iron is relatively uniform and is independent of Cr_2O_3 but shows a strong reciprocal variation with MgO.

Cr#s of accessory chromites in harzburgites range from 19 to 66 and are negatively correlated with Mg#'s (Figure 4-9). The Cr#s increase as the modal proportion of pyroxene decreases and appear to correlate with the degree of partial melting (Dick and Bullen, 1984). Decreasing Mg#s can be due to changing partition coefficients for Mg and Fe between chromite and Ol with increasing chromite Cr#s (Irvine, 1965; Dick and Bullen, 1984). Generally, these

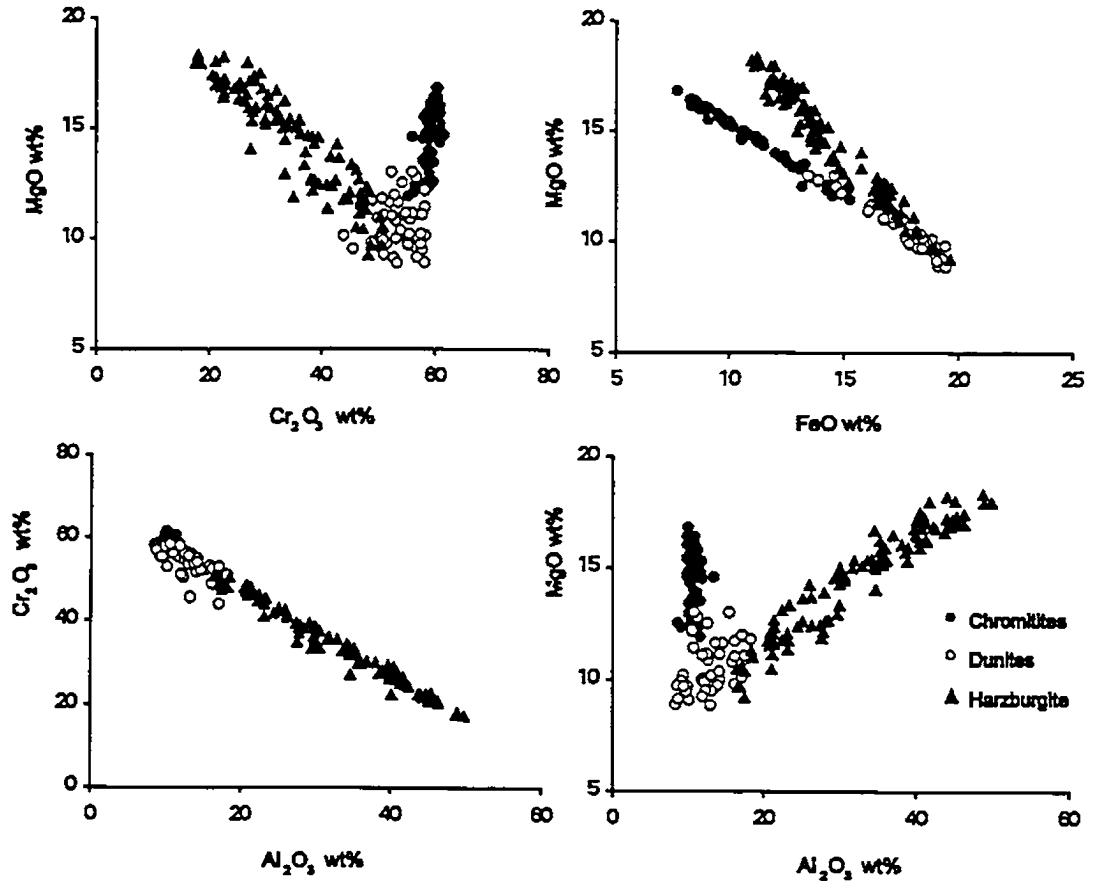


Figure 4-8. Inter-elemental relationships of chromite from the mantle sequence of the Luobusa ophiolite.

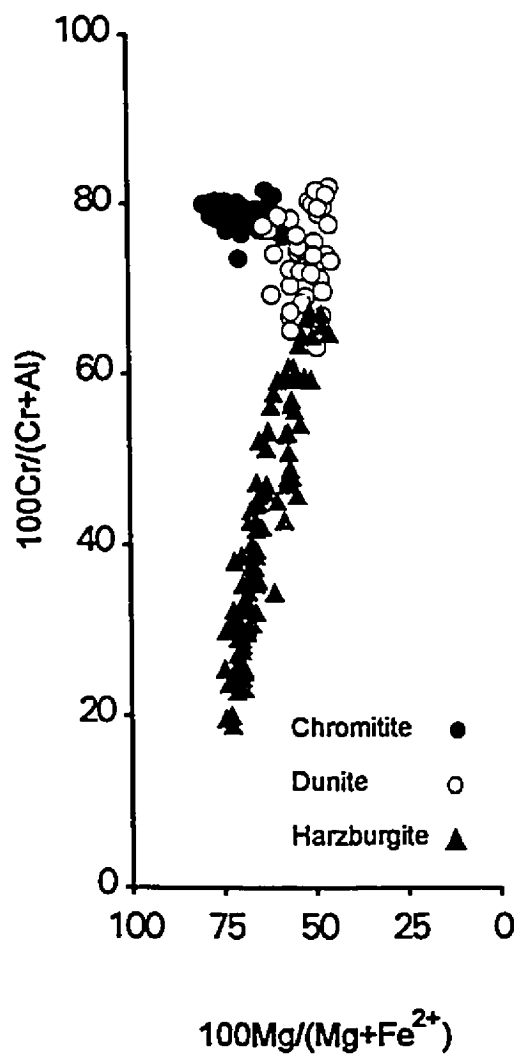


Figure 4-9. Cr# versus Mg# of chromite in dunite, harzburgite, and chromitite in the mantle sequence of the Luobusa ophiolite.

chromites fall within the Alpine field (Irvine, 1967).

Chromites in chromitites have very uniform Cr# (Appendix II-1), ranging from 74 to 82 but show almost the same variations in MgO and FeO_{total} as accessory chromites in the harzburgites (Figure 4-8). They have higher MgO and lower FeO_{total} than the dunites (Figure 4-8). The Mg#s of chromite in chromitites (58-80) are relatively high but decrease with increasing proportions of silicate minerals (Appendix III-1). This relationship has been attributed to subsolidus diffusion, particularly of Fe and Mg, between chromite and silicate minerals during cooling (Irvine, 1965; Roeder et al., 1979; Lehmann, 1983). Such a subsolidus exchange may also have resulted in higher Mg#s of chromites in the chromitites than in the dunites (Figure 4-9).

Generally, residual chromites in the harzburgites are compositionally distinct from those in the chromitites although there is some overlap between the fields of chromitite and dunite (Figure 4-9). Dunites have chromites compositionally intermediate between the harzburgites and chromitites (Figure 4-9). Chromites in the harzburgites have much lower Ti contents than those in chromitites, whereas chromites in chromitites and dunites have similar Ti contents (Figure 4-10).

In sample L29, large grains in nodules have higher Cr₂O₃, Al₂O₃, and Mg#, but lower FeO_{total} and Cr#, than small, disseminated grains in the matrix (Figure 4-11). No significant variation was observed within a single grain. Chromites in many podiform bodies have Fe- and Al-rich margins (e.g. Ahmed,

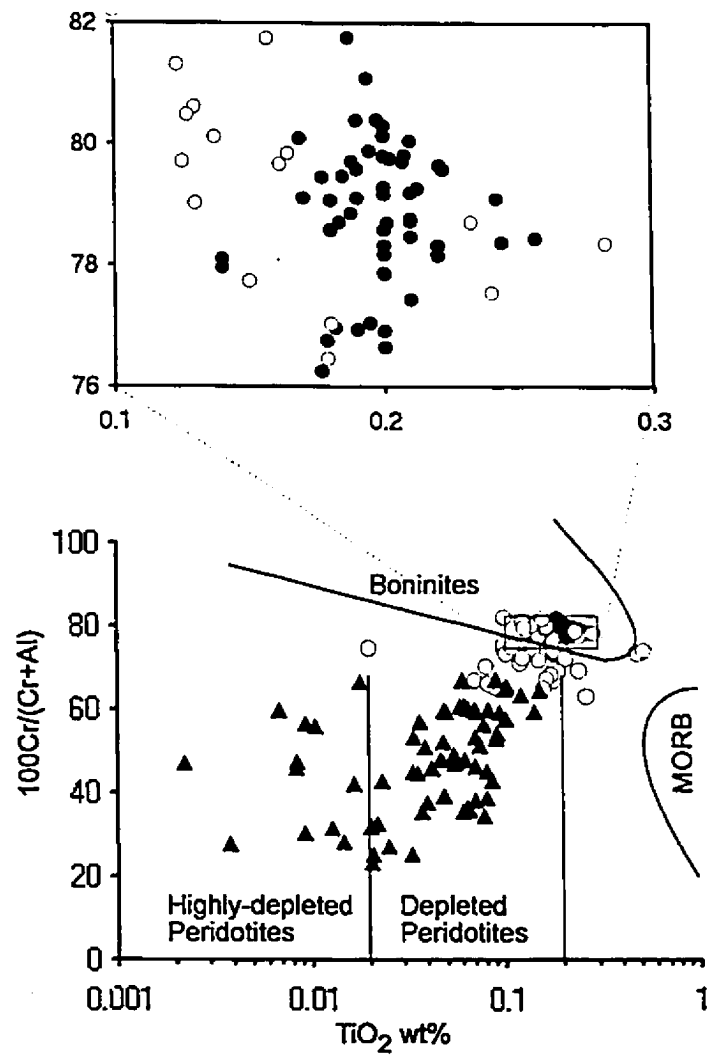


Figure 4-10. Log TiO_2 versus Cr# of chromite, showing distinct fields of boninitic rocks and MORB (after Dick and Bullen, 1984). Fields of depleted peridotites are from Jan and Windley (1990). Chromite in chromitite of Luobusa plots entirely in the boninitic field. Legends as in Figure 4-8.

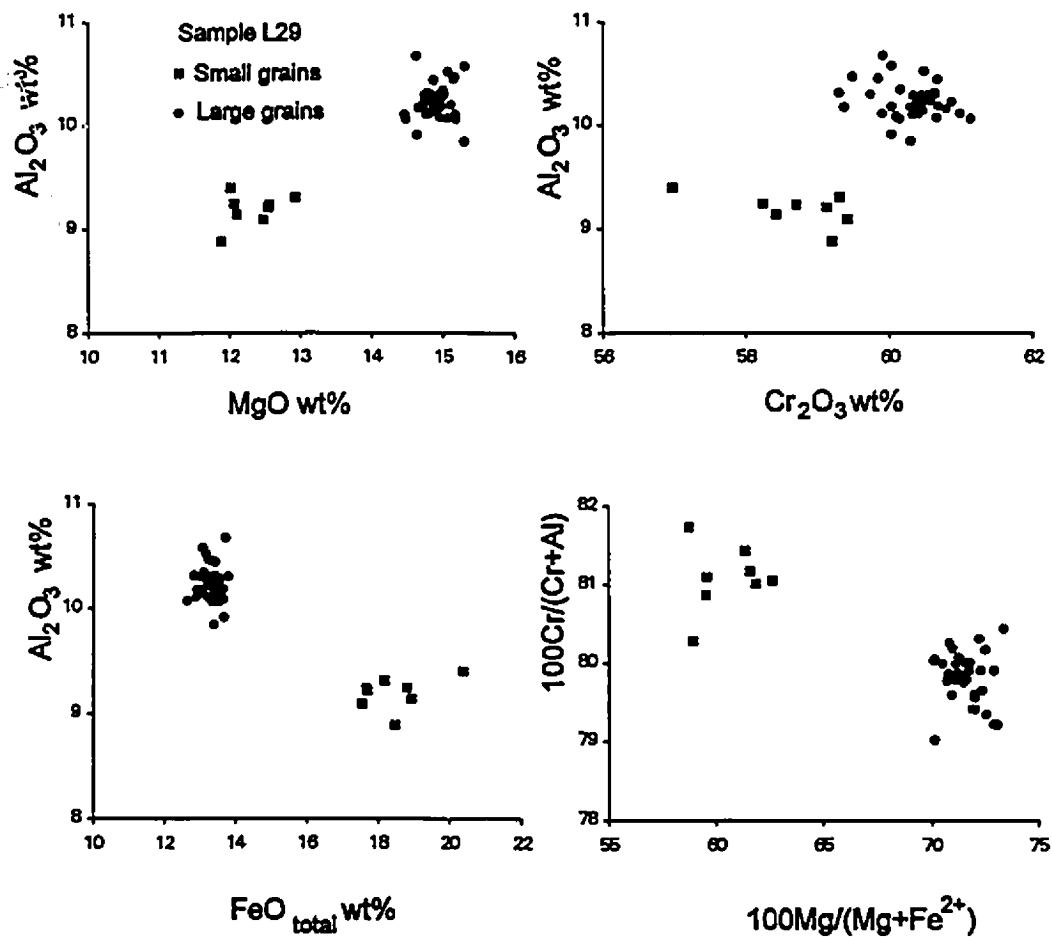


Figure 4-11. Compositional differences between large (nodular) and small (disseminated) chromites in sample L29. Petrographic description as in Figure 3-13D.

1984), which may reflect post-magmatic alteration associated with serpentinization. In Luobusa, there are no significant variations in chromite compositions within a single chromitite body or with depth of the body in the mantle. This is in contrast with many other podiform chromitites which show a positive correlation between Cr content of chromites and depth in the mantle (e.g., Ahmed, 1984).

Chemical analyses were carried out on a 14-cm-wide transition zone from a small chromitite band through dunite to harzburgite to Di-harzburgite host (Figure 3-6A and Table 4-2). Chromites in this transition zone span the entire range of chromite compositions from the mantle sequence of the Luobusa ophiolite. Cr#'s and Cr_2O_3 decrease systematically from the chromitite pod to the Di-harzburgite whereas Al_2O_3 increases (Figure 4-12). Mg#'s and MgO contents decrease systematically from Di-harzburgite to dunite and $\text{FeO}_{\text{total}}$ follows a complementary trend (Figure 4-12). Chromites in the chromitite have higher MgO and lower $\text{FeO}_{\text{total}}$ than those in the adjacent dunites. Ti contents of the chromites decrease from the chromitite to the host peridotites.

4.2.2. Olivine

Olivines in the harzburgites and Di-harzburgites are compositionally uniform with Fo values (90 to 92), higher than those of Ol in most abyssal peridotites (average Fo=90.8, Dick et al., 1984). They represent a residuum after extraction of MORB magmas. Olivines in the massive chromitites are the most magnesian (Fo_{96-97}), but those in disseminated chromitites are also of the

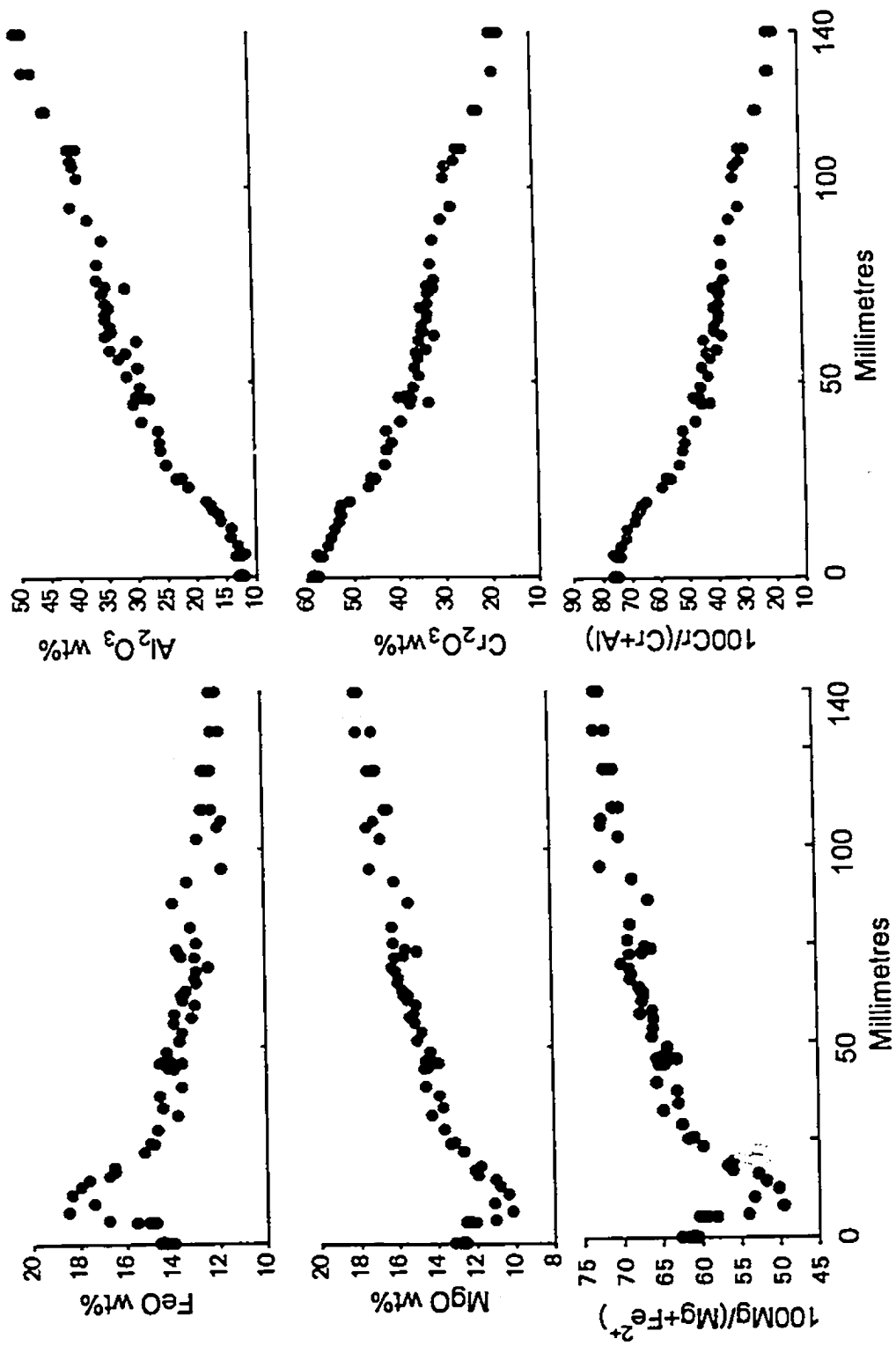


Figure 4-12. Compositional variations of chromite in the reaction zone from chromite to dunite to harzburgite to Di-harzburgite. Petrographic description as in Figure 3-6A.

high-Fo variety (Fo_{93-96}). These Ol grains are too magnesian to have crystallized from a melt and probably owe their composition to Mg-Fe subsolidus exchange between silicates and chromite (Irvine, 1965; Roeder et al., 1979). The dunites also contain Ol of somewhat higher Fo value (91.5-93.5) than the peridotites. This might indicate that the original Ol in chromitites also had high Fo values, although these values were subsequently modified by subsolidus Mg-Fe exchange. The high-Fo Ol in dunites and chromitites suggest that chromitites crystallized from a boninitic magma, as documented by chromite chemistry (Figures 4-9 and 4-10).

Olivines in the mantle rocks of the Luobusa ophiolite have trace amounts of CaO and MnO and variable NiO (Appendix III-2). NiO contents of the Ol in the harzburgites and dunites are similar. However, the high-Fo Ol of the massive chromitites has high Ni contents (Figure 4-13) similar to those of Ol in komatiites. The high-Ni Ol in chromitites may suggest that they were derived from highly refractory melts.

Chemical variations of Ol through a transitional zone from chromitite to dunite to harzburgite to Di-harzburgite are shown in Figure 4-14: NiO and Fo values decrease. These changes cover the whole range of the rock suite in Luobusa as discussed above. Chemical variations of Ol in this reaction zone suggest that the magmas from which chromitites crystallized were not in equilibrium with the host peridotites.

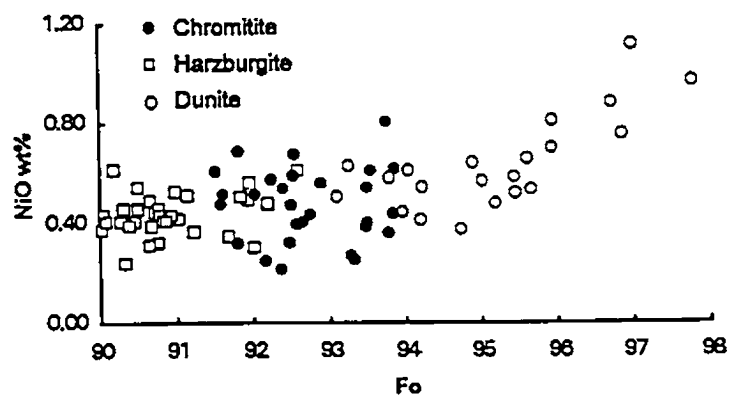


Figure 4-13. Fo versus NiO of Ol in harzburgite, dunite, and chromitite from the mantle sequence of the Luobusa ophiolite.

4.2.3. Pyroxenes

Pyroxenes in harzburgites, dunites and chromitites are compositionally uniform: Opx is all in the enstatite field and Cpx in the diopside field (Figure 4-15). Orthopyroxenes in the harzburgites have En values ranging from 87 to 92. Those in the dunites have relatively narrow En values (90.5 to 92.5). The chromitites have high-En Opx (En=91.5 to 95). In general, these compositions are similar to many other ophiolites (Coleman, 1977).

MgO in Opx correlates negatively with FeO and Al_2O_3 , whereas FeO varies positively with Al_2O_3 (Figure 4-16). Al_2O_3 , FeO, CaO correlate negatively with En (Figure 4-17). CaO in Opx shows no correlation with other oxides, reflecting the fact that Ca in Opx does not correlate with mantle melting. Opx in the harzburgites, dunites, and chromitites has similar Ca contents (CaO=0.25 to 1.0 wt%), with the exception of some Opx grains in the harzburgites that have higher CaO contents (CaO=1 to 2.5 wt%). These grains also have the lowest En values (87 to 89). Interestingly, they form a continuous chemical trend with Opx in the dunites and chromitites. This trend is distinctly different from other Opx in the harzburgites as shown in diagrams of CaO versus Al_2O_3 , MgO, and FeO (Figure 4-16). These Opx crystals have relatively lower Al_2O_3 , and FeO but higher MgO than those in the harzburgites and are believed to be magmatic in origin. Opx in the dunites and high-Ca Opx in the harzburgites may be generated by magma impregnation associated with the formation of chromitites.

Alumina contents in pyroxene are known to be sensitive to the degree of

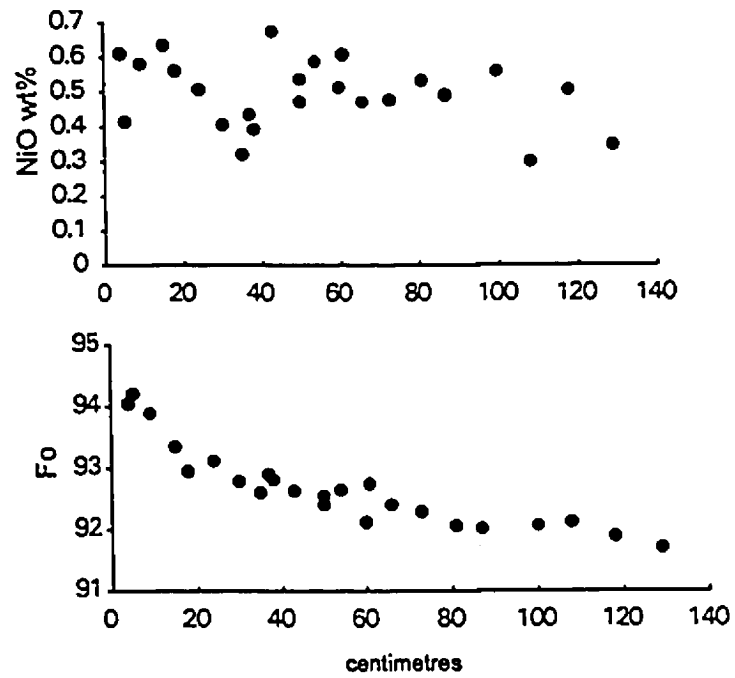


Figure 4-14. Compositional variations of Ol through a transitional zone from chromitite to dunite to harzburgite to Di-harzburgite.

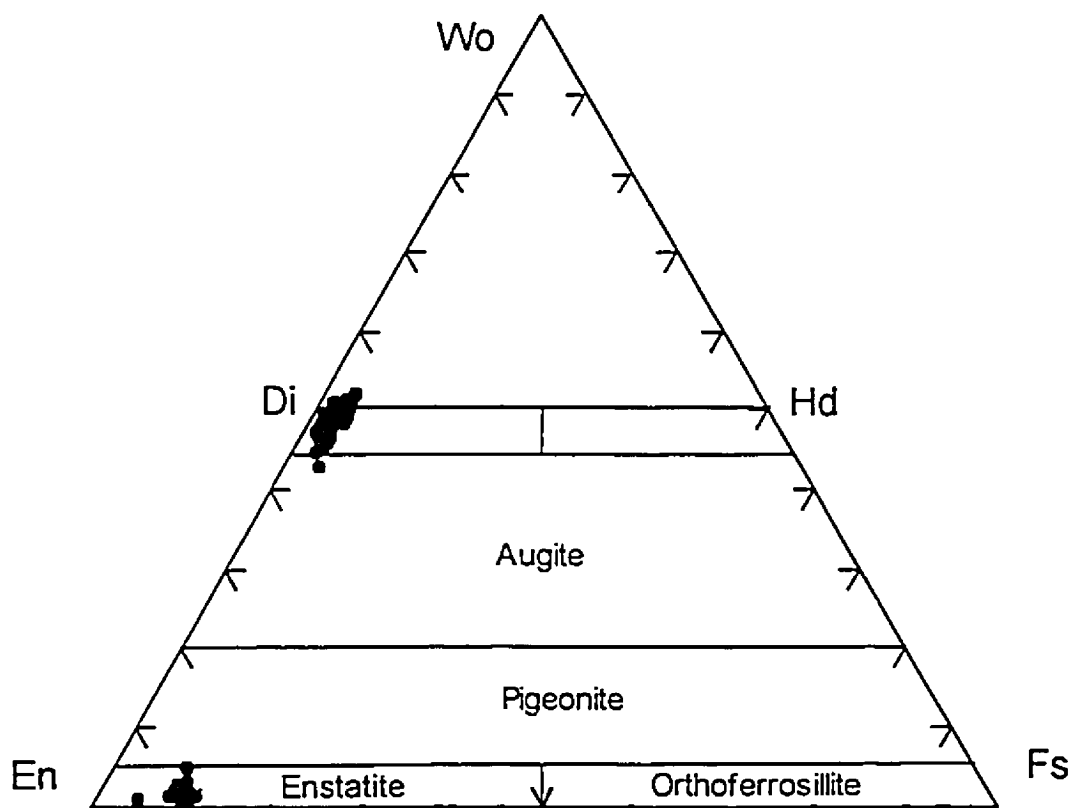


Figure 4-15. "Di-En-Fs" diagram of pyroxenes in harzburgite, dunite and chromitite in the mantle sequence of the Luobusa ophiolite.

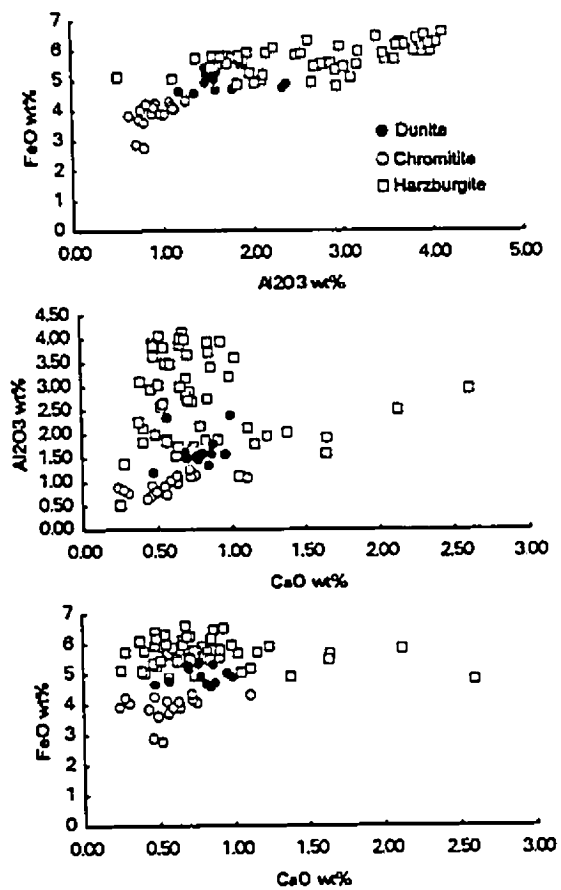


Figure 4-16. Inter-elemental relationships of Opx in harzburgite, dunite and chromitite in the mantle sequence of the Luobusa ophiolite.

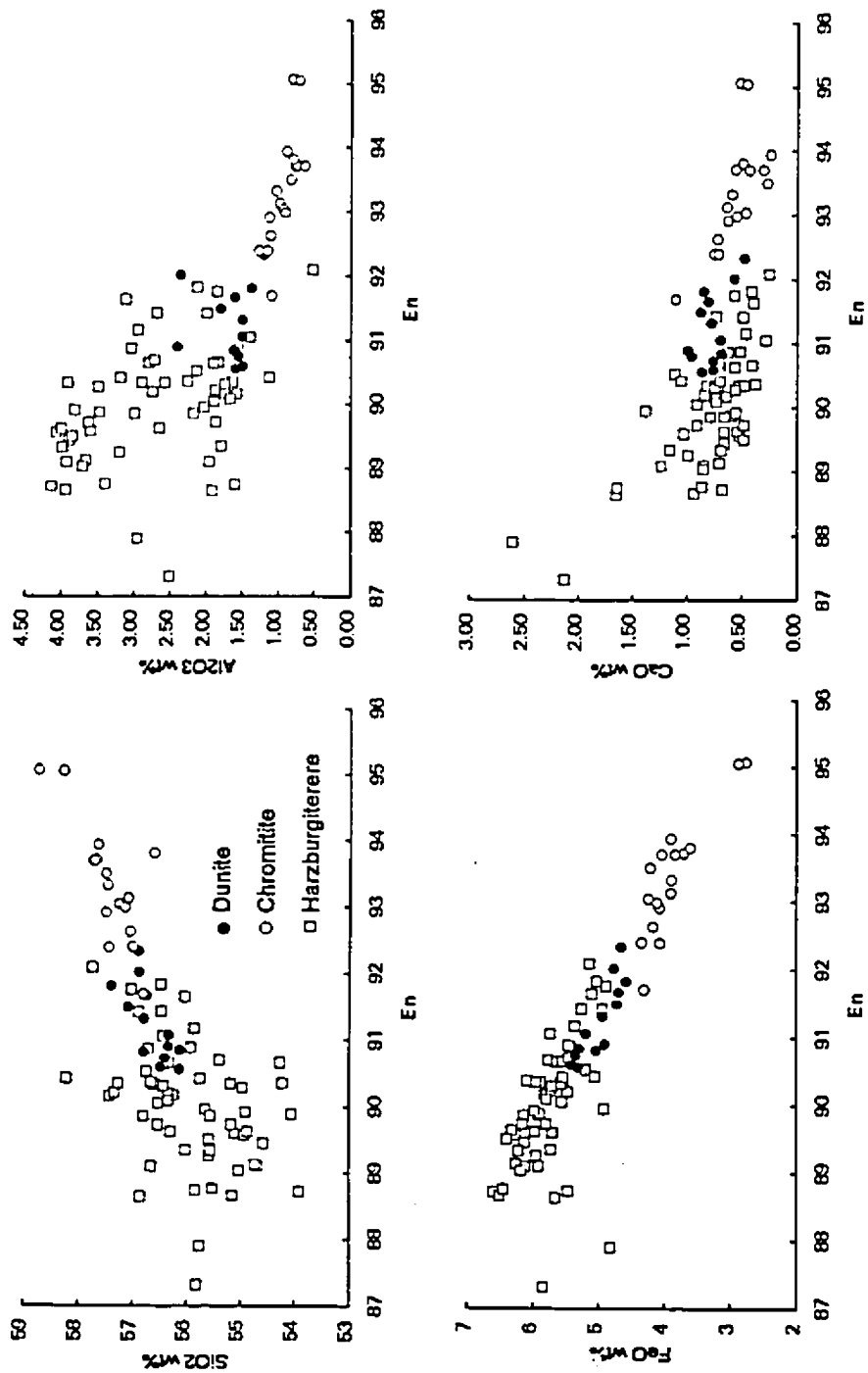


Figure 4-17. En versus oxides of Opx in harzburgite, dunite, and chromitite in the mantle sequence of the Luobusa ophiolite.

mantle melting, decreasing systematically with increasing depletion of peridotites (e.g., Dick, 1977; Dick and Natland, 1995). Al_2O_3 contents (1.0 wt%) of Opx in the harzburgites of Luobusa are much lower than in abyssal peridotites (2.19 to 5.0% from depleted to undepleted harzburgites, Dick and Natland, 1995). This suggests that the Luobusa peridotites are more depleted than normal abyssal peridotites.

Orthopyroxenes in the harzburgites have variable Cr_2O_3 (0.14 and 0.88 wt%) and Na_2O (0.01 to 0.49 wt%) [Appendix III-3]. Those in the dunites have somewhat lower Na_2O (0.01-0.24 wt%), but similar Cr_2O_3 (0.41-0.65 wt%). Cr_2O_3 (0.32-0.82 wt%) of Opx in the chromitites is also similar but Na_2O (0-0.09 wt%) is lower (Appendix III-3). Accordingly, partial melting in the upper mantle does not affect the Cr contents of Opx.

Clinopyroxene in harzburgites has a large range of Mg#s [$100\text{Mg}/(\text{Mg}+\text{Fe}+\text{Ca})$] from 44.5 to 53, whereas that in dunites and chromitites is similar with Mg#s generally between 47 and 52.5.

SiO_2 and Al_2O_3 in Cpx are negatively correlated, but there is a positive relation between FeO and Al_2O_3 (Figure 4-18). Cr_2O_3 and CaO contents do not vary with the rock type and show only a weak correlation with other oxides (Figure 4-18). Both elements in Cpx as well as in Opx are not sensitive to mantle melting. Clinopyroxene in the harzburgites has Cr_2O_3 (0.32 to 1.25 wt%) and Na_2O (0.08 to 0.46 wt%). Those in the dunites have similar Cr_2O_3 (0.54 to 1.19 wt%) and Na_2O (0.16 to 0.35 wt%). Clinopyroxene in the chromitites has

wider ranges of Cr_2O_3 (0.34 to 1.56 wt%), and Na_2O (0.03 to 0.76 wt%).

Clinopyroxene in the dunites and chromitites has relatively higher SiO_2 but lower Al_2O_3 and FeO than that in harzburgites, supporting the view that the chromitites crystallized from a boninitic magma.

Chemical variations of pyroxenes vary through a transitional zone from Di-harzburgite to harzburgite to dunite to chromitite. As shown in Figure 4-19, Al_2O_3 contents of Opx and Cpx decrease, whereas En values and Mg#'s increase. FeO contents of Cpx show a small decrease, whereas CaO contents of Opx increase and then decrease in the chromitite. The low-Ca, low-Al but high-Mg pyroxenes in chromitites suggest that they may have crystallized from a boninitic magma. These variations suggest that the parental magmas of chromitites were not in equilibrium with the host peridotites.

4.3. Summary

Harzburgites (Mg#'s=89 to 91) are depleted in Ca and Al and are essentially residual rocks. Chromitites, which formed by crystallization from magmas, have a distinctly different chemical trend from the harzburgites, whereas dunites are intermediate between the two chemical trends defined by the harzburgites and chromitites. The harzburgites have flat PGE patterns, but the chromitites and dunites have PGE patterns depleted in Pt and Pd. The chromitites have lower Pd/Ir but higher V, Zn, Cr, and Mn contents than the harzburgites. The dunites have Pd/Ir ratios intermediate to the harzburgites and

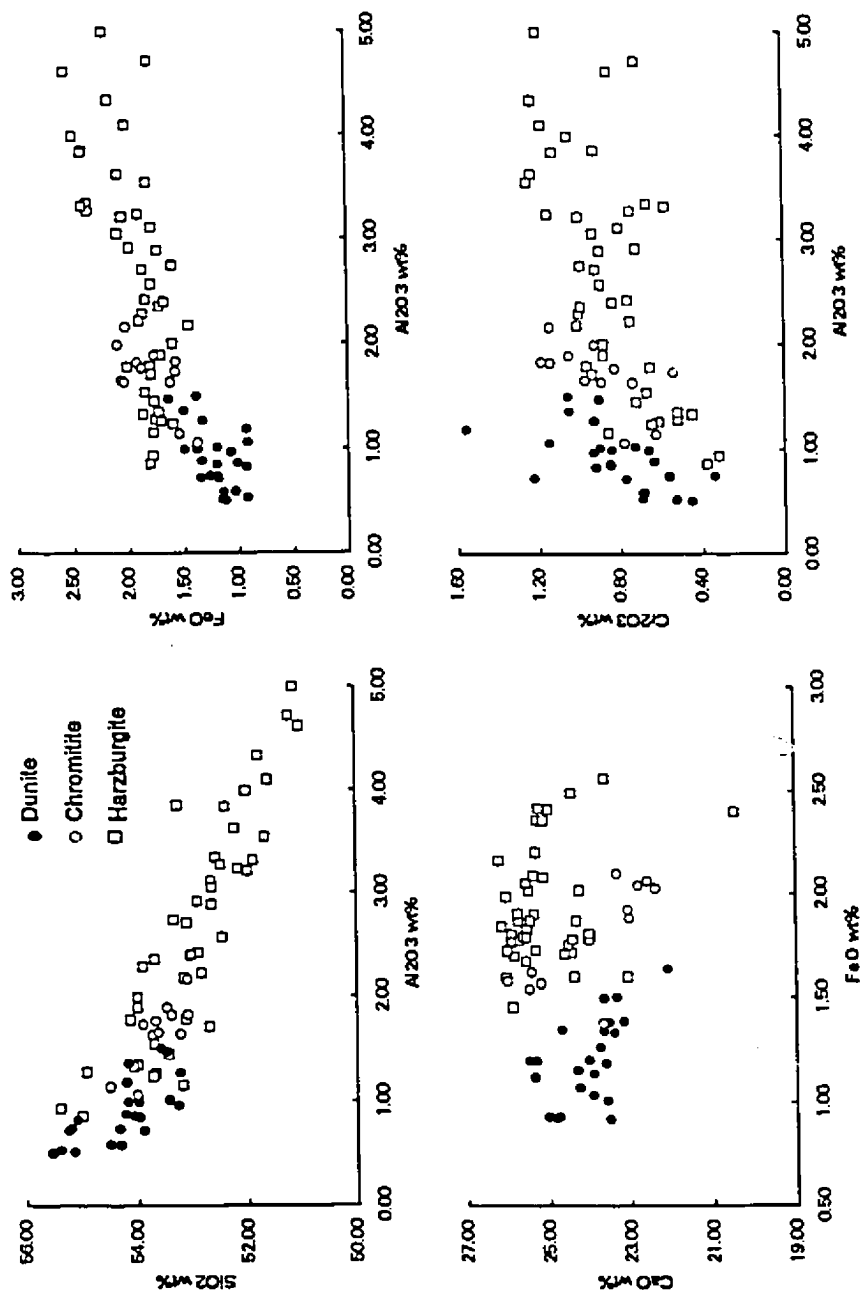


Figure 4-18. Inter-elemental relationships of Cpx in harzburgite, dunite, and chromitite in the mantle sequence of the Luobusa ophiolite.

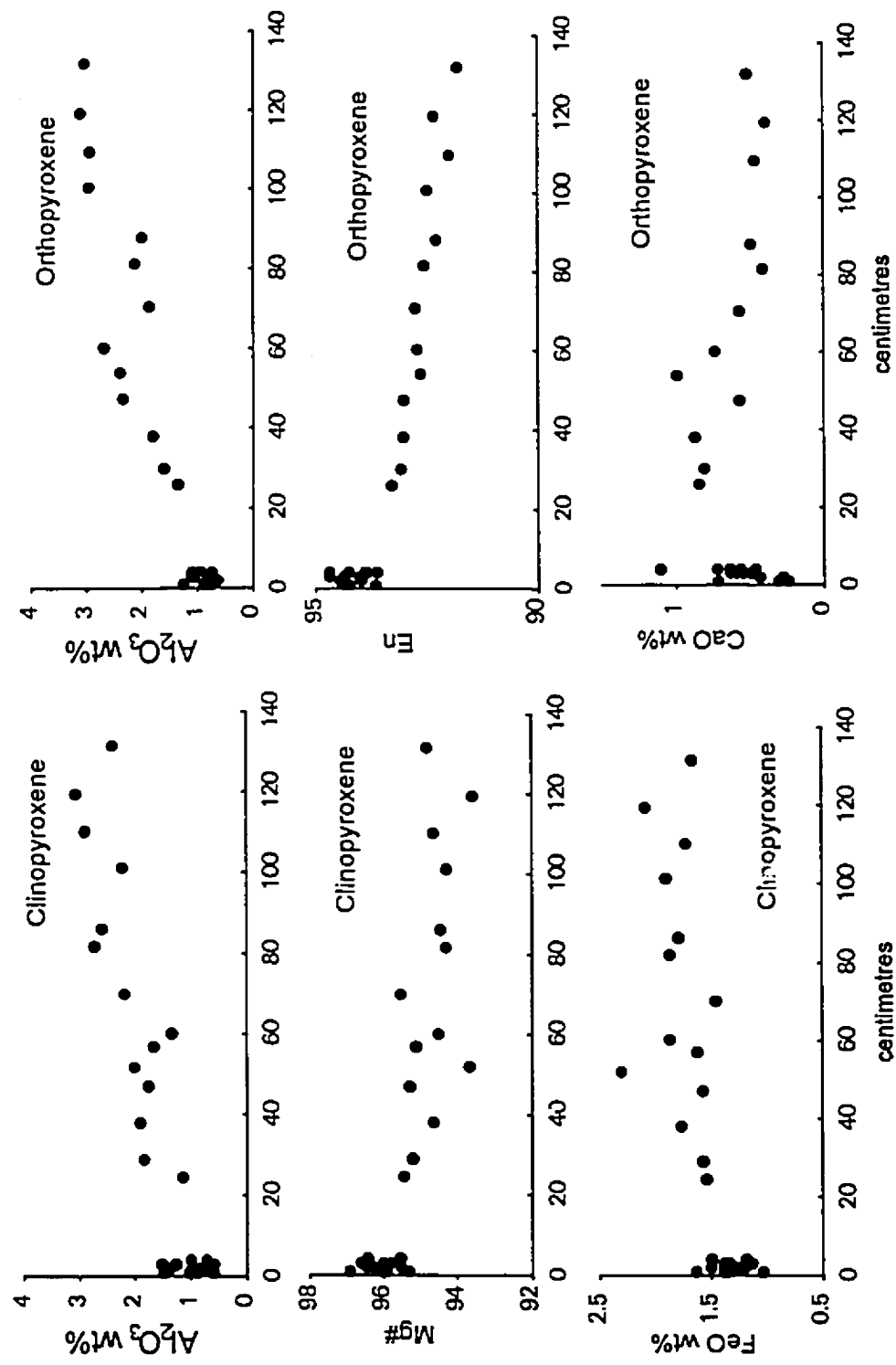


Figure 4-19. Chemical variations of pyroxenes in a transitional zone from chromitite to dunite to harzburgite to Di-harzburgite. Petrographic description in Figure 3-6A.

chromitites.

Chromites in the harzburgites have large variations in Cr#s (18 to 66) and low Ti contents (<0.15 wt% TiO₂) but those in the chromitites are relatively uniform in Cr#s (74 to 82) and have high Ti contents (0.2 wt% TiO₂ on average). The dunites contain chromites intermediate in composition between those of the harzburgites and chromitites. The harzburgites have Ol (Fo=90 to 92), Opx (En=87 to 92), and Cpx (Mg#s=44.5 to 53). Silicates in the chromitites have the highest Mg contents. In the reaction zone, Cr#s of chromites, Fo of Ol, En of Opx and Mg#s of Cpx increase from Di-harzburgite to harzburgite to dunite to chromitite, suggesting that the parental magmas for the chromitites were not in equilibrium with the harzburgites. In addition, both Opx and Cpx in the chromitites have much lower Ca and Al than those in the harzburgites. The low-Ca and low-Al pyroxenes in the chromitites suggest that they crystallized from a boninitic magma.

Chapter 5: PETROGENESIS

5.1. Origin of the harzburgite

Harzburgite in the mantle sequence of the Luobusa ophiolite is believed to be residual in origin, left from partial melting in the upper mantle. Despite extensive overprinting by late-stage deformation (see Chapter 3), the harzburgite in Luobusa retains its original geochemical character. The highly depleted nature of these rocks is interpreted to reflect their origin as the residue of extensive partial melting.

The harzburgites and Di-harzburgites in Luobusa are chemically homogenous (Figures 4-1 and 4-2), a feature that also indicates a large scale melting process (Coleman, 1977; Nicolas and Prinzhofer, 1983). Whole-rock Mg#s and Ca and Al contents of the harzburgite are very similar to those of spinel harzburgites from Finero, northern Italy ($Al_2O_3 = 1.23 \pm 0.49$, $CaO = 1.28 \pm 0.43$) that are interpreted as depleted peridotites formed by about 18% partial melting of primary mantle (Hartmann and Wedepohl, 1993). Mg/Si ratios of the Luobusa peridotites are similar to those of abyssal peridotites, but the Mg#s are slightly lower than those of the very depleted, low-Ca harzburgites from Southern Africa described by Boyd et al. (1993).

The Luobusa peridotites generally have flat, unfractionated PGE distributions (Figure 4-3), similar to MORB-type residues (Edwards, 1990). Os, Ir, and Ru are present in the upper mantle as refractory alloy metals, but Pt and

Pd occur in Fe-Ni-Cu sulphides which lie along grain boundaries (Mitchell and Keays, 1981; Edwards, 1990). During relatively low degrees of partial melting (<25%), S, Cu, Pt and Pd behave as incompatible elements and fractionate into the melt phase (Lorand, 1989; Mathez and Peach, 1989), whereas Os-Ir-Ru alloys remain as solids (Leblanc, 1991). Thus, one would expect strongly fractionated PGE patterns in such residual peridotites. However, because MORB-type magmas are sulfur-saturated, they typically contain an immiscible sulphide liquid, preferentially enriched in Pt and Pd. This melt would likely be retained in the mantle due to its high density, so that the residue would be impregnated with sulfides, thus leading to an unfractionated PGE distribution (Mitchell and Keays, 1981; Edwards, 1990). High degrees (>25%) of mantle melting should produce sulfur-undersaturated melts without an immiscible phase (Keays, 1982; 1994; Sun et al., 1991; Fryer and Greenough, 1992; Zhou, 1994). In this case, the Pd and Pt would be concentrated in these melts and extracted from the mantle, leaving peridotites depleted in these elements. Thus, because they have unfractionated PGE patterns, the Luobusa peridotites are interpreted to have formed by extraction of MORB magmas produced by about 20% of partial melting.

The wide range in Cr#s (18-66) and low Ti contents of accessory chromite in harzburgite are consistent with partial melting of the upper mantle, as documented extensively in the literature (e.g., Irvine, 1965; Dick and Bullen, 1984). These chromites are residual in origin and plot in the field of abyssal

peridotites (Figure 5-1), suggesting formation by extraction of tholeiitic magmas (Dick, 1977; Dick and Bullen, 1984). Thus, chromite compositions further demonstrate that the harzburgites in Luobusa have a MORB affinity.

5.2. Magmatic origin of the podiform chromitites

The textures of the chromitites in Luobusa (Figure 3-12) are typical of podiform varieties (Thayer, 1964; 1969; Leblanc, 1987) and are interpreted as indicating a magmatic origin (Greenbaum, 1977; Brown, 1980; Lago et al., 1982; Duke, 1983; Auge, 1987; Leblanc, 1987; Malpas and Robinson, 1987; Leblanc and Ceuleneer, 1992; Roberts and Neary, 1993).

These chromitites contain high-Mg silicates (Ol, Opx and Cpx) and high-Cr chromite, an assemblage of phenocrysts typical of low-Ca boninites (Crawford et al., 1989). The podiform chromitites in Luobusa also have highly fractionated PGE patterns that show significant depletion of Pt and Pd (Figure 4-5). Because these elements typically reside in sulfides, the depleted nature of the chromitites suggests crystallization from sulfur-undersaturated magmas (Naldrett and von Gruenewaldt, 1989). Abundant evidence suggests that boninitic magmas are sulfur-undersaturated (Keays, 1982; 1994; Hamlyn et al., 1985; Sun et al., 1991), supporting the suggestion that the chromitites of Luobusa were formed from such melts.

Chromites from the chromitites have a narrow compositional range (Figure 4-9) suggesting they crystallized from liquids with similar compositions.

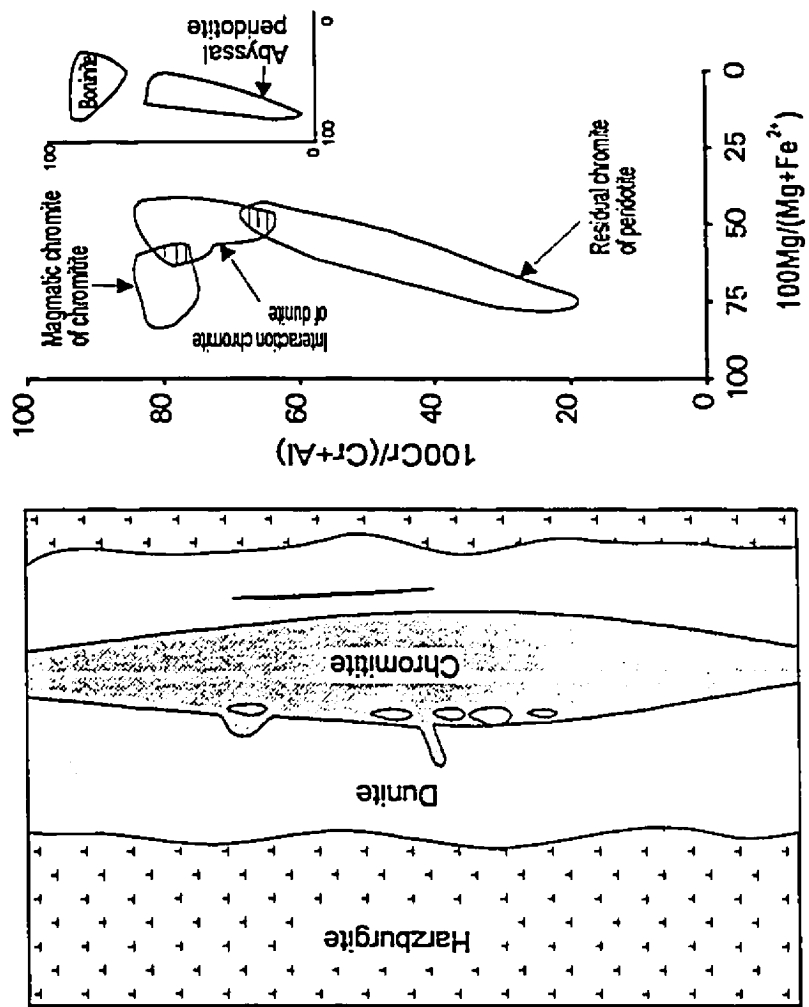


Figure 5-1. Genetic relationships among harzburgite, dunite and chromitite from the mantle sequence of the Luobusa ophiolite. Abyssal peridotite and boninite fields are after Dick and Bullen (1984) and Kepezhinskas et al. (1993), respectively.

They all plot in the boninitic field in the diagram of Cr# versus TiO_2 (Figure 4-10). As summarized in Irvine (1967), Dick and Bullen (1984) and Arai (1992), chromite chemistry can be a guide to parental magma composition. This is particularly true of podiform chromitites, which are believed to have crystallized early, before significant modification of the melts by crystal fractionation. Maurel and Maurel (1982), cited in Auge (1987), have suggested that Al contents of spinel can be related to those of the melt by the formula:

$$Al_2O_3\text{chromite}=0.035Al_2O_3^{2.42}_{\text{melt}} \quad \text{Equation 4.1.}$$

Although many factors can affect chromite composition, this relationship can at least provide a guide to the original melt composition. Using samples from the most massive chromitites, Al_2O_3 contents of the liquids range from 9.8 to 11 wt%. These Al_2O_3 contents compare closely with those of high SiO_2 -high MgO (boninitic) melts from the Troodos ophiolite, Cyprus (Robinson et al., 1983).

Auge (1987) suggests that the magmas from which podiform chromitites of the Semail ophiolite solidified had compositions similar to those from which the cumulate sequences crystallized. In Luobusa, the cumulate sequence of dunite, pyroxenite and gabbro, and associated volcanic sequence with an arc affinity, suggest a supra-subduction zone origin for the ophiolite (Bai et al., 1993; Zhou et al., 1995c). The crustal section of the Luobusa ophiolite thus is compatible with a boninitic parental magma for the podiform chromitites in its

mantle section.

5.3. Melt/rock interaction around the chromitite bodies

Most chromitite bodies in Luobusa have dunite envelopes with a zonal pattern grading outward into harzburgite and Di-harzburgite (Figure 3-6). As discussed in an earlier section, the harzburgites in Luobusa are compatible with a residual origin, whereas the chromitites are believed to have crystallized from a boninitic magma. It is, therefore, likely that interaction between the melt and residual rock formed the dunite envelopes around the chromitite bodies in Luobusa. This melt/rock interaction around the chromitites is similar to that previously documented around dunite, pyroxenite and gabbro dykes in mantle peridotites of other ophiolites (Dick, 1977; Quick, 1981; Bodinier et al., 1990; Kelemen et al., 1992; 1995; Edwards and Malpas, 1995; Kelemen and Dick, 1995; Quick and Gregory, 1995) and in situ oceanic lithosphere (Dick and Natland, 1995).

If melt is produced in the mantle and segregates rapidly, the melt and residue would probably soon be in disequilibrium (Bédard, 1989). In the Mg_2SiO_4 - $CaMgSi_2O_6$ - SiO_2 system, the forsterite liquidus volume expands with decreasing pressure so that primary liquids in equilibrium with Ol, Cpx and Opx at depth should first crystallize Ol at lower pressure (Warner, 1973; Hess, 1993). The upward migration of partial melts through the mantle may lead to reaction with wall rocks especially where the melt flow is focussed. Such reactions will

dissolve pyroxenes at shallower depths (Kelemen et al., 1992; Hess, 1993). It should be recognized that the mantle rocks hosting the chromitites were likely also part of the diapir, but ascended at a slower rate than the melts (Leblanc, 1987; Ceuleneer, 1988; Nicolas, 1989; Leblanc and Ceuleneer, 1992).

Formation of dunites on a centimetre scale has been experimentally demonstrated by reaction of OI-saturated liquid with harzburgite (Daines and Kohlstedt, 1994). Such interaction involves melt infiltration (Watson, 1982) or a percolation-diffusion process (Bodinier et al., 1990; Vasseur et al., 1991) which allows minerals in the peridotites to come in contact with the melt, such that the peridotite behaves like a "chromatographic column" (Navon and Stolper, 1987). When applied to the natural example of Luobusa, this suggests that immediately adjacent to a chromitite pod, both Opx and Cpx would be dissolved to form the dunite envelope with high Mg/Si ratios (Figure 4-2). Farther outward, only Cpx would be dissolved, producing a zone of harzburgite, which would grade into the host Di-harzburgite (Figure 3-6). The OI grains in the dunite envelopes are coarser than those in the harzburgites, consistent with experimental observations that OI can grow on existing crystals (Daines and Kohlstedt, 1994). The poikilitic texture of OI in dunite hosting chromitite (Figure 3-11) demonstrates a magmatic impregnation during the formation of dunites.

The melts from which the Luobusa chromitites crystallized were probably not in equilibrium with the host peridotites because they had migrated from sources deeper in the mantle. In Luobusa, such disequilibrium is indicated by

the large variations in chromite composition across the reaction zones between chromitites and peridotites. Cr#s increase systematically from less than 20 in the host Di-harzburgite to nearly 80 in the chromitite bands, over a distance of about 14 cm (Figure 4-8). This suggests that the original chromite in the Di-harzburgite was modified by reaction with the melt. In particular, the progressive increase of Ti in chromites towards the chromitites (Table 4-2) brings their compositions closer to those crystallizing from the magmas. The high Ti contents are not a residual feature because peridotites in Luobusa typically have chromites with very low Ti contents. High-Ti chromites in the plagioclase lherzolites of the Bay of Islands ophiolite are interpreted as the result of melt/rock interaction (Suhr and Robinson, 1994; Edwards and Malpas, 1995), a process similar to that envisaged here.

Initially, liquid saturated only in Ol reacts with peridotite to produce dunite and increasingly opx-rich liquid compositions. As a result, the modified liquid will become saturated in chromite and Opx. This seems to have occurred in Luobusa, where many chromitites and dunitites contain Opx, although in variable amounts.

Field observations in Luobusa suggest that the dunite envelopes can be produced in an open system by reaction between harzburgite and the migrating boninitic melt from which the podiform chromitites were crystallized. This can account for dunitites with lower Pd/Ir ratios than the harzburgites. At this stage the magma was saturated in Ol and chromite but not Cpx. The residual magmas

continued to move upward to the crust/mantle boundary and formed transition zone dunites, together with abundant pyroxenites at higher levels.

5.4. Mechanism of chromite segregation

The occurrence of dunite envelopes around most podiform chromitites in Luobusa suggests that melt/rock interaction and chromitite formation are closely linked. Removal of pyroxenes to form the dunite envelopes would have modified the primary magmas such that they may have moved into the primary phase field of chromite (Figure 5-2). Thus, melt/rock reaction provides a mechanism by which large volumes of chromite can be extracted from a melt that has only a small chromium content. To form monomineralic layers or pods, chromite must have crystallized alone for a period of time and/or have been concentrated by physical processes.

In the melt/rock interaction model, batches of relatively primitive parental magma rising through the upper mantle react with the host peridotites, dissolving pyroxenes from the wall rock and undergoing compositional modification. Such interaction would increase the silica content of the liquid, as demonstrated by experiments (Fisk, 1986; Kelemen, 1990). The dissolution of Opx would produce a melt with lower Mg/Si ratios and a dunitic residuum with higher Mg/Si ratios (Figure 4-2). As a result, the primitive liquid would move from the Ol-chromite cotectic into the chromite stability field (Figure 5-2), producing a monomineralic aggregate.

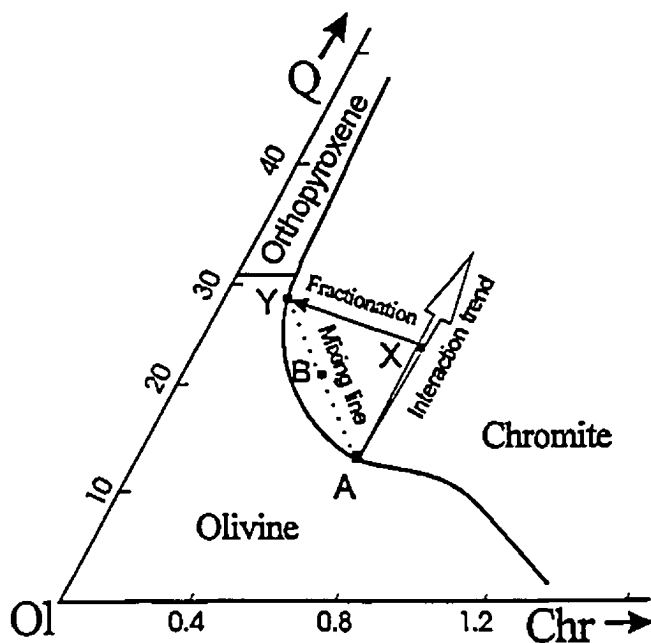


Figure 5-2. Phase relations in the system Ol-quartz-chromite as determined by Irvine (1977). Primitive magma (A) would react with the peridotite host to form a range of compositions along a line such as A-X, all of which would lie in the chromite field. The fractionated magma (Y), mixing with new batches of the primitive magma (A) would form melt (B) which also lies in the chromite field.

Such a change in melt composition is recorded in the chromites from a podiform body in Luobusa. Large grains in nodules and small disseminated grains likely formed at different stages (Figure 3-12). Positive correlation between Al and Cr of large and small grains in sample L29 (Figure 4-11) cannot be due to simple crystal fractionation. In a typical mafic magma, chromium is a trace component, whereas aluminum is a major element. Thus crystallization of chromite should deplete chrome in the melt far more rapidly than aluminum. When Al-bearing silicates (such as Cpx and plagioclase) are absent and only chromite and Ol are crystallized, the chromites should be progressively enriched in Fe and depleted in Cr and Mg, but show little change in Al (Zhou and Kerrich, 1992). Thus, the Al and Cr relation in sample L29 likely reflects the influence of melt/rock interaction rather than crystal fractionation. In mantle peridotites, clinopyroxene is the major carrier of chromium (Dawson et al., 1970; Barnes, 1986; Hevig et al., 1986). The primary melt would have had similar Cr_2O_3 but higher Al_2O_3 and CaO than the pyroxenes in the host peridotites. Thus, this type of melt/rock reaction would introduce mainly Si and Mg, causing dilution of Al and Ca but little change in chromium. The increase in Cr#s of the liquid as crystallization proceeded implies that Al in the liquid was depleted by dilution more rapidly than Cr was consumed by chromite precipitation.

Once a melt has moved into the chromite stability field and chromite starts to precipitate, the melt would move back toward the Ol-chromite cotectic where both Ol and chromite would crystallize. A new magma along the mixing line can

be formed if a batch of relatively primitive magma is injected and mixed with the fractionated melt (Figure 5-2). This mechanism is similar to the magma mixing model proposed for the formation of stratiform chromitites (Irvine, 1977). Irvine's model has since been supported by textural evidence pointing to common cotectic crystallization of chromite and Ol. It also accounts for the presence of laterally extensive chromitite bands within layered intrusions and the observed sequence of layers (Sharpe and Irvine, 1983; Irvine and Sharpe, 1986; Murch and Campbell, 1986; Roeder and Reynolds, 1991; Campbell and Murck, 1993).

The interplay of melt/rock reaction, chromite fractionation and magma mixing would presumably lead to many fluctuations in melt composition, producing both massive and disseminated chromitites and phase layering within a single podiform body, such as observed in Luobusa (Figure 3-12). Continuous interaction would presumably result in the precipitation of chromite alone to form massive ores. If the magmas and host rocks reached equilibrium and interaction ceased, chromite and Ol would precipitate cotectically to produce disseminated chromitites (Figure 3-12). Mixing of fractionated and primitive magmas may also bring the melt into the field of chromite crystallization (Figure 5-2).

Massive and disseminated chromitites may occur together or separately. Clots of Ol with rims of chromite (occluded textures) indicate later growth of chromite around Ol nuclei. These could also be due to melt/rock interaction or magma mixing that moves the liquid into the field of chromite crystallization (Figure 5-2). Nodular and obicular chromitites probably represent aggregates of

chromite grains (Thayer, 1969) rounded by convection in a melt pod to form snow ball-like clots (Malpas and Robinson, 1987).

In stratiform chromitites, the transition from massive to disseminated ores may be sharp or gradational with modal or phase layering. Similar layering is observed in Luobusa chromitites and in many other podiform deposits (Thayer, 1964; Zhou and Bai, 1992) and has been attributed to convection in magma conduits, or to multiple injections of new magma (Leblanc and Ceuleneer, 1992). In the melt/rock interaction model, the layering of the podiform chromitites is best explained by changes in melt composition produced either by melt/rock reaction and/or by repeated injections of more primitive magma.

As noted above, the chromitite bodies are concentrated at a similar level in the peridotites. This suggests that small pods of rising magma coalesce in this zone, close to the mantle/crust transition, leading to larger magma bodies from which the chromitite can crystallize (Figure 5-3). This level coincides with the point at which mantle flow changes from nearly vertical to nearly horizontal beneath a spreading centre (Figure 3-4). According to Nicolas (1989), it is the inability of these magmas to hydraulically fracture their way upward from the zone that causes them to pond.

In a stratiform complex, the depleted hybrid liquid left after extraction of chromite would continue to evolve and precipitate silicate minerals above the chromitite layers (Irvine and Sharpe, 1986). The same conditions may prevail in some podiform bodies that have cumulate textures and phase layering in a

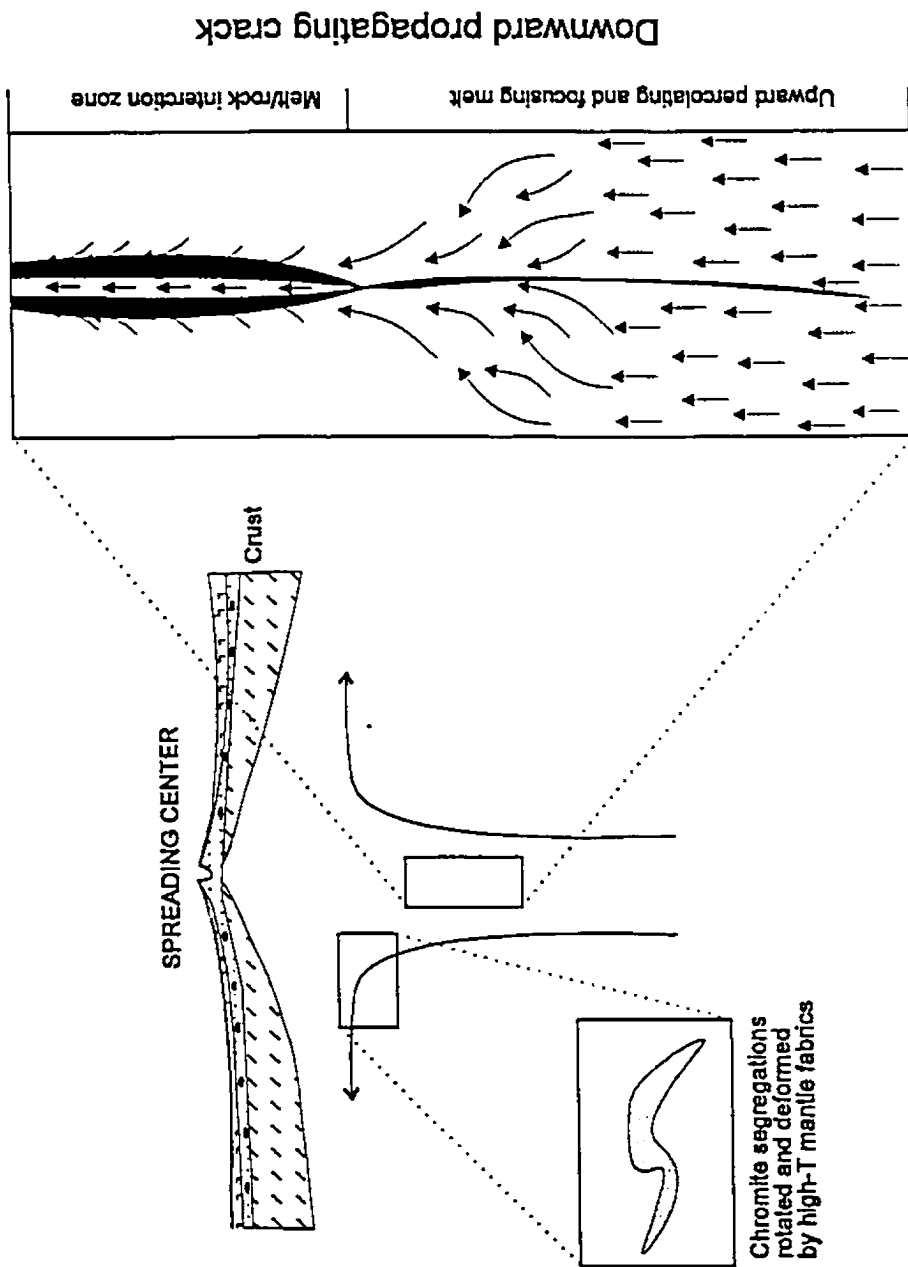


Figure 5-3. A model illustrating the formation of podiform chromitites in the upper mantle.

single body. In the upper mantle and mantle/crust transition zone, where podiform chromitites form, the residual liquids would probably be hot and still relatively buoyant and would continue to move upward by percolation, leaving chromite behind as pods surrounded by envelopes of dunite or depleted harzburgite (Figure 5-3).

5.5. MORB mantle peridotites versus boninitic magmas

As discussed above, petrochemistry, PGE distributions and chromite compositions of the harzburgites in Luobusa suggest that they were formed by partial melting that produced tholeiitic magmas. On the other hand, the petrography and geochemistry of the podiform chromitites in Luobusa strongly suggest that they formed from a boninitic magma (Figure 5-1). Therefore, the mantle sequence of the Luobusa ophiolite likely had two stages of magma generation. The first stage, producing a residual peridotite and tholeiitic melts, occurred possibly in a mature spreading centre (such as mid-oceanic ridge). The depleted residue of the peridotites with unfractionated PGE patterns may represent part of the Neo-Tethyan oceanic lithospheric mantle (Figure 5-4). These peridotites have chromites with low Cr#'s (Figure 4-9), similar to those in the Xigaze ophiolite that is believed to have formed in a MORB setting (Nicolas, 1989). However, the mantle sequence in Luobusa has experienced a second stage of melting at depth forming boninitic magmas (see discussion above). It is likely that the boninitic magmas were produced above a subduction zone. This

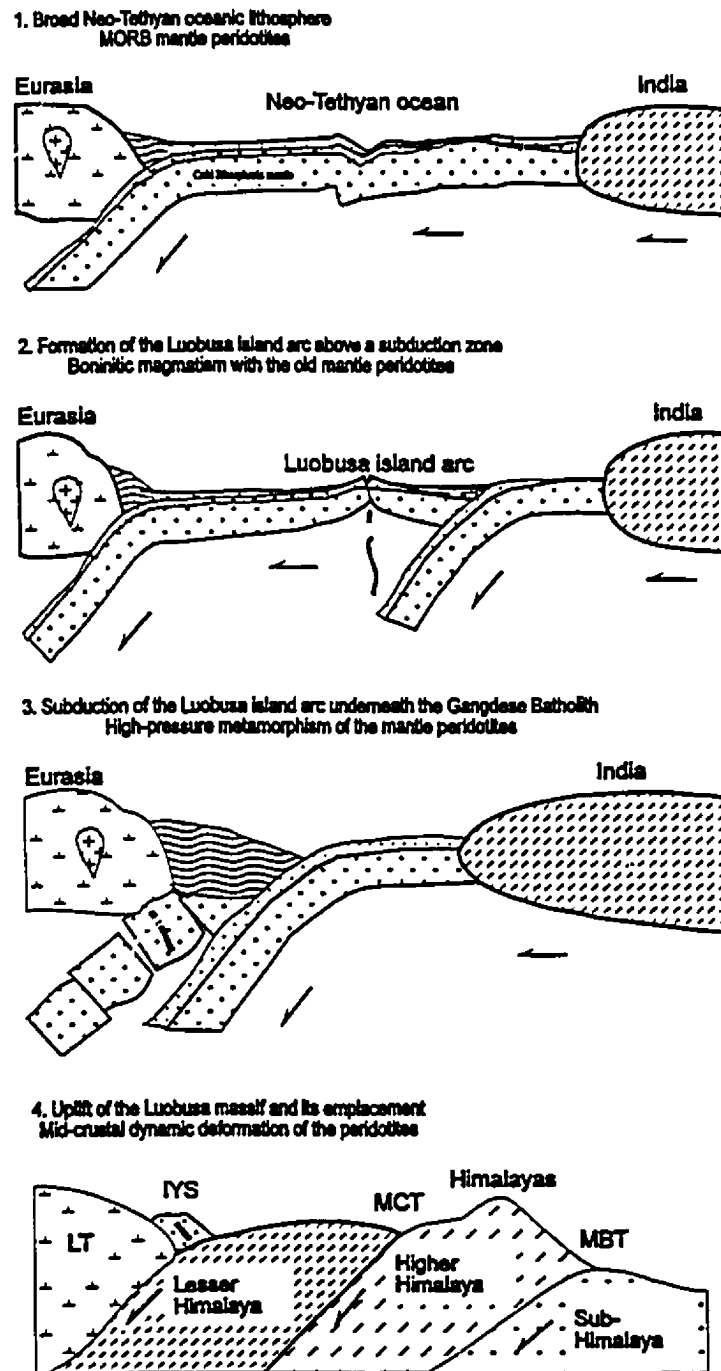


Figure 5-4. Tectonic evolution of the Luobusa massif, showing two stages of magma generation within the mantle peridotites.

subduction zone may have formed through an intra-oceanic thrust due to rapid, northward movement of the ISC, producing the Luobusa island arc (Figure 5-4). The newly-formed boninitic magmas at depth reacted with the old lithospheric mantle peridotites at shallower depth, dissolving Cpx and Opx and producing dunites and chromitites. Such reaction produced large variations in mineral chemistry because of the high degree of disequilibrium between boninitic magmas and MORB peridotites.

In Xigaze, all chromites in the mantle sequence, including those in dunite have consistently low Cr#. There is no evidence that boninitic magmatism occurred in this mantle sequence. Accordingly, the Xigaze ophiolite formed by a single stage of partial melting. This explains why no large bodies of chromitites have been found in the Xigaze ophiolite (see Chapter 6 for further discussion). It is known that the compositions of liquidus minerals might match the compositions of minerals in the residual mantle under the conditions of melting (Elthon, 1989). Although the reaction between such melts and wall-rocks at lower pressure could produce dunite dykes, chemical compositions of minerals through such reaction zones would be less variable as seen in the Xigaze ophiolite (Girardeau and Mercier, 1988), in the Josephine ophiolite (Orogen, United States) [Quick, 1981; Kelemen et al., 1992], and in the Table Mountain ophiolite (Newfoundland, Canada) [R. Herbert, 1995, personal communication].

Andesites of arc tholeiitic affinity in the melange zone of the Luobusa ophiolite might represent the second stage melts. The evidence for boninitic

melts lies in the petrography, mineral chemistry and PGE distributions of the podiform chromitites. To date, no boninitic lavas have been found in the complex. However, the cumulate sequence composed of pyroxenites and gabbros might have been derived from boninitic melts. It is interesting to note that the crustal section of the Xigaze ophiolite is composed of gabbros, troctolites and MORB tholeiitic lavas, supporting its formation in a tectonic setting different from the Luobusa ophiolite.

A similar sequence of melts has been described in the Troodos ophiolite where early arc tholeiite magmas were followed by depleted tholeiites and boninites (Robinson et al., 1983; Mehegan and Robinson, 1990). In Troodos, the sequence of melts was attributed to melting of progressively depleted mantle material in a rising diapir (Mehegan and Robinson, 1990).

5.6. Summary

In Luobusa, the dunites and chromitites in the harzburgites of the mantle sequence are local features formed by interaction between melt and harzburgite or Di-harzburgite. Mineral chemistry and whole-rock PGE distributions suggest that the chromitites in Luobusa were derived from boninitic magmas. To date, no boninitic lavas have been found in the complex, however, the cumulate sequence composed of pyroxenites and gabbros could have formed from boninitic melts.

The harzburgites and chromitites in Luobusa suggest two stages of

magma generation in this complex. Early, sulfur-saturated tholeiitic melts possibly formed in a mature spreading centre and left a moderately depleted residue of harzburgite with unfractionated PGE patterns. A second stage of melting at depth formed boninitic magmas in a supra-subduction zone environment. These magmas reacted with the residual harzburgites at shallower depth, dissolving Cpx and Opx and producing dunites. The reaction process added silica to the original magma, producing high SiO₂-high MgO boninitic or andesitic melts (Fisk, 1986, Kelemen, 1990). Such interaction would have moved the magmas from the Ol-chromite cotectic to the chromite crystallization field, allowing the formation of massive and disseminated chromites and phase layering within a single chromite pod. During melt extraction, porous flow was concentrated into narrow regions now represented by the chromitite and dunite lenses in the harzburgites.

Chapter 6: DISCUSSION

6.1. Controls on high-Cr and high-Al chromitites

As discussed earlier, podiform chromitites include both high-Cr and high-Al varieties (Figure 1-2); the Luobusa chromitites are typical of the high-Cr variety. The melt/rock interaction proposed is believed to have played an important role in the production of the podiform chromitites in Luobusa. This model is also applicable to other chromitites, either high-Cr or high-Al varieties, because all podiform bodies are enveloped by dunites (Thayer, 1964; 1969). However, the mechanism for producing these compositionally different chromitites is not yet clear.

Leblanc and Violette (1983) suggested that high-Al and high-Cr chromitites in the same massif were formed at different times, at different levels, and from different source rocks during upwelling of mantle peridotites. Hock et al. (1986) noted that high-Al and high-Cr chromitites in the Zambales ophiolite occur in two distinct lithologic associations and crystallized from different parental magmas. Based on a comparative study of high-Cr and high-Al podiform chromitites from western China, Zhou and Robinson (1994) suggest that high-Cr and high-Al chromitites crystallized from two compositionally distinct magmas, but similar melt/rock interactions caused the precipitation of chromitites in both cases.

6.1.1. Similarities and differences of high-Cr and high-Al chromitites

The major high-Al chromitites in China occur in the Asiatic orogenic belt that separates the Siberian tectonic plate on the north from the Tarim-Sino Archean Craton on the south (Coleman, 1989; Feng et al., 1989; Zhang et al., 1993) [Figure 1-1]. The Sartohay ophiolite contains the largest, minable high-Al chromitites in this belt, and is located in the west Junggar Mountains of Xinjiang Province. In Sartohay, mantle peridotites form a body that stretches for more than 20 km along strike and include both Di-harzburgite and lherzolite (Figure 6-1). The podiform chromitites occur in harzburgite, associated with abundant troctolite dikes (Figure 6-2A and B) and dunite lenses. The chromite pods are concordant bodies, parallel to the long axis of the peridotite massif. These are lens-shaped bodies enclosed in either dunite or harzburgite and are of the typical podiform type. They can be either disseminated or massive (Figure 6-2A and B). Silicate minerals found in the chromitites include Cpx and plagioclase. There are commonly bands of chlorite separating the chromitites from the enclosing dunite (Figure 6-2C).

The Sartohay ophiolite has distinctly different mineralogical and geochemical features from the Luobusa ophiolite (Table 6-1). Peridotites in Luobusa have higher bulk rock MgO, but lower $\text{FeO}_{\text{total}}$, than those in Sartohay (Figure 6-3). TiO_2 in the Sartohay peridotites ranges from 0.08 to 0.18 wt%, whereas in Luobusa it varies from 0 to 0.06 wt%. Whole-rock Ca/Al ratios are relatively consistent in the Luobusa peridotites and average about 1.5, whereas

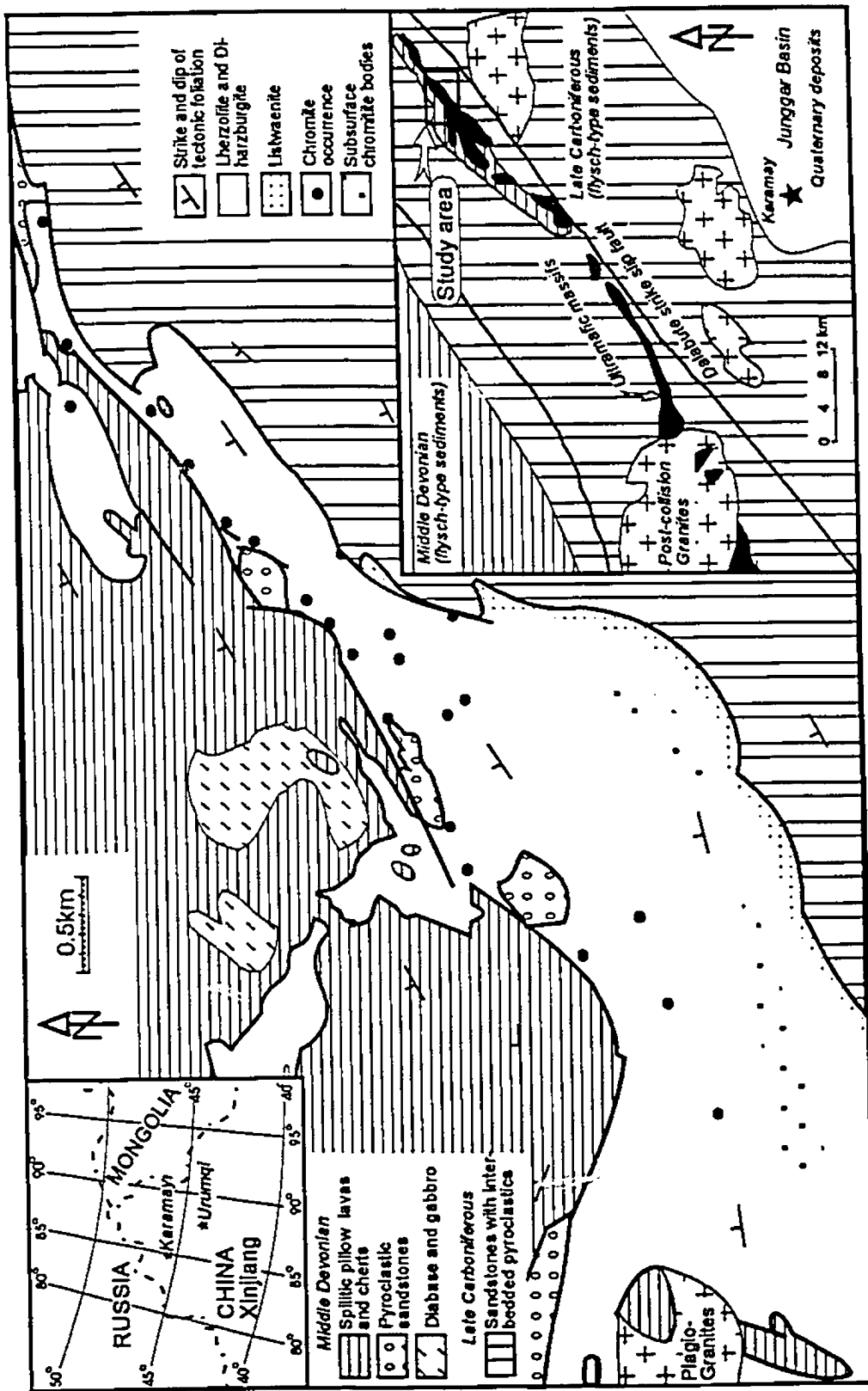


Figure 6-1. Geologic map of the Sartohay ophiolite (after Feng et al., 1989; Zhou and Robinson, 1994), showing distribution of chromitite bodies. Also see location in Figure 1-1.

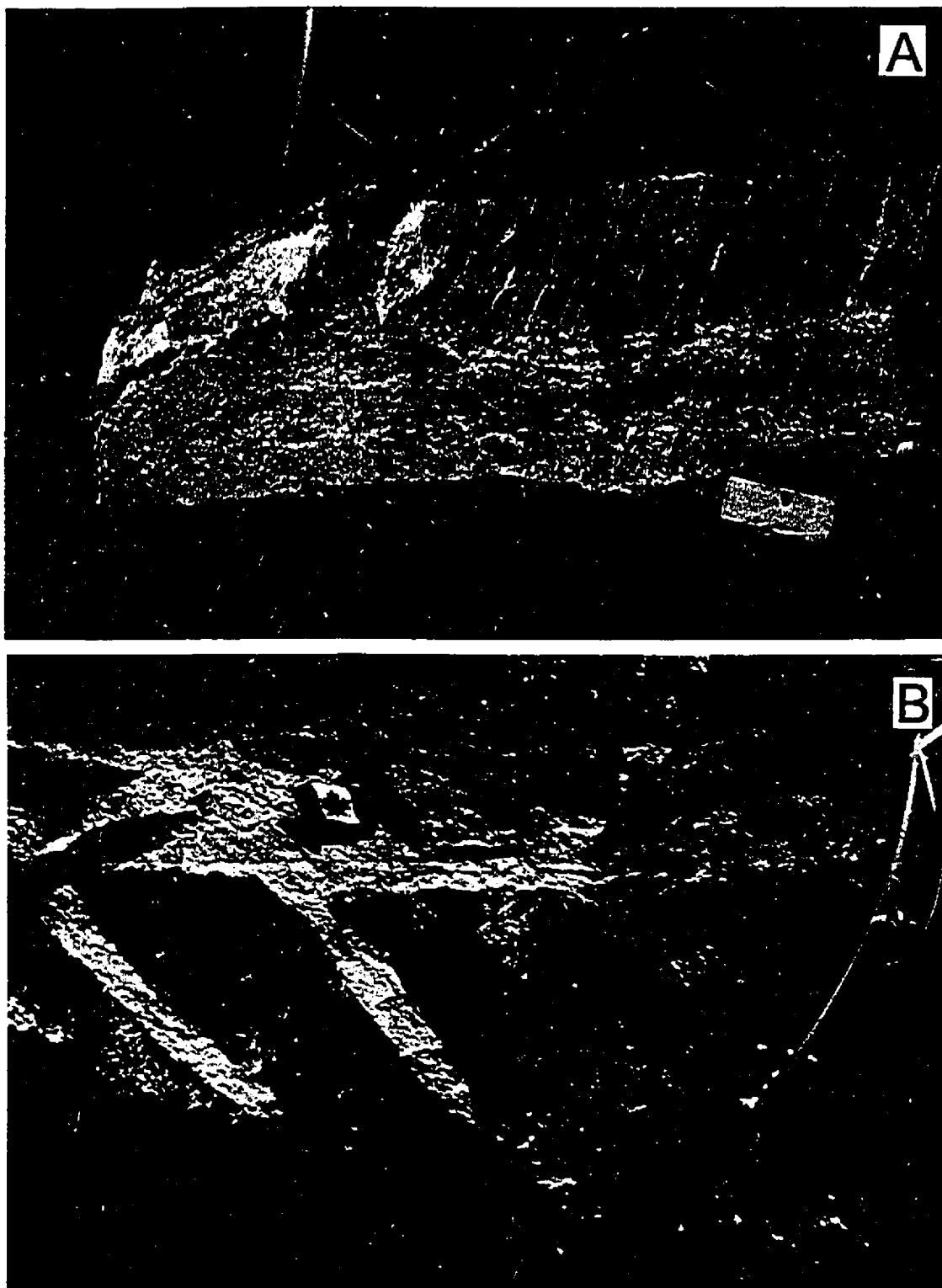


Figure 6-2. Hand specimen photos of chromitites from Sartohay: A. Massive chromitite intruded by a troctolite dyke. B. Disseminated chromitite transitional to dunite, both intruded by troctolite dykes.

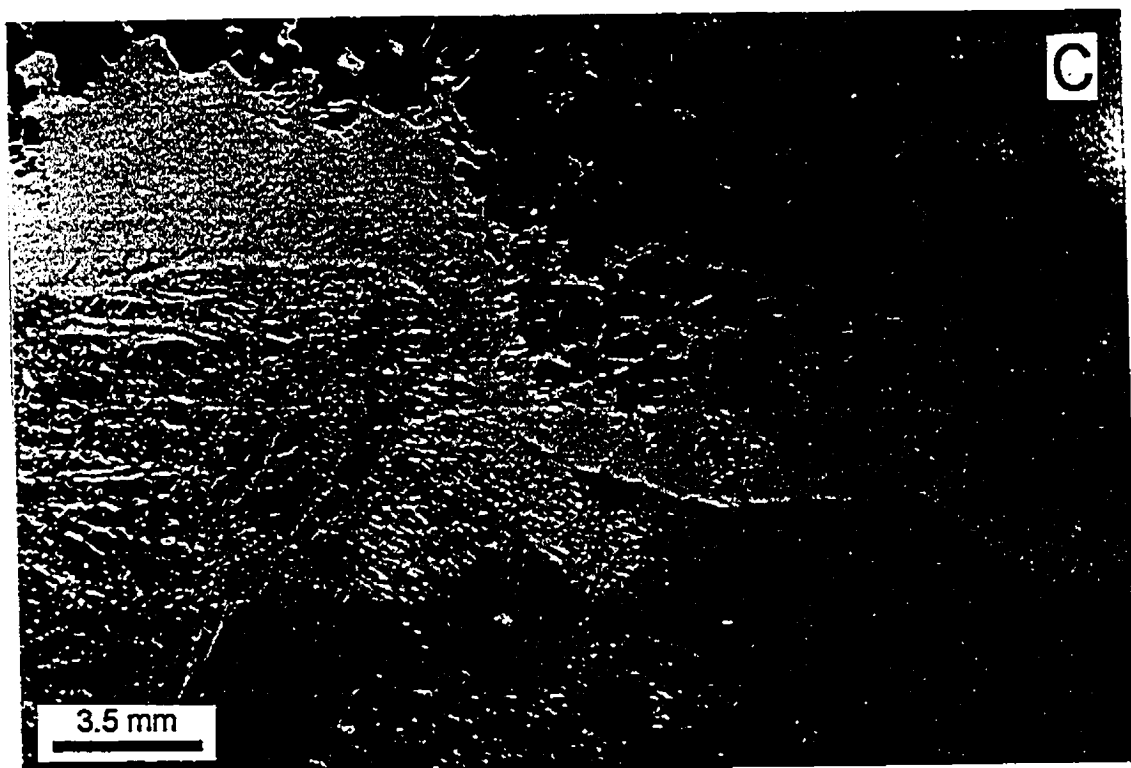


Figure 6-2. C. Massive chromitite separated from dunite by a chlorite rim.

Table 6-1. A mineralogical and geochemical comparison between the Luobusa and Sartohay ophiolites

| | Luobusa | Sartohay |
|---|---|--|
| Chromitite | High-Cr | High-Al |
| Chromite | Cr#>70 TiO ₂ <0.20 wt% | Cr#<60 TiO ₂ >0.20 wt% |
| Opx(Al ₂ O ₃) (CaO) | 0.71-1.26 wt% 0.24-1.10 wt% | 1.32-1.59 wt% 0.38-0.45 wt% |
| Cpx(Al ₂ O ₃) | 0.53-1.51 wt% | 2.02-2.96 wt% |
| Peridotite | Harzburgite | Lherzolite+Di-harzburgite |
| Bulk chemistry | TiO ₂ <0.05wt% MgO=42-51wt% Ca=0.00-1.50wt% Al=0.01-1.20wt% | TiO ₂ >0.08 wt% MgO=36-48 wt% Ca=0.00-3.40wt% Al=0.30-2.20 wt% |
| Mineral chemistry | | |
| Olivine (Fo) | 90-93 | 86-91 |
| Opx(En) (Al ₂ O ₃) (CaO) | 91-92 0.71-4.13wt% 0.48-1.64wt% | 87-88 2.29-5.98wt% 0.92-4.34wt% |
| Cpx (Mg#) (Al ₂ O ₃) | 47-53 2.75-4.72wt% | 43-51 2.21-7.68wt% |

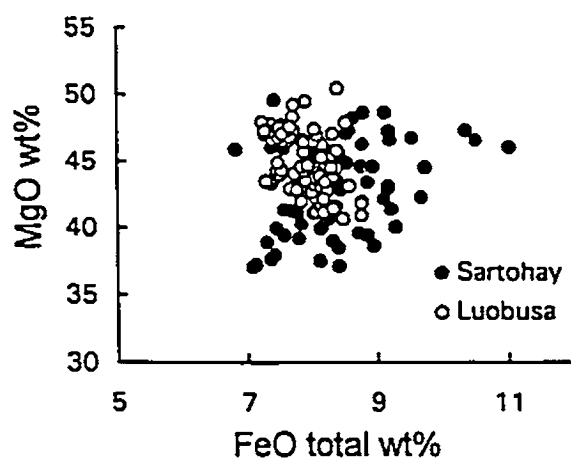


Figure 6-3. MgO versus FeO_{total} of lherzolite, harzburgite and dunite from the Luobusa and Sartohay ophiolites.

in Sartohay there is a much wider range of values and the average for harzburgite and dunite is less than 1 (Figure 6-4). All of the mantle rocks in Sartohay have higher average Al contents than their equivalents in Luobusa. Ca is generally lower and more variable in the peridotites of Sartohay than in those of Luobusa.

Olivines and pyroxenes in mantle peridotites of the Sartohay ophiolite have relatively variable compositions and are lower in MgO, but higher in CaO and Al₂O₃, than those in mantle peridotites from the Luobusa ophiolite (Table 6-1). Chromites in the mantle peridotites of Sartohay have lower Cr#'s than their equivalents in Luobusa. In Sartohay, chromite compositions are similar in both dunites and harzburgites, but in Luobusa, chromites in dunites have higher Cr#'s than those in harzburgites (Figure 4-9).

The chromitites in Sartohay consist of high-Al and high-Ti but low-Cr chromites (Cr# < 60), typical of the high-Al variety, whereas those in Luobusa have high-Cr chromites (Cr# > 70) (Table 6-1, Figures 6-5 and 6-6). The Sartohay chromitites have higher-Al pyroxenes than the Luobusa equivalents (Table 6-1).

Leblanc and Temagoult (1989) describe high-Al chromite pods in the Collo lherzolite massif of Algeria which are hosted in a tabular body of dunite about 10 m wide. The field relationships and geochemistry of these chromitite pods are similar to those in Sartohay. The peridotites in Zambales, which host the high-Al Coto chromitites, are less depleted than those that host the high-Cr

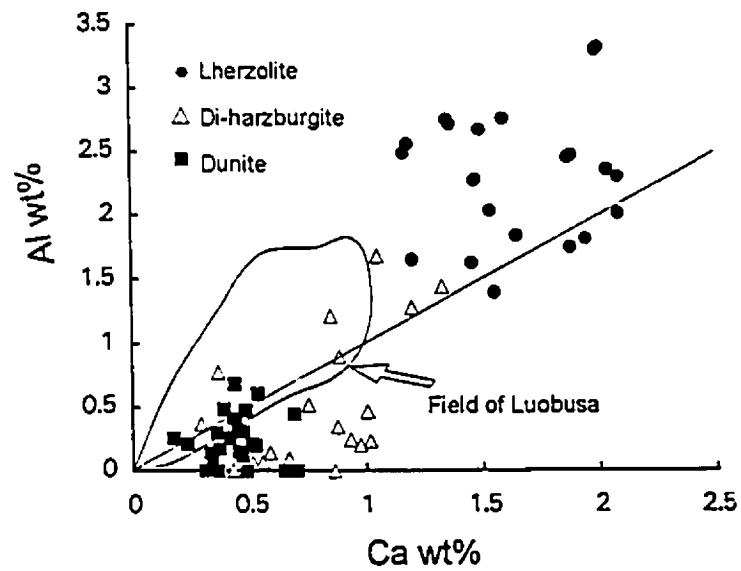


Figure 6-4. Ca versus Al of Lherzolite, Di-harzburgite, and dunite from the Sartohay ophiolite. See Figure 4-2 for details of field of the rocks from Luobusa.

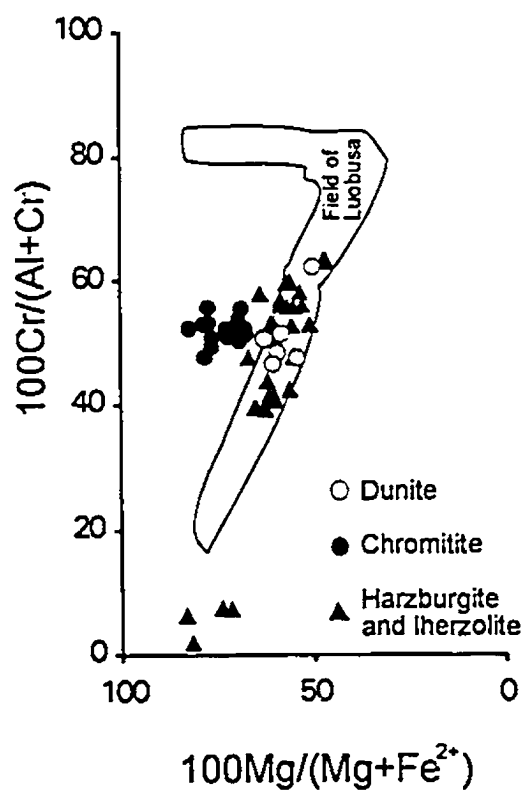


Figure 6-5. Cr# versus Mg# of chromites in lherzolite, Di-harzburgite, dunite, and chromitite from the Sartohay ophiolite. See Figure 4-9 for details of field of chromites in Luobusa. Boninitic and MORB fields are from Dick and Bullen (1984).

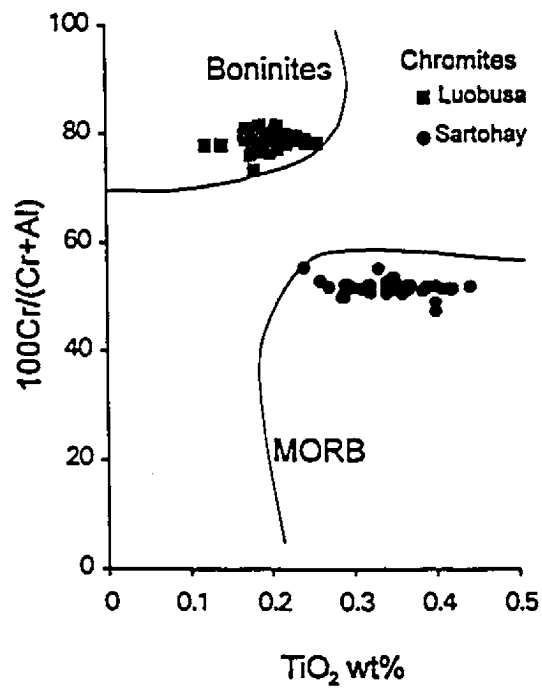


Figure 6-6. TiO₂ versus Cr# of chromites of the high-Al chromites from the Sartohay ophiolite. See Figure 4-10 for details of the high-Cr chromites in Luobusa. Boninitic and MORB fields are from Arai (1992).

Acoje chromitites (Hock et al., 1986; Evans and Hawkins, 1989). In mineral and bulk chemistry, these massifs are comparable to the Sartohay and Luobusa chromitites, respectively.

6.1.2. Effects of partial melting

Al_2O_3 contents of pyroxenes, Fo values of Ol and Mg#s of pyroxenes are useful criteria for estimating degrees of partial melting and depletion in mantle peridotites. Experimental studies have shown that the compositions of the residual phases change with progressive melting; the minerals become depleted in magmaphile elements (Fe, Al, Ca, Ti, Na), the Mg#s of both residual Ol and Opx increase and the Al_2O_3 content of the pyroxene decreases (Mysen and Kushiro, 1977; Jaques and Green, 1980; Michael and Bonatti, 1985). Using these criteria, the mantle peridotites in Sartohay are somewhat less depleted than those in Luobusa.

Variations in the Cr content of residual and magmatic chromites are also believed to be related to the degree of partial melting. Cr#s for residual chromites increase with progressive melting (Dick and Bullen, 1984). The relatively low Cr and high Ti contents of the chromites of the Sartohay ophiolite suggest that the mantle peridotites were formed by lower degrees of partial melting than in Luobusa. In Sartohay, the partial melting residue would be the less depleted lherzolites and Di-harzburgites found locally in the ophiolite. Thus, both the high Cr contents of chromites of Luobusa and the depleted nature of the peridotites in which they occur can be explained by higher degrees of

partial melting. The depleted nature of the Luobusa mantle peridotites is also reflected in their relatively uniform chemistry and lower Ca and Al but higher Mg contents than that of Sartohay.

Chromites crystallized from magmas in Sartohay have higher Al and Ti but lower Cr than those in Luobusa. The Sartohay chromites plot in the MORB field whereas those of Luobusa lie in the boninitic field (Figures 6-5 and 6-6). From equation 1, the parental magmas of the chromitites in Sartohay had higher Al contents (14.7 to 15.9 wt%) than those in Luobusa (9.79 to 11.1 wt%). Accordingly, the high-Al chromitites of Sartohay could have precipitated from mantle melts less refractory than the high-Cr ones of Luobusa.

The above conclusion is consistent with the presence of troctolite and gabbro dikes in the Sartohay ophiolite and pyroxenite and gabbro dikes in Luobusa, because these dikes would have been generated from Al-rich and Al-poor magmas, respectively. In addition, higher Al and Ca contents of pyroxenes in the chromitites of Sartohay than in those from Luobusa also support the above conclusion.

6.1.3. Melt/rock interaction around high-Al chromitites

Based on the geochemical data outlined above, the Cr/Al ratios of chromites in the Sartohay and Luobusa ophiolites reflect different parental magma compositions, which in turn, reflect different degrees of partial melting in the upper mantle. If such is the case, the residual peridotites of Sartohay should be significantly less depleted than those in Luobusa and on a broad scale this is

true. In Sartohay the peridotites include Di-harzburgite and lherzolite whereas in Luobusa only depleted harzburgite and Di-harzburgite are present. However, on a smaller scale the podiform chromitites in both bodies are associated with harzburgite and dunite regardless of the bulk composition of the mantle section. In particular, the dunites and harzburgites that host the high-Al Sartohay chromitite bodies, although less refractory than those of Luobusa, are far too depleted to be the source of the high-Al chromitites. They contain somewhat higher Al and Ti than the Luobusa peridotites, but less than would be expected if they were simply the residue of low degrees of partial melting. In particular, both the dunites and harzburgites are highly depleted in Ca, a feature difficult to explain by low degrees of melting. However, this association of chromitites with dunites and depleted harzburgites in Sartohay can be the result of the melt/rock interaction envisaged for the Luobusa chromitites.

The high-Al chromites of Sartohay may have crystallized from a parental magma formed originally by relatively low degrees of partial melting of mantle lherzolite. As discussed in Chapter 5, magma formed in this way would rise through the upper mantle, reacting with the host lherzolite and crystallizing chromite. Immediately adjacent to the magma pocket, all pyroxene in the host rock would be dissolved to produce the dunite envelope found around the chromitite bodies. Farther outward, only Cpx would be dissolved, producing a zone of harzburgite, which grades into the host lherzolite.

The melt/rock interaction during the formation of high-Al chromitites was

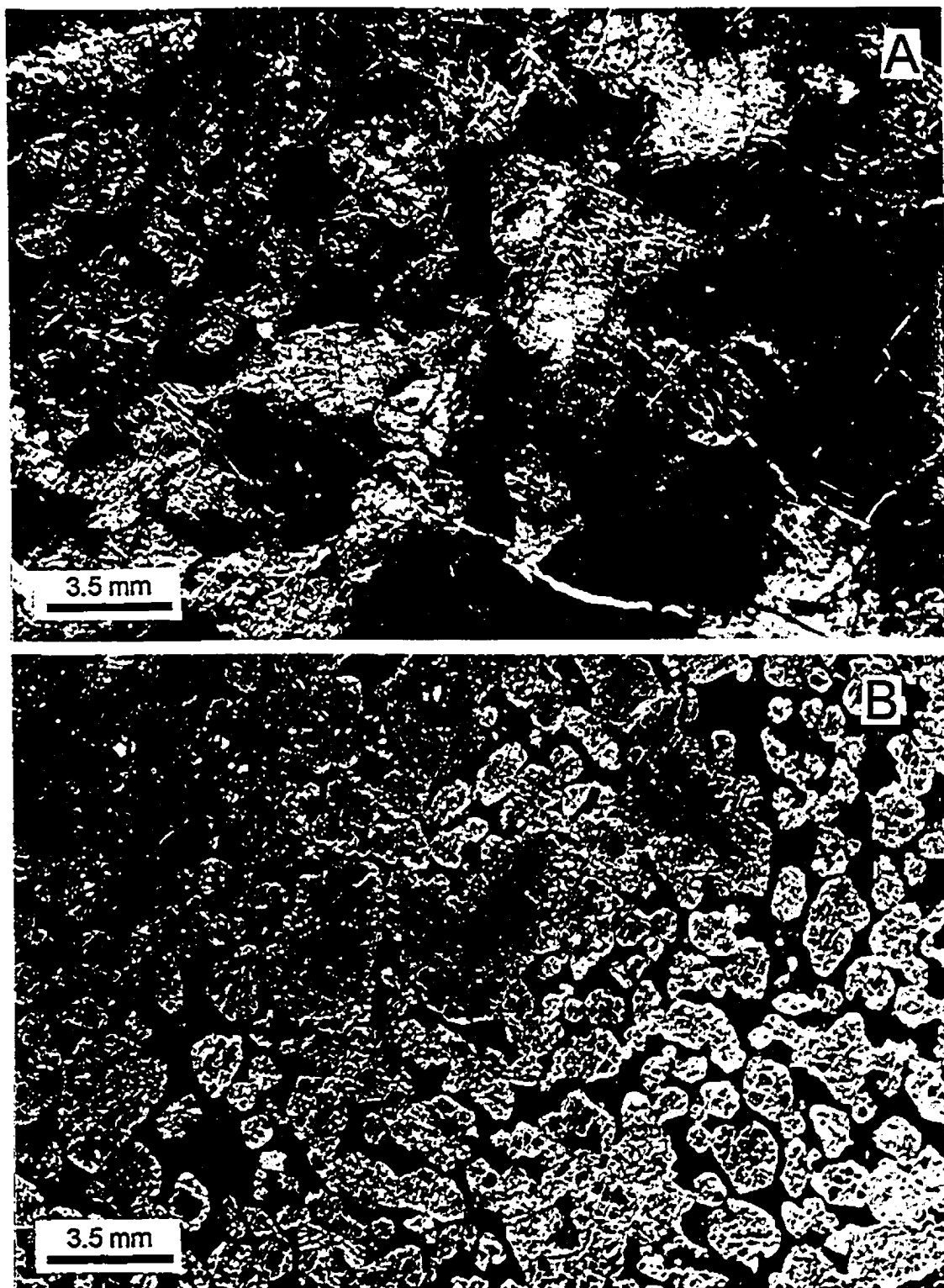


Figure 6-7. Textures illustrating melt impregnation in high-Al chromitites: A. Altered plagioclase (black) interstitial to dunites (light colour), Hegenshan ophiolite, H15b. B. Plagioclase matrix of dunite, Hongguleleng ophiolite; Ho57.

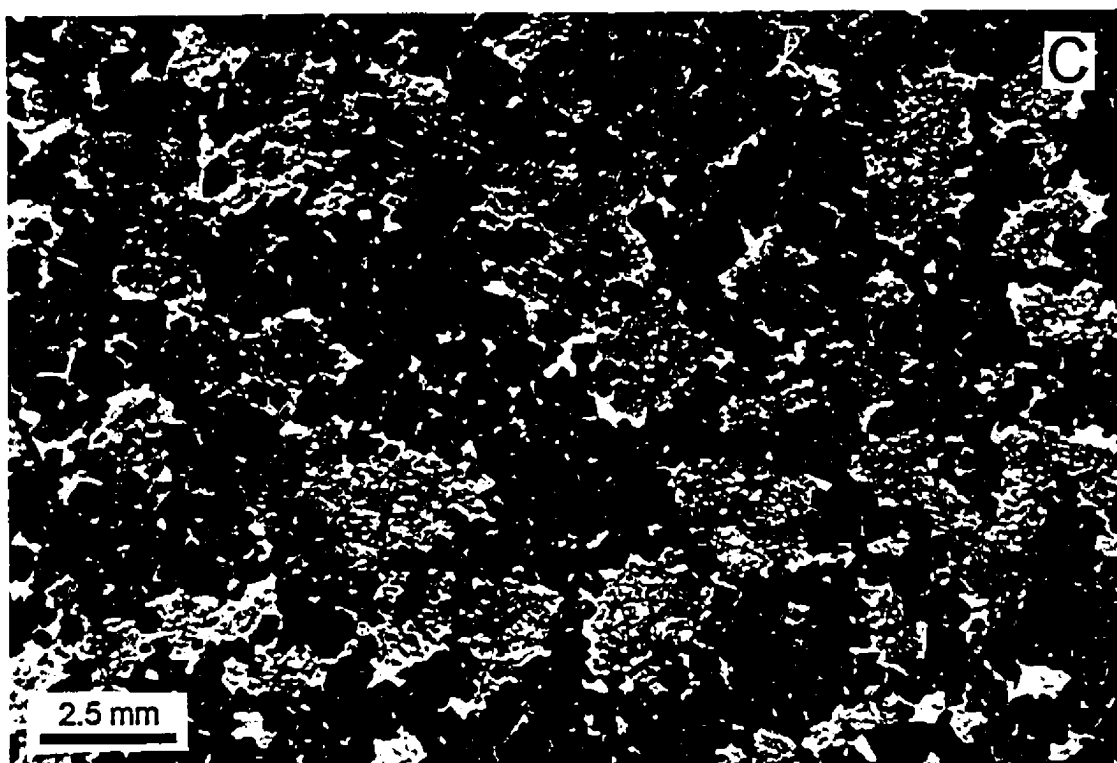


Figure 6-7. C-Chromite and altered Cpx (black) interstitial to dunite, Hongguleleng ophiolite, Ho44.

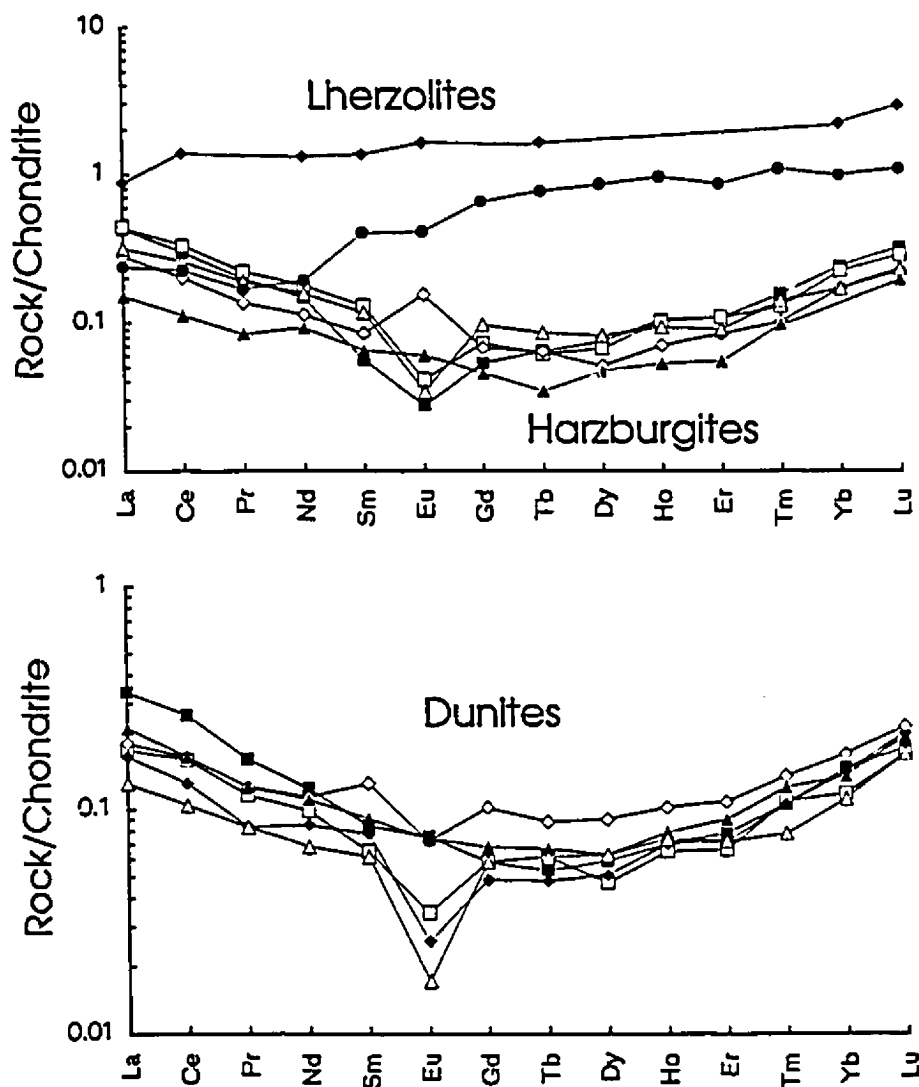


Figure 6-8. Chondrite-normalized REE patterns of dunites and harzburgites adjacent to chromitites and lherzolites of the Sartohay massif.

recorded in the wall-rock texture showing melt impregnation (Figure 6-7). The rocks adjacent to the chromitites have LREE-enriched patterns (Figure 6-8), attributed to the melt/rock interaction.

Quick (1981) and Kelemen et al. (1992) showed that the major element compositions of silicate minerals in reaction zones in the Trinity ophiolite remained nearly constant. The degree to which chromite compositions in the rock might be affected by the reaction process is determined by the magma composition. For example, in Luobusa where the magma had a relatively high Cr/Al ratio, the residual chromites clearly reacted with the melt to become more Cr rich. In Sartohay, where the original magma was much richer in Al, the residual chromites were in equilibrium with the melt composition and thus underwent little modification while the host rock was being changed from lherzolite to harzburgite to dunite. In this model, the higher Al contents of the dunites from Sartohay are due to the presence of high-Al chromite grains. The low Ca contents of the dunites and harzburgites reflect dissolution of Cpx from a lherzolithic parent, leaving only slightly modified Ol and chromite that kept the host rocks high in Fe and Al, respectively.

Accordingly, melt/rock interaction in the upper mantle that involved the formation of high-Al and high-Cr podiform chromitites can be illustrated in Figure 6-9.

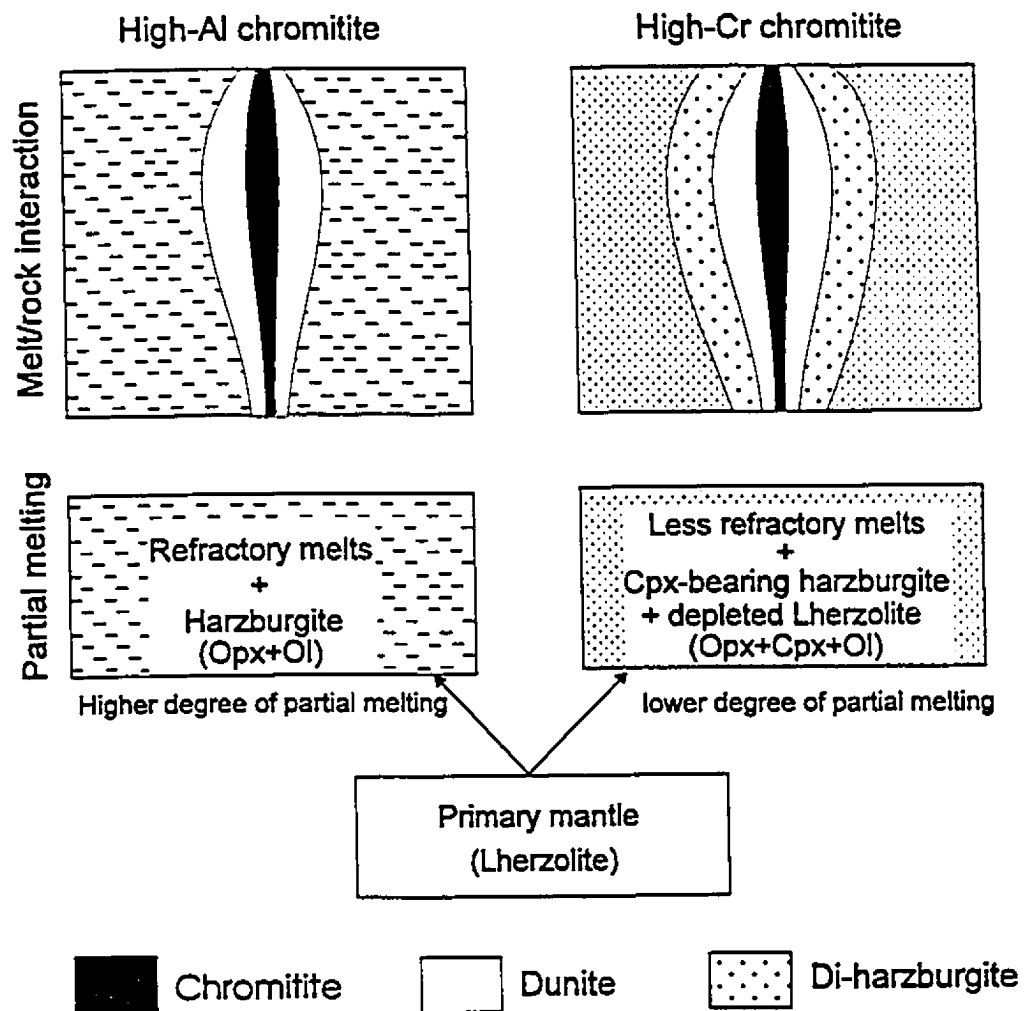


Figure 6-9. Illustration of melt/rock interaction in the upper mantle that produced both high-Al and high-Cr chromitites, respectively (modified from Zhou et al., 1994).

6.2. Tectonic setting of podiform chromitites

Ophiolitic harzburgite has generally been interpreted as a depleted residuum formed by variable degrees of partial melting - the higher the degree of partial melting, the more depleted the residuum (Jaques and Green, 1980; Dick and Bullen, 1984). Podiform chromitites are closely associated with very depleted harzburgites and dunites, and therefore the hosting ophiolites were thought to be the harzburgite ophiolite type (Nicolas, 1989; Nicolas and Al Azi, 1991). Pearce et al. (1984) and Roberts (1988, 1992) suggested that podiform chromitites form in supra-subduction zone environments where mantle peridotites have experienced unusually high degrees of partial melting by addition of volatiles (Bonatti and Michael 1989; McDonough 1990). The Luobusa ophiolite hosting high-Cr chromitites is believed to have formed in such a supra-subduction zone environment (Zhou et al., 1995C).

The Luobusa ophiolite is characterized by depleted mantle peridotites suggesting formation by high degrees of partial melting in a supra-subduction zone environment. Chromites in the Luobusa massif have a wider range of Cr#s, but their compositions are compatible with a supra-subduction zone environment (Dick and Bullen, 1984). CaO contents of pyroxenes are low relative to oceanic peridotites (Dick and Natland, 1995). Diamonds have been reported from the Luobusa ophiolite suggesting emplacement from considerable depth (Bai et al., 1993).

Sparse volcanic rocks in Luobusa include basalts and basaltic andesites

whose compositions are compatible with formation in an arc-related environment. The cumulate sequence in Luobusa consists chiefly of dunite, pyroxenite and gabbro, a feature of supra-subduction zone ophiolites (Pearce, et al., 1984). These are similar to Papua-type ophiolites that contain low-Al tholeiites, Opx-cumulates and Cpx-free harzburgites (Ishiwatari, 1985).

Such mantle materials may contain considerable amounts of hydrous minerals such as amphibole or phlogopite, because island-arc magmas are thought to have high water contents (Anderson, 1975; Delaney et al., 1978; Muenow et al., 1980). For example, arc-related geochemical characteristics suggesting a hydrous upper mantle have been reported in the Miyamori ophiolite, northeast Japan (Ozawa, 1988). These fluid phases or melts may have derived from subducted slab that added H₂O and K₂O-rich fluid or silicate melt to the mantle wedge (Ringwood, 1974; Best, 1975; Hickey and Frey, 1982; Tatsumi and Ishizaka, 1982; Ozawa, 1988).

Hydrous phases have not been observed in the chromitites and peridotites in Luobusa. The lack of hydrous minerals may result from the high degree of partial melting for residual peridotites from "island-arc" ophiolites (e.g., Dick and Bullen, 1984; Hawkins and Evans, 1982, Pearce et al., 1984). Volatile- and alkali-rich mineral and fluid inclusions have been identified in chromite grains of podiform chromitites from several ophiolites, such as those in Al Ays of Saudi Arabia, Troodos in Cyprus, New Caledonia, and Oman (Johan et al., 1983; Johan, 1984; Auge, 1987; Lorand and Cottin, 1989; McElduff and

Stumpfl, 1991). The influence of volatiles also can be seen in many pegmatitic chromitites and associated pegmatitic gabbro and troctolite. Fluid inclusions in some chromitites have primitive upper mantle isotopic signatures (Dunlop and Fouillas, 1985). The volatile- and alkali-rich inclusions indicate high water content in the primitive magma, suggesting that the most probable tectonic setting is subduction-related (Delaney et al., 1978; Muenow et al., 1980).

However, a comparison of the high-Cr and high-Al chromitites in Western China indicates that not all podiform chromitites are hosted in highly depleted mantle peridotites (Zhou and Robinson, 1994). These authors suggest that high-Al chromitites can occur in less depleted mantle sequences (Iherzolite ophiolite type or transitional type) which have been locally modified by melt/rock interaction.

The Sartohay peridotites represent a moderately depleted residue after partial melting, similar to that of the Yakuno-type ophiolite characterized by high-Al tholeiite, Cpx-type cumulates and Cpx-bearing harzburgite (Ishiwatari, 1985). Abundant dykes, including troctolite, gabbro and chromitite, are present in the Sartohay, Hongguleleng and Hegenshan massifs (Zhou and Robinson, 1994). These observations in high-Al chromitite-bearing ophiolites indicate that they are similar to the MORB ophiolites as defined by Pearce et al. (1984). The well-developed cumulate sequences in Hongguleleng and Hegenshan may suggest a fast spreading environment which led to the formation of a thick and continuous plutonic sequence (Nicolas and Al Azi, 1991). The association of troctolites and

gabbros may indicate a lower pressure environment than the association of pyroxenites and gabbros (Thompson, 1972), suggesting that high-Al chromitites may have formed in a lower pressure environment than high-Cr chromitites. Furthermore, hydrous minerals and fluid inclusions were also observed in high-Al chromitites, such as those from the Hegenshan ophiolite of northern China (Bai et al., 1985), suggesting that high-Al chromitites also can be formed in a subduction-related environment.

According to Quick and Gregory (1995), ophiolites may have formed in three different settings: 1). mature spreading centres; 2). nascent spreading centres; and 3). island arcs (Figure 6-10). The mature spreading centres are similar to mid-ocean ridges (Figure 6-10A). Podiform chromitites likely form in the latter two settings that are related to supra-subduction zone environments. It is further suggested that high-Cr chromitites form in an island arc and high-Al chromitites in a nascent spreading centre (or backarc basin) (Figure 6-10B, C).

Microstructures and geochemistry of the mantle sequence of the Luobusa ophiolite allow a reconstruction of its tectonic evolution. The Di-harzburgites and harzburgites in Luobusa were originally formed in a mature spreading centre and subducted underneath the Gangdese magmatic arc. Intraoceanic subduction created the Luobusa oceanic island arc as shown in Figure 6-10C. The old lithospheric mantle immediately beneath the crust was invaded by large volumes of melts generated at depth by melting of the depleted harzburgites. The new magmas rose through and reacted with the old mantle, producing the

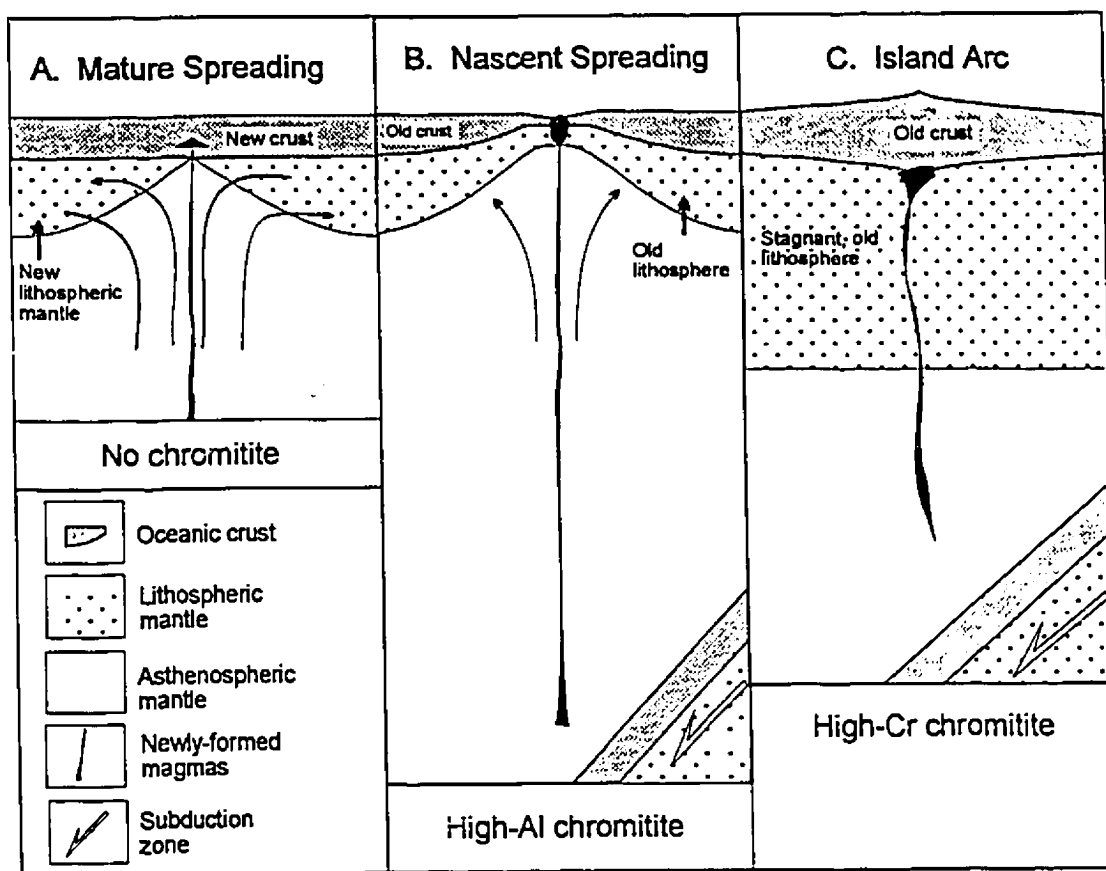


Figure 6-10. Diagrams illustrating three major tectonic settings and their relationships to the podiform chromitites. Podiform chromitites form in supra-subduction zone environments where new magmas reacted with old mantle peridotites.

chromitite and dunite pods. These represent stage 1 of deformation, overprinting the grain-growth-controlled, coarse "fertile" mantle microstructure (Calon, 1995, personal communication).

In the nascent spreading centres, old crust is removed as old lithospheric mantle rises and thins (Figure 6-10B). Melts generated by melting associated with subduction penetrate pre-existing, unrelated lithospheric mantle. Reaction between them produces high-Al chromitites, such as those from the Sartohay ophiolite.

6.3. Applications to chromite exploration

The melt/rock interaction model seems sufficient for explaining the formation of podiform chromitites, although it is necessary to provide further theoretical and experimental evidence for the factors that control the precipitation of chromite during the melt/rock interaction. A knowledge of such factors may be of use in chromite exploration, although exploration criteria are empirical in nature and based in large part on analogy with known chromite deposits.

It is well-documented that melt/rock interaction occurs in the upper mantle and commonly modifies the mineralogy and geochemistry of both the mantle peridotites and the magmas (Fisk, 1986; Kelemen, 1990; Kelemen et al., 1995; Daines and Kohlstedt, 1994; Dick and Natland, 1995). However, some ophiolites, or some dunite lenses, even in the same massif, may or may not

contain podiform bodies. In addition to melt/rock interaction, Cr and volatile contents of the parental magmas are likely controls on chromitite formation.

Normally, chromium would be included in the original magma as a minor component and eventually be incorporated into spinel phases as crystallization takes place. Previously, Roberts (1988; 1992) and Nicolas (1989) suggested that the higher the chromium in the magma, caused by dissolution of the Cr-diopside of the peridotites, the better the chance for chromite segregation into chromite deposits. In Luobusa, whole rock Cr contents do not show any correlations with major oxides or rock types (Figure 4-2). Similarly, Cr contents of pyroxenes do not vary systematically (Figure 4-15). Consequently, Cr contents of the original, basaltic magmas are not believed to be critical for the formation of podiform bodies.

As discussed earlier, the occurrence of volatile- and alkali-rich mineral assemblages suggests that the chromitites may have crystallized from volatile-rich magmas. Hydrous components in magmas may have enhanced the interaction between the magma and wall-rock and therefore have increased the extraction of chromium from the magmas.

In Luobusa, chromitites are distributed along a narrow band (Figure 3-1). According to the melt/rock interaction model, this represents the most extensive reaction zone where chromites precipitated from the magma. Melt/rock interaction may enrich the wall rocks in incompatible elements. In Sartohay, boron anomalies surrounding the large podiform bodies are used in prospecting

(Zhang Lin, 1992, personal communication). Moreover, immediately adjacent to the chromitite bodies, dunites or harzburgites are LREE-enriched, distinctly different from lherzolites (Figure 6-8). As outlined in Li Zijin et al. (1993), dunites hosting the Luobusa chromitites also show LREE-enrichment.

6.4. Summary

The high-Cr chromitites in Luobusa and the high-Al chromitites in Sartohay have distinctly different geochemical characteristics and crystallized from boninitic and tholeiitic magmas, respectively. Melt/rock interaction produced highly depleted dunite envelopes around both types of chromitites. In Sartohay, high-Al magmas reacted with lherzolites to produce high-Al dunites and harzburgites, whereas in Luobusa the reaction between more refractory melts and depleted harzburgites yielded only depleted dunite envelopes. High-Al chromitites occur in the weakly depleted mantle sequences (lherzolitic ophiolite type) that are locally depleted by melt/rock interaction in the immediate vicinity of the chromitite pods.

Podiform chromitites are believed to form in supra-subduction zone environments: high-Cr chromitites in island arc settings and high-Al chromitites in nascent spreading centres, e.g. back arc basins. Their formation involved a volatile-rich magma system caused by dehydration of the downgoing slab which interacted with old lithospheric mantle. Due to reaction with magmas, wall-rock dunites of podiform chromitites are enriched in LREE and other incompatible

elements. These may be used as indicators for chromite exploration.

Chapter 7: CONCLUSIONS AND FUTURE WORK

7.1. Conclusions

The principal conclusions of this study are as follows:

(1) The mantle peridotites and chromitites in Luobusa indicate two stages of magma generation in this complex. Early, sulfur-saturated tholeiitic melts formed possibly in a mature spreading centre left a depleted residue of harzburgite with unfractionated PGE patterns. A second stage of melting at depth formed sulfur-undersaturated boninitic magmas from which high-Cr podiform chromitites with highly-fractionated PGE patterns were crystallized.

(2) Melt/rock interaction in the upper mantle added silica to the magma by dissolving Opx and precipitating Ol. This process, along with magma mixing between relatively primitive and fractionated melts, moved the magmas from the Ol-chromite cotectic into the field of chromite crystallization (Figure 5-2). Crystallization of these melts produced massive and disseminated chromitites and phase layering within a single podiform body.

(3) The Luobusa ophiolite contains abundant high-Cr podiform chromitite; and the Sartohay ophiolite is rich in high-Al podiform chromitites. Both the chromitites formed by crystallization of magmas are petrographically similar and are hosted in mantle peridotites with different degrees of depletion.

(4) Interaction between the residual rocks and magmas produced dunite envelopes around both the high-Cr and high-Al podiform chromitites. These

envelopes grade from dunite to harzburgite to Di-harzburgite or to lherzolite. However, the dunite envelopes in Sartohay are much higher in Al than those in Luobusa.

(5) High-Cr and high-Al podiform chromitites were formed from boninitic and MORB magmas, respectively. High-Cr podiform chromitites are hosted in more refractory, harzburgitic mantle peridotites, whereas high-Al podiform chromitites occur in less-depleted, lherzolitic mantle peridotites which have been locally modified by melt/rock interaction.

(6) Podiform chromitites are likely formed in supra-subduction zone environments. In such environments, volatile-enriched, newly-formed magmas react with relatively stagnant, old lithospheric mantle, to form podiform chromitites. The presence or absence of podiform chromitites and their compositions are controlled by tectonic setting: A. No chromite deposits would form in mature spreading centres, such as mid-oceanic ridges; B. High-Cr chromite deposits form in island arc environments; and C. High-Al chromite deposits reflect nascent spreading centres, such as those in back arc basins.

7.2. Suggestions for future work

The melt/rock interaction model proposed in this thesis provides a means of precipitating relatively large volumes of chromite from mafic magmas having low Cr concentrations. The following suggestions, although beyond the scope of this study, are recommended for further investigations.

(1) It is necessary to provide theoretical and experimental evidence for the factors that control the precipitation of chromite during melt/rock interaction. The magma mixing model has been experimentally documented with respect to phase relationships (Sharpe and Irvine, 1983; Irvine and Sharpe, 1986). Recently, experiments have demonstrated the effects of interaction between harzburgite and basaltic magma (Fisk, 1986; Daines and Kohstedt, 1994; Kelemen et al., 1995). It may be possible to produce experimentally system in which chromites can be formed. In particular, such experiments may provide useful information about the effects of melt/rock reaction on the chemistry of magmas, wall-rocks and chromite composition.

(2) To further test the proposed model will require new analyses on the reaction zone around podiform chromitites. Whole-rock and mineral trace elements, such as Ti, B, and REE, as well as isotopic compositions, are known to be sensitive to partial melting and melt/rock interaction (Johnson et al., 1990; Sen et al., 1993). These data can be obtained by ICP-MS and ion-probe techniques and will provide further geochemical constraints on the melt/rock reaction process.

(3) This study has focused on high-Cr chromitites in Luobusa and high-Al chromitites in Sartohay. In both cases, parental magmas were relatively simple as indicated by the uniform chromite compositions. Other ophiolites may contain podiform chromitites in which chromites have variable compositions. Further study of such chromitites may be required in order to investigate complicated

magma systems and/or *P/T* conditions in the upper mantle during the formation of podiform chromitites.

Appendix I: ANALYTICAL METHODS

I.1. Petrochemistry

Major oxides and some trace elements were analyzed with a Phillips PW1400 sequential X-ray fluorescence spectrometer at the Regional Analytical Facility, Saint Mary's University, Halifax. Fused glass disks were used for major oxides, whereas pressed powder pellets were used for trace element determinations. The analytical precision is better than 5% for major elements and between 5 to 10% for trace elements.

I.2. Whole rock PGE abundances

Preconcentration of PGEs was accomplished by a combination of NiS fusion, and Te coprecipitation (Jackson et al., 1990; Sun et al., 1993; Zhou, 1994). The fusion mixture was prepared using powdered chromitite (7g), nickel (9.6g), sulfur (6.0g), sodium carbonate (18g), lithium tetraborate (25g), and silica (9g) to produce a NiS button. This analytical protocol for chromite-rich samples differs from that for ordinary mafic and ultramafic rock samples as follows: (a) lithium tetraborate was substituted for sodium borate, (b) the fusion temperature was raised from 1000 °C to 1150 °C, and (c) the fusion time was increased from 1.25 hours to 2.5 hours. These modifications were adopted because the conventional method produces a NiS button with a thin layer of new chromite, possibly resulting in incomplete recovery of PGEs. Uncrushed buttons were

dissolved in 100 ml concentrated HCl, and the PGEs were collected by Te coprecipitation.

The final solutions were analyzed for PGEs using an ELAN-5000 inductively coupled plasma-mass spectrometer (ICP-MS) at the University of Saskatchewan. Total procedural blanks are 0.5 ng for Os, Ru and Rh, 2.0 ng for Ir and Pt, and 3.0 ng for Pd. Average detection limits cited as 3σ background are equivalent to Os 0.01, Ir 0.005, Rh 0.07, Pt 0.04 and Pd 0.47 ppb in the rock.

Recovery of precious metals in the geologic reference material, SARM-7, is ca.100%. Average determined abundances of Ru, Rh, Pd, and Ir were found to be within error of the certified values. Precision and accuracy are less than 5% for Ru, Rh and Pd, 10% for Pt and Ir, and 30% for Os.

1.3. Mineral compositions

Chromite, Ol and pyroxenes were analyzed for major oxides with a JEOL 733 electron microprobe equipped with an Oxford Link eXL energy dispersive system at Dalhousie University. The resolution of the detector is 137 eV at 5.9 Kev. An accelerating voltage of 15 Kv was used with a beam current of 12 nA, and each spectrum was accumulated for 40 seconds. Instrument calibration was performed using Cobalt metal and geological standards. Results were corrected using Link's ZAF matrix correction program.

Electron microprobe results are probably accurate to 1% of the value of the results, for each oxide, and precise to 0.1%. Recalculated mineral formulae

are subject to similar accuracy and precision. In Ol analyses, Fo calculations are accurate to roughly 0.3 of the Fo number, but precise to a much higher degree. Similar accuracy and precision apply to analyses of other minerals.

All data tables have been presented with major element oxides quoted to three significant figures, to reflect the levels of error. Mineral recalculations, however, have been presented, as is conventional, to three decimal places.

For chromite, Fe²⁺ and Fe³⁺ were distributed based on the stoichiometry of spinel (Fe²⁺, Mg) (Al, Cr, Fe³⁺)₂O₄. Representative analyses, together with Cr#s and Mg#s, appear in Appendix III-1. Total iron in Ol and pyroxene was considered to be Fe²⁺ and the results appear in Appendix III-2, -3, and -4.

Appendix II Petrochemistry

| | SiO ₂ | Al ₂ O ₃ | Cr ₂ O ₃ | FeO | MgO | CaO |
|-------------|------------------|--------------------------------|--------------------------------|------|-------|------|
| Harzburgite | | | | | | |
| 1 | 45.95 | 1.34 | 0.80 | 7.90 | 43.18 | 0.83 |
| 2 | 44.48 | 0.74 | 0.47 | 8.58 | 45.08 | 0.65 |
| 3 | 45.02 | 0.70 | 0.51 | 8.53 | 44.51 | 0.73 |
| 4 | 43.90 | 1.17 | 0.43 | 9.09 | 43.64 | 1.77 |
| 5 | 43.81 | 1.03 | 0.46 | 8.50 | 44.70 | 1.50 |
| 6 | 44.80 | 0.66 | 0.36 | 8.42 | 45.07 | 0.69 |
| 7 | 44.92 | 1.76 | 0.49 | 8.62 | 42.29 | 1.91 |
| 8 | 44.82 | 1.33 | 0.26 | 7.92 | 44.43 | 1.24 |
| 9 | 44.34 | 1.51 | 0.33 | 8.14 | 44.07 | 1.61 |
| 10 | 45.30 | 1.65 | 0.42 | 7.90 | 43.03 | 1.70 |
| 11 | 45.15 | 1.94 | 0.42 | 7.76 | 43.11 | 1.61 |
| 12 | 45.83 | 0.79 | 0.57 | 8.09 | 44.00 | 0.73 |
| 13 | 44.28 | 1.41 | 0.41 | 8.19 | 44.33 | 1.39 |
| 14 | 44.82 | 1.47 | 0.45 | 8.37 | 43.07 | 1.82 |
| 15 | 43.90 | 1.17 | 0.58 | 7.95 | 45.16 | 1.23 |
| 16 | 45.10 | 1.31 | 0.51 | 8.24 | 43.11 | 1.73 |
| 17 | 45.90 | 1.93 | 0.59 | 8.34 | 41.17 | 2.07 |
| 18 | 46.02 | 1.80 | 0.46 | 8.20 | 41.66 | 1.85 |
| 19 | 45.05 | 1.71 | 0.55 | 8.31 | 42.69 | 1.69 |
| 20 | 45.51 | 1.14 | 0.42 | 8.36 | 42.82 | 1.75 |
| 21 | 44.46 | 1.06 | 0.37 | 8.25 | 44.57 | 1.29 |
| 22 | 46.14 | 1.93 | 0.45 | 8.17 | 41.19 | 2.11 |
| 23 | 45.24 | 1.41 | 0.35 | 8.49 | 43.22 | 1.29 |
| 24 | 44.79 | 0.35 | 0.30 | 8.24 | 45.75 | 0.58 |
| 25 | 45.24 | 0.95 | 0.58 | 8.21 | 44.09 | 0.93 |
| 26 | 44.47 | 1.16 | 0.49 | 8.47 | 43.74 | 1.68 |
| 27 | 44.85 | 0.87 | 0.49 | 8.34 | 44.48 | 0.97 |
| 28 | 44.27 | 1.03 | 0.46 | 8.27 | 44.78 | 1.19 |
| 29 | 44.52 | 1.48 | 0.52 | 8.28 | 43.09 | 2.10 |
| 30 | 44.06 | 0.37 | 0.52 | 8.38 | 46.21 | 0.44 |
| 31 | 44.75 | 0.97 | 0.62 | 7.99 | 44.53 | 1.13 |
| 32 | 44.81 | 1.39 | 0.53 | 8.02 | 43.53 | 1.70 |
| 33 | 44.42 | 0.98 | 0.55 | 7.98 | 44.81 | 1.26 |
| 34 | 44.31 | 0.91 | 0.42 | 7.98 | 45.65 | 0.73 |
| 35 | 44.73 | 1.07 | 0.48 | 8.22 | 44.26 | 1.25 |
| 36 | 43.86 | 1.15 | 0.54 | 8.11 | 45.36 | 0.99 |
| 37 | 43.68 | 0.50 | 0.45 | 8.27 | 46.48 | 0.63 |
| 38 | 44.40 | 1.00 | 0.50 | 7.91 | 45.24 | 0.94 |
| 39 | 44.85 | 1.22 | 0.34 | 8.20 | 44.58 | 0.82 |
| 40 | 43.37 | 0.76 | 0.24 | 8.08 | 46.95 | 0.60 |
| 41 | 45.33 | 0.68 | 0.46 | 7.97 | 44.67 | 0.88 |
| 42 | 43.83 | 0.64 | 0.38 | 7.79 | 46.47 | 0.88 |
| 43 | 47.01 | 0.85 | 0.47 | 7.78 | 42.94 | 0.94 |
| 44 | 45.65 | 1.15 | 0.54 | 7.65 | 43.49 | 1.52 |
| 45 | 44.69 | 0.95 | 0.43 | 8.01 | 44.91 | 1.01 |

Appendix II (continued)

| | SiO ₂ | Al ₂ O ₃ | Cr ₂ O ₃ | FeO | MgO | CaO |
|------------|------------------|--------------------------------|--------------------------------|-------|-------|------|
| 46 | 45.68 | 1.87 | 0.27 | 8.19 | 41.99 | 2.00 |
| 47 | 45.15 | 0.76 | 0.54 | 9.15 | 42.71 | 1.69 |
| 48 | 44.67 | 1.28 | 0.33 | 8.54 | 43.86 | 1.33 |
| 49 | 46.12 | 2.10 | 0.40 | 8.77 | 40.65 | 1.95 |
| 50 | 45.03 | 1.85 | 0.43 | 8.73 | 41.83 | 2.11 |
| 51 | 45.80 | 1.80 | 0.27 | 8.31 | 41.46 | 2.36 |
| 52 | 45.13 | 1.80 | 0.36 | 8.81 | 42.85 | 1.05 |
| 53 | 46.42 | 1.83 | 0.58 | 7.94 | 40.94 | 2.30 |
| 54 | 45.16 | 1.45 | 0.42 | 8.36 | 42.84 | 1.77 |
| 55 | 44.95 | 1.63 | 0.48 | 8.29 | 43.44 | 1.21 |
| 56 | 45.45 | 1.73 | 0.39 | 8.44 | 42.20 | 1.78 |
| Dunite | | | | | | |
| 1 | 42.11 | 0.23 | 0.39 | 7.39 | 49.61 | 0.28 |
| 2 | 41.54 | 0.53 | 0.51 | 8.77 | 47.98 | 0.66 |
| 3 | 41.36 | 0.39 | 0.00 | 10.26 | 47.80 | 0.19 |
| 4 | 40.64 | 0.26 | 0.42 | 6.66 | 51.90 | 0.12 |
| 5 | 41.24 | 0.47 | 0.00 | 7.62 | 50.59 | 0.08 |
| 6 | 42.53 | 0.60 | 0.33 | 5.68 | 50.84 | 0.02 |
| 7 | 40.98 | 0.08 | 0.46 | 8.65 | 49.69 | 0.14 |
| 8 | 40.55 | 0.51 | 0.50 | 6.81 | 51.58 | 0.05 |
| 9 | 42.42 | 0.45 | 0.38 | 8.51 | 47.79 | 0.44 |
| 10 | 40.56 | 0.36 | 0.33 | 7.94 | 50.44 | 0.36 |
| 11 | 41.96 | 0.12 | 0.59 | 8.02 | 49.18 | 0.12 |
| 12 | 42.12 | 0.11 | 0.57 | 7.60 | 49.48 | 0.11 |
| 13 | 44.90 | 1.23 | 0.35 | 8.34 | 44.22 | 0.95 |
| 14 | 45.09 | 1.26 | 0.70 | 8.21 | 43.87 | 0.88 |
| 15 | 45.40 | 1.22 | 0.38 | 8.15 | 43.45 | 1.39 |
| 16 | 45.59 | 1.72 | 0.33 | 8.26 | 42.29 | 1.80 |
| 17 | 44.63 | 0.78 | 0.29 | 7.87 | 45.69 | 0.73 |
| 18 | 44.71 | 1.37 | 0.44 | 8.53 | 42.98 | 1.96 |
| 19 | 43.84 | 0.63 | 0.42 | 8.77 | 45.57 | 0.76 |
| Chromitite | | | | | | |
| 1 | 9.66 | 10.32 | 51.92 | 6.40 | 20.41 | 1.29 |
| 2 | 14.55 | 8.60 | 45.25 | 6.21 | 25.11 | 0.28 |
| 3 | 32.42 | 3.40 | 14.99 | 5.20 | 43.94 | 0.04 |
| 4 | 25.68 | 5.31 | 26.71 | 6.12 | 36.11 | 0.07 |
| 5 | 6.97 | 9.75 | 55.93 | 6.56 | 20.78 | 0.00 |
| 6 | 16.43 | 7.61 | 42.38 | 5.96 | 27.61 | 0.00 |
| 7 | 9.33 | 9.63 | 55.27 | 7.10 | 18.66 | 0.01 |
| 8 | 7.34 | 10.18 | 57.15 | 6.56 | 18.75 | 0.01 |
| 9 | 3.62 | 10.13 | 54.60 | 12.72 | 18.67 | 0.27 |
| 10 | 2.90 | 10.49 | 55.41 | 12.76 | 18.19 | 0.25 |
| 11 | 1.63 | 10.77 | 57.02 | 12.66 | 17.66 | 0.26 |
| 12 | 0.47 | 10.79 | 58.60 | 12.80 | 16.98 | 0.37 |
| 13 | 1.03 | 10.89 | 57.58 | 12.62 | 17.66 | 0.22 |
| 14 | 0.83 | 10.68 | 58.10 | 12.80 | 17.36 | 0.21 |
| 15 | 0.42 | 10.90 | 58.69 | 12.86 | 16.85 | 0.28 |
| 16 | 0.65 | 10.81 | 58.42 | 12.58 | 17.19 | 0.35 |

Appendix II (continued)

| | SiO ₂ | Al ₂ O ₃ | Cr ₂ O ₃ | FeO | MgO | CaO |
|----|------------------|--------------------------------|--------------------------------|-------|-------|------|
| 17 | 5.68 | 10.19 | 52.03 | 12.98 | 19.01 | 0.10 |
| 18 | 9.47 | 7.91 | 49.11 | 14.03 | 19.30 | 0.19 |
| 19 | 2.94 | 10.43 | 56.59 | 12.91 | 16.98 | 0.15 |
| 20 | 7.27 | 9.37 | 50.17 | 13.08 | 19.99 | 0.15 |
| 21 | 1.76 | 10.24 | 57.66 | 12.93 | 17.23 | 0.18 |
| 22 | 3.25 | 10.47 | 55.98 | 13.18 | 16.95 | 0.18 |
| 23 | 1.82 | 11.08 | 57.40 | 12.82 | 16.61 | 0.26 |
| 24 | 1.63 | 11.01 | 57.79 | 12.81 | 16.53 | 0.23 |
| 25 | 0.74 | 11.51 | 58.68 | 13.54 | 15.31 | 0.21 |
| 26 | 4.38 | 10.58 | 54.17 | 13.76 | 16.76 | 0.35 |
| 27 | 3.11 | 10.70 | 55.50 | 13.53 | 16.98 | 0.18 |
| 28 | 2.88 | 10.39 | 56.20 | 12.78 | 17.55 | 0.19 |
| 29 | 1.94 | 11.04 | 57.60 | 12.93 | 16.33 | 0.16 |
| 30 | 5.42 | 9.44 | 53.36 | 13.20 | 18.42 | 0.16 |
| 31 | 2.45 | 11.07 | 56.19 | 12.95 | 17.14 | 0.19 |
| 32 | 2.46 | 10.79 | 56.49 | 12.70 | 17.39 | 0.16 |
| 33 | 2.37 | 10.37 | 55.90 | 13.47 | 17.74 | 0.15 |
| 34 | 1.32 | 10.37 | 57.02 | 13.26 | 17.89 | 0.14 |
| 35 | 1.23 | 10.62 | 57.33 | 13.25 | 17.50 | 0.07 |
| 36 | 4.92 | 3.89 | 56.38 | 14.65 | 19.95 | 0.20 |
| 37 | 0.93 | 10.45 | 57.62 | 13.51 | 17.34 | 0.14 |
| 38 | 2.03 | 10.67 | 55.78 | 13.13 | 18.32 | 0.07 |
| 39 | 3.35 | 10.64 | 55.51 | 12.83 | 17.48 | 0.17 |
| 40 | 2.27 | 10.62 | 56.41 | 13.08 | 17.54 | 0.08 |
| 41 | 1.75 | 10.68 | 57.06 | 12.90 | 17.54 | 0.08 |
| 42 | 3.35 | 9.87 | 53.86 | 14.36 | 18.40 | 0.14 |
| 43 | 3.32 | 10.24 | 55.88 | 13.19 | 17.17 | 0.21 |
| 44 | 5.40 | 10.19 | 52.50 | 13.46 | 18.12 | 0.32 |
| 45 | 3.06 | 10.36 | 56.14 | 12.79 | 17.58 | 0.07 |
| 46 | 4.25 | 10.56 | 54.08 | 12.98 | 17.89 | 0.23 |
| 47 | 2.50 | 8.81 | 57.94 | 14.08 | 16.62 | 0.05 |
| 48 | 1.24 | 10.83 | 58.42 | 13.30 | 16.16 | 0.05 |
| 49 | 2.66 | 10.56 | 55.75 | 13.50 | 17.23 | 0.31 |
| 50 | 2.54 | 10.19 | 56.88 | 13.40 | 16.76 | 0.24 |
| 51 | 1.38 | 10.36 | 57.53 | 12.99 | 17.53 | 0.20 |
| 52 | 1.39 | 10.27 | 58.14 | 12.84 | 17.08 | 0.29 |
| 53 | 1.60 | 10.51 | 57.99 | 13.03 | 16.56 | 0.32 |
| 54 | 9.27 | 10.24 | 46.24 | 12.71 | 21.33 | 0.21 |
| 55 | 6.12 | 10.14 | 52.31 | 12.35 | 18.88 | 0.21 |
| 56 | 2.51 | 10.28 | 57.16 | 12.98 | 16.88 | 0.19 |
| 57 | 1.43 | 10.61 | 58.92 | 12.94 | 15.99 | 0.12 |
| 58 | 1.31 | 10.65 | 58.92 | 12.87 | 16.09 | 0.16 |
| 59 | 1.49 | 10.44 | 58.88 | 12.67 | 16.41 | 0.12 |
| 60 | 0.70 | 10.82 | 59.37 | 12.75 | 16.20 | 0.16 |
| 61 | 0.67 | 10.69 | 59.87 | 12.67 | 15.94 | 0.16 |
| 62 | 0.74 | 10.79 | 59.49 | 12.60 | 16.23 | 0.14 |
| 63 | 0.95 | 10.82 | 60.04 | 12.00 | 16.05 | 0.15 |
| 64 | 0.92 | 10.73 | 59.33 | 12.36 | 16.55 | 0.12 |

Appendix II (continued)

| | SiO ₂ | Al ₂ O ₃ | Cr ₂ O ₃ | FeO | MgO | CaO |
|-----|------------------|--------------------------------|--------------------------------|-------|-------|------|
| 65 | 1.66 | 10.92 | 59.28 | 11.52 | 16.41 | 0.20 |
| 66 | 5.95 | 10.04 | 53.02 | 11.87 | 18.95 | 0.17 |
| 67 | 6.20 | 9.02 | 52.70 | 13.44 | 18.37 | 0.27 |
| 68 | 7.69 | 8.65 | 50.89 | 14.15 | 18.30 | 0.31 |
| 69 | 6.50 | 9.19 | 51.64 | 14.83 | 17.72 | 0.10 |
| 70 | 9.27 | 8.56 | 47.89 | 15.05 | 19.18 | 0.06 |
| 71 | 2.08 | 11.23 | 57.22 | 13.00 | 16.36 | 0.11 |
| 72 | 1.29 | 11.43 | 57.61 | 12.97 | 16.52 | 0.18 |
| 73 | 1.38 | 11.33 | 58.56 | 11.96 | 16.55 | 0.21 |
| 74 | 1.77 | 10.70 | 57.62 | 13.38 | 16.32 | 0.20 |
| 75 | 11.09 | 8.32 | 46.73 | 12.39 | 21.16 | 0.32 |
| 76 | 7.53 | 9.98 | 50.72 | 11.59 | 19.90 | 0.28 |
| 77 | 10.52 | 10.15 | 46.17 | 12.24 | 20.62 | 0.30 |
| 78 | 1.56 | 11.59 | 56.83 | 13.42 | 16.27 | 0.33 |
| 79 | 1.21 | 12.47 | 56.62 | 13.36 | 16.01 | 0.33 |
| 80 | 2.39 | 9.96 | 57.60 | 12.60 | 17.15 | 0.29 |
| 81 | 11.83 | 8.12 | 46.02 | 12.74 | 20.97 | 0.32 |
| 82 | 8.12 | 9.88 | 50.54 | 13.04 | 18.12 | 0.30 |
| 83 | 4.84 | 9.83 | 54.25 | 12.54 | 18.28 | 0.26 |
| 84 | 4.79 | 9.68 | 54.45 | 12.78 | 17.99 | 0.31 |
| 85 | 6.21 | 9.99 | 52.12 | 12.73 | 18.70 | 0.26 |
| 86 | 2.46 | 10.47 | 57.15 | 12.64 | 17.02 | 0.25 |
| 87 | 1.61 | 10.62 | 58.03 | 12.69 | 16.80 | 0.25 |
| 88 | 2.00 | 10.26 | 57.79 | 13.34 | 16.38 | 0.23 |
| 89 | 4.66 | 9.67 | 54.57 | 12.85 | 18.02 | 0.23 |
| 90 | 2.27 | 10.30 | 57.17 | 12.66 | 17.29 | 0.31 |
| 91 | 2.26 | 10.07 | 57.89 | 13.05 | 16.63 | 0.10 |
| 92 | 5.82 | 9.41 | 53.13 | 12.50 | 19.09 | 0.05 |
| 93 | 4.38 | 10.00 | 54.48 | 12.86 | 18.23 | 0.05 |
| 94 | 2.70 | 9.86 | 57.51 | 13.13 | 16.78 | 0.00 |
| 95 | 1.30 | 10.25 | 58.46 | 12.82 | 17.13 | 0.03 |
| 96 | 3.81 | 10.08 | 55.60 | 12.49 | 18.03 | 0.00 |
| 97 | 9.99 | 9.60 | 47.43 | 12.32 | 20.64 | 0.01 |
| 98 | 4.48 | 10.28 | 54.54 | 12.39 | 17.86 | 0.45 |
| 99 | 4.54 | 10.23 | 54.43 | 12.82 | 17.56 | 0.42 |
| 100 | 6.00 | 10.05 | 52.77 | 12.79 | 17.97 | 0.42 |
| 101 | 6.99 | 9.75 | 51.50 | 13.92 | 17.42 | 0.42 |
| 102 | 1.17 | 10.15 | 59.91 | 12.55 | 16.04 | 0.18 |
| 103 | 1.17 | 9.47 | 60.33 | 12.82 | 16.01 | 0.20 |
| 104 | 1.75 | 10.15 | 58.89 | 12.87 | 16.15 | 0.18 |
| 105 | 0.94 | 10.20 | 59.76 | 13.00 | 15.93 | 0.17 |
| 106 | 1.28 | 10.58 | 59.03 | 12.94 | 15.95 | 0.23 |
| 107 | 0.62 | 10.46 | 60.18 | 12.74 | 15.80 | 0.21 |
| 108 | 0.78 | 10.58 | 59.84 | 12.66 | 15.99 | 0.15 |
| 109 | 1.70 | 10.59 | 58.73 | 12.40 | 16.24 | 0.33 |
| 110 | 2.52 | 10.34 | 57.98 | 12.59 | 15.91 | 0.66 |
| 111 | 2.31 | 10.56 | 57.86 | 12.67 | 16.25 | 0.35 |
| 112 | 3.19 | 10.87 | 56.34 | 12.81 | 16.60 | 0.18 |

Appendix II (continued)

| | SiO ₂ | Al ₂ O ₃ | Cr ₂ O ₃ | FeO | MgO | CaO |
|-----|------------------|--------------------------------|--------------------------------|-------|-------|------|
| 113 | 8.69 | 9.35 | 49.81 | 12.41 | 18.85 | 0.89 |
| 114 | 3.40 | 10.40 | 55.69 | 13.76 | 16.22 | 0.52 |
| 115 | 2.48 | 10.49 | 56.98 | 12.19 | 17.32 | 0.53 |
| 116 | 4.37 | 9.59 | 55.07 | 12.36 | 18.09 | 0.53 |
| 117 | 8.17 | 8.48 | 49.52 | 11.64 | 21.62 | 0.56 |
| 118 | 3.05 | 10.54 | 56.76 | 12.20 | 16.95 | 0.49 |
| 119 | 8.45 | 8.30 | 49.43 | 15.24 | 18.05 | 0.54 |
| 120 | 18.41 | 6.75 | 35.44 | 13.30 | 25.23 | 0.87 |
| 121 | 32.32 | 2.98 | 16.00 | 11.25 | 38.87 | 0.58 |
| 122 | 7.88 | 8.90 | 49.57 | 14.70 | 18.43 | 0.52 |
| 123 | 5.21 | 10.37 | 52.62 | 14.02 | 17.26 | 0.52 |
| 124 | 3.79 | 9.68 | 56.23 | 13.14 | 16.75 | 0.41 |
| 125 | 9.69 | 8.89 | 46.23 | 12.40 | 20.71 | 2.08 |
| 126 | 2.00 | 9.66 | 59.77 | 12.26 | 16.15 | 0.15 |
| 127 | 4.69 | 9.96 | 53.24 | 13.01 | 18.80 | 0.30 |
| 128 | 4.89 | 10.37 | 51.77 | 13.09 | 19.29 | 0.59 |
| 129 | 2.43 | 10.50 | 56.62 | 12.84 | 17.48 | 0.13 |
| 130 | 2.67 | 10.29 | 57.16 | 12.64 | 17.08 | 0.15 |
| 131 | 4.38 | 10.05 | 54.14 | 13.13 | 17.85 | 0.45 |
| 132 | 3.90 | 10.16 | 55.20 | 12.39 | 18.27 | 0.08 |
| 133 | 8.19 | 9.06 | 50.11 | 12.70 | 19.78 | 0.15 |
| 134 | 6.28 | 9.75 | 52.67 | 12.75 | 18.14 | 0.41 |
| 135 | 2.86 | 11.03 | 56.34 | 12.66 | 16.91 | 0.19 |
| 136 | 2.12 | 10.17 | 58.10 | 12.55 | 16.88 | 0.19 |
| 137 | 5.50 | 9.08 | 53.87 | 13.88 | 17.57 | 0.11 |
| 138 | 7.64 | 9.01 | 50.87 | 12.26 | 20.01 | 0.21 |
| 139 | 34.12 | 2.03 | 11.44 | 7.64 | 44.59 | 0.19 |
| 140 | 35.25 | 1.45 | 8.94 | 8.00 | 46.14 | 0.22 |
| 141 | 1.39 | 10.11 | 58.69 | 12.95 | 16.70 | 0.17 |
| 142 | 8.52 | 9.45 | 49.30 | 12.07 | 20.43 | 0.23 |
| 143 | 5.16 | 10.08 | 53.27 | 12.63 | 18.44 | 0.43 |
| 144 | 6.55 | 9.36 | 52.14 | 11.87 | 19.79 | 0.30 |
| 145 | 8.08 | 9.83 | 49.94 | 11.92 | 20.03 | 0.20 |
| 146 | 6.37 | 9.93 | 52.31 | 12.54 | 18.63 | 0.22 |
| 147 | 1.84 | 10.75 | 57.88 | 13.13 | 16.24 | 0.17 |
| 148 | 2.11 | 10.86 | 57.22 | 13.91 | 15.73 | 0.17 |
| 149 | 2.44 | 10.38 | 57.22 | 12.56 | 17.21 | 0.19 |
| 150 | 4.64 | 10.48 | 54.66 | 13.08 | 16.45 | 0.69 |
| 151 | 3.40 | 10.21 | 55.81 | 12.89 | 17.52 | 0.17 |
| 152 | 2.53 | 11.29 | 56.40 | 13.27 | 16.20 | 0.30 |
| 153 | 2.33 | 9.98 | 57.69 | 13.30 | 16.57 | 0.14 |
| 154 | 4.08 | 10.63 | 54.87 | 14.08 | 15.86 | 0.48 |
| 155 | 4.89 | 9.64 | 53.96 | 12.59 | 18.39 | 0.53 |
| 156 | 1.12 | 11.33 | 57.57 | 13.80 | 15.88 | 0.30 |
| 157 | 5.82 | 9.52 | 55.25 | 12.94 | 16.33 | 0.12 |
| 158 | 6.30 | 9.86 | 52.73 | 12.54 | 18.37 | 0.19 |
| 159 | 4.52 | 10.33 | 54.26 | 12.66 | 18.01 | 0.22 |
| 160 | 4.03 | 10.84 | 54.89 | 13.24 | 16.83 | 0.17 |

Appendix II (continued)

| | SiO ₂ | Al ₂ O ₃ | Cr ₂ O ₃ | FeO | MgO | CaO |
|-----|------------------|--------------------------------|--------------------------------|-------|-------|------|
| 161 | 3.08 | 10.53 | 56.94 | 12.67 | 16.63 | 0.15 |
| 162 | 8.29 | 9.18 | 50.12 | 12.02 | 18.95 | 1.44 |
| 163 | 37.37 | 1.20 | 6.41 | 7.43 | 47.35 | 0.23 |
| 164 | 3.70 | 9.61 | 56.78 | 11.91 | 17.77 | 0.23 |
| 165 | 5.06 | 10.42 | 54.72 | 11.87 | 17.46 | 0.47 |
| 166 | 3.05 | 10.42 | 56.88 | 12.38 | 17.04 | 0.21 |
| 165 | 8.26 | 9.50 | 49.06 | 11.53 | 21.40 | 0.26 |
| 166 | 5.36 | 10.19 | 53.63 | 11.67 | 18.28 | 0.87 |
| 167 | 6.36 | 9.97 | 51.84 | 12.95 | 18.21 | 0.67 |
| 168 | 4.29 | 9.97 | 54.58 | 12.82 | 18.07 | 0.26 |
| 169 | 4.18 | 9.43 | 54.98 | 13.16 | 17.77 | 0.47 |
| 170 | 10.54 | 8.88 | 46.07 | 12.90 | 20.54 | 1.07 |
| 171 | 1.93 | 10.80 | 58.19 | 12.30 | 16.64 | 0.13 |
| 172 | 28.12 | 5.97 | 19.43 | 9.35 | 36.54 | 0.59 |
| 173 | 4.71 | 11.19 | 53.63 | 12.85 | 17.49 | 0.12 |
| 174 | 9.41 | 9.17 | 46.94 | 13.97 | 20.35 | 0.16 |
| 175 | 4.17 | 10.23 | 54.45 | 13.32 | 17.61 | 0.22 |
| 176 | 12.10 | 8.32 | 45.78 | 12.49 | 21.15 | 0.16 |
| 177 | 4.62 | 11.27 | 53.86 | 12.41 | 16.84 | 1.00 |
| 178 | 2.97 | 12.06 | 54.88 | 13.30 | 16.42 | 0.37 |
| 179 | 2.74 | 9.96 | 57.41 | 13.34 | 16.43 | 0.13 |
| 180 | 5.76 | 9.55 | 52.82 | 12.17 | 19.06 | 0.65 |
| 181 | 4.20 | 10.06 | 54.66 | 13.06 | 17.39 | 0.63 |
| 182 | 6.04 | 10.04 | 52.00 | 12.79 | 18.08 | 1.05 |
| 183 | 21.13 | 6.01 | 31.51 | 10.04 | 30.65 | 0.65 |
| 184 | 4.23 | 9.73 | 54.83 | 11.94 | 18.83 | 0.45 |
| 185 | 6.32 | 9.51 | 52.46 | 11.59 | 19.66 | 0.46 |
| 186 | 4.39 | 10.94 | 54.35 | 12.54 | 17.00 | 0.79 |
| 187 | 18.48 | 7.41 | 34.38 | 10.61 | 28.75 | 0.36 |
| 188 | 3.57 | 11.07 | 54.97 | 12.76 | 17.43 | 0.19 |
| 189 | 3.39 | 9.97 | 56.13 | 13.35 | 17.01 | 0.15 |
| 190 | 12.29 | 8.21 | 44.52 | 11.78 | 23.04 | 0.16 |
| 191 | 12.82 | 11.44 | 40.39 | 15.44 | 18.72 | 1.19 |
| 192 | 6.28 | 11.11 | 51.01 | 13.40 | 17.64 | 0.57 |
| 193 | 14.11 | 7.29 | 44.22 | 11.56 | 22.47 | 0.35 |
| 196 | 21.16 | 6.21 | 34.94 | 10.05 | 27.10 | 0.53 |
| 197 | 12.96 | 8.41 | 44.57 | 10.97 | 22.63 | 0.45 |
| 198 | 26.54 | 5.16 | 27.10 | 9.53 | 31.11 | 0.56 |
| 199 | 2.10 | 10.10 | 58.14 | 12.38 | 16.97 | 0.32 |
| 200 | 19.42 | 6.92 | 36.78 | 11.61 | 24.72 | 0.55 |
| 201 | 11.11 | 9.04 | 46.76 | 11.66 | 21.10 | 0.32 |
| 202 | 5.38 | 10.17 | 53.93 | 12.42 | 17.00 | 1.10 |

Note: Major oxides were recalculated to 100% on volatile-free basis. Total iron was combined as FeO. The data, provided by Li Zijin, are used in Figures 4-2, 4-3 and 4-4. Details of sample locations and petrographic descriptions are available from the Tibetan Geological Survey.

Appendix III Mineral chemistry
III.1. Chromite

| | SiO2 | TiO2 | Al2O3 | Cr2O3 | FeO | MnO | MgO | ZnO | NiO | V2O5 | Co2O | Total | Cr# | Mg# |
|------------|------|------|-------|-------|-------|------|-------|------|------|------|------|-------|-----|-----|
| Chromitite | | | | | | | | | | | | | | |
| XL2-N | 0.11 | 0.19 | 11.58 | 57.91 | 17.09 | 0.51 | 13.51 | 0.15 | 0.05 | 0.50 | 0.04 | 101.7 | 77 | 64 |
| XL2-N | 0.08 | 0.18 | 11.49 | 56.56 | 19.90 | 0.52 | 12.35 | 0.16 | 0.06 | 0.49 | 0.12 | 101.9 | 77 | 59 |
| XL2-N | 0.12 | 0.18 | 11.30 | 56.29 | 17.46 | 0.52 | 12.07 | 0.15 | 0.05 | 0.49 | 0.05 | 98.7 | 77 | 60 |
| L-29-N | 0.04 | 0.22 | 10.20 | 60.43 | 13.35 | 0.46 | 15.11 | 0.17 | 0.09 | 0.49 | 0.09 | 100.6 | 80 | 72 |
| L-29-N | 0.19 | 0.19 | 10.11 | 60.99 | 13.20 | 0.46 | 14.80 | 0.17 | 0.11 | 0.49 | 0.09 | 100.8 | 80 | 71 |
| L-29-N | 0.17 | 0.19 | 9.84 | 60.30 | 13.40 | 0.45 | 15.30 | 0.16 | 0.05 | 0.48 | 0.04 | 100.4 | 80 | 73 |
| L-29-N | 0.10 | 0.20 | 10.32 | 59.30 | 12.85 | 0.43 | 14.80 | 0.18 | 0.09 | 0.51 | 0.07 | 98.9 | 79 | 72 |
| L-29-N | 0.12 | 0.24 | 10.47 | 59.49 | 13.25 | 0.45 | 15.16 | 0.16 | 0.06 | 0.50 | 0.09 | 100.0 | 79 | 73 |
| L-29-N | 0.26 | 0.21 | 10.45 | 59.85 | 13.35 | 0.44 | 15.15 | 0.18 | 0.08 | 0.48 | 0.04 | 100.5 | 79 | 73 |
| L-29-N | 0.20 | 0.21 | 10.08 | 60.10 | 13.67 | 0.49 | 14.95 | 0.14 | 0.12 | 0.49 | 0.05 | 100.5 | 80 | 72 |
| L-29-N | 0.09 | 0.20 | 10.22 | 60.87 | 13.25 | 0.47 | 14.86 | 0.14 | 0.11 | 0.49 | 0.06 | 100.7 | 80 | 71 |
| L-29-N | 0.21 | 0.20 | 10.27 | 60.54 | 13.34 | 0.49 | 14.85 | 0.16 | 0.15 | 0.50 | 0.04 | 100.7 | 80 | 71 |
| L-29-N | 0.13 | 0.22 | 10.18 | 60.34 | 13.52 | 0.47 | 14.98 | 0.15 | 0.14 | 0.50 | 0.07 | 100.7 | 80 | 72 |
| L-29-N | 0.07 | 0.21 | 10.29 | 60.63 | 13.05 | 0.48 | 14.74 | 0.19 | 0.13 | 0.49 | 0.05 | 100.3 | 80 | 71 |
| L-29-N | 0.10 | 0.23 | 10.44 | 60.67 | 13.45 | 0.46 | 14.86 | 0.14 | 0.09 | 0.48 | 0.04 | 101.0 | 80 | 71 |
| L-29-N | 0.06 | 0.22 | 10.34 | 60.16 | 13.12 | 0.44 | 15.00 | 0.16 | 0.10 | 0.52 | 0.04 | 100.2 | 80 | 72 |
| L-29-N | 0.09 | 0.23 | 10.67 | 59.92 | 13.73 | 0.48 | 14.62 | 0.15 | 0.11 | 0.51 | 0.04 | 100.6 | 79 | 70 |
| L-29-N | 0.08 | 0.22 | 10.25 | 60.57 | 13.50 | 0.47 | 14.88 | 0.17 | 0.11 | 0.51 | 0.08 | 100.8 | 80 | 71 |
| L-29-N | 0.10 | 0.19 | 9.91 | 60.04 | 13.69 | 0.43 | 14.63 | 0.17 | 0.12 | 0.51 | 0.06 | 99.9 | 80 | 71 |
| L-29-N | 0.08 | 0.20 | 10.18 | 60.68 | 13.66 | 0.46 | 14.72 | 0.17 | 0.10 | 0.51 | 0.07 | 100.8 | 80 | 71 |
| L-29-N | 0.02 | 0.20 | 10.15 | 60.79 | 13.53 | 0.43 | 14.90 | 0.15 | 0.11 | 0.50 | 0.06 | 100.9 | 80 | 71 |
| L-29-N | 0.16 | 0.20 | 10.17 | 59.37 | 12.93 | 0.45 | 14.87 | 0.15 | 0.13 | 0.53 | 0.05 | 99.0 | 80 | 72 |
| L-29-N | 0.09 | 0.22 | 10.10 | 60.41 | 12.91 | 0.47 | 14.76 | 0.19 | 0.08 | 0.49 | 0.01 | 99.7 | 80 | 71 |
| L-29-N | 0.06 | 0.22 | 10.30 | 59.74 | 13.32 | 0.50 | 14.95 | 0.15 | 0.12 | 0.51 | 0.05 | 99.9 | 80 | 72 |
| L-29-N | 0.16 | 0.20 | 10.14 | 60.46 | 12.98 | 0.47 | 14.85 | 0.15 | 0.13 | 0.50 | 0.04 | 100.1 | 80 | 72 |
| L-29-N | 0.10 | 0.19 | 10.52 | 60.49 | 13.17 | 0.48 | 15.07 | 0.16 | 0.10 | 0.51 | 0.05 | 100.9 | 79 | 72 |
| L-29-N | 0.19 | 0.20 | 10.24 | 60.57 | 13.54 | 0.47 | 14.88 | 0.17 | 0.03 | 0.49 | 0.05 | 100.8 | 80 | 71 |
| L-29-N | 0.18 | 0.21 | 10.06 | 60.15 | 13.55 | 0.50 | 14.48 | 0.14 | 0.14 | 0.50 | 0.07 | 100.0 | 80 | 70 |

Appendix III.1. (continued)

| | SiO2 | TiO2 | Al2O3 | Cr2O3 | FeO | MnO | MgO | ZnO | NiO | V2O5 | Co2O | Total | Cr# | Mg# |
|--------|------|------|-------|-------|-------|------|-------|-------|------|------|------|-------|-----|-----|
| L-29-N | 0.15 | 0.21 | 10.17 | 60.04 | 13.08 | 0.44 | 14.65 | 0.16 | 0.12 | 0.51 | 0.08 | 99.6 | 80 | 71 |
| L-29-N | 0.09 | 0.20 | 10.11 | 59.91 | 13.34 | 0.46 | 15.17 | 0.14 | 0.11 | 0.51 | 0.03 | 100.1 | 80 | 73 |
| L-29-N | 0.07 | 0.22 | 10.28 | 60.34 | 13.59 | 0.48 | 14.94 | 0.16 | 0.12 | 0.50 | 0.07 | 100.8 | 80 | 72 |
| L-29-N | 0.14 | 0.21 | 10.10 | 60.33 | 13.29 | 0.49 | 14.47 | 0.14 | 0.08 | 0.49 | 0.08 | 99.8 | 80 | 70 |
| L-29-N | 0.06 | 0.22 | 10.57 | 60.04 | 13.10 | 0.45 | 15.30 | 0.14 | 0.11 | 0.51 | 0.04 | 100.5 | 79 | 73 |
| L-29-N | 0.52 | 0.21 | 10.06 | 61.14 | 13.35 | 0.46 | 15.18 | 0.16 | 0.12 | 0.49 | 0.04 | 101.7 | 80 | 72 |
| L-29-N | 0.06 | 0.22 | 10.23 | 60.51 | 13.22 | 0.45 | 14.93 | 0.15 | 0.10 | 0.50 | 0.05 | 100.4 | 80 | 72 |
| L-29-N | 0.16 | 0.20 | 10.22 | 60.45 | 13.45 | 0.45 | 14.73 | 0.17 | 0.08 | 0.50 | 0.04 | 100.4 | 80 | 71 |
| L-29-N | 0.10 | 0.20 | 10.32 | 60.63 | 13.44 | 0.46 | 14.76 | 0.18 | 0.09 | 0.49 | 0.06 | 100.7 | 80 | 71 |
| L-29-N | 0.13 | 0.23 | 10.17 | 60.31 | 13.50 | 0.44 | 14.96 | 0.16 | 0.05 | 0.52 | 0.03 | 100.5 | 80 | 72 |
| L29-5N | 0.10 | 0.18 | 10.26 | 60.38 | 13.52 | 0.44 | 14.98 | 0.15 | 0.10 | 0.51 | 0.04 | 100.7 | 80 | 72 |
| L29-5N | 0.26 | 0.23 | 10.28 | 60.46 | 13.52 | 0.42 | 14.74 | 0.15 | 0.07 | 0.49 | 0.08 | 100.7 | 80 | 71 |
| L29-5N | 0.11 | 0.20 | 10.29 | 60.55 | 13.41 | 0.48 | 14.86 | 0.14 | 0.06 | 0.51 | 0.03 | 100.6 | 80 | 71 |
| L29-5N | 0.09 | 0.21 | 10.30 | 60.64 | 13.81 | 0.43 | 15.02 | 0.16 | 0.08 | 0.51 | 0.05 | 101.3 | 80 | 71 |
| L29-5N | 0.12 | 0.19 | 10.07 | 60.66 | 12.65 | 0.42 | 15.05 | 0.16 | 0.10 | 0.51 | 0.08 | 100.0 | 80 | 72 |
| L29-5N | 0.09 | 0.21 | 9.21 | 59.13 | 17.71 | 0.49 | 12.55 | 0.17 | 0.08 | 0.51 | 0.07 | 100.2 | 81 | 62 |
| L29-5N | 0.05 | 0.18 | 9.30 | 59.31 | 18.19 | 0.46 | 12.94 | 0.15 | 0.06 | 0.51 | 0.07 | 101.2 | 81 | 63 |
| S2-N | 0.11 | 0.19 | 9.09 | 59.42 | 17.58 | 0.51 | 12.49 | 0.17 | 0.05 | 0.52 | 0.07 | 100.2 | 81 | 61 |
| S2-N | 0.26 | 0.21 | 9.23 | 58.72 | 17.69 | 0.54 | 12.57 | 0.18 | 0.04 | 0.50 | 0.10 | 100.0 | 81 | 62 |
| S2-N | 0.16 | 0.21 | 8.88 | 59.21 | 18.48 | 0.54 | 11.88 | 0.17 | 0.07 | 0.51 | 0.09 | 100.2 | 82 | 59 |
| S2-N | 0.13 | 0.18 | 9.39 | 56.99 | 20.39 | 0.49 | 12.01 | 0.16 | 0.08 | 0.49 | 0.07 | 100.4 | 80 | 59 |
| S2-N | 0.05 | 0.21 | 9.24 | 58.24 | 18.81 | 0.48 | 12.07 | 0.17 | 0.08 | 0.50 | 0.08 | 99.9 | 81 | 60 |
| S2-N | 0.19 | 0.17 | 9.14 | 58.43 | 18.94 | 0.48 | 12.11 | 0.17 | 0.06 | 0.49 | 0.10 | 100.3 | 81 | 60 |
| XL1-N | 0.02 | 0.19 | 8.75 | 58.43 | 16.73 | 0.47 | 12.51 | 0.16 | 0.09 | 0.51 | 0.05 | 97.9 | 82 | 63 |
| XL1-N | 0.15 | 0.17 | 10.02 | 60.06 | 13.31 | 0.41 | 14.72 | 0.16 | 0.06 | 0.54 | 0.06 | 99.7 | 80 | 71 |
| XI-2-N | 0.10 | 0.18 | 11.58 | 55.43 | 19.59 | 0.48 | 11.90 | 0.17 | 0.08 | 0.52 | 0.10 | 100.1 | 76 | 58 |
| XI-2-N | 0.11 | 0.19 | 11.58 | 57.91 | 17.09 | 0.51 | 13.51 | 0.15 | 0.05 | 0.50 | 0.04 | 101.7 | 77 | 64 |
| XI-2-N | 0.08 | 0.18 | 11.49 | 56.56 | 19.90 | 0.52 | 12.35 | 0.16 | 0.06 | 0.49 | 0.12 | 101.9 | 77 | 59 |
| XI-2-N | 0.12 | 0.18 | 11.30 | 56.29 | 17.46 | 0.52 | 12.07 | 0.15 | 0.05 | 0.49 | 0.05 | 98.7 | 77 | 60 |
| L28-N | 0.13 | 0.21 | 10.40 | 60.82 | 12.42 | 0.43 | 15.17 | 0.00 | 0.13 | 0.11 | 0.08 | 99.9 | 80 | 73 |
| L28-N | 0.11 | 0.20 | 9.87 | 60.32 | 13.21 | 0.42 | 15.40 | -0.01 | 0.15 | 0.09 | 0.03 | 99.8 | 80 | 74 |
| L28-N | | 0.19 | 10.39 | 60.33 | 13.00 | 0.12 | 16.00 | | 0.20 | | | 100.2 | 80 | 76 |

Appendix III.1. (continued)

| | SiO2 | TiO2 | Al2O3 | Cr2O3 | FeO | MnO | MgO | ZnO | NiO | V2O5 | Co2O | Total | Ct# | Mg# |
|-------|------|------|-------|-------|-------|------|-------|------|------|------|------|-------|-----|-----|
| L28-N | | 0.20 | 11.27 | 59.05 | 14.01 | 0.14 | 14.80 | | 0.17 | | | 99.6 | 78 | 71 |
| L28-N | | 0.21 | 10.74 | 59.18 | 12.92 | 0.13 | 15.80 | | 0.19 | | | 99.2 | 79 | 75 |
| L28-N | | 0.21 | 11.18 | 59.15 | 14.23 | 0.15 | 15.00 | | 0.15 | | | 100.1 | 78 | 71 |
| L28-N | | 0.20 | 10.64 | 59.36 | 14.02 | 0.11 | 15.00 | | 0.18 | | | 99.5 | 79 | 72 |
| L28-N | | 0.22 | 10.78 | 59.46 | 14.70 | 0.15 | 14.50 | | 0.14 | | | 100.0 | 79 | 69 |
| L28-N | | 0.12 | 11.20 | 59.20 | 14.24 | 0.14 | 15.00 | | 0.17 | | | 100.1 | 78 | 71 |
| L28-N | | 0.20 | 11.27 | 59.09 | 14.01 | 0.14 | 14.90 | | 0.17 | | | 99.8 | 78 | 71 |
| L28-N | | 0.21 | 11.05 | 60.00 | 14.22 | 0.11 | 14.70 | | 0.11 | | | 100.4 | 78 | 70 |
| L28-N | | 0.22 | 10.91 | 58.74 | 13.90 | 0.13 | 15.70 | | 0.12 | | | 99.7 | 78 | 74 |
| L23-M | 0.17 | 0.20 | 10.87 | 59.82 | 11.91 | 0.39 | 16.37 | | 0.24 | 0.08 | 0.01 | 100.0 | 79 | 78 |
| L23-M | 0.04 | 0.18 | 10.85 | 59.77 | 11.60 | 0.36 | 16.14 | 0.01 | 0.16 | 0.10 | 0.02 | 99.2 | 79 | 77 |
| L23-M | 0.09 | 0.19 | 10.85 | 60.26 | 11.57 | 0.37 | 16.31 | 0.00 | 0.19 | 0.10 | 0.02 | 99.9 | 79 | 77 |
| L23-M | | 0.17 | 10.59 | 59.72 | 13.63 | 0.13 | 15.60 | | 0.16 | | | 100.0 | 79 | 74 |
| L23-M | | 0.21 | 10.48 | 60.10 | 12.74 | 0.12 | 16.00 | | 0.21 | | | 99.9 | 79 | 76 |
| L23-M | | 0.19 | 9.96 | 60.84 | 12.84 | 0.11 | 16.00 | | 0.20 | | | 100.1 | 80 | 76 |
| L23-M | | 0.20 | 10.05 | 60.39 | 12.61 | 0.12 | 16.40 | | 0.20 | | | 100.0 | 80 | 78 |
| L23-M | | 0.18 | 10.65 | 59.93 | 12.89 | 0.12 | 16.10 | | 0.20 | | | 100.1 | 79 | 76 |
| L23-M | | 0.22 | 11.11 | 59.25 | 14.67 | 0.17 | 13.80 | | 0.16 | | | 99.4 | 78 | 67 |
| L23-M | | 0.20 | 10.20 | 58.17 | 13.55 | 0.16 | 15.50 | | 0.18 | | | 98.0 | 79 | 75 |
| L23-M | | 0.21 | 10.09 | 60.31 | 12.23 | 0.13 | 16.80 | | 0.22 | | | 100.0 | 80 | 79 |
| L23-M | | 0.18 | 13.47 | 56.06 | 13.86 | 0.15 | 14.60 | | 0.15 | | | 98.5 | 74 | 70 |
| L23-M | | 0.20 | 10.47 | 59.29 | 12.14 | 0.12 | 16.11 | | 0.22 | | | 98.6 | 79 | 77 |
| L23-M | | 0.19 | 11.78 | 58.57 | 12.78 | 0.13 | 15.30 | | 0.15 | | | 98.9 | 77 | 73 |
| L23-M | | 0.20 | 11.02 | 59.32 | 13.20 | 0.11 | 15.90 | | 0.20 | | | 100.0 | 78 | 75 |
| L23-M | | 0.19 | 10.54 | 59.46 | 12.64 | 0.11 | 16.00 | | 0.20 | | | 99.1 | 79 | 76 |
| L23-M | | 0.14 | 11.21 | 59.10 | 13.67 | 0.14 | 15.40 | | 0.17 | | | 99.8 | 78 | 73 |
| L23-M | | 0.21 | 10.46 | 59.29 | 12.64 | 0.13 | 16.00 | | 0.19 | | | 98.9 | 79 | 76 |
| L23-M | | 0.21 | 11.52 | 58.92 | 14.00 | 0.12 | 15.00 | | 0.10 | | | 99.9 | 77 | 71 |
| L23-M | | 0.22 | 11.00 | 59.19 | 13.25 | 0.12 | 16.00 | | 0.14 | | | 99.9 | 78 | 76 |
| L23-M | | 0.20 | 11.35 | 60.59 | 11.86 | 0.10 | 15.80 | | 0.12 | | | 100.0 | 78 | 75 |
| L23-M | | 0.20 | 10.79 | 58.97 | 15.45 | 0.13 | 14.00 | | 0.10 | | | 99.6 | 79 | 67 |
| L23-M | | 0.14 | 11.20 | 59.51 | 15.15 | 0.10 | 13.86 | | 0.09 | | | 100.1 | 78 | 66 |

Appendix III.1. (continued)

| | SiO2 | TiO2 | Al2O3 | Cr2O3 | FeO | MnO | MgO | ZnO | NiO | V2O5 | Co2O | Total | Cr# | Mg# |
|----------------|------|------|-------|-------|-------|------|-------|-------|------|------|------|-------|-----|-----|
| L23-M | | 0.21 | 10.67 | 58.95 | 15.18 | 0.15 | 14.47 | | 0.12 | | | 99.8 | 79 | 69 |
| L23-M | | 0.20 | 11.77 | 58.44 | 14.67 | 0.13 | 14.73 | | 0.14 | | | 100.1 | 77 | 70 |
| L23-M | | 0.20 | 10.05 | 59.15 | 14.11 | 0.15 | 14.60 | | 0.10 | | | 98.4 | 80 | 71 |
| L23-M | | 0.20 | 11.85 | 57.95 | 14.99 | 0.17 | 14.50 | | 0.08 | | | 99.7 | 77 | 69 |
| L23-M | | 0.18 | 10.66 | 58.28 | 16.43 | 0.18 | 13.60 | | 0.08 | | | 99.4 | 79 | 66 |
| L26-D | 0.16 | 0.24 | 10.37 | 58.48 | 16.69 | 0.52 | 13.26 | -0.02 | 0.10 | 0.09 | 0.08 | 100.0 | 79 | 64 |
| L26-D | 0.17 | 0.22 | 10.17 | 59.05 | 16.53 | 0.53 | 12.92 | 0.02 | 0.07 | 0.09 | 0.08 | 99.9 | 80 | 63 |
| L26-D | 0.18 | 0.22 | 10.11 | 58.92 | 16.09 | 0.48 | 13.37 | -0.02 | 0.08 | 0.08 | 0.06 | 99.6 | 80 | 65 |
| L26-D | 0.15 | 0.19 | 10.39 | 60.81 | 12.75 | 0.47 | 14.92 | 0.01 | 0.11 | 0.10 | 0.04 | 99.9 | 80 | 72 |
| L26-D | 0.17 | 0.20 | 10.36 | 60.83 | 13.49 | 0.44 | 14.32 | -0.01 | 0.08 | 0.08 | 0.03 | 100.0 | 80 | 69 |
| L26-D | 0.14 | 0.20 | 10.14 | 61.58 | 13.20 | 0.46 | 14.66 | 0.00 | 0.07 | 0.10 | 0.03 | 100.6 | 80 | 70 |
| L27-D | 0.22 | 0.24 | 10.92 | 58.99 | 16.92 | 0.49 | 12.36 | 0.01 | 0.07 | 0.11 | 0.09 | 100.4 | 78 | 60 |
| L27-D | 0.13 | 0.26 | 11.01 | 59.66 | 15.43 | 0.49 | 13.43 | 0.03 | 0.08 | 0.11 | 0.08 | 100.7 | 78 | 65 |
| L27-D | 0.12 | 0.21 | 10.49 | 59.76 | 16.39 | 0.51 | 12.55 | 0.00 | 0.12 | 0.08 | 0.07 | 100.3 | 79 | 61 |
| L24-D | 0.12 | 0.18 | 10.52 | 60.59 | 12.52 | 0.44 | 15.58 | 0.02 | 0.09 | 0.07 | 0.06 | 100.2 | 79 | 74 |
| L24-D | 0.07 | 0.19 | 10.29 | 60.86 | 12.63 | 0.44 | 15.70 | 0.00 | 0.13 | 0.07 | 0.00 | 100.4 | 80 | 75 |
| L24-D | 0.08 | 0.18 | 10.54 | 60.77 | 12.19 | 0.38 | 15.68 | -0.01 | 0.10 | 0.09 | 0.04 | 100.0 | 79 | 75 |
| Di-harzburgite | | | | | | | | | | | | | | |
| L20 | 0.09 | 0.05 | 27.80 | 38.48 | 18.96 | 0.43 | 12.18 | 0.33 | 0.05 | 0.71 | 0.08 | 99.1 | 48 | 56 |
| L20 | 0.08 | 0.04 | 27.66 | 35.02 | 23.11 | 0.34 | 11.87 | 0.31 | 0.01 | 0.69 | 0.07 | 99.2 | 46 | 55 |
| L20 | 0.20 | 0.06 | 28.11 | 38.36 | 19.67 | 0.34 | 12.60 | 0.30 | 0.05 | 0.71 | 0.10 | 100.5 | 48 | 57 |
| L20 | 0.17 | 0.06 | 28.07 | 38.73 | 19.03 | 0.32 | 12.62 | 0.29 | 0.07 | 0.72 | 0.08 | 100.2 | 48 | 57 |
| L20 | 0.25 | 0.05 | 28.51 | 38.07 | 19.36 | 0.34 | 12.68 | 0.26 | 0.05 | 0.72 | 0.08 | 100.4 | 47 | 57 |
| L20 | 0.17 | 0.05 | 27.48 | 39.51 | 19.50 | 0.35 | 12.43 | 0.29 | 0.06 | 0.72 | 0.10 | 100.7 | 49 | 56 |
| LH2 | 0.12 | 0.06 | 22.94 | 40.61 | 21.08 | 0.30 | 11.56 | | | 0.35 | 0.12 | 97.1 | 54 | 55 |
| LH2 | 0.13 | 0.06 | 22.97 | 40.65 | 21.35 | 0.08 | 11.33 | 0.01 | 0.25 | 0.28 | | 97.1 | 54 | 54 |
| LH2 | 0.23 | 0.09 | 23.20 | 41.07 | 21.49 | 0.21 | 11.37 | 0.16 | 0.17 | 0.26 | 0.06 | 98.3 | 54 | 54 |
| LH3 | 0.14 | | 38.83 | 27.59 | 15.72 | 0.20 | 15.33 | 0.38 | 0.37 | 0.17 | 0.07 | 98.8 | 32 | 66 |
| LH3 | 0.20 | | 40.50 | 27.00 | 15.47 | 0.15 | 15.93 | 0.35 | 0.22 | 0.16 | 0.16 | 100.1 | 31 | 67 |
| LH3 | 0.20 | | 38.58 | 27.68 | 15.91 | 0.42 | 15.71 | 0.27 | 0.31 | 0.26 | 0.00 | 99.3 | 32 | 68 |
| LH4 | 0.17 | | 44.56 | 22.00 | 14.47 | 0.17 | 16.86 | 0.15 | 0.39 | 0.13 | | 98.9 | 25 | 70 |
| LH4 | 0.19 | | 43.69 | 22.56 | 15.03 | 0.23 | 16.61 | 0.38 | 0.18 | 0.22 | | 99.1 | 26 | 70 |

Appendix III.1. (continued)

| | SiO2 | TiO2 | Al2O3 | Cr2O3 | FaO | MnO | MgO | ZnO | NiO | V2O5 | Co2O | Total | Cr# | Mg# |
|-------------|------|------|-------|-------|-------|------|-------|------|------|------|------|-------|-----|-----|
| LH4 | 0.11 | | 44.18 | 21.94 | 14.47 | 0.08 | 17.02 | 0.33 | 0.21 | 0.09 | | 98.4 | 25 | 71 |
| LH5 | 0.07 | | 46.24 | 20.56 | 14.70 | 0.15 | 17.44 | | 0.18 | 0.25 | | 99.6 | 23 | 72 |
| LH5 | 0.17 | | 45.08 | 21.87 | 15.36 | 0.23 | 16.99 | 0.00 | 0.16 | 0.19 | 0.15 | 100.2 | 25 | 70 |
| LH5 | 0.10 | 0.03 | 44.72 | 22.69 | 15.01 | 0.21 | 17.20 | 0.26 | 0.16 | 0.12 | 0.10 | 100.6 | 25 | 71 |
| LH5 | 2.32 | 0.03 | 40.19 | 22.48 | 15.86 | 0.21 | 16.41 | 0.17 | 0.12 | 0.22 | 0.01 | 98.0 | 27 | 71 |
| LH5 | 0.19 | 0.02 | 45.39 | 22.89 | 14.69 | 0.19 | 16.99 | 0.29 | 0.15 | 0.27 | 0.03 | 101.1 | 25 | 70 |
| LH5 | 0.19 | 0.02 | 46.26 | 21.06 | 14.94 | 0.17 | 16.98 | 0.18 | 0.15 | 0.01 | | 100.0 | 23 | 70 |
| LH1-1 | 0.11 | 0.07 | 35.71 | 29.98 | 18.32 | 0.37 | 15.17 | 0.14 | 0.13 | 0.32 | 0.14 | 100.4 | 36 | 65 |
| LH1-1 | 0.08 | 0.06 | 36.14 | 29.91 | 17.57 | 0.36 | 15.37 | 0.21 | 0.11 | 0.22 | 0.01 | 100.0 | 36 | 66 |
| LH1-1 | 0.12 | 0.04 | 36.92 | 30.38 | 16.09 | 0.40 | 16.50 | 0.36 | 0.14 | 0.22 | | 101.2 | 36 | 70 |
| LH1-1 | 0.14 | 0.06 | 35.89 | 30.81 | 17.86 | 0.36 | 15.93 | 0.25 | 0.14 | 0.25 | 0.02 | 101.7 | 37 | 68 |
| LH1-1 | 0.16 | 0.04 | 35.27 | 31.89 | 16.93 | 0.38 | 15.78 | 0.13 | 0.13 | 0.15 | 0.17 | 101.0 | 38 | 68 |
| LH1-1 | 0.08 | 0.05 | 33.68 | 32.76 | 17.49 | 0.42 | 15.34 | 0.31 | 0.17 | 0.21 | | 100.5 | 39 | 67 |
| LH1-1 | 0.17 | 0.08 | 34.70 | 27.35 | 22.71 | 0.36 | 14.05 | 0.24 | 0.16 | 0.40 | 0.12 | 100.3 | 35 | 61 |
| LH1-1 | 0.14 | 0.09 | 29.62 | 33.43 | 22.12 | 0.44 | 12.92 | 0.26 | 0.14 | 0.12 | 0.08 | 99.4 | 43 | 58 |
| Harzburgite | | | | | | | | | | | | | | |
| S4-2 | 0.10 | 0.09 | 21.41 | 46.68 | 16.57 | 0.28 | 12.68 | 0.44 | 0.10 | 0.28 | 0.28 | 98.9 | 59 | 60 |
| S4-2 | 0.17 | 0.08 | 23.41 | 45.27 | 16.08 | 0.06 | 13.32 | 0.18 | | 0.28 | 0.02 | 98.9 | 56 | 62 |
| S4-2 | 0.18 | 0.10 | 22.50 | 46.16 | 16.29 | 0.26 | 13.11 | 0.03 | 0.30 | 0.21 | 0.13 | 99.3 | 58 | 61 |
| S4-2 | 0.26 | 0.07 | 25.16 | 43.01 | 16.41 | 0.25 | 13.64 | 0.17 | 0.08 | 0.33 | | 99.4 | 53 | 62 |
| S4-2 | 0.09 | 0.05 | 26.08 | 42.66 | 15.11 | 0.38 | 14.26 | | 0.12 | 0.18 | 0.20 | 99.1 | 52 | 65 |
| S4-2 | 0.12 | 0.07 | 26.29 | 41.58 | 15.76 | 0.49 | 13.71 | 0.29 | 0.21 | 0.20 | 0.26 | 98.7 | 51 | 63 |
| S4-2 | 0.26 | 0.05 | 26.47 | 42.58 | 15.54 | 0.26 | 13.88 | | 0.00 | 0.01 | 0.05 | 99.4 | 52 | 63 |
| S4-2 | 0.15 | 0.01 | 29.27 | 39.42 | 14.22 | 0.16 | 14.56 | 0.24 | 0.01 | 0.19 | | 98.2 | 47 | 66 |
| S4-3 | 0.43 | 0.03 | 30.60 | 37.49 | 15.36 | 0.46 | 14.63 | | 0.10 | 0.09 | | 99.2 | 45 | 65 |
| S4-3 | 0.67 | 0.02 | 30.60 | 33.46 | 19.34 | 0.61 | 14.46 | 0.43 | 0.08 | 0.22 | 0.23 | 100.1 | 42 | 65 |
| S4-3 | 0.50 | 0.00 | 27.89 | 37.15 | 18.78 | 0.62 | 13.91 | 0.30 | 0.08 | 0.23 | | 99.5 | 47 | 63 |
| S4-3 | 0.42 | 0.04 | 28.23 | 38.54 | 16.03 | 0.60 | 14.45 | 0.23 | 0.07 | 0.20 | | 98.8 | 48 | 65 |
| S4-3 | 0.28 | 0.03 | 28.88 | 39.74 | 15.54 | 0.54 | 14.15 | 0.15 | 0.04 | 0.29 | | 99.7 | 48 | 64 |
| S4-3 | 0.21 | 0.01 | 30.16 | 38.27 | 15.49 | 0.51 | 14.59 | | 0.03 | 0.14 | 0.06 | 99.5 | 46 | 65 |
| S4-3 | 0.57 | 0.04 | 29.51 | 36.67 | 17.46 | 0.59 | 14.31 | 0.20 | 0.08 | 0.12 | 0.14 | 99.7 | 45 | 64 |
| S4-3 | 0.47 | 0.02 | 31.65 | 35.50 | 16.32 | 0.48 | 15.00 | 0.23 | 0.07 | 0.24 | 0.30 | 100.3 | 43 | 66 |

Appendix III.1. (continued)

| | SiO2 | TiO2 | Al2O3 | Cr2O3 | FeO | MnO | MgO | ZnO | NiO | V2O5 | Co2O | Total | Cr# | Mg# |
|------|------|------|-------|-------|-------|------|-------|------|------|------|------|-------|-----|-----|
| S4-3 | 1.12 | 0.04 | 29.85 | 36.23 | 17.03 | 0.49 | 14.76 | 0.16 | 0.14 | 0.11 | 0.05 | 100.0 | 45 | 66 |
| S4-3 | 0.15 | | 32.98 | 35.53 | 15.59 | 0.44 | 15.12 | 0.13 | 0.07 | 0.11 | | 100.1 | 42 | 66 |
| S4-3 | 0.43 | | 31.87 | 35.98 | 15.21 | 0.46 | 15.36 | 0.14 | 0.04 | 0.13 | | 99.6 | 43 | 68 |
| S4-3 | 0.11 | | 34.56 | 33.79 | 14.98 | 0.42 | 15.15 | 0.06 | 0.07 | 0.29 | 0.20 | 99.6 | 40 | 66 |
| S4-3 | 0.94 | | 29.97 | 35.28 | 17.00 | 0.50 | 15.03 | 0.01 | 0.13 | 0.33 | | 99.2 | 44 | 67 |
| S4-3 | 0.24 | | 35.29 | 31.94 | 15.75 | 0.39 | 15.46 | 0.38 | 0.08 | 0.16 | 0.10 | 99.8 | 38 | 67 |
| S4-3 | 0.07 | | 34.42 | 34.72 | 15.20 | 0.43 | 15.67 | 0.25 | 0.08 | 0.30 | 0.06 | 101.2 | 40 | 67 |
| S4-3 | 0.15 | | 34.20 | 34.33 | 14.78 | 0.38 | 15.42 | 0.16 | 0.06 | 0.11 | 0.20 | 99.8 | 40 | 67 |
| S4-3 | 0.04 | | 34.47 | 34.57 | 14.81 | 0.42 | 15.70 | 0.29 | 0.08 | 0.30 | | 100.7 | 40 | 68 |
| S4-3 | 0.31 | | 35.27 | 33.51 | 14.18 | 0.39 | 15.94 | 0.52 | 0.03 | 0.18 | | 100.3 | 39 | 69 |
| S4-3 | 0.06 | | 35.22 | 33.41 | 14.48 | 0.37 | 15.92 | | 0.09 | 0.32 | 0.02 | 99.9 | 39 | 69 |
| S4-3 | 0.18 | | 34.60 | 34.85 | 14.31 | 0.40 | 16.06 | | 0.09 | 0.18 | 0.06 | 100.7 | 40 | 69 |
| S4-3 | 0.08 | | 35.22 | 33.31 | 14.05 | 0.37 | 16.24 | | 0.06 | 0.23 | 0.01 | 99.6 | 39 | 70 |
| S4-3 | 0.18 | | 35.85 | 33.37 | 14.20 | 0.39 | 16.08 | | 0.04 | 0.19 | | 100.3 | 38 | 69 |
| S4-3 | 0.18 | | 35.65 | 32.94 | 15.12 | 0.40 | 15.63 | 0.14 | 0.13 | 0.09 | 0.00 | 100.3 | 38 | 67 |
| S4-3 | 0.98 | | 31.74 | 32.05 | 19.48 | 0.49 | 14.97 | | 0.07 | 0.15 | | 99.9 | 40 | 66 |
| S4-3 | 0.16 | | 35.25 | 33.40 | 15.43 | 0.41 | 15.54 | 0.19 | 0.10 | 0.22 | 0.13 | 100.8 | 39 | 67 |
| S4-4 | 0.16 | | 36.65 | 31.91 | 14.45 | 0.37 | 16.15 | 0.04 | 0.08 | 0.21 | 0.09 | 100.1 | 37 | 69 |
| S4-4 | 0.12 | | 36.52 | 32.59 | 14.87 | 0.36 | 16.19 | | 0.13 | 0.22 | 0.00 | 101.0 | 37 | 69 |
| S4-4 | 0.12 | | 35.61 | 32.00 | 16.10 | 0.40 | 15.37 | 0.03 | 0.08 | 0.24 | 0.03 | 100.0 | 38 | 66 |
| S4-4 | 0.05 | | 38.06 | 30.11 | 14.97 | 0.32 | 16.06 | 0.32 | 0.08 | 0.09 | | 100.1 | 35 | 68 |
| S4-4 | 0.12 | | 40.88 | 27.93 | 13.14 | 0.23 | 17.34 | 0.11 | 0.13 | 0.32 | 0.25 | 100.5 | 31 | 72 |
| S4-4 | 0.15 | | 39.76 | 29.33 | 14.45 | 0.31 | 16.77 | 0.21 | 0.12 | 0.20 | 0.12 | 101.4 | 33 | 70 |
| S4-4 | 0.13 | | 40.46 | 28.93 | 13.73 | 0.28 | 17.48 | 0.12 | 0.11 | 0.22 | 0.08 | 101.5 | 32 | 72 |
| S4-4 | 0.20 | | 40.78 | 27.06 | 13.26 | 0.26 | 17.12 | 0.37 | 0.19 | 0.20 | 0.10 | 99.5 | 31 | 72 |
| S5 | 0.12 | | 41.21 | 25.25 | 13.91 | 0.19 | 16.34 | 0.28 | 0.32 | 0.18 | 0.03 | 97.8 | 29 | 70 |
| S5 | 0.16 | | 39.90 | 26.54 | 14.18 | 0.21 | 16.52 | 0.11 | 0.24 | 0.13 | 0.26 | 98.2 | 31 | 71 |
| S5 | 0.15 | | 40.44 | 26.52 | 14.38 | 0.39 | 16.44 | 0.03 | 0.04 | 0.19 | | 98.6 | 31 | 70 |
| S6 | 0.13 | | 44.84 | 22.34 | 13.97 | 0.05 | 17.11 | 0.21 | 0.39 | 0.12 | 0.22 | 99.4 | 25 | 71 |
| S6 | 0.09 | | 45.38 | 22.26 | 13.63 | | 17.39 | 0.12 | 0.13 | 0.15 | 0.07 | 99.2 | 25 | 72 |
| S6 | 0.10 | | 45.01 | 21.72 | 14.20 | 0.05 | 16.97 | 0.12 | 0.09 | 0.12 | 0.12 | 98.5 | 24 | 71 |
| S7 | 0.22 | | 48.85 | 18.36 | 13.26 | 0.19 | 17.95 | 0.24 | 0.51 | 0.05 | 0.13 | 99.8 | 20 | 73 |

Appendix III.1. (continued)

| | SiO2 | TiO2 | Al2O3 | Cr2O3 | FeO | MnO | MgO | ZnO | NiO | V2O5 | Co2O | Total | Cr# | Mg# |
|-------|------|------|-------|-------|-------|------|-------|------|------|------|------|-------|-----|-----|
| S7 | 0.06 | | 47.30 | 18.33 | 13.63 | 0.16 | 17.16 | 0.36 | 0.27 | 0.14 | 0.09 | 97.5 | 21 | 72 |
| S8 | 0.13 | | 49.79 | 17.52 | 13.30 | | 17.98 | | 0.34 | 0.16 | | 99.2 | 19 | 73 |
| S8 | 0.17 | | 50.09 | 16.95 | 13.20 | 0.28 | 17.96 | 0.26 | 0.29 | 0.13 | 0.06 | 99.4 | 19 | 73 |
| S8 | 0.14 | | 48.91 | 18.80 | 13.50 | 0.12 | 17.86 | 0.49 | 0.18 | 0.23 | 0.19 | 100.4 | 20 | 72 |
| L6 | 0.10 | | 48.72 | 17.90 | 13.46 | 0.06 | 18.34 | 0.12 | 0.18 | 0.12 | 0.05 | 99.1 | 20 | 74 |
| L6 | 0.02 | 0.01 | 42.19 | 24.88 | 15.70 | 0.16 | 16.87 | 0.09 | 0.17 | 0.11 | 0.05 | 100.2 | 28 | 70 |
| L6 | 0.10 | | 40.75 | 26.07 | 15.44 | 0.17 | 16.81 | 0.10 | 0.12 | 0.10 | 0.03 | 99.7 | 30 | 71 |
| L6 | 0.18 | | 41.30 | 25.37 | 15.48 | 0.15 | 17.03 | 0.09 | 0.11 | 0.12 | | 99.8 | 29 | 71 |
| L6 | 0.12 | 0.00 | 42.48 | 24.40 | 14.98 | 0.17 | 16.80 | 0.10 | 0.15 | 0.10 | 0.02 | 99.3 | 28 | 70 |
| L6 | 0.21 | 0.01 | 40.40 | 26.38 | 15.85 | 0.17 | 16.21 | 0.08 | 0.09 | 0.12 | | 99.5 | 30 | 68 |
| L10 | 0.24 | 0.01 | 40.41 | 28.01 | 13.82 | 0.15 | 17.21 | 0.12 | 0.07 | 0.07 | 0.01 | 100.1 | 32 | 72 |
| L10 | 0.07 | | 41.73 | 26.75 | 13.23 | 0.12 | 17.97 | 0.12 | 0.11 | 0.05 | 0.02 | 100.2 | 30 | 74 |
| L10-s | 0.18 | | 43.93 | 22.59 | 14.43 | 0.13 | 17.24 | 0.19 | 0.12 | 0.08 | 0.05 | 98.9 | 28 | 72 |
| L10-L | 0.09 | 0.02 | 40.03 | 28.03 | 14.53 | 0.17 | 17.14 | 0.11 | 0.15 | 0.06 | 0.01 | 100.3 | 32 | 72 |
| L19 | 0.03 | 0.06 | 20.77 | 46.95 | 18.85 | 0.42 | 11.54 | 0.06 | 0.01 | 0.30 | 0.08 | 99.1 | 60 | 55 |
| L19 | 0.12 | 0.06 | 20.59 | 47.90 | 18.16 | 0.45 | 11.72 | 0.07 | 0.02 | 0.30 | 0.07 | 99.5 | 61 | 55 |
| L19 | 0.03 | 0.05 | 21.06 | 46.89 | 17.96 | 0.42 | 11.75 | 0.09 | 0.05 | 0.28 | 0.07 | 98.6 | 60 | 56 |
| L19-s | 0.10 | 0.05 | 21.42 | 47.03 | 17.68 | 0.41 | 11.62 | 0.10 | 0.01 | 0.30 | 0.05 | 98.8 | 60 | 55 |
| L19 | 0.14 | 0.08 | 21.47 | 47.98 | 17.36 | 0.42 | 12.33 | 0.04 | 0.05 | 0.27 | 0.07 | 100.2 | 60 | 57 |
| L19 | 0.21 | 0.06 | 20.92 | 48.59 | 17.23 | 0.42 | 12.11 | 0.09 | 0.03 | 0.26 | 0.09 | 100.0 | 61 | 57 |
| L12 | 0.45 | 0.03 | 24.48 | 41.80 | 20.10 | 0.39 | 12.39 | 0.10 | 0.01 | 0.24 | 0.09 | 100.1 | 53 | 57 |
| L12 | 0.15 | 0.04 | 26.35 | 40.93 | 18.69 | 0.37 | 12.41 | 0.10 | 0.04 | 0.25 | 0.08 | 99.4 | 51 | 57 |
| L22 | 0.03 | 0.07 | 21.02 | 47.14 | 19.03 | 0.45 | 11.93 | 0.07 | 0.07 | 0.25 | 0.05 | 100.1 | 60 | 56 |
| L22 | 0.06 | 0.07 | 21.34 | 46.89 | 18.94 | 0.42 | 12.07 | 0.08 | 0.04 | 0.24 | 0.06 | 100.2 | 60 | 56 |
| L22 | 0.24 | 0.07 | 21.64 | 46.89 | 19.19 | 0.40 | 12.04 | 0.10 | 0.02 | 0.25 | 0.06 | 100.9 | 59 | 56 |
| L17 | 0.21 | | 44.06 | 21.90 | 15.42 | 0.11 | 17.77 | 0.09 | 0.19 | 0.09 | 0.05 | 99.9 | 25 | 73 |
| L17 | | | 45.01 | 21.02 | 15.12 | 0.10 | 18.04 | 0.12 | 0.15 | 0.09 | 0.05 | 99.7 | 24 | 74 |
| L17 | 0.15 | | 44.00 | 22.48 | 14.64 | 0.12 | 18.24 | 0.10 | 0.21 | 0.05 | 0.04 | 100.0 | 26 | 75 |
| H14 | 0.19 | | 45.27 | 21.14 | 13.47 | 0.07 | 17.35 | 0.32 | 0.28 | 0.19 | | 98.3 | 24 | 72 |
| H14 | 0.10 | | 45.77 | 20.47 | 14.42 | 0.13 | 17.26 | 0.71 | 0.25 | 0.18 | 0.15 | 99.4 | 23 | 71 |
| H2 | 0.12 | | 41.34 | 26.26 | 14.46 | 0.05 | 16.22 | 0.57 | 0.19 | 0.14 | | 99.3 | 30 | 69 |
| H2 | 0.06 | 0.02 | 38.96 | 28.23 | 14.53 | 0.23 | 15.93 | 0.19 | 0.22 | 0.06 | | 98.4 | 33 | 68 |

Appendix III. 1. (continued)

| | SiO2 | TiO2 | Al2O3 | Cr2O3 | FeO | MnO | MgO | ZnO | NiO | V2O5 | Co2O | Total | Cr# | Mg# |
|--------|------|-------|-------|-------|-------|------|-------|------|------|------|------|-------|-----|-----|
| H2 | 0.18 | | 39.81 | 27.37 | 14.44 | 0.20 | 15.81 | 0.02 | 0.34 | 0.09 | 0.09 | 98.4 | 32 | 68 |
| H1 | 0.19 | 0.01 | 23.21 | 43.96 | 18.57 | 0.14 | 11.75 | 0.20 | 0.29 | 0.33 | 0.10 | 98.8 | 56 | 55 |
| H1 | 0.19 | 0.01 | 21.17 | 46.79 | 19.76 | 0.35 | 11.12 | 0.35 | 0.20 | 0.41 | 0.23 | 100.6 | 60 | 52 |
| H1 | 0.25 | 0.01 | 23.19 | 44.99 | 18.21 | 0.22 | 12.07 | 0.13 | 0.11 | 0.35 | | 99.5 | 57 | 56 |
| H1 | 0.17 | 0.04 | 22.42 | 44.64 | 17.70 | 0.41 | 11.77 | 0.08 | 0.17 | 0.22 | | 97.6 | 57 | 56 |
| H395 | 0.10 | 0.02 | 17.02 | 50.84 | 18.59 | 0.34 | 10.54 | 0.23 | 0.35 | | | 98.0 | 67 | 52 |
| H395 | 0.18 | | 17.62 | 51.79 | 18.10 | 0.37 | 10.80 | 0.33 | 0.09 | 0.29 | 0.02 | 99.6 | 66 | 52 |
| H395 | 0.11 | | 18.55 | 50.49 | 17.72 | 0.20 | 11.01 | 0.02 | 0.36 | 0.45 | 0.04 | 98.9 | 65 | 53 |
| L6A | 0.16 | 0.01 | 26.22 | 42.40 | 17.52 | 0.38 | 13.41 | 0.27 | 0.06 | 0.31 | 0.03 | 100.8 | 52 | 61 |
| L6A | 2.98 | -0.01 | 17.12 | 34.10 | 32.77 | 0.49 | 11.40 | 0.33 | 0.07 | 0.19 | | 99.4 | 57 | 56 |
| Harz | | 0.14 | 21.05 | 46.13 | 20.50 | 0.18 | 10.50 | | 0.11 | | | 98.6 | 60 | 50 |
| Harz | | 0.15 | 17.47 | 47.40 | 23.11 | 0.23 | 10.40 | | 0.09 | | | 98.9 | 65 | 50 |
| Harz | | 0.06 | 16.60 | 50.71 | 21.70 | 0.26 | 9.70 | | 0.07 | | | 99.1 | 67 | 47 |
| Harz | | 0.12 | 18.37 | 47.95 | 21.44 | 0.20 | 11.30 | | 0.10 | | | 99.5 | 64 | 54 |
| Harz | | 0.09 | 25.13 | 42.42 | 19.01 | 0.20 | 12.60 | | 0.10 | | | 99.6 | 53 | 58 |
| Harz | | 0.09 | 16.47 | 50.99 | 20.76 | | 10.50 | | | | | 98.8 | 67 | 51 |
| Harz | | 0.08 | 29.93 | 36.91 | 17.85 | | 13.33 | | | | | 98.1 | 45 | 60 |
| Harz | | 0.08 | 34.65 | 33.05 | 14.42 | 0.15 | 15.01 | | 0.17 | | | 97.5 | 39 | 66 |
| Harz | | 0.07 | 29.96 | 38.65 | 17.11 | 0.16 | 14.30 | | 0.12 | | | 100.4 | 46 | 63 |
| Harz | | 0.07 | 34.54 | 31.88 | 15.71 | 0.15 | 16.70 | | 0.15 | | | .2 | 38 | 72 |
| ZHK11 | 0.42 | | 29.74 | 35.69 | 19.50 | 0.35 | 13.36 | 0.18 | 0.07 | 0.38 | 0.06 | 99.8 | 45 | 60 |
| ZHK11 | 0.22 | | 29.18 | 36.29 | 18.84 | 0.37 | 14.26 | 0.20 | 0.08 | 0.27 | | 99.7 | 45 | 64 |
| ZHK11 | 0.19 | | 29.13 | 38.26 | 18.10 | 0.36 | 13.59 | 0.21 | 0.07 | 0.38 | 0.04 | 100.3 | 47 | 61 |
| ZHK10 | 0.10 | | 24.02 | 45.05 | 17.33 | 0.46 | 12.68 | 0.15 | 0.04 | 0.30 | 0.12 | 100.3 | 56 | 58 |
| ZHK10 | 0.23 | | 22.60 | 47.09 | 17.37 | 0.52 | 12.55 | 0.26 | 0.03 | 0.30 | 0.07 | 101.0 | 58 | 58 |
| ZHK10 | 0.23 | | 24.06 | 45.03 | 17.91 | 0.44 | 12.55 | 0.58 | 0.04 | 0.37 | 0.03 | 101.2 | 56 | 57 |
| Dunite | | | | | | | | | | | | | | |
| L8 | 0.13 | 0.48 | 12.21 | 50.80 | 25.43 | 0.56 | 10.05 | 0.07 | 0.09 | 0.26 | 0.11 | 100.2 | 74 | 49 |
| L8 | 0.10 | 0.52 | 12.40 | 50.38 | 25.42 | 0.60 | 9.60 | 0.07 | 0.08 | 0.28 | 0.06 | 99.5 | 73 | 48 |
| L8 | 0.10 | 0.51 | 12.08 | 50.22 | 26.12 | 0.55 | 9.54 | 0.08 | 0.10 | 0.25 | 0.10 | 99.7 | 74 | 47 |
| L8 | 0.10 | 0.49 | 12.26 | 51.04 | 25.38 | 0.55 | 9.90 | 0.07 | 0.10 | 0.24 | 0.07 | 100.2 | 74 | 49 |
| L8 | 0.18 | 0.49 | 12.34 | 50.72 | 25.50 | 0.57 | 9.55 | 0.05 | 0.09 | 0.24 | 0.12 | 99.8 | 73 | 47 |

Appendix III.1. (continued)

| | SiO2 | TiO2 | Al2O3 | Cr2O3 | FeO | MnO | MgO | ZnO | NiO | V2O5 | Co2O | Total | Cr# | Mg# |
|---------|------|------|-------|-------|-------|------|-------|------|-------|------|------|-------|-----|-----|
| L8 | 0.13 | 0.52 | 11.98 | 51.13 | 25.60 | 0.55 | 9.24 | 0.08 | 0.11 | 0.28 | 0.04 | 99.6 | 74 | 46 |
| L9 | 0.14 | 0.09 | 17.73 | 50.01 | 18.99 | 0.49 | 10.89 | 0.07 | 0.01 | 0.32 | 0.08 | 98.8 | 65 | 53 |
| L9 | 0.07 | 0.08 | 17.51 | 51.24 | 19.12 | 0.51 | 11.05 | 0.09 | 0.02 | 0.28 | 0.08 | 100.0 | 66 | 53 |
| L9 | 0.60 | 0.10 | 13.00 | 53.46 | 21.19 | 0.51 | 8.88 | 0.11 | 0.02 | 0.27 | 0.07 | 98.2 | 73 | 45 |
| L18 | 0.01 | 0.16 | 9.74 | 56.82 | 23.44 | 0.60 | 9.57 | 0.06 | 0.07 | 0.15 | 0.12 | 100.7 | 80 | 47 |
| L18 | 0.11 | 0.13 | 9.39 | 57.67 | 21.78 | 0.56 | 10.19 | 0.05 | 0.08 | 0.17 | 0.09 | 100.2 | 80 | 51 |
| L18 | 0.16 | 0.16 | 9.79 | 57.77 | 22.43 | 0.62 | 9.48 | 0.07 | 0.07 | 0.14 | 0.11 | 100.8 | 80 | 47 |
| L18-7-1 | 0.08 | 0.14 | 9.24 | 55.47 | 23.62 | 0.58 | 9.95 | 0.08 | 0.08 | 0.16 | 0.13 | 99.5 | 80 | 50 |
| L18-7-2 | 0.12 | 0.16 | 8.65 | 57.67 | 22.80 | 0.55 | 9.74 | 0.05 | 0.08 | 0.16 | 0.07 | 100.0 | 82 | 49 |
| L18 | 0.10 | 0.13 | 8.62 | 57.84 | 22.10 | 0.57 | 9.84 | 0.05 | 0.05 | 0.16 | 0.13 | 99.6 | 82 | 49 |
| L18 | 0.22 | 0.14 | 8.79 | 57.87 | 22.70 | 0.58 | 9.86 | 0.03 | 0.04 | 0.16 | 0.08 | 100.5 | 82 | 49 |
| L18 | 0.18 | 0.14 | 8.64 | 58.24 | 22.59 | 0.54 | 9.66 | 0.05 | 0.07 | 0.18 | 0.16 | 100.5 | 82 | 48 |
| L18 | 0.19 | 0.12 | 8.79 | 56.96 | 23.60 | 0.59 | 9.13 | 0.06 | 0.09 | 0.16 | 0.10 | 99.8 | 81 | 46 |
| L18 | 0.17 | 0.13 | 9.46 | 55.37 | 24.34 | 0.53 | 9.72 | 0.03 | 0.06 | 0.16 | 0.08 | 100.1 | 80 | 48 |
| L15 | 0.24 | 0.12 | 12.68 | 55.74 | 19.71 | 0.51 | 10.83 | 0.09 | 0.03 | 0.27 | 0.11 | 100.3 | 75 | 53 |
| L15 | 0.17 | 0.11 | 12.89 | 55.54 | 20.02 | 0.53 | 10.81 | 0.09 | 0.06 | 0.24 | 0.09 | 100.5 | 74 | 53 |
| L15 | 0.20 | 0.12 | 12.41 | 55.67 | 20.64 | 0.51 | 10.32 | 0.08 | 0.04 | 0.26 | 0.08 | 100.3 | 75 | 51 |
| L15 | 0.04 | 0.11 | 12.56 | 56.21 | 20.10 | 0.52 | 11.11 | 0.06 | 0.07 | 0.25 | 0.09 | 101.1 | 75 | 54 |
| L15 | 0.08 | 0.12 | 13.72 | 53.67 | 19.88 | 0.48 | 11.61 | 0.06 | 0.07 | 0.26 | 0.09 | 100.0 | 72 | 56 |
| L13 | 0.16 | 0.26 | 10.87 | 58.79 | 18.79 | 0.50 | 11.86 | 0.02 | 0.09 | 0.13 | 0.06 | 101.5 | 78 | 57 |
| L13 | 0.19 | 0.28 | 10.81 | 58.29 | 18.71 | 0.56 | 11.41 | 0.04 | 0.05 | 0.11 | 0.04 | 100.5 | 78 | 56 |
| L13 | 0.12 | 0.23 | 10.59 | 58.32 | 18.04 | 0.53 | 12.17 | 0.01 | 0.06 | 0.13 | 0.07 | 100.3 | 79 | 59 |
| L16 | 0.18 | 0.08 | 4.22 | 65.00 | 22.61 | 0.72 | 7.10 | 0.07 | 0.03 | 0.29 | 0.12 | 100.4 | 91 | 37 |
| L16 | 0.09 | 0.08 | 4.42 | 64.58 | 22.08 | 0.67 | 7.66 | 0.06 | 0.04 | 0.28 | 0.13 | 100.1 | 91 | 40 |
| L16 | 0.21 | 0.09 | 4.41 | 65.29 | 22.24 | 0.70 | 7.55 | 0.04 | 0.02 | 0.28 | 0.10 | 100.9 | 91 | 39 |
| L16 | 0.08 | 0.09 | 4.36 | 64.53 | 22.59 | 0.70 | 7.24 | 0.07 | 0.03 | 0.27 | 0.12 | 100.1 | 91 | 38 |
| L16 | 0.15 | 0.10 | 4.45 | 64.50 | 23.33 | 0.73 | 6.86 | 0.09 | -0.01 | 0.27 | 0.13 | 100.6 | 91 | 36 |
| L16 | 0.14 | 0.09 | 4.34 | 64.50 | 23.74 | 0.70 | 6.55 | 0.08 | -0.01 | 0.30 | 0.12 | 100.6 | 91 | 34 |
| L16 | 0.15 | 0.09 | 4.30 | 64.19 | 23.77 | 0.72 | 6.21 | 0.15 | 0.06 | 0.31 | 0.12 | 100.1 | 91 | 33 |
| S11 | 0.12 | 0.08 | 18.13 | 47.18 | 21.44 | 0.45 | 8.99 | 0.23 | 0.06 | 0.39 | 0.12 | 97.2 | 64 | 45 |
| S11 | 0.23 | 0.10 | 17.00 | 48.79 | 21.45 | 0.42 | 9.69 | 0.63 | 0.06 | 0.37 | 0.02 | 98.7 | 66 | 48 |
| S11 | 0.19 | 0.10 | 17.45 | 48.34 | 21.59 | 0.43 | 9.24 | 0.11 | 0.06 | 0.24 | 0.02 | 97.8 | 65 | 46 |

Appendix III.1. (continued)

| | SiO ₂ | TiO ₂ | Al ₂ O ₃ | Cr ₂ O ₃ | FeO | MnO | MgO | ZnO | NiO | V ₂ O ₅ | Co ₂ O | Total | Cr# | Mg# |
|--------|------------------|------------------|--------------------------------|--------------------------------|-------|------|-------|------|------|-------------------------------|-------------------|-------|-----|-----|
| S4-1 | 0.18 | 0.18 | 12.02 | 58.65 | 16.18 | | 12.56 | 0.16 | 0.09 | 0.10 | 0.01 | 100.1 | 77 | 61 |
| S4-1 | 0.17 | 0.23 | 12.92 | 57.61 | 15.64 | | 12.72 | | 0.09 | 0.23 | 0.07 | 99.7 | 75 | 61 |
| S4-1 | 0.12 | 0.24 | 12.33 | 58.56 | 15.71 | | 12.83 | 0.31 | 0.09 | 0.20 | 0.04 | 100.4 | 76 | 62 |
| S4-1 | 0.14 | 0.22 | 12.44 | 58.99 | 15.51 | | 13.16 | 0.32 | 0.12 | 0.13 | 0.05 | 101.1 | 76 | 63 |
| S4-1 | 0.13 | 0.23 | 12.47 | 58.33 | 15.70 | 0.81 | 12.65 | | 0.09 | | | 100.4 | 76 | 61 |
| S4-1 | 0.17 | 0.22 | 12.46 | 58.65 | 15.57 | 0.79 | 12.71 | 0.35 | 0.07 | | 0.17 | 101.2 | 76 | 61 |
| S4-1 | 0.12 | 0.21 | 13.22 | 57.57 | 16.33 | | 12.56 | 0.06 | 0.07 | 0.13 | 0.06 | 100.3 | 75 | 60 |
| S4-1 | 0.12 | 0.23 | 13.32 | 57.39 | 16.77 | | 12.09 | 0.13 | 0.09 | 0.06 | | 100.2 | 74 | 58 |
| S4-1 | 0.52 | 0.19 | 12.89 | 57.61 | 16.44 | | 12.51 | 0.28 | 0.12 | 0.16 | 0.35 | 101.1 | 75 | 60 |
| S4-1 | 0.22 | 0.20 | 12.45 | 56.80 | 17.76 | 0.78 | 12.30 | 0.06 | 0.05 | 0.07 | 0.06 | 100.7 | 75 | 59 |
| S4-1 | 0.27 | 0.19 | 13.21 | 57.50 | 16.15 | 0.78 | 12.58 | | 0.05 | 0.26 | 0.08 | 101.1 | 74 | 60 |
| S4-1 | 0.25 | 0.18 | 11.96 | 57.90 | 18.15 | 0.80 | 11.06 | 0.15 | 0.04 | 0.01 | 0.08 | 100.6 | 76 | 54 |
| S4-1 | 0.15 | 0.18 | 13.10 | 55.62 | 20.71 | 0.82 | 10.19 | 0.43 | 0.06 | 0.07 | 0.03 | 101.4 | 74 | 50 |
| S4-1 | 0.11 | 0.21 | 14.26 | 54.93 | 19.79 | 0.83 | 11.12 | | 0.07 | 0.14 | 0.06 | 101.5 | 72 | 53 |
| S4-1 | 0.10 | 0.15 | 14.22 | 54.06 | 20.89 | 0.85 | 10.37 | 0.15 | 0.07 | 0.06 | 0.06 | 101.0 | 72 | 50 |
| S4-1 | 0.02 | 0.19 | 15.93 | 53.21 | 19.66 | 0.74 | 10.81 | | 0.03 | 0.18 | 0.07 | 100.8 | 69 | 52 |
| S4-1 | 0.11 | 0.17 | 16.28 | 52.55 | 19.44 | 0.78 | 11.01 | 0.09 | 0.07 | 0.21 | | 100.7 | 68 | 53 |
| S4-1 | 0.20 | 0.16 | 17.20 | 53.00 | 18.30 | 0.75 | 11.90 | 0.18 | 0.05 | | 0.13 | 101.9 | 67 | 56 |
| S4-1 | 0.23 | 0.16 | 17.70 | 52.64 | 17.83 | 0.76 | 12.09 | 0.13 | 0.05 | 0.15 | 0.17 | 101.9 | 67 | 57 |
| S4-1 | 0.13 | 0.16 | 18.26 | 50.84 | 17.83 | 0.69 | 11.80 | 0.25 | 0.07 | 0.12 | 0.07 | 100.2 | 65 | 56 |
| ZHK8 | 0.17 | 0.20 | 15.31 | 53.40 | 18.45 | 0.65 | 12.14 | 0.39 | 0.09 | 0.19 | 0.11 | 101.1 | 70 | 58 |
| ZHK8 | 0.17 | 0.16 | 14.11 | 55.18 | 18.32 | 0.67 | 12.01 | 0.01 | 0.09 | 0.11 | 0.07 | 100.9 | 72 | 57 |
| ZHK8 | 0.15 | 0.17 | 14.06 | 54.41 | 18.47 | 0.68 | 11.77 | 0.29 | 0.11 | 0.17 | 0.13 | 100.4 | 72 | 57 |
| ZHK9 | 0.15 | 0.11 | 13.29 | 55.26 | 18.44 | 0.65 | 11.21 | 0.14 | 0.08 | 0.33 | 0.18 | 99.8 | 74 | 55 |
| ZHK9 | 0.15 | 0.10 | 13.53 | 55.40 | 18.46 | 0.65 | 11.29 | 0.25 | 0.06 | 0.21 | 0.04 | 100.1 | 73 | 55 |
| ZHK9 | 0.21 | 0.09 | 13.70 | 56.09 | 18.18 | 0.66 | 11.31 | 0.34 | 0.09 | 0.31 | 0.04 | 101.0 | 73 | 55 |
| ZHK6-2 | 0.21 | 0.05 | 12.59 | 55.12 | 19.33 | 0.68 | 11.91 | 0.33 | 0.09 | 0.14 | 0.16 | 100.6 | 75 | 58 |
| ZHK6-2 | 0.13 | 0.07 | 11.67 | 54.96 | 20.44 | 0.70 | 10.72 | | 0.12 | 0.13 | 0.14 | 99.1 | 76 | 53 |
| ZHK6-2 | 0.08 | 0.06 | 11.52 | 55.41 | 20.12 | 0.70 | 10.82 | 0.11 | 0.12 | 0.27 | 0.03 | 99.2 | 76 | 54 |
| ZHK6-2 | 0.08 | 0.08 | 11.65 | 55.10 | 20.58 | 0.71 | 10.92 | 0.19 | 0.08 | 0.26 | 0.00 | 99.7 | 76 | 54 |
| ZHK6-2 | 0.18 | 0.04 | 10.76 | 55.72 | 20.76 | 0.64 | 10.76 | 0.35 | 0.09 | 0.20 | | 99.5 | 78 | 53 |
| ZHK6-2 | 0.11 | 0.06 | 13.87 | 56.65 | 14.34 | 0.57 | 14.31 | | 0.12 | 0.30 | 0.07 | 100.4 | 73 | 68 |

Appendix III.1. (continued)

| | SiO ₂ | TiO ₂ | Al ₂ O ₃ | Cr ₂ O ₃ | FeO | MnO | MgO | ZnO | NiO | V ₂ O ₅ | Co ₂ O | Total | Cr# | Mg# |
|--------|------------------|------------------|--------------------------------|--------------------------------|-------|------|-------|------|------|-------------------------------|-------------------|-------|-----|-----|
| ZHK6-2 | 0.10 | 0.08 | 13.89 | 56.44 | 13.80 | 0.61 | 14.42 | 0.01 | 0.10 | 0.13 | | 99.6 | 73 | 69 |
| ZHK6-2 | 0.23 | 0.06 | 14.48 | 56.45 | 13.34 | 0.57 | 14.61 | | 0.15 | 0.18 | | 100.1 | 72 | 69 |
| DUN1 | | 0.10 | 23.64 | 41.38 | 20.60 | 0.24 | 13.10 | | 0.12 | | | 99.2 | 54 | 60 |
| DUN1 | | 0.16 | 23.89 | 38.65 | 23.00 | 0.31 | 13.10 | | 0.15 | | | 99.3 | 52 | 60 |
| DUN1 | | 0.26 | 17.15 | 43.95 | 27.40 | 0.26 | 10.10 | | 0.14 | | | 99.3 | 63 | 49 |
| DUN1 | | 0.12 | 23.17 | 44.92 | 18.77 | 0.20 | 12.80 | | 0.09 | | | 100.1 | 57 | 59 |
| DUN1 | | 0.02 | 12.77 | 56.48 | 19.14 | 0.25 | 11.04 | | 0.07 | | | 99.8 | 75 | 54 |
| DUN1 | | 0.24 | 15.50 | 52.42 | 19.20 | 0.13 | 13.00 | | 0.07 | | | 100.6 | 69 | 61 |
| DUN1 | | 0.10 | 12.63 | 55.38 | 19.89 | 0.22 | 11.00 | | 0.07 | | | 99.3 | 75 | 54 |
| DUN1 | | 0.12 | 14.26 | 53.40 | 21.39 | 0.24 | 10.00 | | 0.06 | | | 99.5 | 72 | 49 |
| DUN1 | | 0.10 | 10.83 | 58.35 | 25.04 | 0.25 | 10.70 | | 0.06 | | | 105.3 | 78 | 50 |
| DUN1 | | 0.13 | 9.99 | 56.05 | 23.38 | 0.30 | 9.70 | | 0.08 | | | 99.6 | 79 | 48 |
| DUN1 | | 0.10 | 10.37 | 59.28 | 18.75 | 0.23 | 10.80 | | 0.06 | | | 99.6 | 79 | 53 |
| DUN1 | | 0.10 | 8.47 | 58.29 | 22.20 | 0.26 | 8.90 | | 0.05 | | | 98.3 | 82 | 45 |
| DUN1 | | 0.10 | 10.10 | 58.91 | 18.59 | 0.25 | 11.13 | | 0.06 | | | 99.1 | 80 | 55 |
| DUN1 | | 0.12 | 14.06 | 51.73 | 23.60 | 0.28 | 9.75 | | 0.07 | | | 99.6 | 71 | 48 |
| DUN1 | | 0.10 | 11.90 | 55.21 | 21.91 | 0.27 | 10.00 | | 0.07 | | | 99.5 | 76 | 49 |
| DUN1 | | 0.08 | 14.66 | 52.17 | 20.53 | 0.23 | 11.60 | | 0.11 | | | 99.4 | 70 | 56 |
| DUN1 | | 0.18 | 16.27 | 48.85 | 22.04 | 0.18 | 11.70 | | 0.12 | | | 99.3 | 67 | 56 |
| DUN1 | | 0.18 | 13.24 | 45.61 | 30.06 | 0.32 | 9.50 | | 0.14 | | | 99.1 | 70 | 47 |
| DUN1 | | 0.18 | 11.35 | 56.72 | 18.25 | 0.22 | 12.78 | | 0.13 | | | 99.6 | 77 | 62 |
| DUN1 | | 0.13 | 9.42 | 58.37 | 23.56 | 0.26 | 10.15 | | 0.09 | | | 102.0 | 81 | 49 |
| DUN1 | | 0.24 | 10.90 | 56.11 | 18.91 | 0.19 | 13.00 | | 0.11 | | | 99.5 | 78 | 63 |
| DUN1 | | 0.20 | 10.35 | 55.68 | 21.81 | 0.19 | 11.95 | | 0.13 | | | 100.3 | 78 | 58 |
| DUN1 | | 0.20 | 12.66 | 54.34 | 20.11 | 0.18 | 12.50 | | 0.10 | | | 100.1 | 74 | 60 |
| DUN1 | | 0.20 | 12.40 | 50.40 | 26.07 | 0.28 | 10.00 | | 0.12 | | | 99.5 | 73 | 49 |
| DUN1 | | 0.15 | 10.16 | 52.87 | 27.10 | 0.31 | 9.10 | | 0.09 | | | 99.8 | 78 | 45 |
| DUN1 | | 0.14 | 12.56 | 54.57 | 20.53 | 0.22 | 11.00 | | 0.06 | | | 99.1 | 74 | 54 |
| DUN1 | | 0.07 | 16.21 | 48.95 | 24.14 | 0.36 | 9.80 | | | | | 99.5 | 67 | 47 |

Appendix III. Mineral chemistry
III.2. Olivine

| | SiO ₂ | FeO | MnO | MgO | CaO | NiO | Total | Fo |
|--------------------|------------------|------|------|------|------|------|-------|----|
| Chromitite | | | | | | | | |
| ZHK | 42.0 | 5.71 | 0.11 | 53.3 | | 0.54 | 101.8 | 94 |
| ZHK | 42.3 | 5.10 | 0.05 | 53.7 | 0.05 | 0.64 | 101.8 | 95 |
| ZHK | 41.3 | 5.23 | 0.00 | 52.8 | 0.01 | 0.38 | 99.9 | 95 |
| ZHK6-2 | 42.2 | 4.29 | 0.14 | 54.0 | 0.02 | 0.66 | 101.4 | 96 |
| ZHK6-2 | 42.3 | 4.02 | 0.07 | 54.3 | 0.00 | 0.81 | 101.6 | 96 |
| IIIIV6 | 41.2 | 5.89 | 0.08 | 52.1 | | 0.45 | 99.6 | 94 |
| L26 | 41.5 | 4.56 | 0.15 | 52.4 | 0.05 | 0.48 | 98.9 | 95 |
| L26 | 42.1 | 4.45 | 0.10 | 53.6 | 0.02 | 0.52 | 100.6 | 95 |
| L28 | 41.6 | 2.92 | 0.10 | 54.7 | 0.01 | 1.11 | 100.4 | 97 |
| L28 | 42.2 | 2.23 | | 55.0 | 0.01 | 0.97 | 100.7 | 98 |
| L25 | 41.8 | 3.21 | 0.05 | 54.0 | 0.00 | 0.88 | 99.9 | 97 |
| L25 | 41.7 | 3.07 | 0.05 | 54.0 | | 0.75 | 99.5 | 97 |
| L27 | 41.3 | 4.76 | 0.07 | 51.7 | 0.04 | 0.57 | 98.3 | 95 |
| L27 | 41.8 | 4.47 | 0.08 | 53.3 | 0.05 | 0.59 | 100.2 | 95 |
| L29 | 42.0 | 4.35 | | 53.7 | | 0.53 | 100.6 | 96 |
| L29 | 41.9 | 3.99 | 0.11 | 54.3 | | 0.70 | 101.0 | 96 |
| S4 | 41.2 | 5.90 | 0.01 | 52.4 | 0.07 | 0.61 | 100.4 | 94 |
| S4 | 41.4 | 5.76 | 0.02 | 52.6 | | 0.41 | 100.2 | 94 |
| S4 | 41.8 | 6.10 | 0.10 | 52.6 | 0.08 | 0.58 | 101.0 | 94 |
| S4 | 41.8 | 6.67 | 0.10 | 52.5 | 0.08 | 0.63 | 101.8 | 93 |
| S4 | 41.1 | 6.78 | 0.02 | 51.5 | 0.03 | 0.51 | 99.9 | 93 |
| R-37 | 43.0 | 3.18 | 0.00 | 53.8 | 0.03 | | 100.0 | 97 |
| R-38 | 42.8 | 3.73 | 0.21 | 53.2 | 0.01 | | 100.0 | 96 |
| R-67 | 41.7 | 3.02 | 0.12 | 54.4 | 0.03 | | 99.3 | 97 |
| R-76 | 36.6 | 7.51 | 0.06 | 55.4 | 0.03 | | 99.6 | 93 |
| Harzburgite | | | | | | | | |
| L6 | 41.4 | 8.96 | 0.11 | 47.4 | 0.07 | 0.46 | 98.5 | 90 |
| L6 | 40.8 | 9.69 | 0.05 | 49.3 | 0.01 | 0.38 | 100.2 | 90 |
| L12 | 41.0 | 9.13 | 0.12 | 50.3 | 0.01 | 0.49 | 101.2 | 91 |
| H14 | 40.5 | 9.57 | 0.15 | 49.4 | 0.04 | 0.44 | 100.0 | 90 |
| H1 | 40.8 | 8.86 | 0.22 | 49.5 | 0.08 | 0.39 | 99.8 | 91 |
| L17 | 40.8 | 9.44 | 0.26 | 50.0 | 0.04 | 0.62 | 101.2 | 90 |
| L17 | 40.9 | 9.17 | 0.07 | 49.4 | | 0.55 | 100.0 | 90 |
| L22 | 41.0 | 8.80 | | 49.8 | 0.04 | 0.53 | 100.3 | 91 |
| L22 | 40.6 | 8.88 | 0.23 | 49.9 | 0.00 | 0.44 | 100.0 | 91 |
| L10 | 40.6 | 8.88 | 0.10 | 49.5 | | 0.46 | 99.7 | 91 |
| L10 | 41.1 | 8.54 | 0.10 | 49.9 | 0.04 | 0.51 | 100.3 | 91 |
| L19 | 40.6 | 8.69 | 0.17 | 50.5 | 0.04 | 0.42 | 100.5 | 91 |
| L19 | 40.5 | 8.73 | 0.09 | 49.6 | 0.08 | 0.43 | 99.3 | 91 |
| S4-3 | 41.3 | 7.16 | 0.16 | 51.4 | 0.05 | 0.61 | 100.5 | 93 |
| S4-3 | 41.4 | 7.58 | 0.21 | 51.7 | 0.11 | 0.47 | 101.5 | 92 |
| S4-3 | 41.1 | 7.58 | 0.09 | 50.9 | 0.00 | 0.48 | 100.0 | 92 |
| S4-3 | 41.3 | 7.89 | 0.09 | 51.3 | | 0.53 | 101.0 | 92 |

Appendix III.2. (continued)

| | SiO ₂ | FeO | MnO | MgO | CaO | NiO | Total | Fo |
|--------|------------------|------|------|------|------|------|-------|----|
| S4-3 | 41.4 | 7.88 | 0.08 | 50.9 | 0.04 | 0.49 | 100.7 | 92 |
| L6A | 41.1 | 8.93 | 0.12 | 49.9 | 0.00 | 0.32 | 100.4 | 91 |
| ZHK11 | 41.5 | 9.01 | 0.14 | 50.5 | 0.02 | 0.44 | 101.6 | 91 |
| ZHK11 | 41.1 | 9.29 | 0.13 | 50.3 | 0.05 | 0.46 | 101.2 | 90 |
| ZHK10 | 41.4 | 9.09 | 0.00 | 50.4 | | 0.41 | 101.3 | 91 |
| ZHK10 | 41.3 | 9.08 | 0.20 | 50.4 | 0.03 | 0.31 | 101.2 | 91 |
| ZHK10 | 41.5 | 8.60 | 0.06 | 50.5 | 0.02 | 0.37 | 101.0 | 91 |
| L8 | 40.4 | 9.07 | 0.27 | 48.7 | 0.19 | 0.41 | 99.2 | 90 |
| L8 | 40.5 | 8.90 | | 49.7 | 0.13 | 0.41 | 99.6 | 91 |
| L8 | 40.8 | 9.36 | 0.16 | 49.8 | 0.08 | 0.46 | 100.4 | 90 |
| R-63 | 40.6 | 8.3 | 0.13 | 51.3 | 0.03 | | 100.3 | 92 |
| R-76 | 41.5 | 8.03 | 0 | 49.5 | 0.01 | | 98.9 | 92 |
| R76-1 | 40.0 | 7.91 | 0.11 | 51.9 | 0.00 | | 99.9 | 92 |
| R105 | 40.0 | 8.08 | 0.12 | 51.4 | 0.02 | | 99.6 | 92 |
| R105-1 | 40.3 | 8.94 | 0.17 | 50.5 | 0.00 | | 100.0 | 91 |
| R166 | 41.5 | 8.23 | 0.13 | 48.9 | 0.04 | | 98.7 | 91 |
| 1D | 40.4 | 9.35 | 0.07 | 49.2 | 0.06 | | 99.0 | 90 |
| R5 | 41.1 | 8.82 | 0.09 | 49.7 | 0.03 | | 99.8 | 91 |
| R5-1 | 41.2 | 8.74 | 0.17 | 48.3 | 0.03 | | 98.4 | 91 |
| R87 | 40.6 | 7.86 | 0.19 | 51.3 | 0.01 | | 100.0 | 92 |
| LH3 | 40.9 | 9.39 | 0.09 | 49.6 | | 0.24 | 100.2 | 90 |
| LH3 | 40.8 | 9.28 | 0.14 | 50.1 | 0.01 | 0.41 | 100.6 | 90 |
| LH4 | 40.8 | 9.56 | 0.14 | 49.4 | | 0.41 | 100.2 | 90 |
| LH4 | 40.8 | 9.37 | 0.11 | 50.0 | 0.05 | 0.39 | 100.9 | 90 |
| S4-4 | 41.4 | 7.84 | 0.12 | 51.0 | 0.03 | 0.56 | 100.8 | 92 |
| S4-4 | 41.3 | 7.70 | 0.10 | 50.4 | 0.06 | 0.30 | 99.9 | 92 |
| S4-4 | 40.9 | 7.91 | 0.05 | 50.2 | 0.02 | 0.51 | 99.6 | 92 |
| S4-4 | 41.1 | 8.12 | 0.02 | 50.4 | 0.01 | 0.35 | 99.9 | 92 |
| Dunite | | | | | | | | |
| S4-2 | 41.1 | 7.49 | 0.01 | 51.2 | | 0.54 | 100.3 | 92 |
| ZHK6-2 | 41.7 | 6.45 | 0.07 | 52.5 | | 0.40 | 101.3 | 93 |
| ZHK6-2 | 41.8 | 6.45 | 0.08 | 52.5 | 0.02 | 0.39 | 101.4 | 93 |
| L16 | 40.7 | 7.96 | 0.05 | 50.4 | 0.01 | 0.69 | 101.1 | 92 |
| L16 | 40.9 | 7.95 | 0.12 | 50.6 | 0.03 | 0.32 | 99.8 | 92 |
| L9 | 41.1 | 8.17 | 0.12 | 50.8 | 0.07 | 0.52 | 100.6 | 92 |
| L9 | 41.1 | 8.25 | 0.13 | 50.7 | | 0.61 | 100.6 | 92 |
| L9 | 41.1 | 8.20 | 0.16 | 51.0 | 0.09 | 0.48 | 100.8 | 92 |
| L13 | 41.6 | 6.08 | 0.04 | 52.5 | 0.13 | 0.62 | 100.9 | 94 |
| L13 | 41.1 | 6.11 | 0.06 | 52.1 | 0.07 | 0.36 | 99.7 | 94 |
| L18 | 41.7 | 6.25 | | 52.7 | 0.05 | 0.81 | 101.4 | 94 |
| L18 | 41.1 | 6.28 | 0.15 | 51.9 | 0.04 | 0.54 | 99.9 | 93 |
| ZHK9 | 41.7 | 7.58 | 0.02 | 51.6 | 0.06 | 0.21 | 101.0 | 92 |
| ZHK9 | 41.8 | 7.72 | 0.08 | 52.0 | 0.10 | 0.57 | 102.4 | 92 |
| ZHK8 | 42.1 | 6.27 | 0.23 | 52.9 | 0.04 | 0.61 | 102.2 | 94 |
| ZHK8 | 42.1 | 6.63 | 0.05 | 52.4 | 0.04 | 0.25 | 101.7 | 93 |
| ZHK8 | 42.2 | 6.15 | 0.04 | 52.9 | | 0.44 | 102.0 | 94 |

Appendix III.2. (continued)

| | SiO ₂ | FeO | MnO | MgO | CaO | NiO | Total | Fo |
|--------|------------------|------|------|------|------|------|-------|----|
| ZHK8 | 42.1 | 6.69 | 0.09 | 52.8 | 0.01 | 0.27 | 102.2 | 93 |
| S4 | 41.0 | 7.00 | 0.24 | 50.7 | 0.09 | 0.39 | 99.4 | 93 |
| S4 | 41.4 | 7.08 | 0.06 | 52.3 | 0.07 | 0.56 | 101.4 | 93 |
| S4 | 41.0 | 7.12 | 0.13 | 51.3 | | 0.41 | 99.9 | 93 |
| S4 | 42.0 | 7.48 | 0.13 | 52.5 | 0.02 | 0.32 | 102.3 | 92 |
| S4 | 41.4 | 7.10 | 0.16 | 52.1 | 0.04 | 0.44 | 101.2 | 93 |
| S4-2 | 41.3 | 7.85 | 0.10 | 51.5 | 0.02 | 0.52 | 101.1 | 92 |
| S4-2 | 41.3 | 7.31 | 0.12 | 51.6 | | 0.59 | 100.9 | 93 |
| S4-2 | 41.2 | 7.36 | 0.05 | 51.2 | 0.06 | 0.47 | 100.2 | 93 |
| S4-2 | 41.4 | 7.31 | 0.09 | 51.6 | | 0.67 | 101.0 | 93 |
| III V6 | 41.0 | 7.55 | 0.13 | 50.7 | 0.00 | 0.25 | 99.2 | 92 |
| 1D | 42.1 | 7.73 | 0.11 | 48.1 | 0.10 | | 98.1 | 92 |

Appendix III. Mineral chemistry
III.3. Orthopyroxene

| | SiO ₂ | Al ₂ O ₃ | FeO | MgO | CaO | Cr ₂ O ₃ | Na ₂ O | Total | En | Fs | Wo |
|-------------|------------------|--------------------------------|------|------|------|--------------------------------|-------------------|-------|------|------|-----|
| Harzburgite | | | | | | | | | | | |
| H1-1 | 58.2 | 1.74 | 5.82 | 34.2 | 0.64 | 0.42 | 0.14 | 99.0 | 90.2 | 8.6 | 1.2 |
| H1-2 | 58.4 | 1.38 | 5.73 | 34.8 | 0.28 | 0.62 | 0.09 | 99.2 | 91.1 | 8.4 | 0.5 |
| H1-3 | 58.3 | 1.82 | 5.75 | 34.2 | 0.41 | 0.58 | 0.12 | 99.1 | 90.7 | 8.6 | 0.8 |
| L12-1 | 58.5 | 1.89 | 5.55 | 34.1 | 0.91 | 0.76 | 0.07 | 99.9 | 90.1 | 8.2 | 1.7 |
| L12-2 | 56.4 | 1.80 | 5.62 | 34.5 | 0.57 | 0.76 | 0.10 | 99.8 | 90.6 | 8.3 | 1.1 |
| L12-3 | 58.0 | 1.79 | 5.72 | 33.9 | 1.16 | 0.57 | 0.10 | 99.2 | 89.4 | 8.5 | 2.2 |
| H14-1 | 54.7 | 3.92 | 6.11 | 33.0 | 0.85 | 0.63 | 0.09 | 99.2 | 89.1 | 9.3 | 1.6 |
| H14-2 | 54.7 | 3.67 | 6.26 | 33.0 | 0.71 | 0.68 | 0.08 | 99.4 | 89.1 | 9.5 | 1.4 |
| S4-3-c | 58.5 | 2.88 | 4.94 | 35.2 | 0.74 | 0.75 | 0.12 | 101.1 | 91.4 | 7.2 | 1.4 |
| S4-3-d | 57.0 | 1.85 | 4.88 | 35.0 | 0.57 | 0.39 | 0.00 | 99.7 | 91.8 | 7.2 | 1.1 |
| S4-3-e | 58.5 | 2.12 | 5.03 | 35.0 | 0.41 | 0.39 | 0.16 | 99.7 | 91.8 | 7.4 | 0.8 |
| S4-3-f | 58.9 | 1.99 | 5.25 | 35.2 | 0.49 | 0.25 | 0.07 | 100.1 | 91.4 | 7.7 | 0.9 |
| L6A-1 | 58.7 | 1.95 | 5.81 | 34.4 | 1.24 | 0.73 | 0.15 | 101.2 | 89.1 | 8.6 | 2.3 |
| L6A-2 | 58.8 | 2.17 | 5.91 | 34.4 | 0.79 | 0.63 | 0.10 | 100.9 | 89.9 | 8.7 | 1.5 |
| L6A-4 | 58.8 | 1.91 | 5.65 | 34.0 | 1.65 | 0.58 | 0.32 | 101.2 | 88.6 | 8.3 | 3.1 |
| ZHK11-4 | 55.8 | 2.51 | 5.84 | 33.1 | 2.13 | 0.74 | 0.10 | 100.3 | 87.3 | 8.6 | 4.0 |
| ZHK11-5 | 58.6 | 2.57 | 5.87 | 34.4 | 0.53 | 0.61 | 0.21 | 101.2 | 90.3 | 8.7 | 1.0 |
| ZHK11-6 | 58.6 | 2.25 | 6.09 | 34.6 | 0.38 | 0.52 | 0.22 | 100.9 | 90.4 | 8.9 | 0.7 |
| ZHK10-8 | 57.4 | 1.57 | 5.78 | 34.7 | 0.75 | 0.49 | 0.13 | 100.9 | 90.2 | 8.4 | 1.4 |
| ZHK10-9 | 57.3 | 1.87 | 5.71 | 35.0 | 0.82 | 0.66 | 0.17 | 101.9 | 90.2 | 8.3 | 1.5 |
| ZHK10-1 | 57.3 | 1.63 | 5.53 | 34.6 | 0.82 | 0.61 | 0.13 | 100.8 | 90.4 | 8.1 | 1.5 |
| Fg-3 | 56.3 | 2.74 | 5.47 | 33.8 | 0.84 | 0.63 | 0.00 | 99.8 | 90.2 | 8.2 | 1.6 |
| R14 | 55.7 | 2.03 | 4.91 | 33.6 | 1.38 | 0.73 | 0.87 | 99.1 | 90.0 | 7.4 | 2.7 |
| R41 | 56.7 | 2.13 | 5.19 | 35.5 | 1.11 | 0.56 | 0.01 | 101.2 | 90.5 | 7.4 | 2.0 |
| R63 | 55.2 | 2.89 | 5.56 | 34.0 | 0.72 | 0.66 | 0.02 | 99.1 | 90.3 | 8.3 | 1.4 |
| R63-1 | 54.3 | 2.79 | 5.54 | 35.0 | 0.70 | 0.57 | 0.01 | 98.9 | 90.7 | 8.0 | 1.3 |
| 78 | 58.2 | 1.12 | 5.05 | 33.9 | 1.05 | 0.41 | 0.08 | 99.8 | 90.4 | 7.6 | 2.0 |
| R166 | 55.8 | 1.59 | 5.46 | 33.4 | 1.64 | 0.55 | 0.49 | 99.0 | 88.7 | 8.1 | 3.1 |
| R105 | 55.1 | 3.60 | 5.69 | 33.9 | 1.03 | 0.61 | 0.01 | 99.9 | 89.6 | 8.4 | 2.0 |
| 1D | 54.2 | 3.91 | 5.85 | 34.5 | 0.48 | 0.55 | 0.01 | 99.6 | 90.4 | 8.7 | 0.9 |
| 77D | 53.9 | 4.13 | 6.60 | 33.0 | 0.68 | 0.58 | 0.08 | 98.9 | 88.7 | 10.0 | 1.3 |
| L17-1 | 54.9 | 4.06 | 6.26 | 33.4 | 0.52 | 0.71 | 0.17 | 99.9 | 89.6 | 9.4 | 1.0 |
| L17-2 | 56.3 | 2.65 | 6.32 | 34.0 | 0.55 | 0.37 | 0.06 | 100.2 | 89.6 | 9.3 | 1.0 |

Appendix III.3. (continued)

| | SiO ₂ | Al ₂ O ₃ | FeO | MgO | CaO | Cr ₂ O ₃ | Na ₂ O | Total | En | Fs | Wo |
|----------------|------------------|--------------------------------|------|------|------|--------------------------------|-------------------|-------|------|-----|-----|
| L22-1 | 56.7 | 1.55 | 5.42 | 34.8 | 0.63 | 0.52 | 0.23 | 100.1 | 90.9 | 7.9 | 1.2 |
| L22-2 | 57.7 | 0.52 | 5.13 | 35.6 | 0.25 | 0.14 | 0.19 | 99.5 | 92.1 | 7.4 | 0.5 |
| L19-1 | 58.4 | 1.74 | 5.58 | 34.1 | 0.74 | 0.58 | 0.09 | 99.1 | 90.3 | 8.3 | 1.4 |
| L19-3 | 58.5 | 1.88 | 5.80 | 34.1 | 0.91 | 0.58 | 0.06 | 98.8 | 89.7 | 8.5 | 1.7 |
| L19-4 | 58.3 | 1.66 | 5.78 | 34.3 | 0.73 | 0.61 | 0.28 | 100.0 | 90.1 | 8.5 | 1.4 |
| L10-1 | 55.0 | 3.49 | 5.70 | 33.5 | 0.58 | 0.81 | 0.23 | 99.2 | 90.3 | 8.8 | 1.1 |
| L10-2 | 54.1 | 3.47 | 5.89 | 33.2 | 0.59 | 0.80 | 0.15 | 98.0 | 89.9 | 9.0 | 1.2 |
| L6-1 | 54.6 | 3.89 | 6.13 | 33.1 | 0.66 | 0.82 | 0.08 | 99.4 | 89.4 | 9.3 | 1.3 |
| L6-2 | 55.8 | 3.85 | 6.39 | 33.6 | 0.48 | 0.81 | 0.19 | 101.3 | 89.5 | 9.6 | 0.9 |
| Di-harzburgite | | | | | | | | | | | |
| S4-4-g | 55.8 | 2.95 | 4.81 | 33.2 | 2.60 | 0.65 | 0.15 | 100.2 | 87.9 | 7.1 | 5.0 |
| S4-4-h | 55.9 | 2.94 | 5.35 | 34.5 | 0.47 | 0.55 | 0.06 | 99.6 | 91.2 | 7.9 | 0.9 |
| S4-4-i | 58.0 | 3.11 | 5.10 | 34.5 | 0.39 | 0.77 | 0.07 | 100.2 | 91.6 | 7.6 | 0.7 |
| S4-4-j | 55.8 | 3.03 | 5.45 | 34.2 | 0.52 | 0.55 | 0.16 | 99.7 | 90.9 | 8.1 | 1.0 |
| R5 | 55.8 | 3.18 | 5.53 | 34.0 | 0.70 | 0.31 | 0.08 | 99.6 | 90.4 | 8.2 | 1.3 |
| R87 | 55.4 | 2.71 | 5.45 | 34.8 | 0.71 | 0.65 | 0.03 | 99.8 | 91.7 | 8.0 | 1.3 |
| 78L22 | 55.6 | 2.99 | 6.13 | 34.7 | 0.68 | 0.59 | 0.00 | 100.6 | 89.9 | 8.9 | 1.2 |
| LH4-1 | 54.9 | 4.00 | 5.97 | 33.0 | 0.68 | 0.64 | 0.17 | 99.2 | 89.6 | 9.1 | 1.3 |
| LH4-5 | 55.2 | 3.93 | 6.51 | 33.8 | 0.93 | 0.65 | 0.33 | 101.4 | 88.7 | 9.6 | 1.8 |
| LH4-2 | 55.5 | 3.40 | 6.45 | 33.5 | 0.86 | 0.34 | 0.15 | 100.1 | 88.8 | 9.6 | 1.8 |
| LH4-3 | 55.0 | 3.71 | 6.18 | 33.2 | 0.85 | 0.65 | 0.23 | 99.8 | 89.0 | 9.3 | 1.6 |
| LH4-4 | 55.2 | 3.62 | 6.16 | 33.2 | 0.48 | 0.65 | 0.09 | 99.3 | 89.7 | 9.3 | 0.9 |
| LH3-1 | 55.6 | 3.20 | 5.95 | 33.7 | 0.99 | 0.60 | 0.17 | 100.0 | 89.3 | 8.9 | 1.9 |
| LH3-2 | 54.9 | 3.82 | 5.98 | 33.5 | 0.55 | 0.88 | 0.00 | 99.6 | 89.9 | 9.0 | 1.1 |
| LH4-5 | 55.6 | 3.98 | 6.22 | 33.4 | 0.69 | 0.68 | 0.24 | 100.8 | 89.3 | 9.3 | 1.3 |
| Dunite | | | | | | | | | | | |
| S4-a | 56.7 | 1.60 | 4.88 | 35.3 | 0.81 | 0.61 | 0.15 | 99.7 | 91.7 | 8.8 | 1.5 |
| S4-b | 57.1 | 1.79 | 4.71 | 35.2 | 0.87 | 0.59 | 0.24 | 100.8 | 91.5 | 8.9 | 1.6 |
| S4-c | 57.4 | 1.38 | 4.57 | 35.6 | 0.84 | 0.41 | 0.16 | 100.4 | 91.8 | 8.6 | 1.6 |
| S4-2-a | 58.3 | 2.39 | 4.80 | 34.6 | 0.99 | 0.65 | 0.10 | 99.9 | 90.9 | 7.2 | 1.9 |
| S4-2-b | 58.9 | 2.35 | 4.76 | 35.5 | 0.57 | 0.63 | 0.16 | 100.9 | 92.0 | 8.9 | 1.1 |
| IIIV8-1 | 58.8 | 1.58 | 5.03 | 34.7 | 0.96 | 0.63 | 0.02 | 100.0 | 90.8 | 7.4 | 1.8 |
| IIIV8-2 | 58.8 | 1.48 | 4.93 | 35.0 | 0.78 | 0.58 | 0.01 | 99.6 | 91.3 | 7.2 | 1.5 |
| IIIV8-17 | 58.1 | 1.58 | 5.31 | 34.5 | 0.86 | 0.44 | 0.00 | 98.9 | 90.6 | 7.8 | 1.6 |
| IIIV8-18 | 58.9 | 1.19 | 4.65 | 35.5 | 0.48 | 0.46 | 0.00 | 99.3 | 92.3 | 6.8 | 0.9 |
| IIIV8-19 | 58.3 | 1.49 | 5.19 | 34.8 | 0.70 | 0.53 | 0.01 | 99.2 | 91.1 | 7.6 | 1.3 |
| IIIV8-20 | 58.4 | 1.55 | 5.35 | 34.7 | 0.76 | 0.57 | 0.01 | 99.4 | 90.7 | 7.8 | 1.4 |

Appendix III.3. (continued)

| | SiO ₂ | Al ₂ O ₃ | FeO | MgO | CaO | Cr ₂ O ₃ | Na ₂ O | Total | En | Fs | Wo |
|------------|------------------|--------------------------------|------|------|------|--------------------------------|-------------------|-------|------|-----|-----|
| IIIV8-21 | 56.1 | 1.61 | 5.29 | 34.4 | 0.69 | 0.59 | 0.03 | 98.9 | 90.8 | 7.6 | 1.3 |
| IIIV8-22 | 56.5 | 1.48 | 5.41 | 34.6 | 0.77 | 0.50 | 0.03 | 99.3 | 90.6 | 8.0 | 1.4 |
| Chromitite | | | | | | | | | | | |
| R67-a | 58.7 | 0.80 | 2.76 | 37.1 | 0.52 | 0.58 | 0.09 | 100.5 | 95.1 | 4.0 | 1.0 |
| R67-b | 58.3 | 0.71 | 2.87 | 37.3 | 0.46 | 0.32 | 0.00 | 99.9 | 95.1 | 4.1 | 0.8 |
| R168 | 57.4 | 1.14 | 4.06 | 34.2 | 0.75 | 0.42 | 0.19 | 98.2 | 92.4 | 6.1 | 1.5 |
| IIIV8-3 | 57.7 | 0.77 | 4.03 | 36.9 | 0.31 | 0.82 | 0.00 | 100.6 | 93.7 | 5.7 | 0.6 |
| IIIV8-4 | 57.6 | 0.89 | 3.90 | 36.5 | 0.24 | 0.48 | 0.00 | 100.0 | 93.9 | 5.6 | 0.4 |
| IIIV8-5 | 57.1 | 0.98 | 3.89 | 35.8 | 0.84 | 0.51 | 0.01 | 98.9 | 93.1 | 5.7 | 1.2 |
| IIIV8-6 | 57.7 | 0.74 | 3.89 | 36.9 | 0.56 | 0.33 | 0.00 | 100.1 | 93.7 | 5.3 | 1.0 |
| IIIV8-7 | 57.2 | 0.93 | 4.23 | 36.2 | 0.47 | 0.54 | 0.00 | 99.9 | 93.0 | 6.1 | 0.9 |
| IIIV8-8 | 56.8 | 1.08 | 4.30 | 35.4 | 1.10 | 0.42 | 0.00 | 99.2 | 91.7 | 6.2 | 2.1 |
| IIIV8-9 | 57.0 | 1.11 | 4.16 | 35.9 | 0.72 | 0.42 | 0.01 | 99.3 | 92.6 | 6.0 | 1.3 |
| IIIV8-10 | 57.4 | 1.03 | 3.88 | 36.4 | 0.59 | 0.49 | 0.00 | 98.9 | 93.3 | 5.6 | 1.1 |
| IIIV8-11 | 56.6 | 0.80 | 3.59 | 35.9 | 0.49 | 0.36 | 0.00 | 97.8 | 93.8 | 5.3 | 0.9 |
| IIIV8-12 | 57.5 | 1.12 | 4.07 | 35.9 | 0.63 | 0.44 | 0.02 | 99.9 | 92.9 | 5.9 | 1.2 |
| IIIV8-13 | 57.1 | 0.91 | 4.10 | 35.8 | 0.55 | 0.45 | 0.00 | 99.0 | 93.0 | 6.0 | 1.0 |
| IIIV8-14 | 57.0 | 1.28 | 4.34 | 35.9 | 0.72 | 0.45 | 0.00 | 99.6 | 92.4 | 6.3 | 1.3 |
| IIIV8-15 | 57.7 | 0.63 | 3.83 | 36.8 | 0.43 | 0.47 | 0.00 | 99.6 | 93.7 | 5.5 | 0.8 |
| IIIV8-16 | 57.5 | 0.62 | 4.21 | 36.8 | 0.28 | 0.44 | 0.00 | 100.0 | 93.5 | 6.0 | 0.5 |

Appendix III. Mineral chemistry
III.4. Clinopyroxene

| | SiO ₂ | TiO ₂ | Al ₂ O ₃ | FeO | MgO | CaO | Cr ₂ O ₃ | Na ₂ O | Total | En | Fs | Wo |
|-------------|------------------|------------------|--------------------------------|------|------|------|--------------------------------|-------------------|-------|------|-----|------|
| Harzburgite | | | | | | | | | | | | |
| H-w3 | 53.3 | | 2.75 | 1.60 | 17.4 | 23.1 | 0.99 | 0.25 | 99.3 | 49.8 | 2.6 | 47.6 |
| H-w4 | 53.3 | | 3.86 | 2.40 | 18.1 | 20.5 | 0.92 | 0.30 | 99.2 | 52.9 | 3.9 | 43.1 |
| H-w1 | 51.2 | | 4.72 | 1.80 | 16.2 | 24.0 | 0.71 | 0.08 | 98.7 | 47.0 | 2.9 | 50.1 |
| H-w2 | 51.0 | | 4.62 | 2.56 | 16.2 | 23.6 | 0.85 | 0.15 | 99.0 | 48.8 | 4.2 | 49.1 |
| ZHK11-1 | 54.0 | 0.07 | 2.01 | 1.60 | 18.5 | 24.4 | 0.88 | 0.14 | 101.5 | 50.1 | 2.4 | 47.4 |
| ZHK11-2 | 53.9 | 0.03 | 2.30 | 1.87 | 18.4 | 24.3 | 1.00 | 0.16 | 101.9 | 49.8 | 2.8 | 47.3 |
| ZHK11-3 | 53.7 | 0.15 | 2.36 | 1.72 | 18.1 | 24.4 | 0.99 | 0.15 | 101.4 | 49.4 | 2.6 | 48.0 |
| ZHK11-4 | 54.0 | 0.02 | 1.90 | 1.71 | 18.4 | 24.6 | 0.88 | 0.10 | 101.6 | 49.7 | 2.6 | 47.7 |
| ZHK10-5 | 55.4 | | 0.94 | 1.76 | 19.3 | 24.0 | 0.32 | 0.15 | 101.9 | 51.4 | 2.7 | 45.9 |
| ZHK10-6 | 54.9 | | 1.29 | 1.76 | 18.9 | 24.5 | 0.52 | 0.08 | 102.0 | 50.4 | 2.6 | 47.0 |
| ZHK10-7 | 55.0 | | 0.86 | 1.81 | 19.0 | 24.0 | 0.38 | 0.09 | 101.1 | 51.0 | 2.7 | 46.3 |
| L6A-1 | 54.1 | 0.04 | 1.79 | 2.02 | 17.8 | 24.2 | 0.65 | 0.25 | 100.9 | 49.0 | 3.1 | 47.9 |
| L17-1 | 52.6 | 0.15 | 3.35 | 2.36 | 17.1 | 25.3 | 0.66 | 0.28 | 101.5 | 46.7 | 3.6 | 49.7 |
| L17-2 | 52.5 | 0.14 | 3.28 | 2.36 | 16.9 | 25.1 | 0.74 | 0.23 | 101.1 | 46.8 | 3.6 | 49.7 |
| L17-3 | 52.9 | 0.16 | 2.92 | 1.99 | 17.1 | 26.0 | 0.72 | 0.24 | 101.9 | 46.3 | 3.0 | 50.7 |
| L22-1 | 53.7 | 0.09 | 1.55 | 1.85 | 17.7 | 25.5 | 0.67 | 0.17 | 101.2 | 47.8 | 2.8 | 49.4 |
| L22-2 | 53.2 | 0.04 | 1.16 | 1.77 | 17.6 | 25.7 | 0.66 | 0.22 | 100.7 | 47.7 | 2.7 | 49.6 |
| L10-1 | 52.2 | 0.10 | 3.63 | 2.08 | 16.4 | 25.1 | 1.23 | 0.41 | 101.1 | 46.1 | 3.3 | 50.6 |
| L10-2 | 51.7 | 0.09 | 3.55 | 1.83 | 16.3 | 25.5 | 1.25 | 0.46 | 100.6 | 45.7 | 2.9 | 51.4 |
| L10-3 | 52.2 | 0.14 | 3.24 | 1.90 | 16.4 | 25.3 | 1.15 | 0.26 | 100.5 | 46.0 | 3.0 | 51.0 |
| L19-1 | 53.7 | 0.01 | 1.27 | 1.70 | 17.8 | 25.8 | 0.61 | 0.15 | 101.1 | 47.7 | 2.6 | 49.7 |
| L19-2 | 54.0 | | 1.36 | 1.72 | 18.1 | 26.0 | 0.52 | 0.25 | 101.9 | 47.9 | 2.6 | 49.5 |
| L6-1 | 51.8 | 0.13 | 4.34 | 2.16 | 16.1 | 26.2 | 1.23 | 0.09 | 101.9 | 44.6 | 3.4 | 52.0 |
| L6-2 | 52.9 | 0.07 | 2.43 | 1.84 | 17.3 | 26.1 | 0.76 | 0.15 | 101.5 | 46.6 | 2.8 | 50.6 |
| L12-1 | 53.1 | | 1.79 | 1.80 | 17.5 | 25.9 | 0.66 | 0.21 | 101.3 | 47.1 | 2.7 | 50.1 |
| L12-2 | 53.4 | 0.02 | 1.46 | 1.77 | 17.5 | 25.9 | 0.72 | 0.24 | 101.1 | 47.2 | 2.7 | 50.1 |
| H14-1 | 51.1 | 0.22 | 5.00 | 2.20 | 16.0 | 25.3 | 1.19 | 0.41 | 101.2 | 45.2 | 3.5 | 51.3 |
| H14-2 | 51.9 | 0.21 | 3.32 | 2.41 | 17.0 | 25.0 | 0.57 | 0.19 | 100.4 | 46.9 | 3.7 | 49.4 |
| H1-2 | 53.7 | 0.07 | 1.24 | 1.60 | 17.8 | 26.0 | 0.64 | 0.20 | 101.2 | 47.6 | 2.4 | 50.0 |
| H1-3 | 52.7 | 0.12 | 1.72 | 1.79 | 17.4 | 25.6 | 0.94 | 0.41 | 100.6 | 47.3 | 2.7 | 50.0 |
| S4-3-d | 54.1 | 0.08 | 1.34 | 1.67 | 18.1 | 25.7 | 0.45 | 0.26 | 101.8 | 48.1 | 2.8 | 49.1 |
| S4-3-e | 53.2 | 0.10 | 2.18 | 1.45 | 17.4 | 25.9 | 1.01 | 0.33 | 101.4 | 47.3 | 2.2 | 50.5 |

Appendix III.4. (continued)

| | SiO ₂ | TiO ₂ | Al ₂ O ₃ | FeO | MgO | CaO | Cr ₂ O ₃ | Na ₂ O | Total | En | Fs | Wo |
|----------------|------------------|------------------|--------------------------------|------|------|------|--------------------------------|-------------------|-------|------|-----|------|
| S4-3-f | 53.1 | 0.22 | 2.72 | 1.67 | 17.4 | 25.5 | 0.92 | 0.28 | 101.7 | 47.3 | 2.9 | 49.6 |
| S4-3-g | 52.5 | 0.04 | 2.56 | 1.79 | 17.1 | 25.5 | 0.90 | 0.22 | 100.6 | 46.9 | 2.6 | 50.3 |
| Di-harzburgite | | | | | | | | | | | | |
| L-w1 | 52.7 | | 3.12 | 1.78 | 16.8 | 24.4 | 0.80 | 0.10 | 99.7 | 47.6 | 2.8 | 49.8 |
| LH4-1 | 52.0 | 0.12 | 3.99 | 2.49 | 17.3 | 24.4 | 1.05 | 0.21 | 101.4 | 47.7 | 3.9 | 48.4 |
| LH4-2 | 51.6 | 0.20 | 4.10 | 2.02 | 16.5 | 25.5 | 1.18 | 0.26 | 101.1 | 45.8 | 3.2 | 51.0 |
| LH3-1 | 52.0 | 0.09 | 3.22 | 2.05 | 16.7 | 25.5 | 1.00 | 0.42 | 100.9 | 46.1 | 3.2 | 50.7 |
| LH3-2 | 52.4 | 0.06 | 3.84 | 2.42 | 16.7 | 25.2 | 1.13 | 0.33 | 102.0 | 46.1 | 3.7 | 50.1 |
| S4-4-h | 52.8 | 0.08 | 2.23 | 1.90 | 17.7 | 25.7 | 0.75 | 0.27 | 101.4 | 47.4 | 2.9 | 49.7 |
| S4-4-i | 52.6 | 0.14 | 2.69 | 1.73 | 17.1 | 25.3 | 0.90 | 0.18 | 100.8 | 47.2 | 2.7 | 50.1 |
| S4-4-j | 52.6 | 0.13 | 3.06 | 2.09 | 17.1 | 25.4 | 0.93 | 0.25 | 101.4 | 46.9 | 3.2 | 49.9 |
| S4-4-k | 53.0 | 0.07 | 2.41 | 1.67 | 17.2 | 25.6 | 0.83 | 0.27 | 101.0 | 47.1 | 2.6 | 50.3 |
| Chromitite | | | | | | | | | | | | |
| IIIV6-1 | 53.5 | 0.05 | 1.48 | 1.64 | 18.7 | 22.1 | 0.90 | 0.18 | 98.4 | 52.6 | 2.6 | 44.8 |
| IIIV6-2 | 54.0 | 0.07 | 1.03 | 1.39 | 18.2 | 23.2 | 0.73 | 0.15 | 98.7 | 51.2 | 2.2 | 46.7 |
| IIIV6-3 | 54.5 | 0.02 | 0.59 | 1.04 | 18.3 | 23.9 | 0.69 | 0.09 | 98.1 | 50.7 | 1.6 | 47.7 |
| IIIV6-4 | 54.2 | 0.04 | 0.89 | 1.34 | 18.2 | 23.7 | 0.64 | 0.15 | 99.1 | 50.7 | 2.1 | 47.2 |
| IIIV6-5 | 54.0 | 0.08 | 1.00 | 1.38 | 18.1 | 23.5 | 0.66 | 0.12 | 98.6 | 50.6 | 2.2 | 47.2 |
| IIIV6-6 | 54.3 | 0.04 | 0.75 | 1.28 | 18.3 | 23.7 | 0.58 | 0.15 | 99.1 | 50.7 | 2.0 | 47.4 |
| IIIV6-7 | 54.0 | 0.03 | 0.85 | 1.20 | 18.4 | 24.0 | 0.85 | 0.14 | 99.5 | 50.7 | 1.9 | 47.4 |
| IIIV6-8 | 54.2 | 0.05 | 1.37 | 1.50 | 18.0 | 23.3 | 1.05 | 0.19 | 99.6 | 50.6 | 2.4 | 47.1 |
| IIIV6-9 | 53.2 | 0.05 | 1.28 | 1.34 | 18.0 | 23.4 | 0.93 | 0.17 | 98.4 | 50.6 | 2.1 | 47.3 |
| IIIV6-10 | 54.3 | 0.05 | 0.59 | 1.14 | 18.3 | 23.9 | 0.69 | 0.09 | 99.0 | 50.6 | 1.8 | 47.6 |
| IIIV6-11 | 53.6 | 0.06 | 1.51 | 1.39 | 17.8 | 23.2 | 1.06 | 0.19 | 98.6 | 50.5 | 2.2 | 47.3 |
| IIIV6-12 | 53.9 | 0.05 | 0.72 | 1.19 | 18.0 | 23.6 | 0.77 | 0.10 | 98.3 | 50.5 | 1.9 | 47.6 |
| IIIV6-13 | 54.2 | 0.05 | 1.00 | 1.50 | 18.1 | 23.7 | 0.84 | 0.13 | 99.4 | 50.3 | 2.3 | 47.3 |
| ZHK6-2 | 55.4 | 0.07 | 0.53 | 0.93 | 18.4 | 24.8 | 0.69 | 0.20 | 101.0 | 50.1 | 1.4 | 48.5 |
| ZHK6-2 | 55.2 | | 0.52 | 1.15 | 18.7 | 24.3 | 0.53 | 0.33 | 100.7 | 50.8 | 1.8 | 47.5 |
| ZHK-a | 55.2 | | 0.73 | 1.35 | 18.1 | 24.7 | 1.23 | 0.43 | 101.7 | 49.4 | 2.1 | 48.5 |
| ZHK-b | 55.5 | 0.08 | 0.51 | 1.12 | 18.3 | 25.4 | 0.45 | 0.33 | 101.6 | 49.3 | 1.7 | 49.1 |
| R37 | 54.2 | 1.19 | 0.93 | 0.93 | 18.5 | 24.6 | 1.56 | 0.76 | 99.9 | 47.4 | 1.5 | 51.1 |
| R36 | 50.7 | 1.07 | 0.83 | 0.92 | 16.7 | 23.5 | 1.15 | 5.97 | 100.0 | 48.9 | 1.5 | 49.6 |
| 78R67 | 55.1 | | 0.83 | 0.93 | 17.9 | 25.0 | 0.82 | 0.25 | 101.0 | 49.2 | 1.4 | 49.4 |
| R71 | 55.2 | | 0.75 | 1.20 | 18.1 | 25.3 | 0.34 | 0.03 | 100.9 | 48.9 | 1.8 | 49.3 |
| R67 | 54.1 | | 0.87 | 1.01 | 18.4 | 23.6 | 0.85 | 0.30 | 99.1 | 51.3 | 1.6 | 47.2 |
| R76 | 53.3 | | 0.97 | 1.07 | 17.7 | 24.3 | 0.93 | 1.70 | 99.9 | 49.6 | 1.7 | 48.7 |
| R168 | 53.4 | | 1.02 | 1.20 | 16.9 | 25.5 | 0.90 | 1.54 | 100.5 | 47.2 | 1.9 | 51.0 |

Appendix III.4. (continued)

| | SiO ₂ | TiO ₂ | Al ₂ O ₃ | FaO | MgO | CaO | Cr ₂ O ₃ | Na ₂ O | Total | En | Fs | Wo |
|----------|------------------|------------------|--------------------------------|------|------|------|--------------------------------|-------------------|-------|------|-----|------|
| Dunite | | | | | | | | | | | | |
| S4-a | 54.5 | 0.07 | 1.15 | 1.54 | 18.1 | 25.5 | 0.63 | 0.33 | 101.7 | 48.6 | 2.3 | 49.1 |
| S4-b | 53.1 | 0.09 | 1.83 | 1.57 | 17.5 | 25.2 | 1.19 | 0.25 | 100.6 | 48.0 | 2.4 | 49.6 |
| S4-c | 53.5 | 0.08 | 1.90 | 1.77 | 17.6 | 25.9 | 1.05 | 0.31 | 102.0 | 47.3 | 2.7 | 50.0 |
| S4-2-a | 53.7 | 0.15 | 1.64 | 1.62 | 17.8 | 25.4 | 0.74 | 0.35 | 101.3 | 48.1 | 2.5 | 49.5 |
| S4-2-b | 54.0 | 0.10 | 2.00 | 2.10 | 19.2 | 23.3 | 0.93 | 0.19 | 101.7 | 51.7 | 3.2 | 45.1 |
| S4-2-c | 53.9 | 0.08 | 1.74 | 1.58 | 17.9 | 26.0 | 0.54 | 0.27 | 101.9 | 47.8 | 2.4 | 49.9 |
| IIIV6-14 | 54.0 | 0.05 | 1.07 | 1.38 | 17.9 | 23.7 | 0.70 | 0.17 | 99.0 | 50.1 | 2.2 | 47.7 |
| IIIV6-15 | 53.1 | 0.08 | 2.17 | 2.03 | 18.2 | 22.4 | 1.15 | 0.16 | 99.1 | 51.3 | 3.2 | 45.4 |
| IIIV6-16 | 53.4 | 0.04 | 1.83 | 1.92 | 17.3 | 23.0 | 1.14 | 0.21 | 98.9 | 49.6 | 3.1 | 47.3 |
| IIIV6-17 | 53.7 | 0.05 | 1.78 | 1.88 | 17.8 | 23.0 | 0.83 | 0.19 | 99.2 | 50.3 | 3.0 | 46.7 |
| IIIV6-18 | 53.6 | 0.06 | 1.66 | 2.07 | 17.9 | 22.6 | 0.97 | 0.21 | 99.0 | 50.7 | 3.3 | 46.0 |
| IIIV6-19 | 53.2 | 0.04 | 1.65 | 2.04 | 17.6 | 22.8 | 0.89 | 0.21 | 98.4 | 50.1 | 3.3 | 46.6 |

BIBLIOGRAPHY

- Ahmed, Z., 1984. Stratigraphic and textural variations in the chromite composition of the ophiolitic Sakhakot-Qila complex, Pakistan. *Econ. Geol.* 79, 1334-1359.
- Alapieti, T. T., Kujanpaa, J., Lahtinen, J. J., and Papunen, H., 1989. The Kemi stratiform chromitite deposit, Northern Finland. *Econ. Geol.* 84, 1057-1077.
- Allegre, C. J., and other 34 authors, 1984. Structure and evolution of the Himalaya-Tibet orogenic belt. *Nature* 307, 17-22.
- Anderson, A. T., 1975. Some basaltic and andesitic gases. *Rev. Geophys. Space Phys.* 13, 37-55.
- Arai, S., 1980. Dunite-harzburgite-chromitite complexes as refractory residue in the Sangun-Yamaguchi zone, Western Japan. *J. Petrol.* 21, 141-165.
- Arai, S., 1992. Chemistry of chromian spinel in volcanic rocks as a potential guide to magma chemistry. *Mineral. Mag.* 56, 173-184.
- Auge, T., 1987. Chromite deposits in the northern Oman ophiolite: mineralogical constraints. *Mineral. Deposita* 22, 1-10.
- Ave Lallemant, H. G., 1985. Subgrain rotation and dynamic recrystallization of olivine, upper mantle diapirism, and extension of the basin- and -range province. *Tectonophy.* 119, 89-117.
- Bacuta, G. C., Kay, R. W., Gibbs, A. K., and Bruce, R. L., 1990. Platinum-group element abundance and distribution in chromite deposits of the Acoje Block, Zambales ophiolite complex, Philippines. *J. Geochem. Explor.* 37, 113-145.
- Bai, W.-J., Li, H., and Le Bel, L., 1985. Petrographical studies of the ophiolitic complex of Hegenshan in Inner Mongolia, China. *Res. Pap. Collect. (in Chinese)* 3, 41-63.
- Bai, W.-J., Zhou, M.-F., and Robinson, P. T., 1993. Possible diamond-bearing mantle peridotites and chromitites in the Luobusa and Donqiao ophiolites, Tibet. *Can. J. Earth Sci.* 30, 1650-1659.
- Barnes, S.-J., Naldrett, A. J., and Gorton, M. P., 1985. The origin of the

fractionation of platinum-group elements in terrestrial magmas. *Chem. Geol.* 53, 303-323.

Barnes, S.J., 1986. The distribution of chromium among orthopyroxene, spinel and silicate liquid at atmospheric pressure. *Geochim. Cosmochim. Acta* 50, 1889-1909.

Bédard, J., 1989. Disequilibrium mantle melting. *Earth Planet. Sci. Lett.* 91, 359-366.

Best, M. G., 1975. Migration of hydrous fluids in the upper mantle and potassium variation in calc-alkalic rocks. *Geol.* 3, 429-432.

Bodinier, J. L., Vasseur, G., Vernieres, J., Dupuy, C., and Fabries, J., 1990. Mechanisms of mantle metasomatism: geochemical evidence from the Lherz orogenic peridotite. *J. Petrol.* 31, 597-628.

Bonatti, E., and Michael, P. J., 1989. Mantle peridotites from continental rifts to ocean basins to subduction zones. *Earth Planet. Sci. Lett.* 91, 297-311.

Boudreau, A. E., 1988. Investigations of the Stillwater complex. IV. The role of volatiles in the petrogenesis of the J-M Reef, Minneapolis Adit section. *Can. Mineral.* 26, 193-208.

Boullier, A.-M., and Gueguen, Y., 1975. SP-mylonites: origin of some mylonites by superplastic flow. *Contrib. Mineral. Petrol.* 50, 93-104.

Boyd, F. R., 1989. Compositional distinction between oceanic and cratonic lithosphere. *Earth Planet. Sci. Lett.* 96, 15-26.

Boyd, F. R., Pearson, D. G., Nixon, P. H., and Mertzman, S. A., 1993. Low-calcium garnet harzburgites from southern Africa: their relations to cratons structure and diamond crystallization. *Contrib. Mineral. Petrol.* 113, 352-366.

Brown, M., 1980. Textural and geochemical evidence for the origin of some chromite deposits in the Oman ophiolite. In Panayiotou, A. (ed.) *Ophiolites. Proc. Int. Ophiolite Symp.*, p. 714-721.

Calon, T. J., 1979. A study of the Alpine-type peridotites in the Seve-Koli nappe complex, Central Swedish Caledonides, with special reference to the Kittelfjall peridotite. unpubl. PhD thesis, 236pp..

Cameron, E. N., 1980. Evolution of the lower critical zone, centre sector, eastern

Bushveld complex. *Econ. Geol.* 75, 845-871.

Cameron, E. N., and Desborough, G. A., 1969. Occurrence and characteristics of chromite deposits-eastern Bushveld complex, South Africa. *Econ. Geol. Monogr.* 4, 23-40.

Campbell, I. H., and Murck, B. W., 1993. Petrology of the G and H chromitite zones in the Mountain View Area of the Stillwater complex, Montana. *J. Petrol.* 34, 291-316.

Cassard, D., Moutte, J., Nicolas, A., Leblanc, M., Robinovitch, M., Prinzhofer A., and Routhier, P., 1981. Structure classification of chromite pods from New Caledonia. *Econ. Geol.* 76, 805-831.

Ceuleneer, G., Nicolas, A., and Boudier, F., 1988. Mantle flow patterns at an oceanic spreading centre: the Oman peridotites record. *Tectonophy.* 151, 1-26.

Chang, C., Pan, Y. and Sun, Y., 1989. The tectonic evolution of Qinghai-Tibet plateau: a review. In Sengor, A. M. C. (ed.) *Tectonic evolution of the Tethyan Region*. Dordrecht: Kluwer Acad. Publ., p.415-476.

Coleman, R.G., 1977. *Ophiolites, ancient oceanic lithosphere?* Berlin-Heidelberg-New York: Springer, 220pp.

Coleman, R. G., 1989. Continental growth of northwest China. *Tectonics* 8, 621-635.

Crawford, A. J., Falloon, T. J., and Green, D. H., 1989. Classification, petrogenesis and tectonic setting of boninites. In Crawford, A. J. (ed.) *Boninites*. London: Unwin Hyman, p.1-49.

Daines, M. J., and Kohlstedt, D. L., 1994. The transition from porous to channelized flow due to melt/rock reaction during melt migration. *Geophy. Res. Lett.* 21, 145-148.

Dawson, J. B., Powell, D. G., and Reid, A. M., 1970. Ultrabasic xenoliths and lava from the Lashaine volcano, northern Tanzania. *J. Petrol.* 11, 519-548.

Debon, F., Le Fort, P., Sheppard, S. M. F., and Sonet, J., 1986. The four plutonic belt of the Transhimalaya-Himalaya: a chemical, mineralogical, isotopic, and chronological synthesis along a Tibet-Nepal section. *J. Petrol.* 27, 219-250.

Delaney, J. S., Muenow, D. W., and Graham, D. G., 1978. Abundance and distribution of water, carbon and sulfur in the glassy rims of submarine pillow basalts. *Geochim. Cosmochim. Acta* 42, 581-594.

Dewey, J. F., F. R. S., Shackleton, R. M., F. R. S., Chang, C. and Sun, Y., 1988. The tectonic evolution of the Tibetan plateau. *Phil. Trans. R. Soc. Lond. A* 327, 379-413.

Dick, H. J. B., 1977. Partial melting in the Josephine peridotite-I, The effect of mineral composition and its consequence from geobarometry and geothermometry. *Am. J. Sci.* 227, 801-832.

Dick, H. J. B., and Bullen, T., 1984. Chromian spinel as a petrogenetic indicator in abyssal and Alpine-type peridotites and spatially associated lavas. *Contrib. Mineral. Petrol.* 86, 54-76.

Dick, H. J. B., Fisher, R. L., and Bryan, W. B., 1984. Mineralogic variability of the uppermost mantle along mid-ocean ridges. *Earth Planet. Sci. Lett.* 69, 88-106.

Dick, H. J. B., and Natland, J. H., 1995. Late-stage melt evolution and transport in the shallow mantle beneath the East Pacific Rise. *Sci. Results* 147 (submitted MS).

Dickey, J. S. Jr., 1975. A hypothesis of origin for podiform chromite deposits. *Geochim. Cosmochim. Acta* 39, 61-72.

Dickey, J. S. Jr., Yoder, H. S. Jr., and Schairer, J. F., 1971. Chromium in silicate-oxide systems. *Carnegie Inst. Washington Ybk.* 70, 118-122.

Dickey, J. S. Jr., and Yoder, H. S., Jr., 1972. Partitioning of chromium and aluminum between clinopyroxene and spinel. *Carnegie Inst. Washington Ybk.* 71, 384-392.

Duke, J. M., 1983. Ore deposit models 7. Magmatic segregation models of chromite. *Geosci. Can.* 10, 15-24.

Dungan, M. A., and Ave Lallemand, H. G., 1977. Formation of small dunite bodies by metasomatic transformation of harzburgite in the Canyon Mountain ophiolite, northeast Oregon. In Dick, H. J. B. (ed.) *Magma genesis*. Oregon Dep. Geol. Mineral. Ind. Bull. 96, 109-128.

Dunlop, H. M., and Fouillac, A. M., 1985. Isotope geochemistry of Oman basic-

ultrabasic rocks and chromite deposits. In Gallagher, M. J., Ixer, R. A., Neary, C. R., and Prichard, H. M. (eds.) *Metallogeny of basic and ultrabasic rocks*. London: Inst. Mining Metallurgy, p.291-304.

Edwards, S. J., 1990. Harzburgites and refractory melts in the Lewis Hills massif, Bay of Island ophiolite complex: the base-metals and precious-metals story. *Can. Mineral.* 28, 537-552.

Edwards, S. J., and Malpas, J., 1995. Multiple origins for mantle harzburgites: Examples from the Lewis Hills massif, Bay of Islands ophiolite, Newfoundland. *Can. J. Earth Sci.* (in press).

Elthon, D., 1989. Pressure of origin of primary mid-ocean ridge basalts. In Saunders, A. D., and Norry, M. J. (eds.) *Magmatism in the ocean basins*. *Geol. Soc. Spec. Publ.* 42, p.125-136.

Evans, C., and Hawkins, J. W., 1989. Compositional heterogeneities in upper mantle peridotites from the Zambales Range ophiolite, Luzon, Philippines. *Tectonophy.* 168, 23-41.

Feng, Y., Coleman, R. G., Tilton, G., and Xiao, X., 1989. Tectonic evolution of the West Junggar region, Xinjiang, China. *Tectonics* 8, 729-752.

Fisk, M. R., 1986. Basalt-magma interactions with harzburgite and the formation of high magnesium andesites. *Geophy. Res. Lett.* 13, 467-470.

Fryer, B. J., and Greenough, J. D., 1992. Evidence for mantle heterogeneity from platinum-group element abundances in Indian Ocean basalts. *Can. J. Earth Sci.* 29, 2329-2340.

Garuti, G., Gorgoni, C., and Sighinolfi, G. P., 1984. Sulfide mineralogy and chalcophile and siderophile element abundances in the Ivrea-Verbano mantle peridotites. *Earth Planet. Sci. Lett.* 70, 69-87.

Geological Team 2 of Tibetan Geological Bureau (GTTGB), 1981. Geological exploration reports of the Luobusa chromite mine, Tibet (in Chinese), Unpubl.

Geological Team 2 of Tibetan Geological Bureau (GTTGB), 1989. Geological exploration reports of the Xiankashan chromite mine, Luobusa, Tibet (in Chinese), Unpubl.

Girardeau, J., Mercier, J. C. C., and Wang Xibin, 1985. Petrology of the mafic rocks of the Xigaze ophiolite, Tibet: Implications for the genesis of the oceanic

lithosphere. *Contrib. Mineral. Petrol.* 90, 309-321.

Girardeau, J., and Mercier, J. C. C., 1988. Petrology and texture of the ultramafic rocks of the Xigaze ophiolite (Tibet), constraints for mantle structure beneath slow spreading ridges. *Tectonophy.* 147, 33-58.

Girardeau, J., Marcoux, J., and Montenat, C., 1989. The Neo-cimmerian ophiolite belt in Afghanistan and Tibet: comparison and evolution. In Sengor, A.M.C. (ed.) *Tectonic Evolution of the Tethyan Region*. Dordrecht: Kluwer Acad. Publ., p.477-504.

Glasser, F. P., and Osborn, F. F., 1958. Phase equilibrium in the system $\text{CaO-Cr}_2\text{O}_3\text{-SiO}_2$. *J. Amer. Ceram. Soc.* 41, 358-367.

Golding, H. G., and Johnson, K. R., 1971. Variation in gross chemical composition and related physical properties of podiform chromite in the Coolac district, NSW, Australia. *Econ. Geol.* 66, 1017-1027.

Gopel, C., Allegre, C. J., and Xu, R., 1984. Lead isotope study of the Xigaze ophiolite (Tibet): the problem of the relationship between magmatites (gabbros, dolerites, lavas) and tectonites (harzburgites). *Earth Planet. Sci. Lett.* 6, 301-310.

Grafenauer, S., 1977. Genesis of chromite in Yugoslavian peridotite. In Klemm, D.D., and Schneider, H.J. (eds.) *Time- and strata-bound ore deposits*. Berlin Heidelberg New York: Springer-Verlag, P.327-351.

Greenbaum, D., 1977. The chromitiferous rocks of the Troodos ophiolite complex. *Econ. Geol.* 72,1175-1194.

Guo Tieying, Liang Dingyi, Zhang Yizhi, and Zhao Chonghe, 1991. *Geology of Ngari, Tibet* (in Chinese). Wuhan: China Univ. Geosci. Press, 464pp..

Hamlyn, P. R., Keays, R. R., Cameron, W. E., Crawford, A. J., and Waldron, H. M., 1985. Precious metals in magnesian low-Ti lavas: implications for metallogenesis and sulfur saturation in primary magmas. *Geochim. Cosmochim. Acta* 49, 1797-1811.

Harte, B., 1977. Rock nomenclature with particular relation to deformation and recrystallization textures in olivine-bearing xenoliths. *J. Geol.* 85, 279-288.

Hartmann, G., and Wedepohl, K. H., 1993. The composition of peridotite tectonites from the Ivrea complex, northern Italy: residues from melt extraction.

Geochim. Cosmochim. Acta 57, 1761-1782.

Hatton, C. J., and von Gruenewaldt, G., 1987. The geological setting and petrogenesis of the Bushveld chromitite layers. In Stowe, C. W. (ed.) Evolution of chromium ore fields. New York: Van Nostrand-Reinhold, p.109-143.

Hawkins, J. W., and Evans, C. A., 1982. Geology of the Zambales Range, Luzon, Philippine islands: ophiolite derived from an island arc-back arc basin pair. In Hayes, D. E. (ed.) The tectonic evolution of southeast Asian seas and islands Part II. Geophys. Monogr. Ser. 27, AGU Washington, p.95-123.

Hervig, R. L., Smith, J. V., and Dawson, J. B., 1986. Lherzolite xenoliths in Kimberlites and basalts: petrogenetic and crystallochemical significance of some minor and trace elements in olivine, pyroxenes, garnet and spinel. Trans. R. Soc. Edinburgh 77, 181-201.

Hess, P. C., 1993. Phase equilibria constraints on the origin of ocean floor basalt. In Morgan, J. P., Blackman, D. K., and Sinton, J. M. (eds.) Mantle Flow and Melt Generation at mid-ocean ridge. Geophys. Monograph 71, Am. Geophys. Union, 67-102.

Hickey, R. L., and Frey, F. A., 1982. Geochemical characteristics of boninite series volcanics: implications for their source. Geochim. Cosmochim. Acta 46, 2099-2115.

Hock, M., Friedrich, G., Pluger, W. L., and Wichowskik, A., 1986. Refractory- and Metallurgical-type chromite ores, Zambales ophiolite, Luzone, Philippines. Mineral. Deposita 21, 190-199.

Irvine, T. N., 1965. Chromian spinel as a petrogenetic indicator: part I, theory. Can. J. Earth Sci. 2, 648-671.

Irvine, T. N., 1967. Chromium spinels as a petrogenetic indicator. II, Petrologic applications. Can. J. Earth Sci. 4, 71-103.

Irvine, T. N., 1975. Crystallization sequences in the Muskox intrusion and other layered intrusions-II. Origin of chromite layers and similar deposits of other magmatic ores. Geochim. Cosmochim. Acta 39, 991-1020.

Irvine, T. N., 1977. Origin of chromite layers in the Muskox intrusion and other intrusions: a new interpretation. Geol. 5, 273-277.

Irvine, T. N., and Sharpe, M. R., 1986. Magma mixing and the origin of stratiform

oxide ore zones in the Bushveld and Stillwater complexes. In Gallagher, M. J., Ixer, R. A., Neary, C. R., and Prichard, H. M. (eds.) *Metallogeny of basic and ultrabasic rocks*. London: Inst. Mining Metallurgy, p.183-198.

Ishiwatari, A., 1985. Igneous petrogenesis of the Yakuno ophiolite (Japan) in the context of the diversity of ophiolites. *Contrib. Mineral. Petrol.* 89, 155-167.

Jagoutz, E., Palme, H., Hildegard Baddenhausen, Blum, K., Cendales, M., Gerlind Dreibus, Spettel, B., Lorenz, V., and Wanke, H., 1979. The abundances of major, minor and trace elements in the earth's mantle as derived from primitive ultramafic nodules. *Proc. Lunar Planet. Sci. Conf.* 10th, 2031-2050.

Jan, M. Q., and Windley, B. F., 1990. Chromian spinel-silicate chemistry in ultramafic rocks of the Jijal complex, northwest Pakistan. *J. Petrol.* 31, 667-715.

Jaques, A. L., and Green, D. H., 1980. Anhydrous melting of peridotite at 0-15 kb pressure and the genesis of tholeiitic basalts. *Contrib. Mineral. Petrol.* 73, 287-310.

Johan, Z., 1984. Genesis of chromite deposits in the Massif du Sud ophiolitic complex, New Caledonia: example of a high-temperature, fluid-rich, ore-forming system. 27th Inter. Geol. Congress. Abstr. 6, Section 12, 146-147.

Johan, Z., 1986a. Chromite deposits of New Caledonian ophiolite nappes. In Petrascheck, W., and others (eds.) *Chromites*, Athens: Theophrastus, p.311-339.

Johan, Z., 1986b. Chromite deposits in the Massif Du Sud ophiolite, New Caledonia: genetic considerations. In Karamata, S. (ed.) *Chromites*. Unesco's IGCP-197 Project, *Metallogeny of Ophiolites*, p.311-339.

Johan, Z., Dunlop, H., Le Bel, L., Robert, J. L., and Volfinger, M., 1983. Origin of chromite deposits in ophiolitic complexes: evidence for a volatile- and sodium-rich reducing fluid phase. *Fortsch. Mineral.* 61, 105-107.

Johnson, K. T. M., Dick, H. T. B., and Shimizu, N., 1990. Melting in the oceanic upper mantle: an ion microprobe study of diopsides in abyssal peridotites. *J. Geophys. Res.* 95, 2661-2678.

Keays, R. R., 1982. Palladium and iridium in komatiites and associated rocks: application to petrogenetic problems. In Arndt, N. T., and Nisbet, E. G. (eds.) *Komatiites*. London: Allen & Unwin, p.435-457.

- Keays, R. R., 1994. The role of komatiitic and picritic magmatism and S-saturation in the formation of ore deposits. *Lithos* 34, 1-18.
- Keith, M. L., 1954. The system $MgO-Cr_2O_3-SiO_2$. *J. Amer. Ceram. Soc.* 37, 390-496.
- Kelemen, P. B., 1990. Reaction between ultramafic rock and fractionating basaltic magma I. Phase relations, the origin of calc-alkine magma series, and the formation of discordant dunite. *J. Petrol.* 31, 51-98.
- Kelemen, P. B., and Dick, H. J. B., 1995. Focused melt flow and localized deformation in the upper mantle: Juxtaposition of replacive dunite and ductile shear zones in the Josephine peridotite, SW Oregon. *J. Geophys. Res.* 100, 423-438.
- Kelemen, P. B., Dick, H. J. B., and Quick, J. E., 1992. Formation of harzburgite by pervasive melt/rock reaction in the upper mantle. *Nature* 358, 635-641.
- Kelemen, P. B., Whitehead, J. A., Aharonov, E., and Jordahl, K. A., 1995. Experiments on flow focusing in soluble porous media, with applications to melt extraction from the mantle. *J. Geophys. Res.* 100, 475-496.
- Kepezhinskas, P. K., Taylor, R. N., and Tanaka, H., 1993. Geochemistry of plutonic spinels from the north Kamchatka arc: comparisons with spinels from other tectonic settings. *Mineral. Mag.* 57, 575-589.
- Konstantopoulou, U. G., and Economou, M., 1991. Distribution of platinum-group elements and gold within the Vourinos chromite ores, Greece. *Econ. Geol.* 86, 1672-1682.
- Lago, B., Rabinowicz, M., and Nicolas, A., 1982. Podiform chromite ore bodies: a genetic model. *J. Petrol.* 23, 103-125.
- Leblanc, M., 1980. Chromite growth, dissolution and deformation from a morphological view point: SEM investigations. *Mineral. Deposita* 15, 201-210.
- Leblanc, M., 1987. Chromite in oceanic arc environment: New Caledonia. In Stowe, C. W. (ed.) *Evolution of chromium ore fields*. New York: Van Nostrand-Reinhold, p.265-296.
- Leblanc, M., 1991. Platinum-group elements and gold in ophiolite complexes: distribution and fractionation from mantle to oceanic floor. In Peters, T., Nicolas, A., and Coleman, R. G. (eds.) *Ophiolite genesis and evolution of the oceanic*

lithosphere. Dordrecht: Kluwer Acad. Publ., p.231-260.

Leblanc, M., and Violette, J. F., 1983. Distribution of Al-rich and Cr-rich chromite pods in ophiolites. *Econ. Geol.* 78, 293-301.

Leblanc, M., and Temagout, A., 1989. Chromite pods in a lherzolite massif (Collo, Algeria): evidence of oceanic-type mantle rocks along the west Mediterranean Alpine belt. *Lithos* 23, 153-162.

Leblanc, M., and Ceuleneer, G., 1992. Chromite crystallization in a multicellular magma flow: evidence from a chromitite dike in the Oman ophiolite. *Lithos* 27, 231-257.

Le Fort, P., 1988. Granites in the tectonic evolution of the Himalaya, Karakoram and southern Tibet. *Phil. Trans. R. Soc. Lond. A* 326, 281-299.

Lehmann, J., 1983. Diffusion between olivine and spinel: application to geothermometry. *Earth Planet. Sci. Lett.* 64, 123-138.

Lipin, B., 1993. Pressure increases, the formation of chromite seams, and the development of the ultramafic series in the Stillwater complex, Montana. *J. Petrol.* 34, 955-976.

Li Zijin, and others, 1993. Prospecting for the chromite ores in the Luobusa ophiolite, Tibet (in Chinese). Wuhan: China Univ. Geosci. Press, 166pp.

Lorand, J. P., 1989. Abundance and distribution of Cu-Fe-Ni sulfides, sulfur, copper and platinum-group elements in orogenic-type spinel lherzolite massifs of Ariège (northeastern Pyrenees, France). *Earth Planet. Sci. Lett.* 93, 50-64.

Lorand, J. P., and Cottin, J. Y., 1989. Silicate and base-metal sulfide inclusions in chromites from the Maqsad area (Oman ophiolite, Gulf of Oman): a model for entrapment. *Lithos* 22, 173-190.

Lorand, J. P., Keays, R. R., and Bodinier, J. L., 1993. Copper and noble metal enrichments across the lithosphere-asthenosphere boundary of mantle diapirs: evidence from the Lanzo lherzolite massif. *J. Petrol.* 34, 1111-1140.

Malpas, J., 1978. Magma generation in the upper mantle, field evidence from ophiolite suites and application to the generation of oceanic lithosphere. *Phil. Trans. Soc. London*, 288A, 527-546.

Malpas, J., and Robinson, P. T., 1987. Chromite mineralization in the Troodos

ophiolite, Cyprus. In Stowe, C. W. (ed.) Evolution of chromium ore fields. New York: Van Nostrand-Reinhold, p.220-237.

Marcoux, J., De Wever, P., Nicolas, A., Girardeau, J., Xiao, X., Chang, C., Wang, N., Zao, Y., Bassoulet, J. P., Colchen, M., and Mascle, G., 1982. Preliminary report on depositional sediments on top of volcanic member: the Xigaze ophiolite (Yarlung-Zangbo suture zone, Xizang, China). *Ophioliti* 6, 31-32.

Mathez, E. A., and Peach, C. L., 1989. The geochemistry of the platinum-group elements in mafic and ultramafic rocks. In Whitney, J. A., and Naldrett, A. J. (eds.) Ore deposition associated with magmas, *Rev. Econ. Geol.* 4, 33-43.

McDonald, J. A., 1965. Liquid immiscibility as one factor in chromitite seam formation in the Bushveld Igneous Complex. *Econ. Geol.* 60, 1674-1683.

McDonough, W. F., 1990. Constraints on the composition of the continental lithospheric mantle. *Earth Planet. Sci. Lett.* 101, 1-18.

McElduff, B., and Stumpfl, E. F., 1991. The chromite deposits of the Troodos complex, Cyprus-evidence for the role of a fluid phase accompanying chromite formation. *Mineral. Deposita* 26, 307-318.

Mehegan, J. M., and Robinson, P. T., 1991. Lava groups and volcanic stratigraphy of the CCSP Boreholes CY-1 and CY-1A, Troodos ophiolite, Cyprus. In Gibson, I. L., Malpas, J., Robinson, P. T., and Xenophontos, C. (eds.) Cyprus crustal study project, Initial report, Holes Cy-1 and 1A. *Geol. Survey Can. Paper* 90-20, p.177-185.

Mercier, J.-C. C., and Nicolas, A., 1975. Textures and fabrics of upper mantle peridotites as illustrated by xenoliths from basalts. *J. Petrol.* 16, 454-496.

Michael, P. T., and Bonatti, E., 1985. Peridotite composition from the North Atlantic: regional and tectonic variations and implications for partial melting. *Earth Planet. Sci. Lett.* 73, 91-104.

Mitchell, R. H., and Keays, R. R., 1981. Abundance and distribution of gold, palladium and iridium in some spinel and garnet lherzolites: implications for the nature and origin of precious metal-rich intergranular components in the upper mantle. *Geochim. Cosmochim. Acta* 45, 2425-2442.

Muan, A., 1975. Phase relations in chromium oxide-containing systems at elevated temperatures. *Geochim. Cosmochim. Acta* 39, 781-802.

Muan, A., and Somiya, S. H., 1960. Phase equilibria in the system iron oxide Cr_2O_3 - SiO_2 in air. *J. Amer. Cera. Soc.* 43, 204-209.

Muenow, D. W., Liu, N. W. K., Garcia, M. O., and Saunders, A. D., 1980. Volatiles in submarine volcanic rocks from the spreading axis of the East Scotia Sea back-arc basin. *Earth Planet. Sci. Lett.* 47, 272-278.

Murck, B. W., and Campbell, I. H., 1986. The effects of temperature, oxygen fugacity and melt composition on the behaviour of chromium in basic and ultrabasic melts. *Geochim. Cosmochim. Acta* 50, 1871-1887.

Mysen, B., and Kushiro, I., 1977. Compositional variations of coexisting phases with degree of melting of peridotite in the upper mantle. *Am. Mineral.* 62, 843-865.

Naldrett, A. J., and Duke, J. M., 1980. Platinum metals in magmatic sulfide ores. *Science* 208, 1417-1428.

Naldrett, A. J., and von Gruenewaldt, G., 1989. Association of platinum-group elements with chromitite in layered intrusions and ophiolite complexes. *Econ. Geol.* 84, 180-187.

Navon, O., and Stolper, E., 1987. Geochemical consequences of melt percolation: the upper mantle as a chromatographic column. *J. Geol.* 95, 285-307.

Neary, C. R., and Brown, M. A., 1979. Chromites from the Al Ays complex, Saudi Arabia and the Semail complex, Oman. In Al Shanti, M. S. (ed.) *Evolution and mineralization of the Arabian Shield*, *Inst. Arab. Geol. Bull.* 2, 193-205.

Nicolas, A., 1989. *Structures of ophiolites and dynamics of oceanic lithosphere*. Dordrecht: Kluwer Acad. Publ., 367pp.

Nicolas, A., and Poirier, J. P., 1976. *Crystalline plasticity and solid state flow in metamorphic rocks*. London: John Wiley & Sons, 444pp.

Nicolas, A., and Prinzhofer, A., 1983. Cumulative or residual origin for the transition zone in ophiolites: Structural evidence. *J. Petrol.* 24, 188-206.

Nicolas, A., and Al Azi, H., 1991. Chromite-rich and chromite-poor ophiolites: the Oman case. In Peters, Tj., Nicolas, A., and Coleman, R. G. (eds.) *Ophiolite genesis and evolution of the oceanic lithosphere*. London: Kluwer Acad. Publ., p. 261-274.

Nicolas, A., Girardeau, J., Marcoux, J., Dupre, B., Wang, X., Cao, Y., Zheng, H., and Xiao, X., 1981. The Xigaze ophiolite (Tibet): a peculiar oceanic lithosphere. *Nature* 294, 414-417.

Ozawa, K., 1988. Ultramafic tectonite of the Miyamori ophiolitic complex in the Kitakami Mountains, northeast Japan: hydrous upper mantle in an island arc. *Contrib. Mineral. Petrol.* 99, 159-175.

Page, N. J., and Talkington, R. W., 1984. Palladium, platinum, rhodium, ruthenium and iridium in peridotites and chromitites from ophiolite complexes in Newfoundland. *Can. Mineral.* 22, 137-149.

Paktunc, A. D., 1990. Origin of podiform chromite deposits by multistage melting, melt segregation and magma mixing in the upper mantle. *Ore Geol. Rev.* 5, 211-222.

Patriat, P. and Achache, J., 1984. India-Eurasia collision chronology has implications for crustal shortening and driving mechanisms of plates. *Nature* 311, 615-621.

Pavlov, N. V., and Chuprynina, I. I., 1966. Conclusions on formation of chromite deposits within Kempirsay ultrabasic massif. *Intern. Geol. Rev.* 8, 16-27.

Pavlov, N. V., Grigoryeva, I. I., and Tsepin, A. I., 1977. Chromite nodules as an indicator of liquation of a magmatic melt. *Int. Geol. Rev.* 19, 43-56.

Pearce, J. A., Lippard, S. J., and Roberts, S., 1984. Characteristics and tectonic significance of suprasubduction zone ophiolites. In Kokelaar, B. P., and Howells, M. F. (eds.) *Marginal basin geology*. Geol. Soc., London, Spec. Publ. 16, 77-94.

Pozzi, J.P., Weatphal, M., Girardeau, J., Besse, J., Yao Xin Zhou, Xian Yao Chen and Li Sheng Xing, 1984. Paleomagnetism of the Xigaze ophiolite and flysch (Yarlung Zangbo suture zone, southern Tibet): latitude and direction of spreading. *Earth Planet. Sci. Lett.* 70, 383-394.

Quick, J. E., 1981. The origin and significance of large, tabular dunite bodies in the Trinity peridotite, Northern California. *Contrib. Mineral. Petrol.* 78, 413-422.

Quick, J. E., and Gregory, R. T., 1995. Significance of melt-wall reaction: a comparative anatomy of three ophiolites. *J. Geol.* 103, 187-198.

Ringwood, A. E., 1974. The petrological evolution of island arc systems. *J. Geol.*

Soc. Lond. 130, 183-204.

Roberts, S., 1988. Ophiolitic chromitite formation: a marginal basin phenomenon? *Econ. Geol.* 83, 1034-1036.

Roberts, S., 1992. Influence of the partial melting regime on the formation of ophiolitic chromitite, in Parson, L. M., Murton, B. J., and Browning, P. (eds.) *Ophiolites and their modern oceanic analogues. Geol. Soc. Spec. Publ. No.60*, p.203-217.

Roberts, S., and Neary, C., 1993. Petrogenesis of ophiolitic chromitites. In Prichard, H. M., Alabaster, T., Harris, N. B. W., and Neary, C. R. (eds.) *Magmatic processes and plate tectonics. Geol. Soc. Spec. Publ. 76*, p.257-272.

Robinson, P. T., Melson, W. G., O'Hearn, T., and Schmincke, H. V., 1983. Volcanic glass composition of the Troodos ophiolite, Cyprus. *Geol.* 11, 400-404.

Roeder, P. L., Campbell, I. H., and Jamieson, H. E., 1979. A re-evaluation of the olivine-spinel geothermometer. *Contrib. Mineral. Petrol.* 68, 325-335.

Roeder, P. L., and Reynolds, I., 1991. Crystallization of chromite and chromium solubility in basaltic melts. *J. Petrol.* 32, 909-934.

Sampson, E., 1932. Magmatic chromitite deposits in southern Africa. *Econ. Geol.* 27, 113-144.

Sen, G., Frey, F. A., Shimizu, N. and Leeman, W. P., 1993. Evolution of the lithosphere beneath Oahu, Hawaii: rare earth element abundants in mantle xenolith. *Earth Planet. Sci. Lett.* 119, 53-69.

Sengupta, S., Ray, K. K., Acharyya, S. K., and de Smeth, J. B., 1990. Nature of ophiolite occurrences along the eastern margin of the Indian plate and their tectonic significance. *Geol.* 18, 439-442.

Sharer, U., Xu, R.-H., and Allegre, C. J., 1984. U-Pb geochronology of Gandise (Transhimalaya) plutonism in the Lhasa-Xigaze region, Tibet. *Earth Planet. Sci. Lett.* 69, 311-320.

Sharpe, M. R., and Irvine, T. N., 1983. Melting relations of the two Bushveld chilled margin rocks and implications for the origin of chromitite. *Carnegie Inst. Washington Ybk.* 82, 295-300.

Sinigoi, S., Comin-Chiaramonti, P., Demarchi, G., and Siena, F., 1983.

- Differentiation of partial melts in the mantle: Evidence from the Balmuccia peridotite, Italy. *Contrib. Mineral. Petrol.* 82, 351-359.
- Stockman, H. W., and Hlava, P. F., 1984. Platinum-group minerals in Alpine chromitites from southwestern Orogen. *Econ. Geol.* 79, 491-508.
- Stowe, C. W., 1987. Distribution of chromite ore field. In Stowe C. W. (ed.) *Evolution of chromium ore fields*. New York: Van Nostrand-Reinhold, p.49-70.
- Streckeisen, A. L., 1973. Plutonic rocks, classification and nomenclature recommended by the IUGS subcommission on the systematics of igneous rocks. *Geotimes* 18, 26-30.
- Suhr, G., and Robinson, P. T., 1994. Origin of mineral chemical stratification in the mantle section of the Table Mountain massif (Bay of Islands ophiolite, Newfoundland, Canada). *Lithos* 31, 81-102.
- Sun, M., Jain, J., Zhou, M.-F., and Kerrich, R., 1993. A procedural modification for enhanced recovery of precious metals (Au, PGE) following nickel sulphide fire assay and tellurium coprecipitation: applications for analysis of geological samples by Inductively Coupled Plasma Mass Spectrometry. *Can. J. Appl. Spectr.* 38, 103-108.
- Sun, S.-S., Wallace, D. A., Hoatson, D. M., Glikson, A. Y., and Keays R. R., 1991. Use of geochemistry as a guide to platinum group element potential of mafic-ultramafic rocks: examples from the west Pilbara Block and Halls Creek Mobile Zone, Western Australia. *Precam. Res.* 50, 1-35.
- Talkington, R. W., and Malpas, J., 1980. Spinel phases of the White Hills peridotite, St. Anthony Complex, Newfoundland: part 1 occurrence and chemistry. In A. Panayiotou (ed.) *Ophiolites proceedings international ophiolite symposium Cyprus 1979*. Cyprus: Geol. Survey Dept., p.607-619.
- Talkington, R. W., and Lipin, B. R., 1986. Platinum-groups minerals in chromite seams of the Stillwater Complex, Montana. *Econ. Geol.* 81, 1179-1186.
- Tapponnier, P., and others, 1981. The Tibetan side of the India-Eurasia collision. *Nature* 294, 393-399.
- Tatsumi, Y. and Ishizaka, K., 1982. Origin of high-magnesia andesites in the Setouchi volcanic belt, southwest Japan, I. Petrographical and chemical characteristics. *Earth Planet. Sci. Lett.* 60, 293-304.

- Thakur, V. C., and Misra, D. K., 1984. Tectonic frame work of the Indus and Shyok suture zones in eastern Ladakh, Northwest Himalaya. *Tectonophy.* 101, 207-220.
- Thayer, T. P., 1946. Preliminary chemical correlation of chromite with the containing rocks. *Econ. Geol.* 41, 202-217.
- Thayer, T. P., 1964. Principal features and origin of podiform chromite deposits, and some observations on the Guleman-Soridag district, Turkey. *Econ. Geol.* 59, 1497-1524.
- Thayer, T. P., 1969. Gravity differentiation and magmatic reemplacement of podiform chromite deposits. *Econ. Geol. Monogr.* 4, 132-146.
- Thayer, T. P., 1973. Chromium. U.S.G.S. Prof. Pap. 820, 111-121.
- Thompson, R. N., 1972. The oxygen fugacity within graphite capsules in piston-cylinder apparatus at high pressures. *Carnegie Inst. Washington Ybk.* 71, 615-616.
- Ulmer, G. C., 1969. Experimental investigation on chromite spinels. *Econ. Geol. Monogr.* 4, 114-131.
- Vasseur, G., Vernieres, J., and Bodinier, J.-L., 1991. Modelling of trace element transfer between mantle melt and heterogranular peridotite matrix. *J. Petrol. special lherzolite issue*, 41-54.
- von Gruenewaldt, G., Hulbert, L. J., and Naldrett, A. J., 1989. Contrasting platinum-group element concentration patterns in cumulates of the Bushveld complex. *Mineral. Deposita* 24, 219-229.
- Wang Hesheng, Bai, W.-J., Wang Bixi, and Chai Yuchi, 1983. Chromite deposits of China (in Chinese). Beijing: Sci. Press, 227pp.
- Wang Xibin, 1965. Ultramafic rocks in Xizhang and their chromites (in Chinese). Beijing: Sci. Press, 98pp.
- Wang Xibin, Bao Pisheng, Deng Wanming, and Wang Fangguo, 1987. Xizang ophiolite. *Geol. Memoirs* 8 (in Chinese), 215-288.
- Warner, R. D., 1973. Liquidus relations in the system CaO-MgO-SiO₂-H₂O at 10 Kbar and their petrological significance. *Am. J. Sci.* 273, 925-946.

Watson, E. B., 1982. Melt infiltration and magma evolution. *Geology* 10, 236-240.

Xiao Xuchang, and others, 1988. General review of the tectonic evolution of the crustal-mantle of the Qinghai-Xizhang (Tibet) plateau (in Chinese). Beijing: Geol. Publ. House, 236pp.

Xu, R.-H., Scharer, U., and Allegre, J., 1985. Magmatism and metamorphism in the Lhasa Block (Tibet): a geochronological study. *J. Geol.* 93, 41-57.

Yin, A., Harrison, T. M., Ryerson, F. J., Chen, W., Kidd, W. S. F., and Copeland, P., 1994. Tertiary structural evolution of the Gangdese thrust system, southeastern Tibet. *J. Geophys. Res.* 99, 18175-18201.

Zhang, C., Zhai, M., Allen, M. B., Saunders, A. D., Wang, G., and Huang, X., 1993. Implications of palaeozoic ophiolites from west Junggar, NW China, for the tectonics of central Asia. *J. Geol. Soc. London* 150, 551-561.

Zhang, Z.h.-M., Liou, J. G., and Coleman, R. G., 1984. An outline of the plate tectonics of China. *Geol. Soc. Am. Bull.* 95, 295-312.

Zhou, M.-F., 1994. PGE distribution in 2.7-Ga layered komatiite flows from the Belingwe greenstone belt, Zimbabwe. *Chem. Geol.* 118, 155-172.

Zhou, M.-F., and Bai, W.-J., 1992. Chromite deposits in China and their origin. *Mineral. Deposita* 27, 192-199.

Zhou, M.-F., and Kerrich, R., 1992. Morphology and composition of chromite in komatiites from the Belingwe greenstone belt, Zimbabwe. *Can. Mineral.* 30, 303-317.

Zhou, M.-F., and Robinson, P. T., 1994. High-Cr and high-Al chromitites in western China: their relationship to partial melting and melt/rock interaction in the upper mantle. *Intern. Geol. Rev.* 36, 678-686.

Zhou, M.-F., Robinson, P. T., and Bai, W.-J., 1994. Formation of podiform chromitites by melt/rock interaction in the upper mantle. *Mineral. Deposita* 29, 98-101.

Zhou, M.-F., Robinson, P. T., Malpas, J., and Li, Z., 1995a. Podiform chromitites of the Luobusa ophiolite (southern Tibet): Evidence for the melt/rock interaction and chromite segregation in the upper mantle. *J. Petrol.* (in press).

Zhou, M.-F., Robinson, P. T., Sun, M., Kerrich, R., Reynolds, P. H., and Malpas, J., 1995b. Tectonic evolution and chromite mineralization of the Qilian-Kunlun-Himalaya tectonic domain, Western China. In Greccula, P. (ed.) Variscan metallogeny in the Alpine orogenic belt (in press).

Zhou, M.-F., Robinson, P. T., Reynolds, P. H., Malpas, J., Bai, W., Davies, G., Suhr, G., and Hu, X., 1995c. Suprasubduction zone origin of the Luobusa ophiolite, Indus-Yarlung Zangbo Suture zone, Tibet. GAC/MAC abstract program, Victoria.